

**High Track Density:
Challenges in Magnetic
Disk Drives**

**May 22, 1998
8:30 am to 4:30 pm**

Presented by

IIST

Santa Clara University
School of Engineering
Santa Clara, CA 95053

Phone: (408) 554-6853 * Fax: (408) 554-7841 *
iist@iist.scu.edu * <http://www.iist.scu.edu>

**High Track Density:
Challenges in Magnetic Disk Drives**

**Institute for Information Storage Technology
Santa Clara University, May 22, 1998**

**Instructor: Dan Malone
IBM Corporation, San Jose**

High Track Density:
Challenges in Magnetic Disk Drives

Institute for Information Storage Technology
Santa Clara University, May 22, 1998

Density trends, design challenges, TPI targets

Head & disk track density considerations

Noise sources

Track Misregistration

Additional track density considerations

Offtrack, adjacent track interference, 747

Error rate estimations and modeling

Dan Malone, IIST, 5/22/98, (scuintr1.doc)

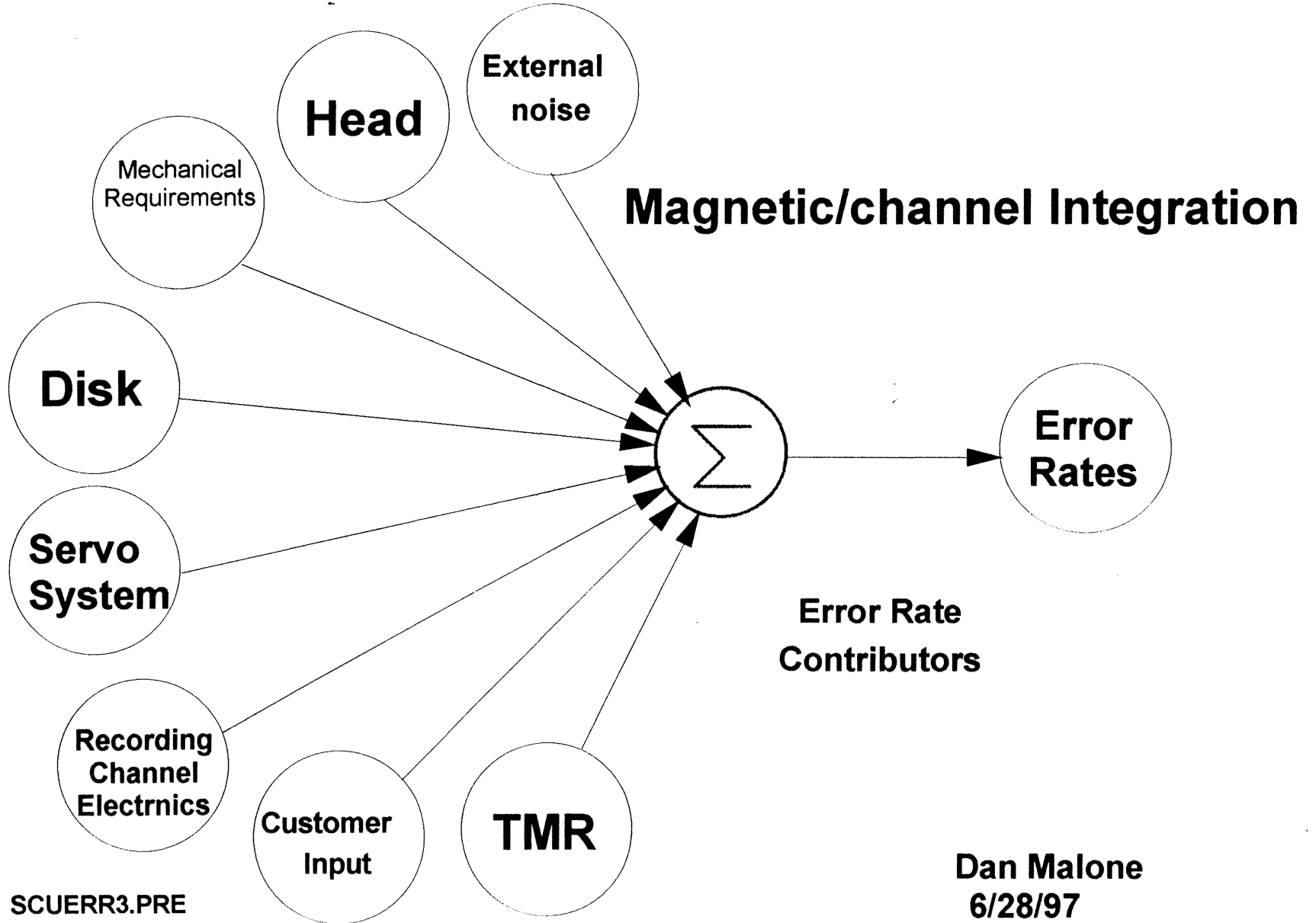
Track Edge Effects

- o Erase Bands**
- o Curved Transitions**
- o Effects due to skewing of the head**
- o Unsymmetrical reading effects of MR/GMR head**

Effected or Driven by:

- o Writing Gap length**
- o Actuator skew angle**
- o Disk magnetic film orientation**
- o Magnetic fly height**
- o Pole tip shape, with or without trimming**

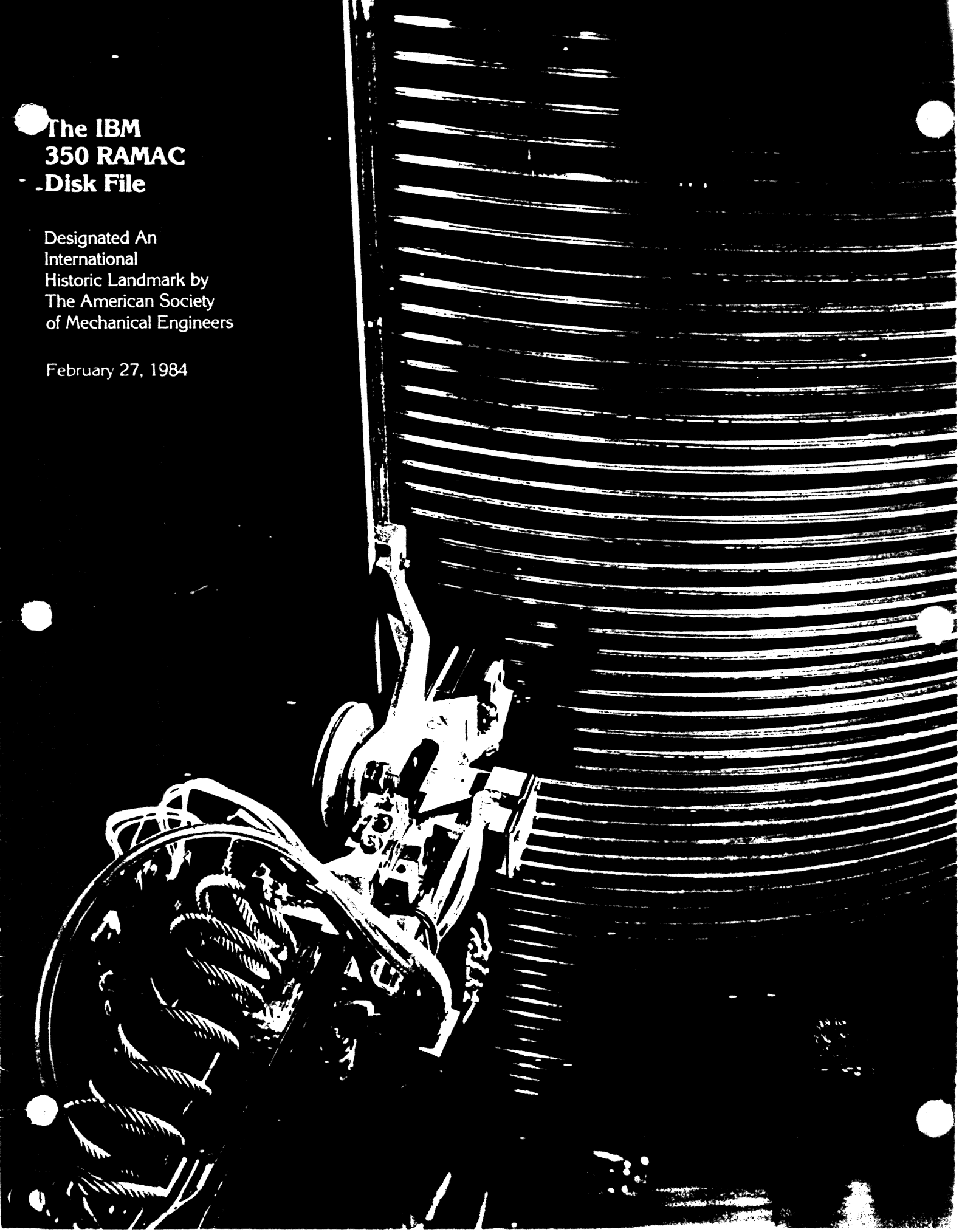
Track Density Considerations



**The IBM
350 RAMAC
Disk File**

Designated An
International
Historic Landmark by
The American Society
of Mechanical Engineers

February 27, 1984



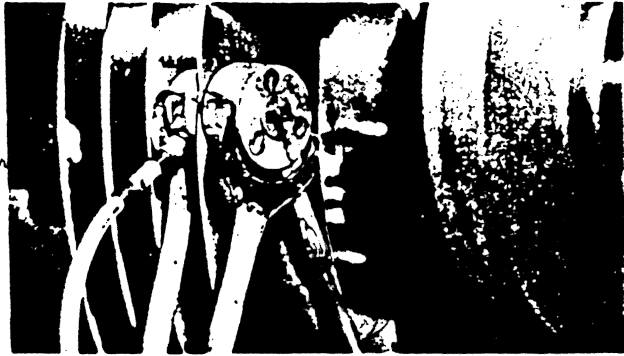
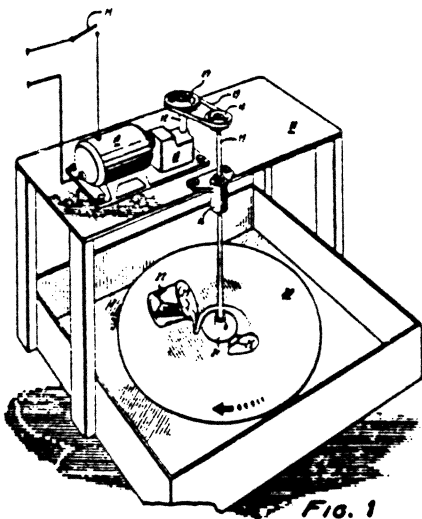
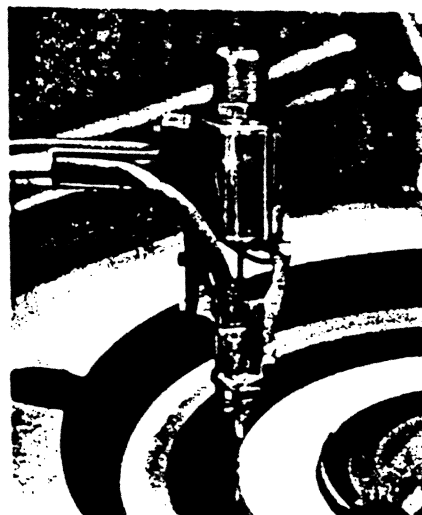


Figure 1 First air bearing magnetic head, tested on June 2, 1953.

Taken from IBM Journal of Research and Development
Vol. 25, No. 5, September 1981



Patent for Magnetic Recording Surface by
J. J. Hagopian.



Today's process for spin-coating disk surfaces.

Taken from "Input/Output 8/83", IBM Corporation,
General Products Division, San Jose, August, 1983

Table 1 Development of technologies in key areas of magnetic head and its air bearing support, disk substrate and its coating, head-positioning actuator, and read/write electronics.

<i>Year of first ship</i>	1957	1961	1962	1963	1966	1971	1973	1976	1979	1979	1981
Product	350	1405	1301	1311	2314	3330	3340	3350	3310	3370	3380
Recording density											
Areal density (Mb/in. ²)	0.002	0.009	0.026	0.051	0.22	0.78	1.69	3.07	3.8	7.8	>12
Linear bit density (bpi)	100	220	520	1025	2200	4040	5636	6425	8530	12134	15200
Track density (tpi)	20	40	50	**	100	192	300	478	450	635	>800
Key geometric parameters (microin.)											
Head-to-disk spacing	800	650	250	125	85	50	18	**	13	**	<13
Head gap length	1000	700	500	250	105	100	60	50	40	25	**
Medium thickness	1200	900	543	250	85	50	41	**	25	41	<25
Air bearing & magnetic element											
Bearing type	hydrostatic		hydrodynamic	**	**	**	**	**	**	**	**
Surface contour	flat	**	cylindrical	**	**	**	taper flat	**	**	**	**
Slider material	Al	**	stainless steel	ceramic	**	**	ferrite	**	**	ceramic	**
Core material	laminated mu-metal	**	**	**	ferrite	**	**	**	**	film	**
Slider/core bond	epoxy	**	**	**	**	glass	integral	**	**	deposited	**
Disk											
Diameter (in.)	24	**	*	14	**	**	**	**	8.3	14	**
Substrate thickness (in.)	0.100	**	**	0.050	**	0.075	**	**	**	**	>0.075
Rpm	1200	**	1800	1500	2400	3600	2964	3600	3125	2964	3620
Fixed/removable	fixed	**	**	removable pack	**	**	module	fixed	**	**	**
Data surfaces/spindle	100	**	**	10	20	19	6	15	11	12	15
Actuator											
Access geometry	x-y	**	linear	radial	**	**	**	**	rotary	linear	**
Heads	2 heads/actuator		1 head/surface	**	**	**	2 heads/surface	1 h/s	2 h/s	**	**
Positioning	motor-clutch	**	hydraulic	**	**	**	voice coil motor	**	**	**	**
Final position	detent	**	**	**	**	**	servo surface	(+sector)	servo surface	**	**
Actuators/spindle (max. no.)	3	**	2	1	**	**	**	**	1	2	**
Avg. seek time (ms)	600	**	165	150	60	30	25	**	27	20	16
Read/write electronics											
Data rate (Kbytes/s)	8.8	17.5	68	69	312	806	885	1198	1031	1859	3000
Encoding	NRZI	**	**	**	2 f	mfm	**	**	mfm	2, 7	**
Detection	ampl	**	**	**	peak	delta	**	**	**	delta c ²	**
Clocking	2 osc	**	clk trk	osc	vfo	**	**	**	**	**	**

**Same as in preceding column.

The evolution of the whole technology is given in the overview paper [3], and the progress in disk file manufacturing and in selected innovations in materials, processes, and testing is discussed in the paper by Mulvany and Thompson [4]. The present paper traces the development of each part of the technologies in four key areas:

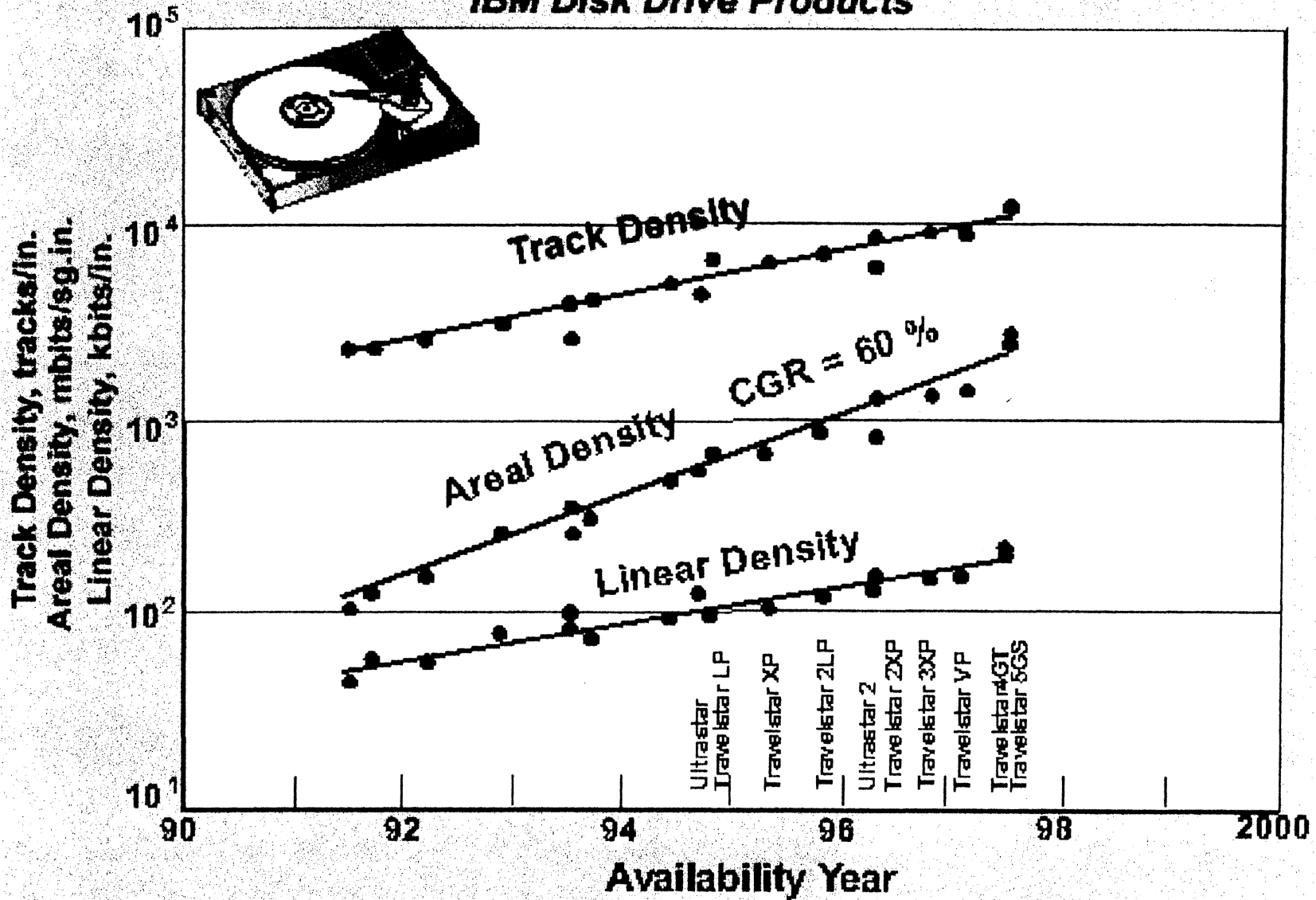
- The development of the magnetic head and its air bearing support that provides the close spacing between the disk surface and read/write head necessary for high-density magnetic recording.
- The development of the disk substrate and its magnetic coating.
- The mechanical design aspects of the actuator that positions the read/write heads over concentric tracks of a rotating disk.
- The key innovations in logic and electronics required to read and write data reliably and accurately from a disk.

Much of this development has been based upon the work of many individuals who have created, over the past quarter of a century, a technological base that has permitted the improvement of almost four orders of magnitude in areal density shown in Table 1 and also enhancements in performance, function, and reliability. Two individuals in particular deserve mention because their influence was so pervasive through the early days of development. They certainly deserve credit for motivation and for active participation in many of the innovations to be discussed. They are R. B. Johnson, who had the vision that such a device was needed and could be built, and L. D. Stevens, who provided the engineering management that realized the first successful product [5].

Air bearing spacing and magnetic heads

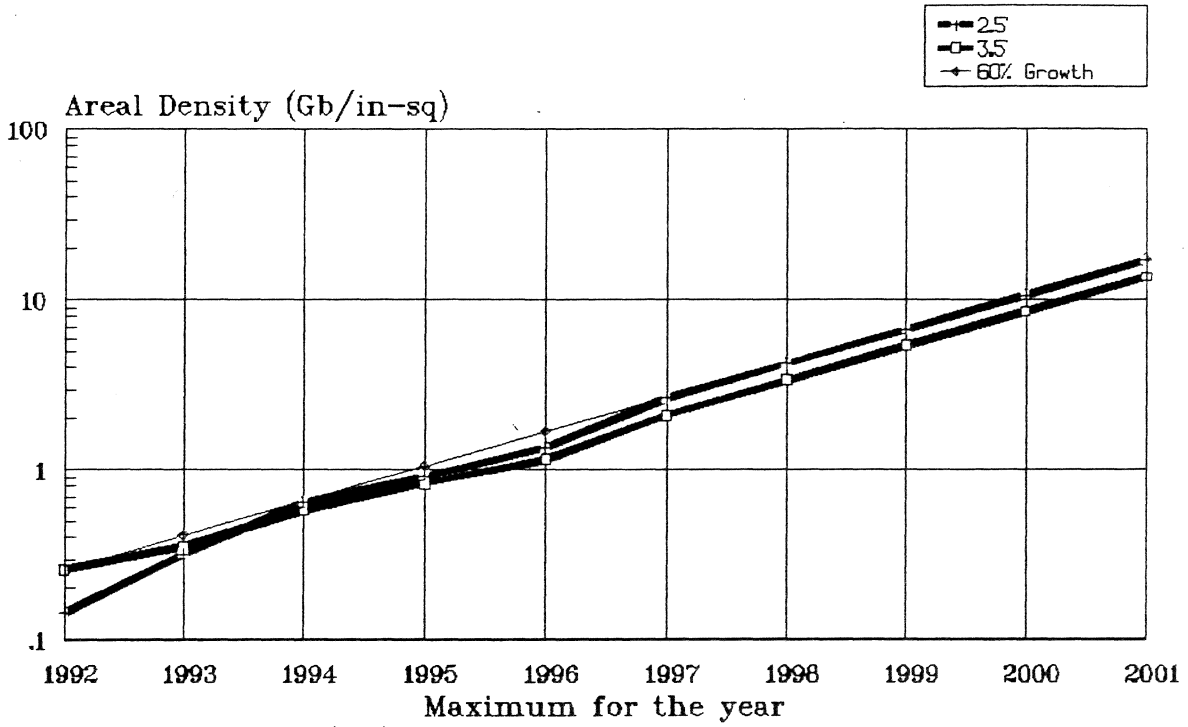
Film bearings, both self-acting and externally pressurized, have been in common use for over a hundred years.

Track, Areal, Linear Density Perspective IBM Disk Drive Products



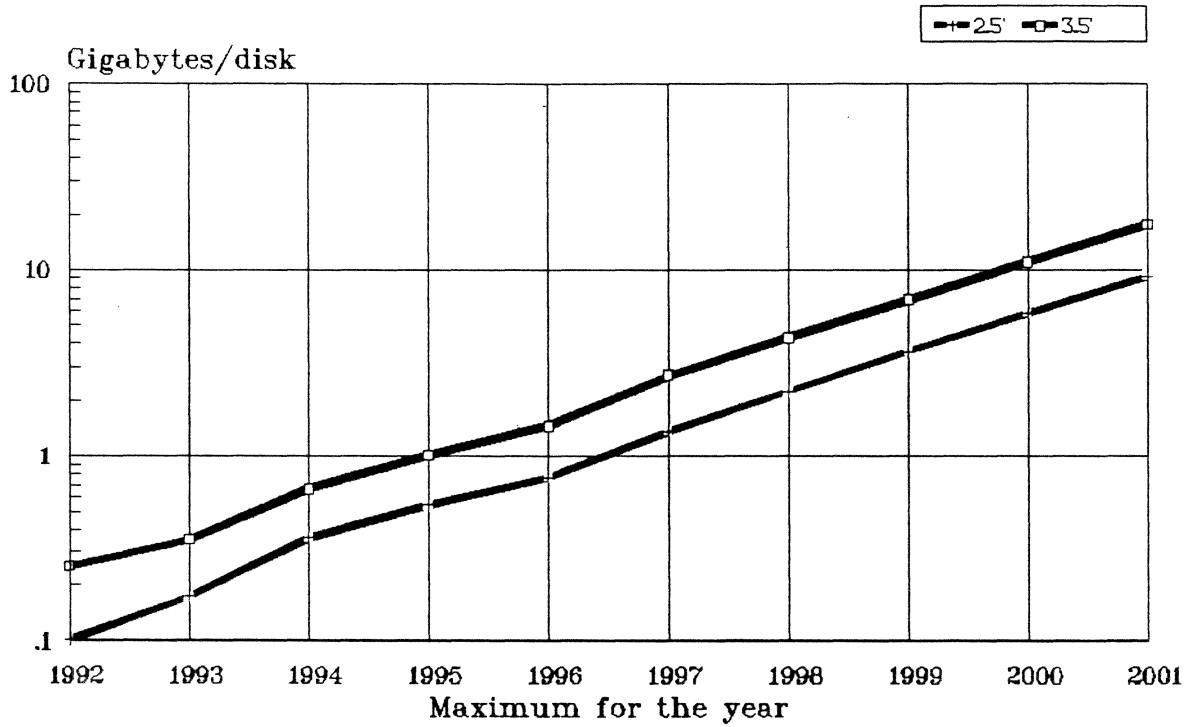
Areal Density Trends

Source: Jim Porter - Disk Trend report at IEEE Meeting 6-10-97
Projections for years 1998-2001



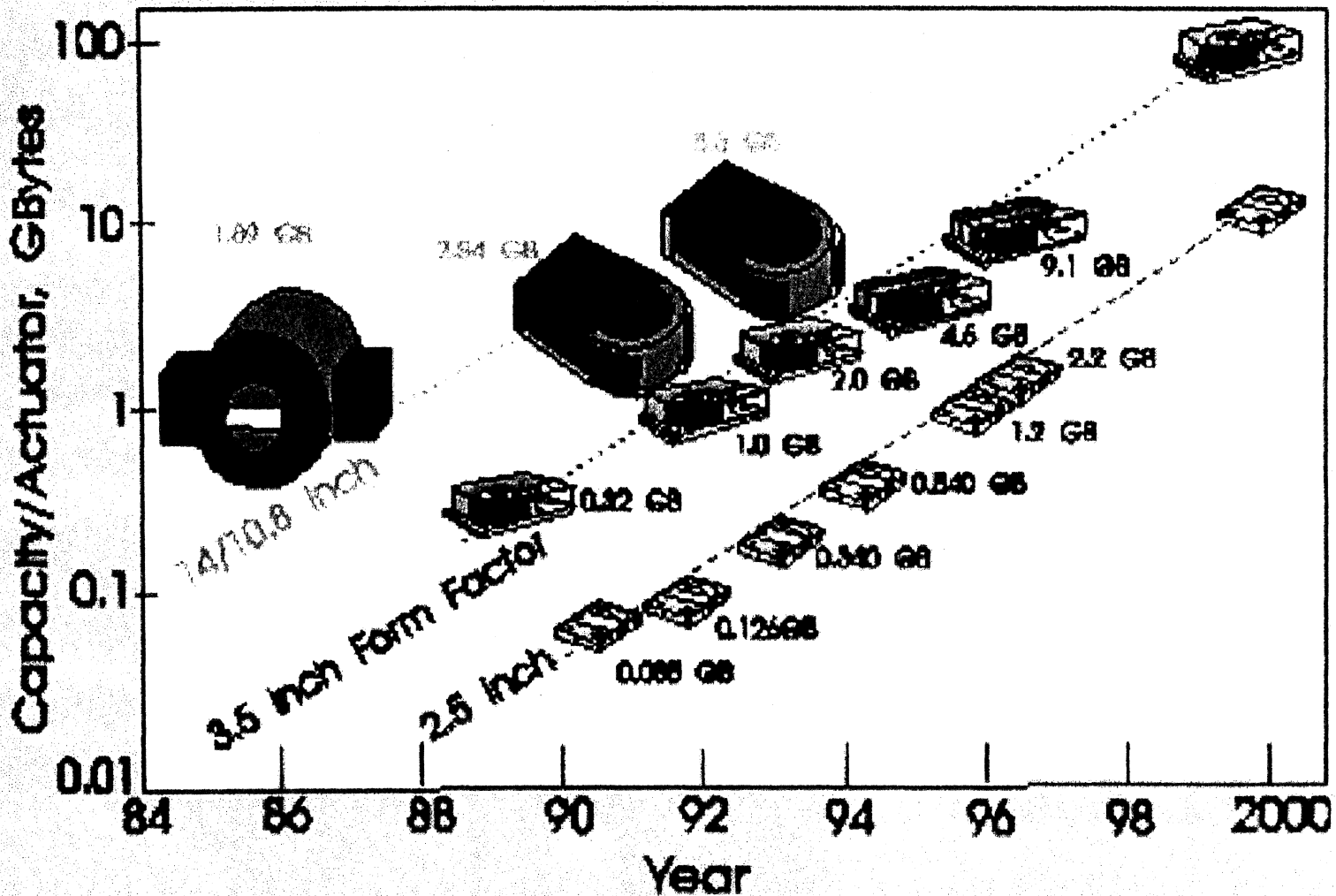
Gigabytes per Disk

Source: Jim Porter - Disk Trend report at IEEE Meeting 6-10-97
Projections for years 1998-2001



Dan Malone, IIST, 6/24/97

Disk drive form factor evolution



IBM Advanced Technology

FUTURE STORAGE TECHNOLOGIES

Magnetic Tape

1 TByte/In³
200 kbpI
5 ktpI
0.125 mil tape
25 MByte/sec

500 GByte/QIC
40 GByte/RDAT

Magnetic Disk

10 Gbit/In²
400 kbpI
25 ktpI
15 MByte/sec

150 GByte/3.5" drive
1.5 GByte/1" drive

Magneto-Optic Disk

10 Gbit/In²
165 kbpI
64 ktpI
10 MByte/sec

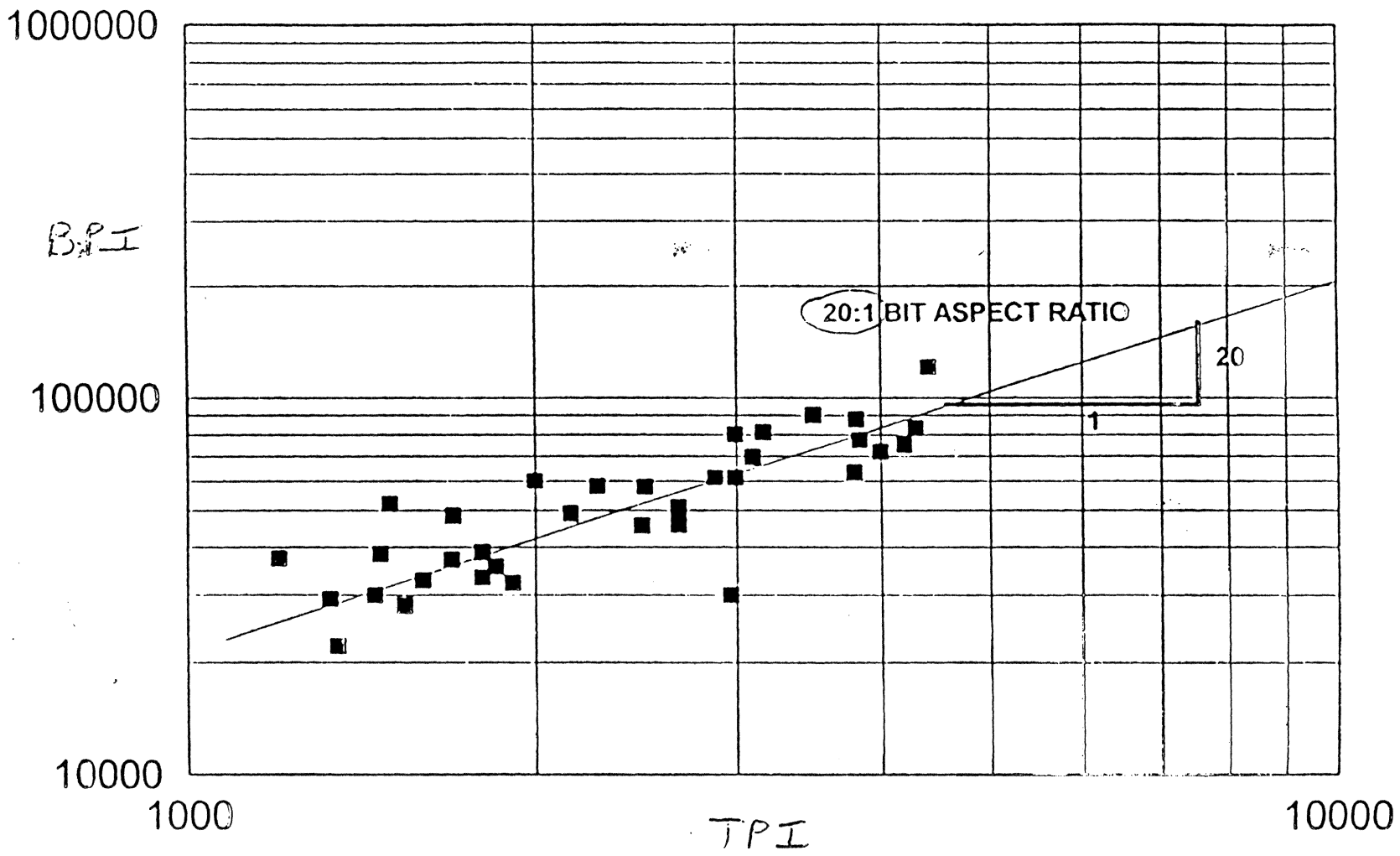
6 GByte/2" removable disk

High Performance Drive - Year 2000

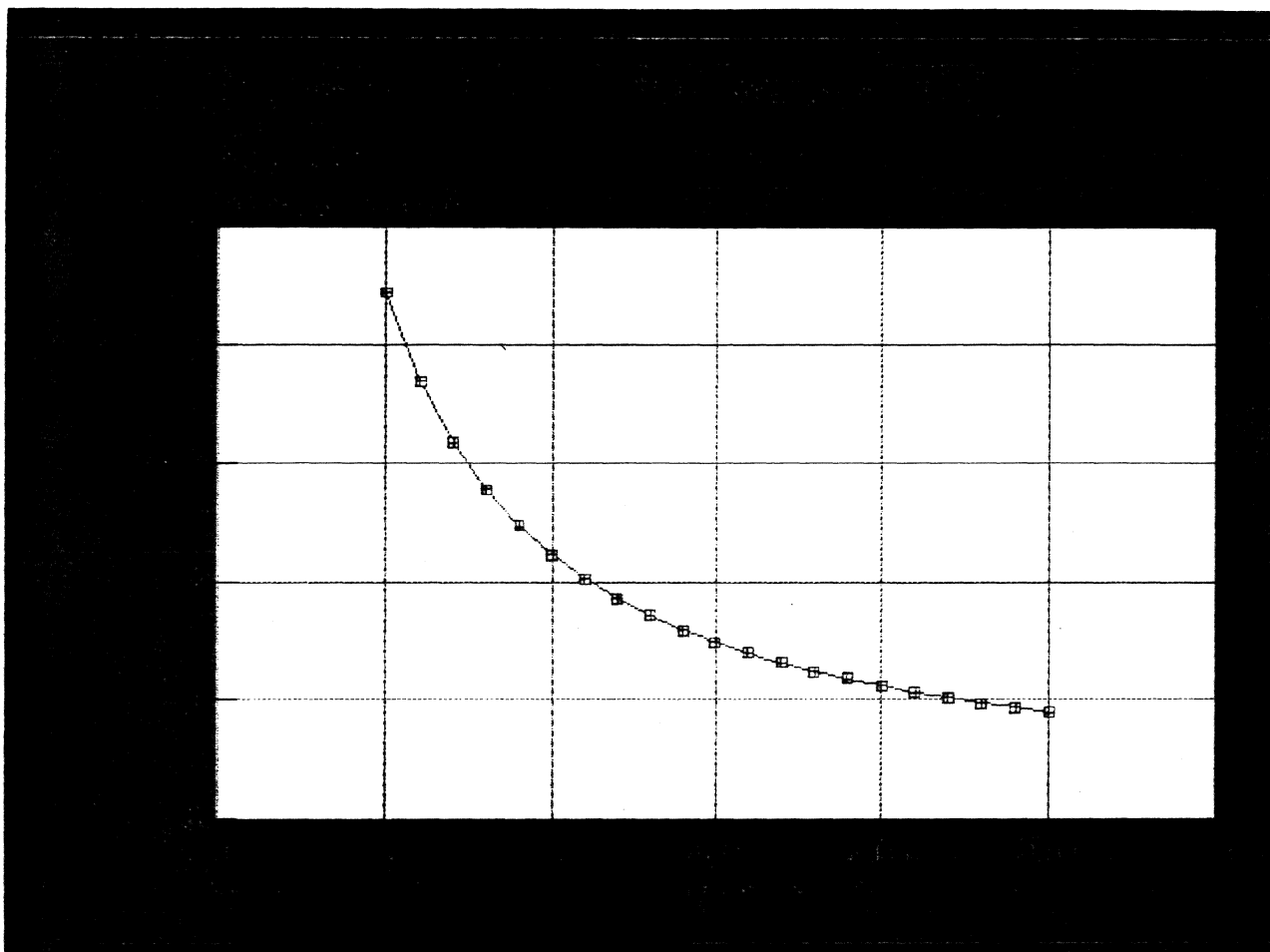


	Scorpion 9GB	Year 2000 72GB
Form Factor	3 1/2", 43 mm	3 1/2", 43 mm
Disks/Heads	9 Disks/18 Heads	10 Disks/20 Heads
Areal Density	0.85 Gbits/in ²	8 Gbits/in ²
Linear Density	140 kbits/in.	373 kbits/in.
Track Density	6300 tracks/in.	21400 tracks/in.
RPM	7200	10000
Average Access Time	7.5 msec.	6.0 msec.
Media Data Rate	15 Mbytes/sec.	62 Mbytes/sec.
Average Power	<20 watts	>20 watts
OEM Price	\$950	\$950
Price per MB	11¢	1.5¢

PRODUCT BIT ASPECT RATIO TREND



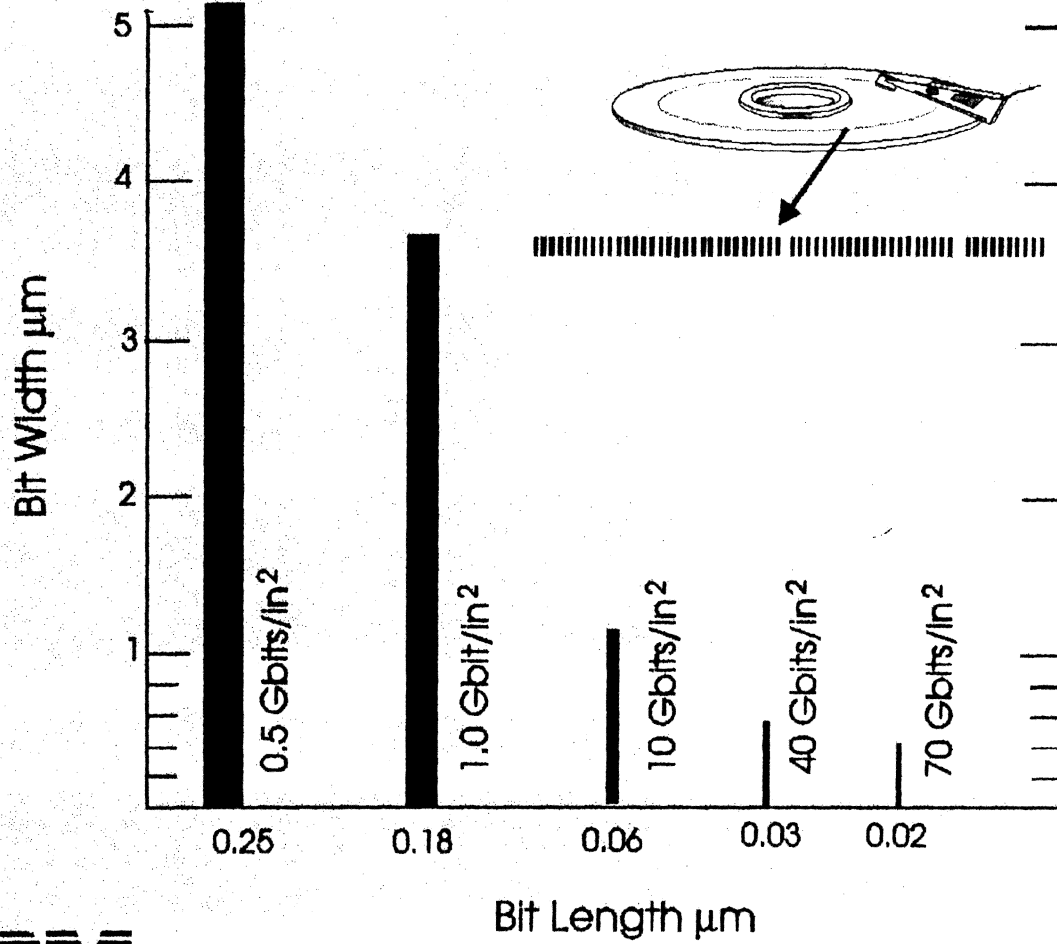
Magnetic Track Width Considerations:



The chart above uses a “7/8’s rule” to estimate the required **magnetic** corewidth for a particular TPI. It is usually somewhat more complicated to pick the proper width, but a technique like this can be used to give one guidance.

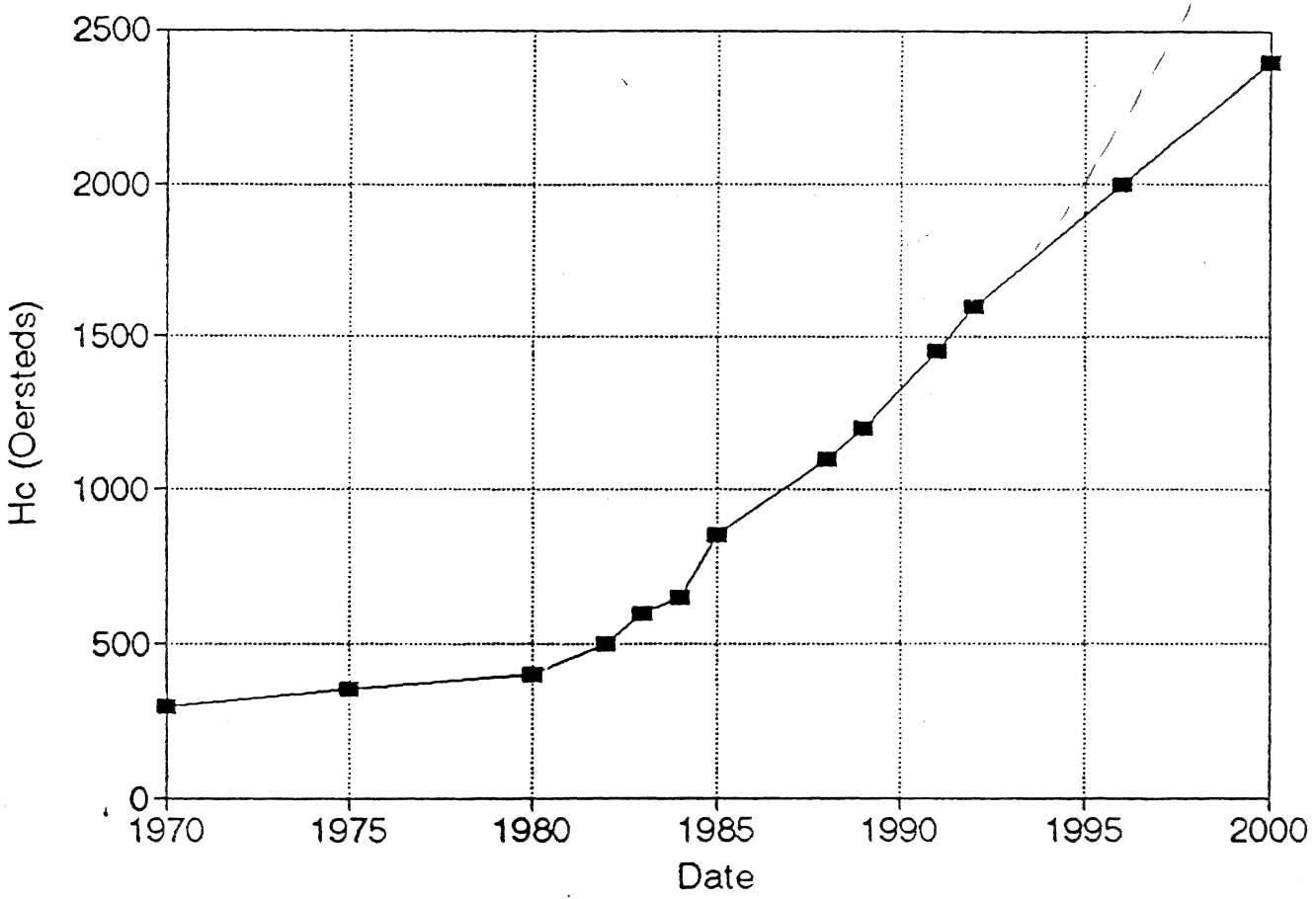
Important: -- The **physical** width of the head must be selected base on the magnetic corewidth requirements. The **physical** width of the head elements will most certainly be different from the **magnetic** widths.

Bit Cell Scaling

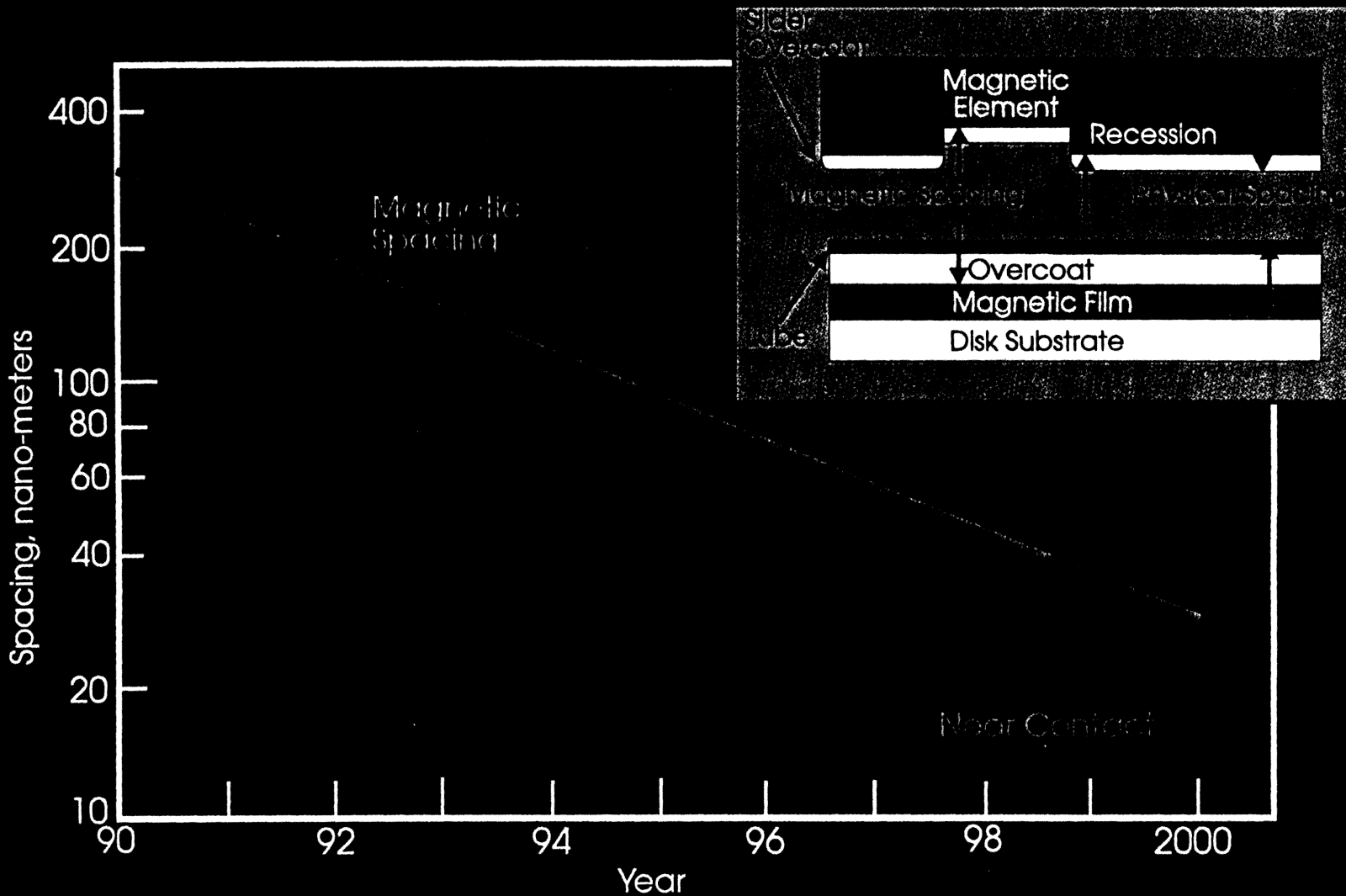


IBM Advanced Technology

Disk Coercivity vs Date



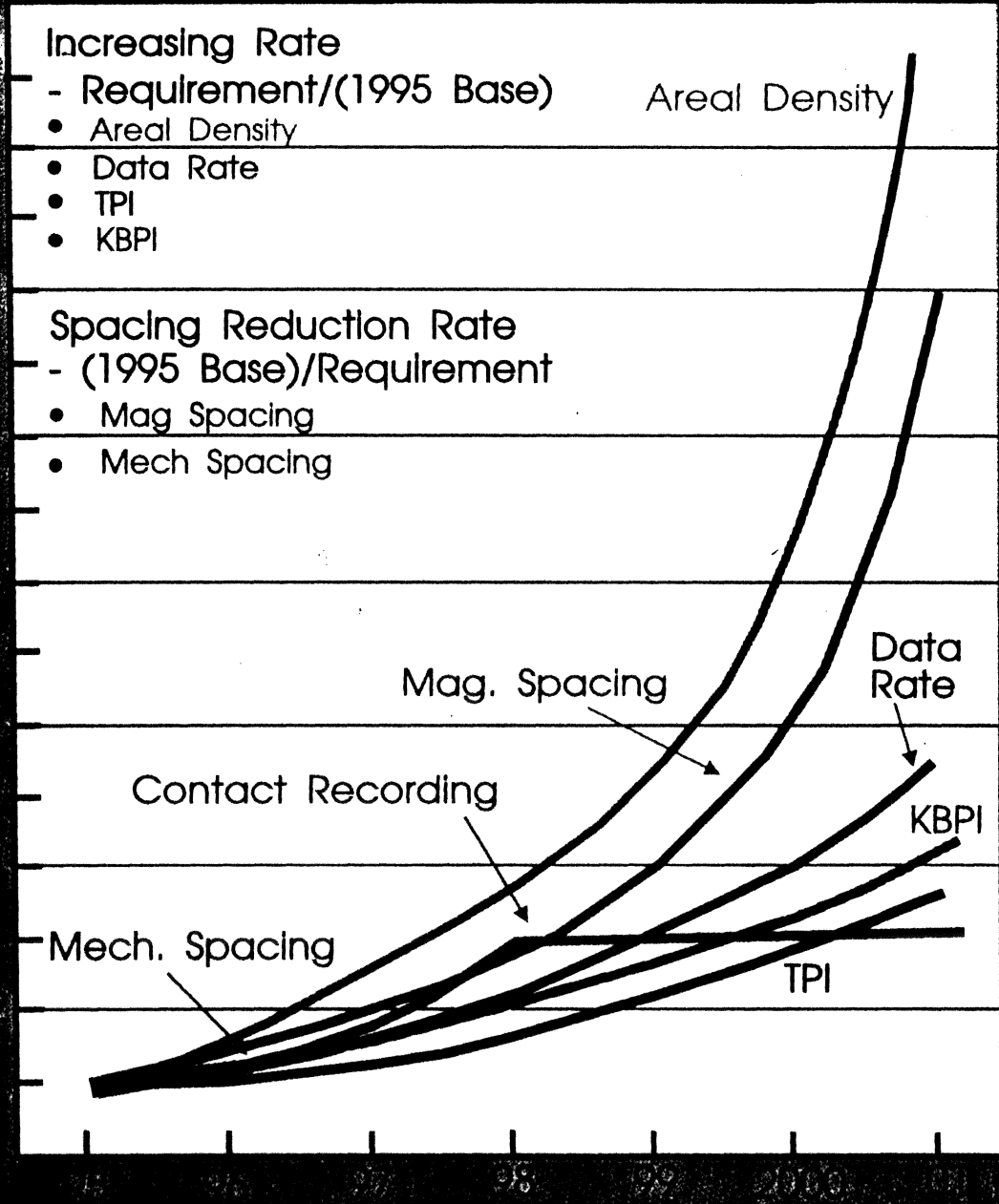
Magnetic/Physical spacing evolution



IBM Advanced Technology

Technology Challenges

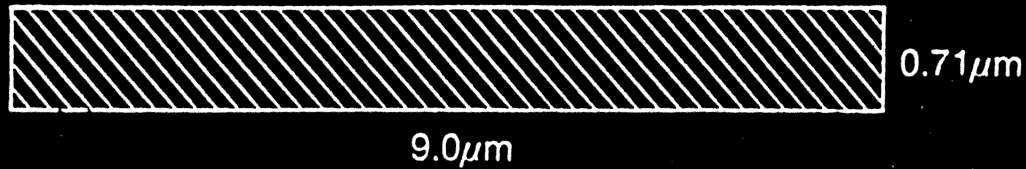
Storage Capacity Growth Rate (1995 Base)



IBM Advanced Storage Technology

TRENDS IN AREAL DENSITY: IMPACT ON BIT SIZES

100 Mb/in²



(35 kfc i x 2200 tpi)

GRAIN SIZE
 $d = 30 \pm 10 \text{ nm}$

1 Gb/in²



(175 kfc i x 6600 tpi)

GRAIN SIZE
 $d = 15 \pm 5 \text{ nm}$

10 Gb/in²

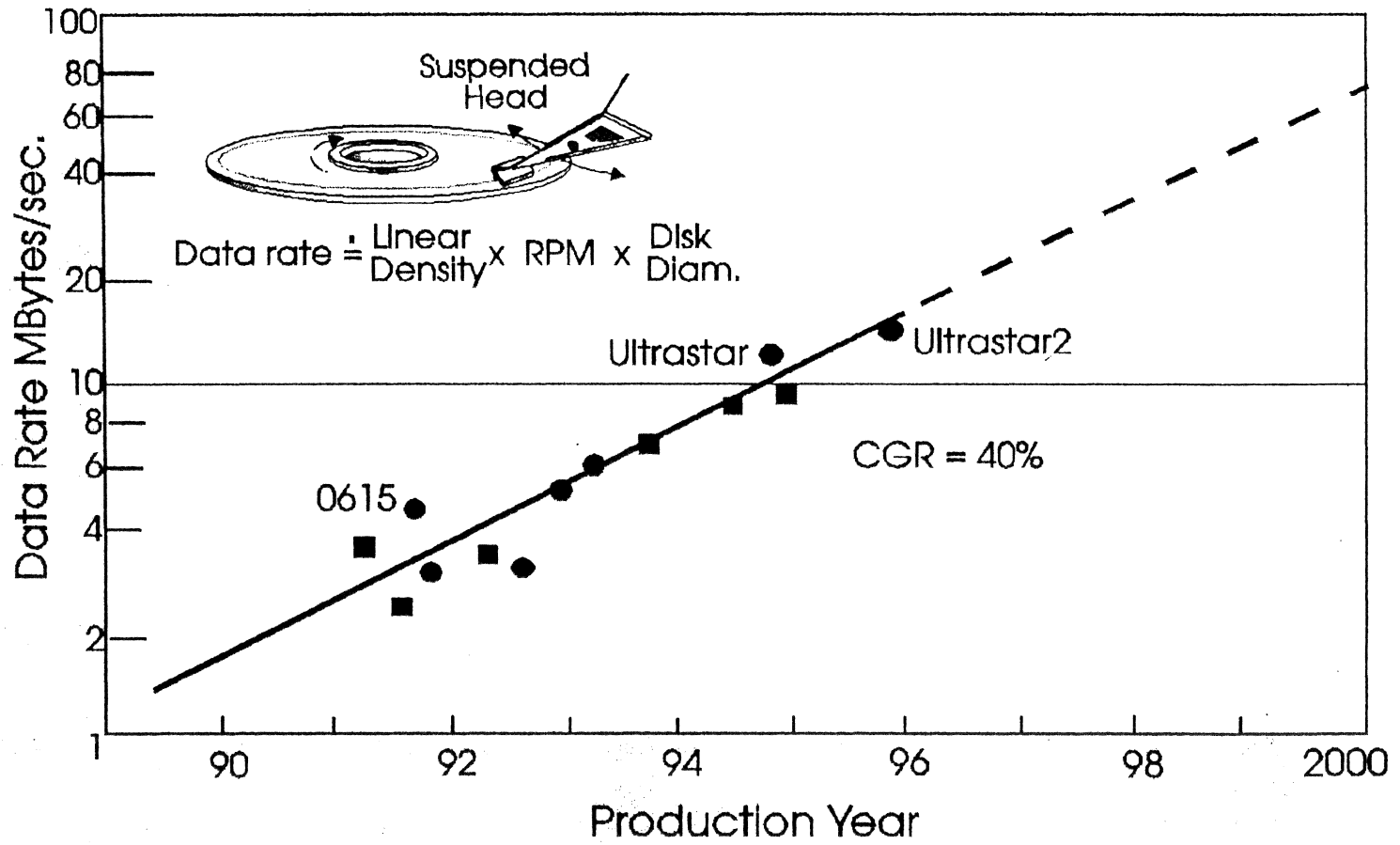


0.8 μm

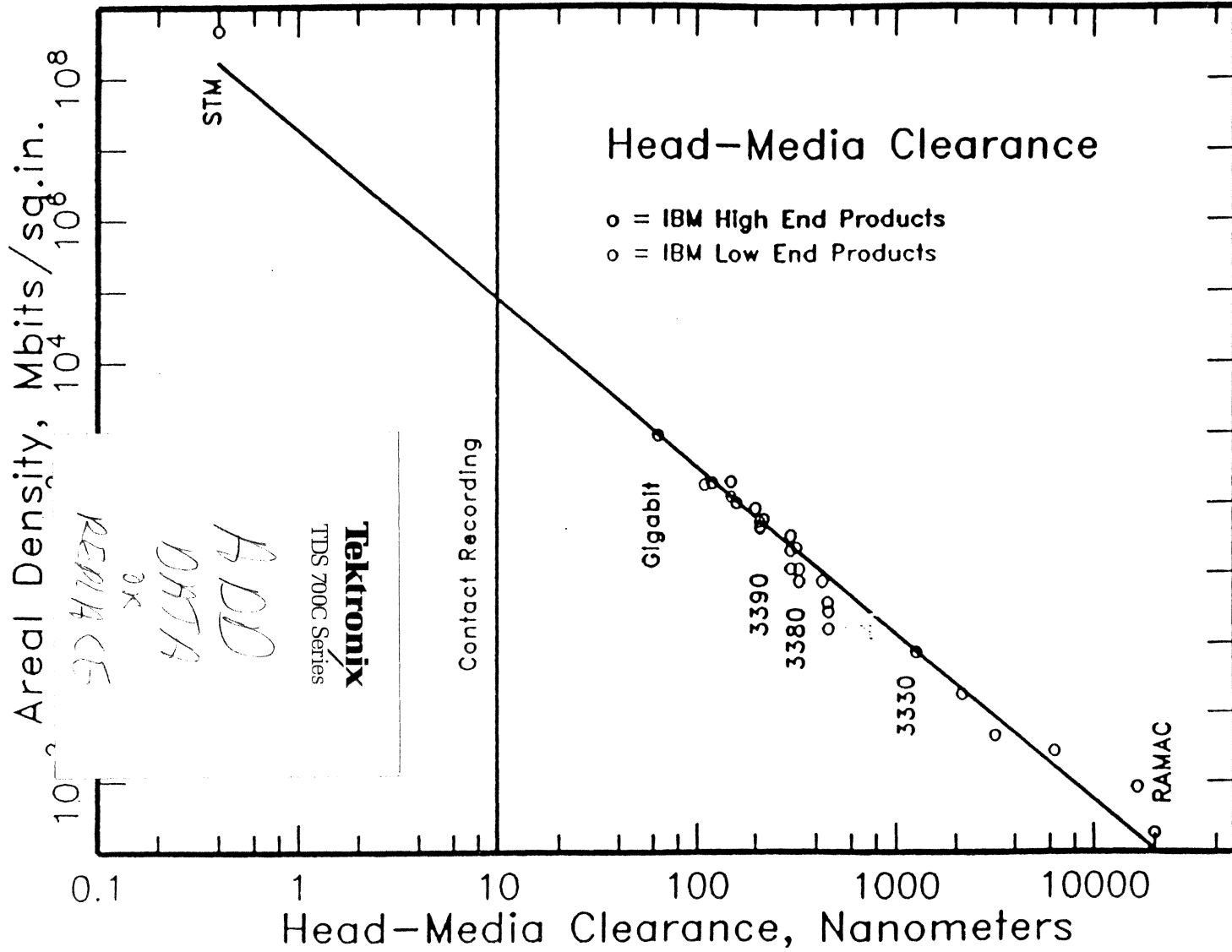
(400 kfc i x 25 ktpi)

GRAIN SIZE
(projected)
 $d \approx 8-10 \text{ nm}$

Internal (media) data rate trend

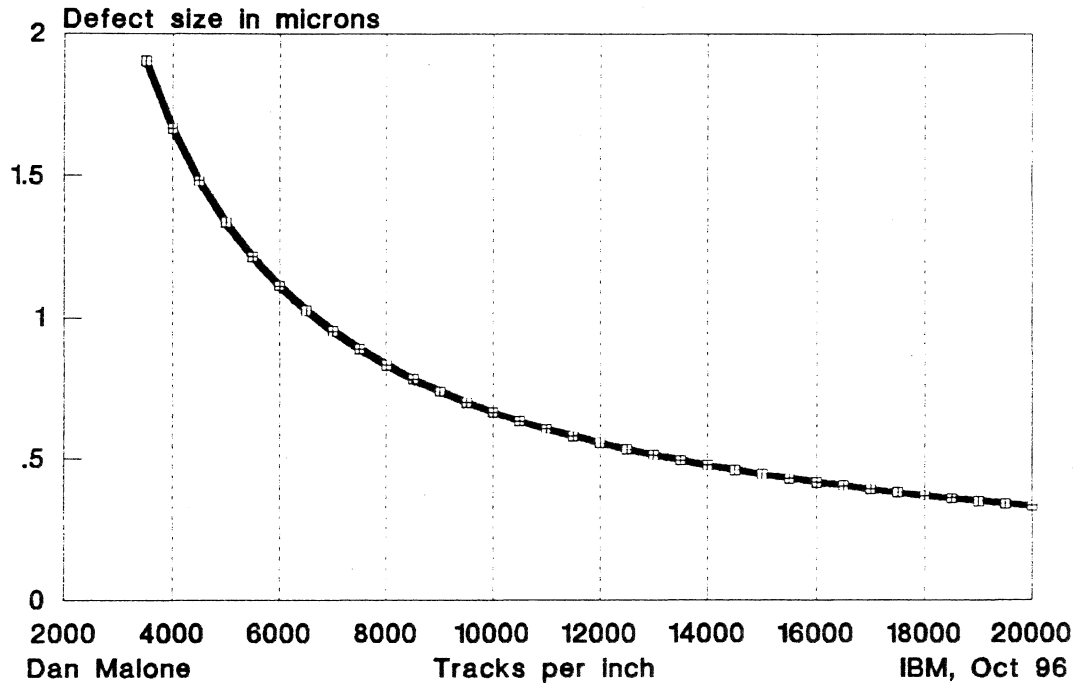


IBM Advanced Technology



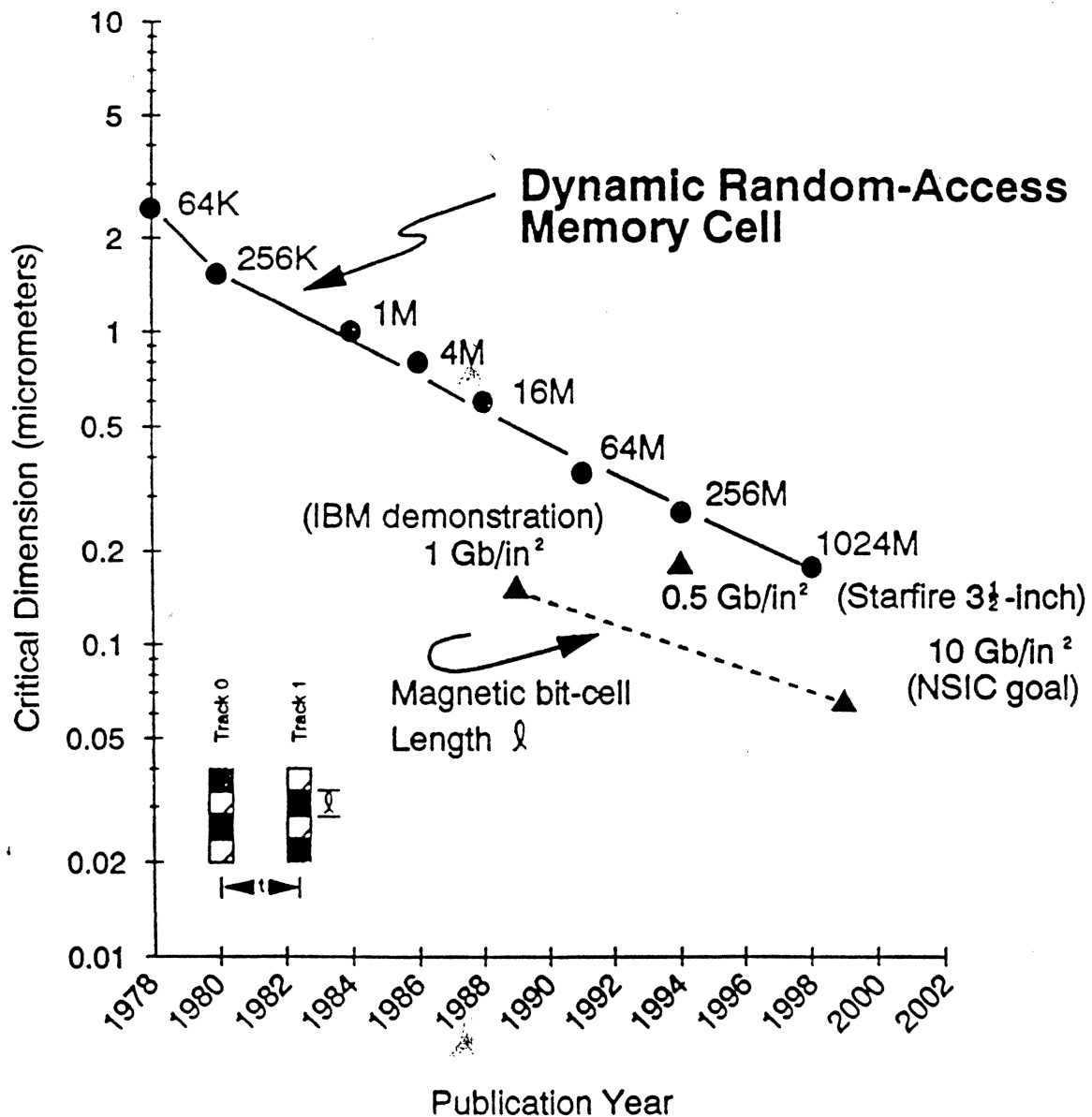
Critical Defect Size vs TPI

30% of "magnetic track width"



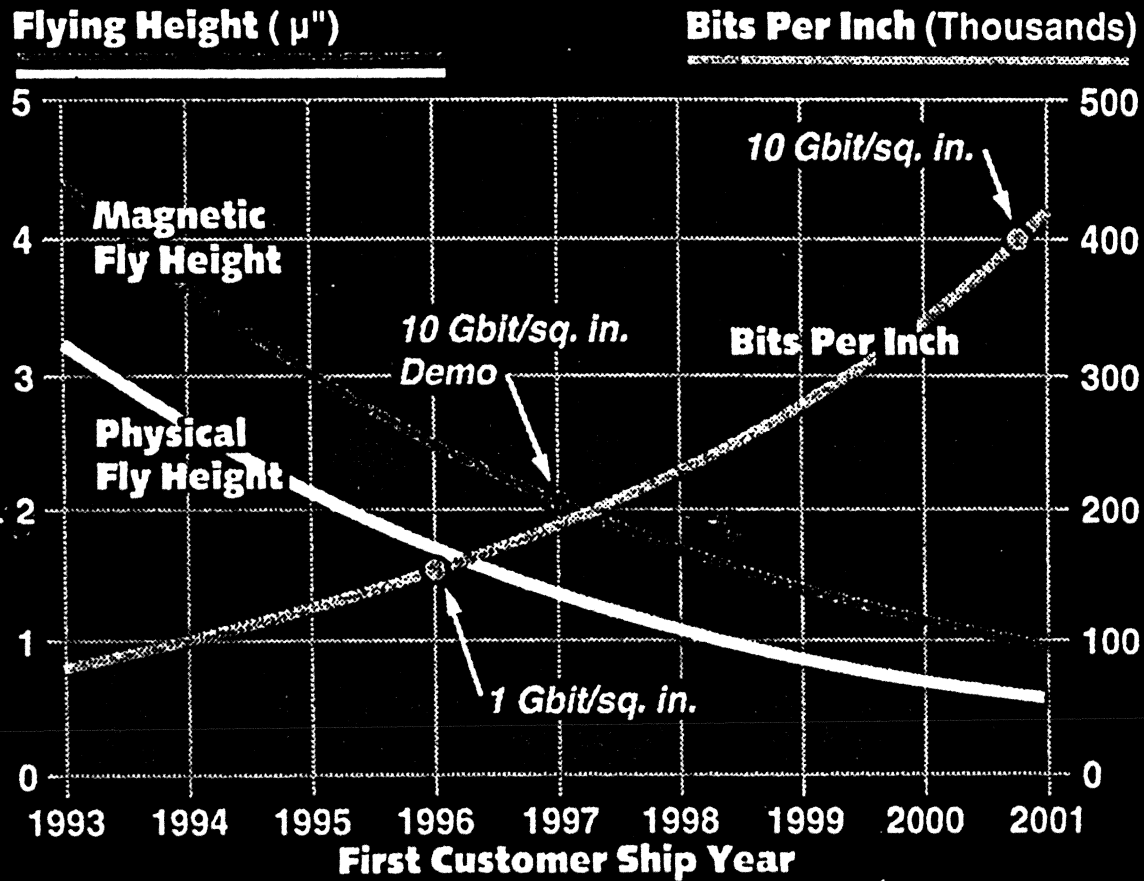
Semiconductor Memory Versus Magnetic Storage

Critical Dimensions



Future Recording Trends

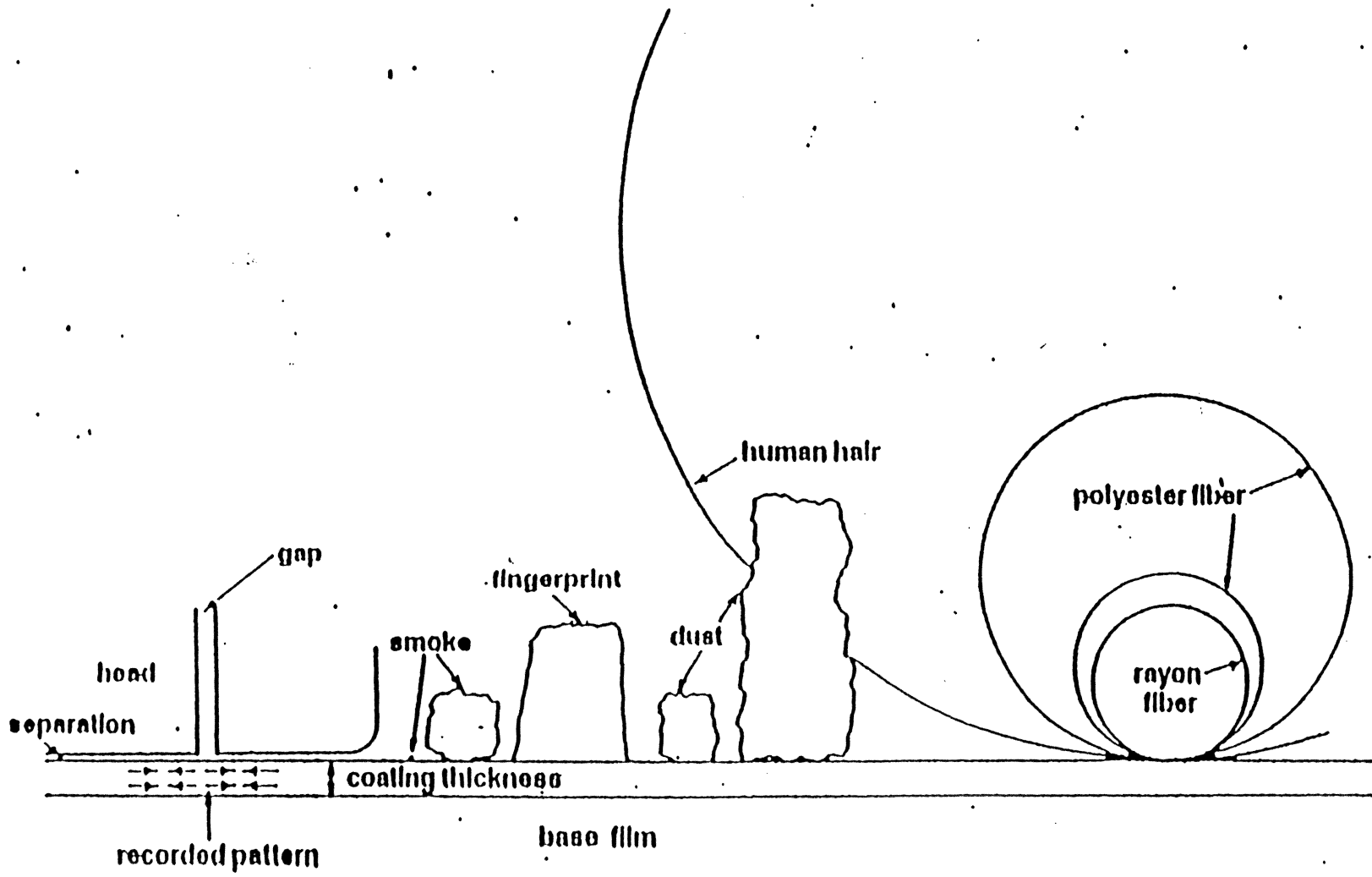
IBM 60% CAGR - MR Technology



331 1 Source: NSIC

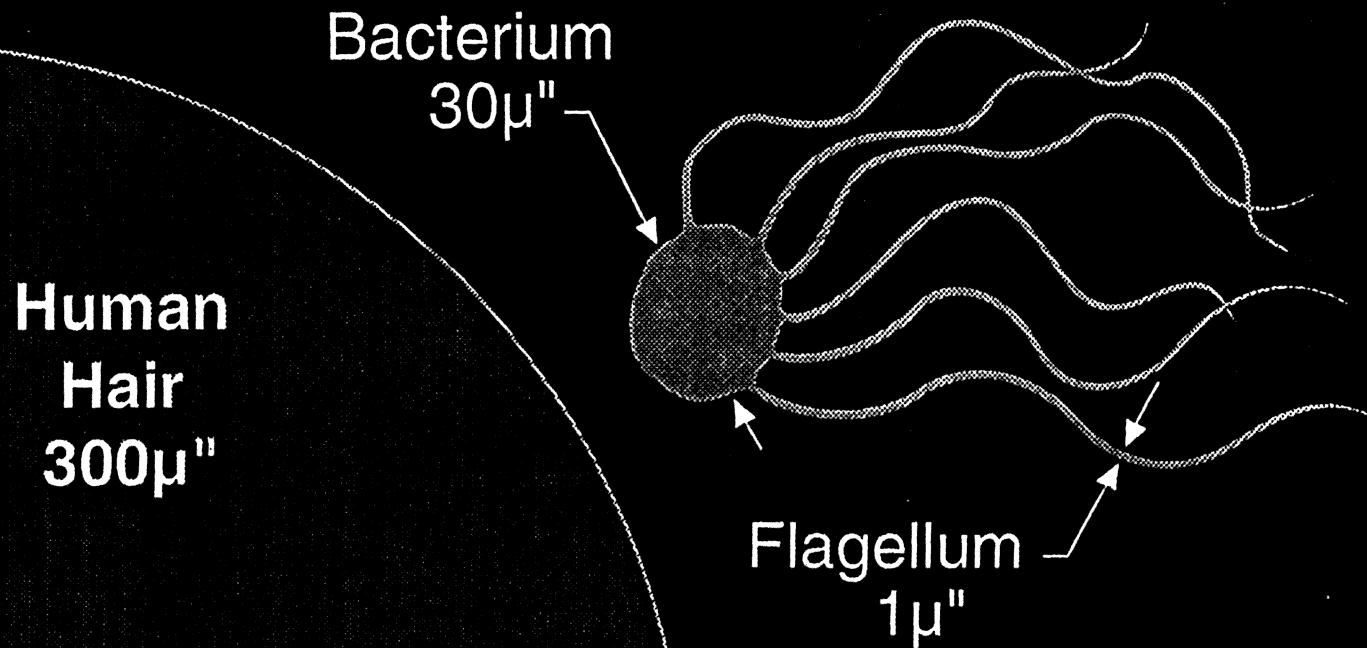
 Applied Magnetics

Head—Disk Interface



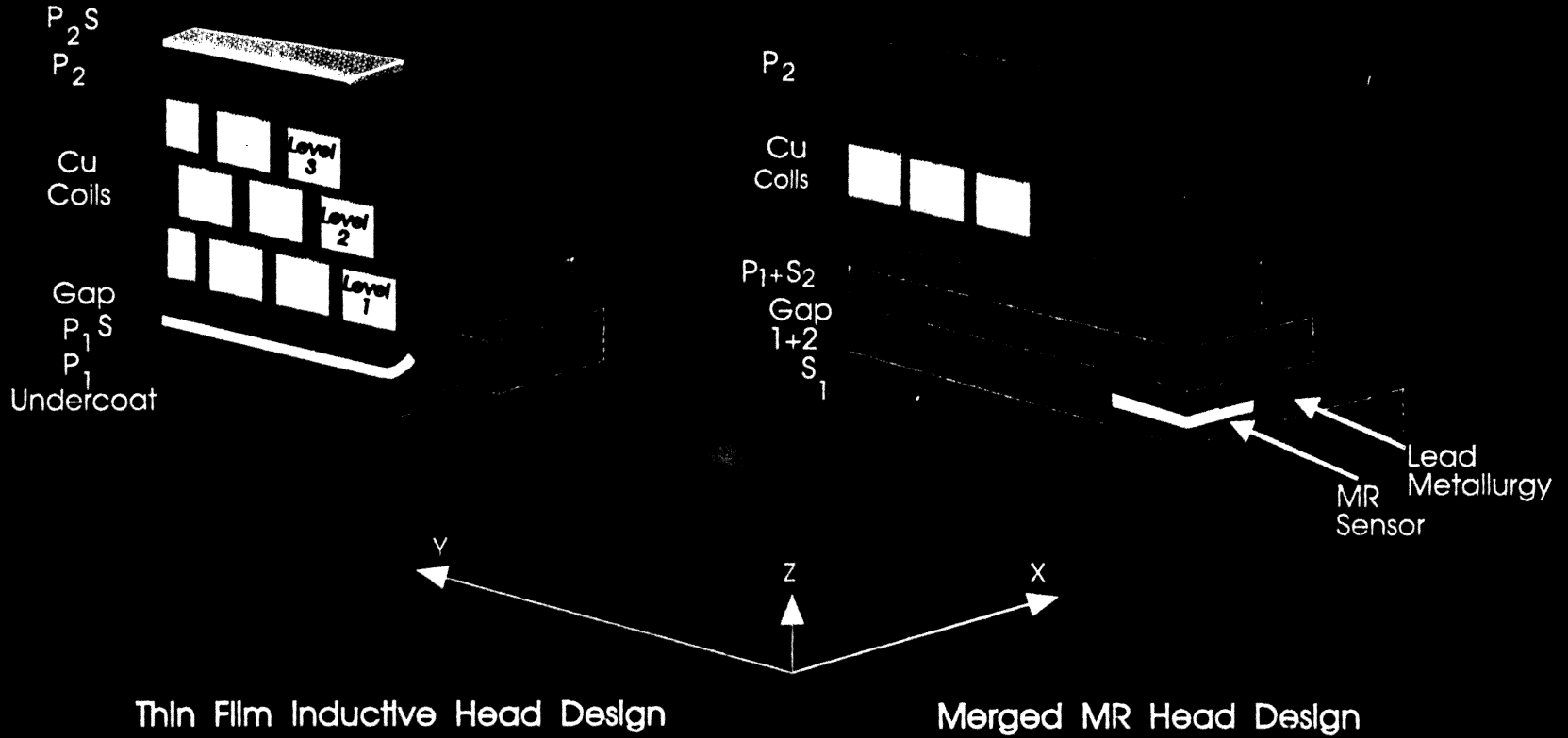
26

From Human Hair To Bacterial "Hair"



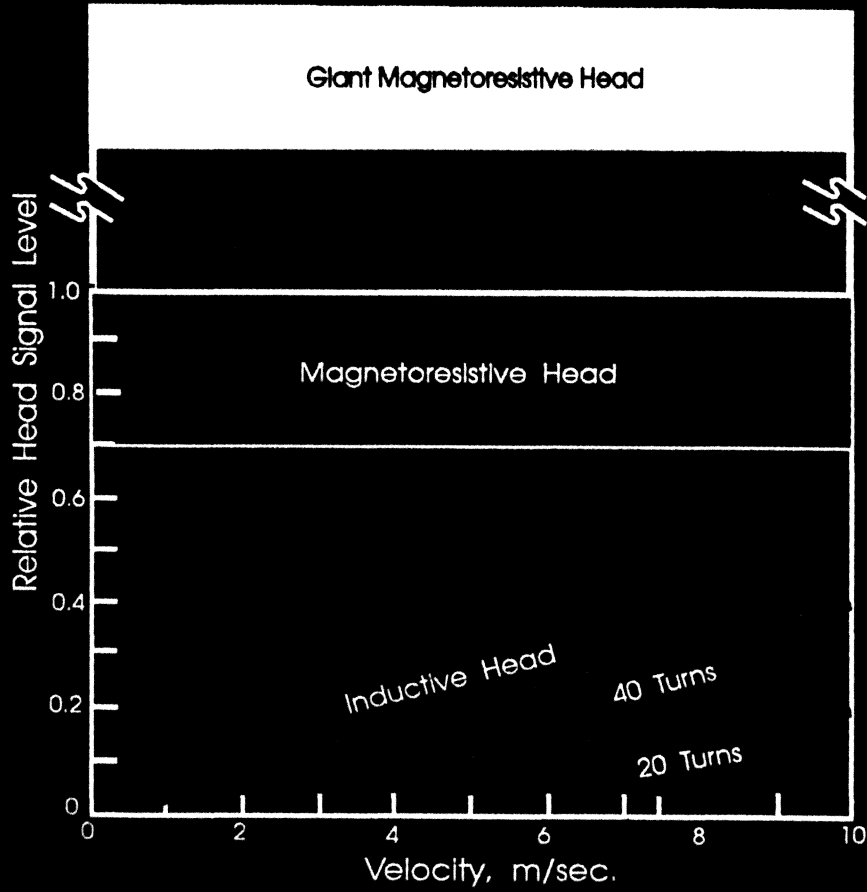
Magnetic Recording Heads

Magnetic Head Design



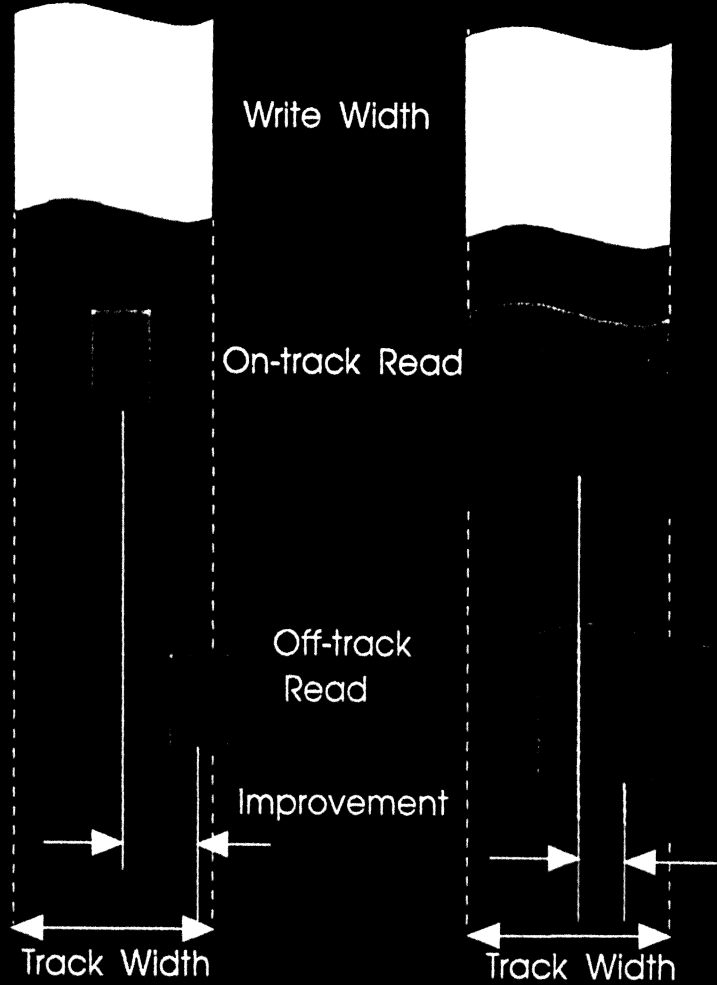
IBM Advanced Technology

Improved Performance - MR/GMR Heads



Magnetostrictive

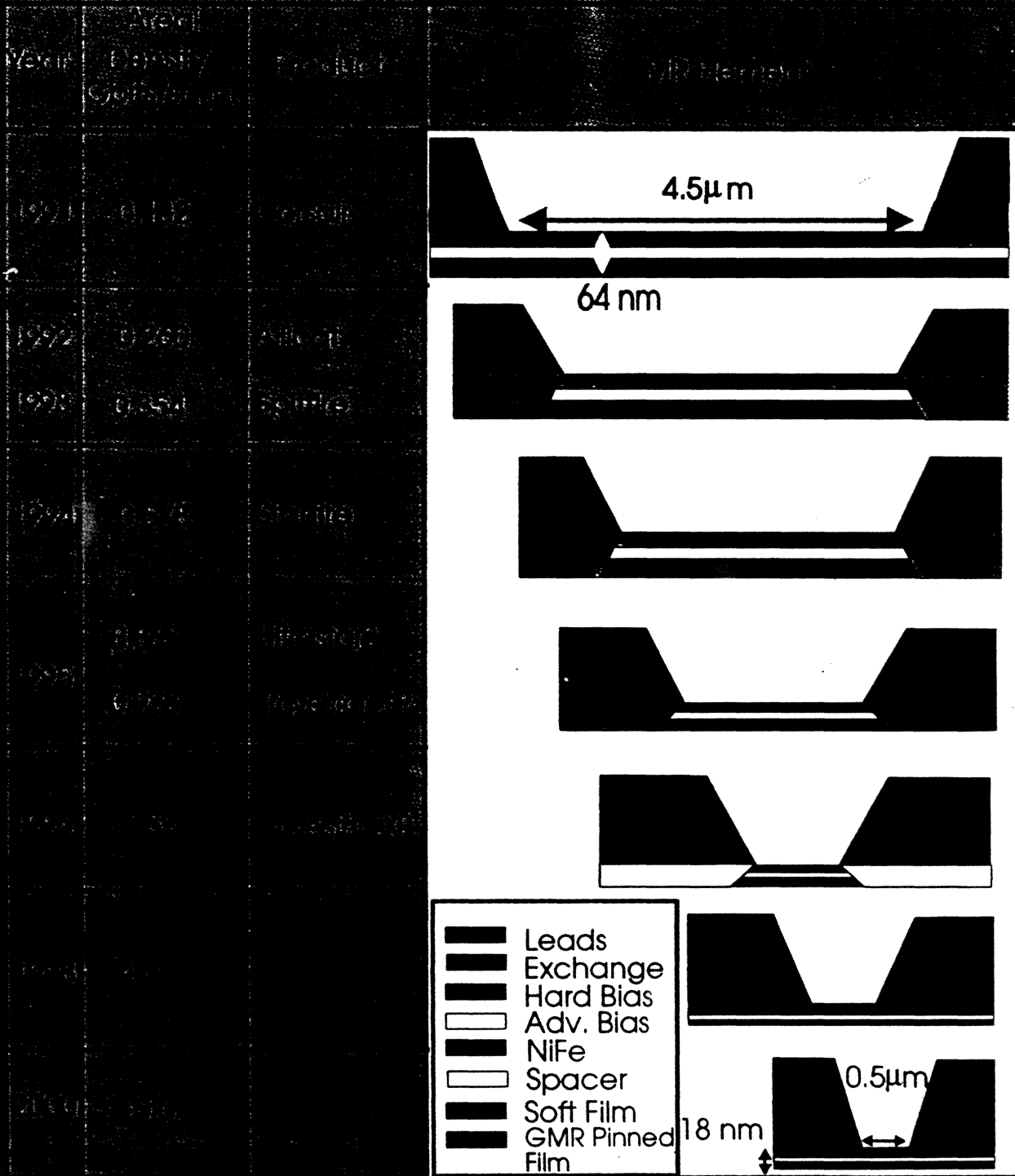
Inductive



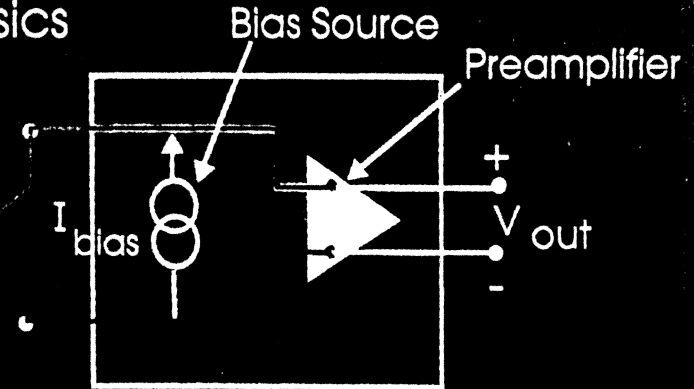
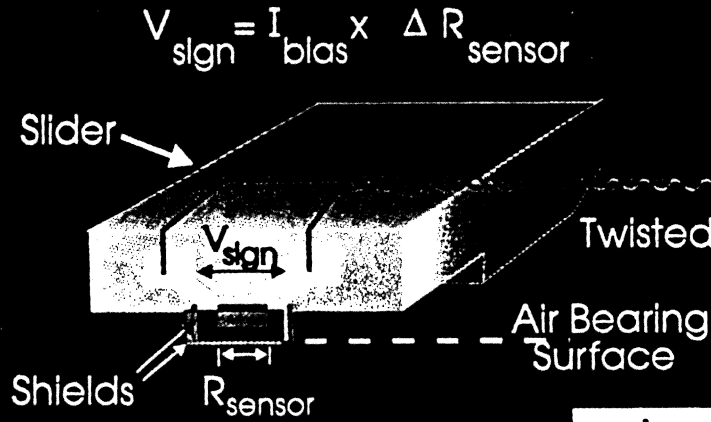
IBM Advanced Technology



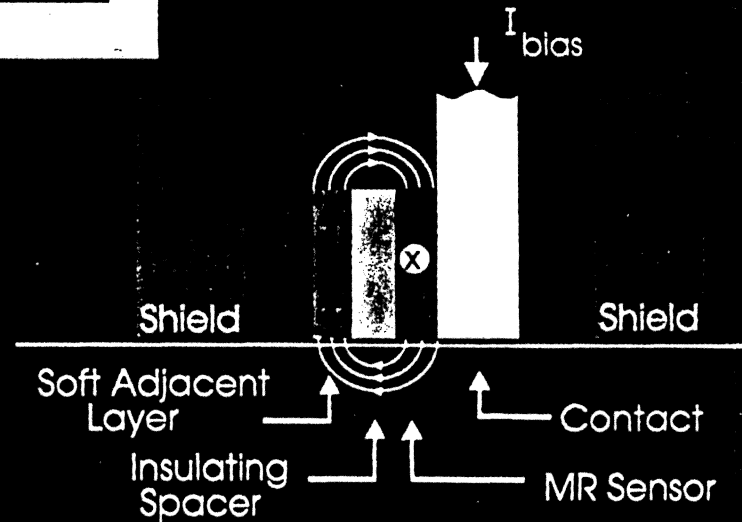
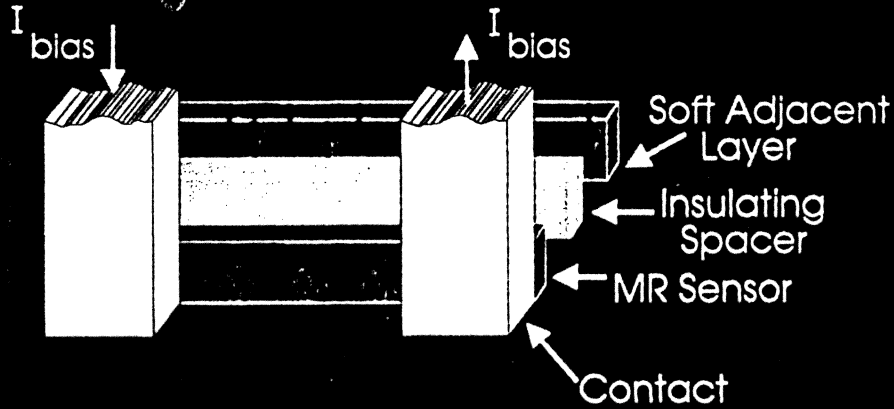
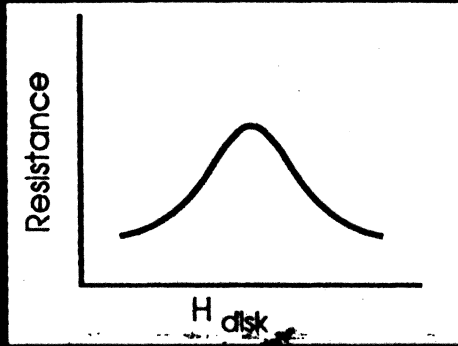
Projected IBM MR Head Evolution



MR Head Basics

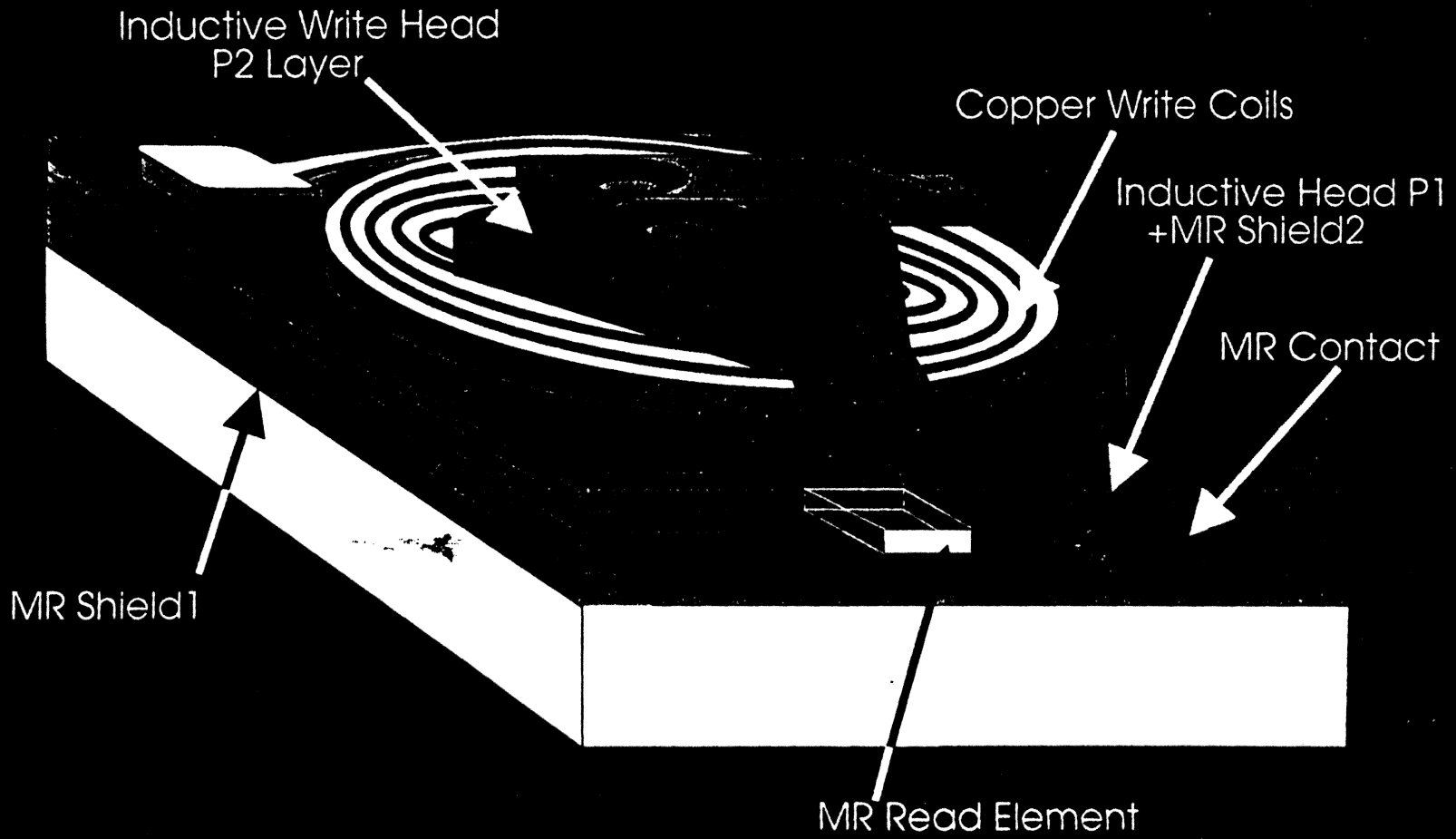


Arm Electronics Module

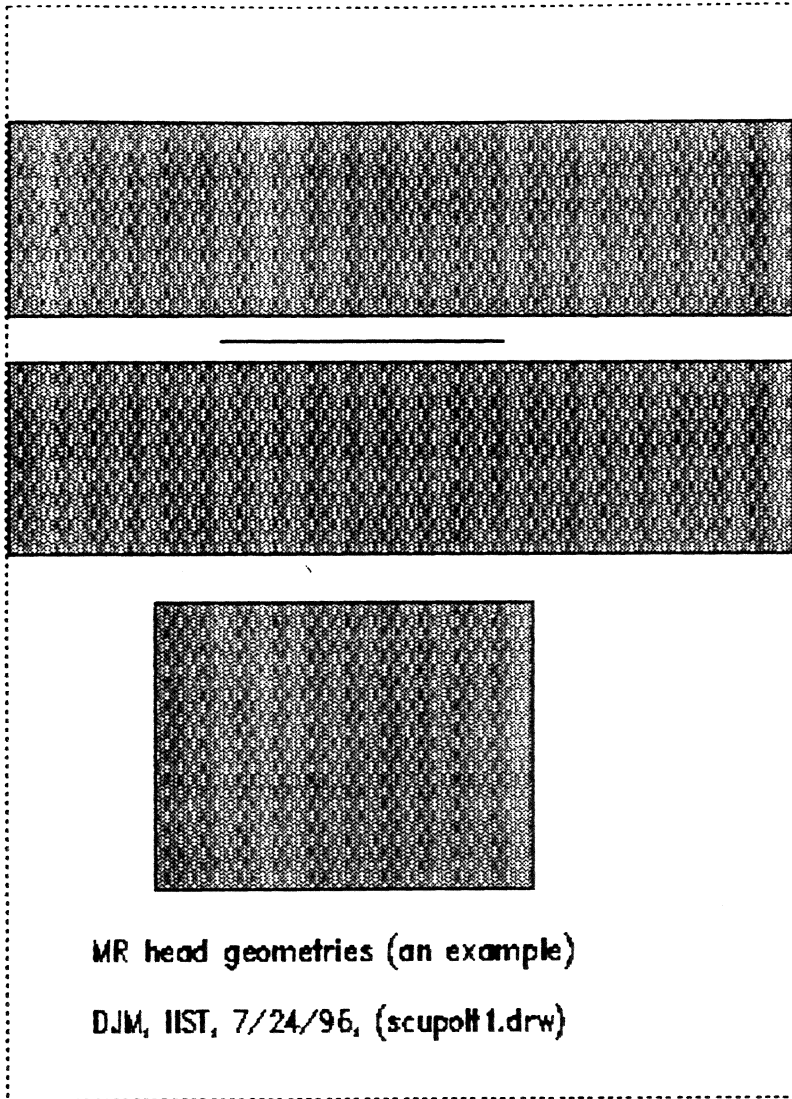


IBM Advanced Technology

Merged Magneto-resistive Head



IBM Advanced Technology



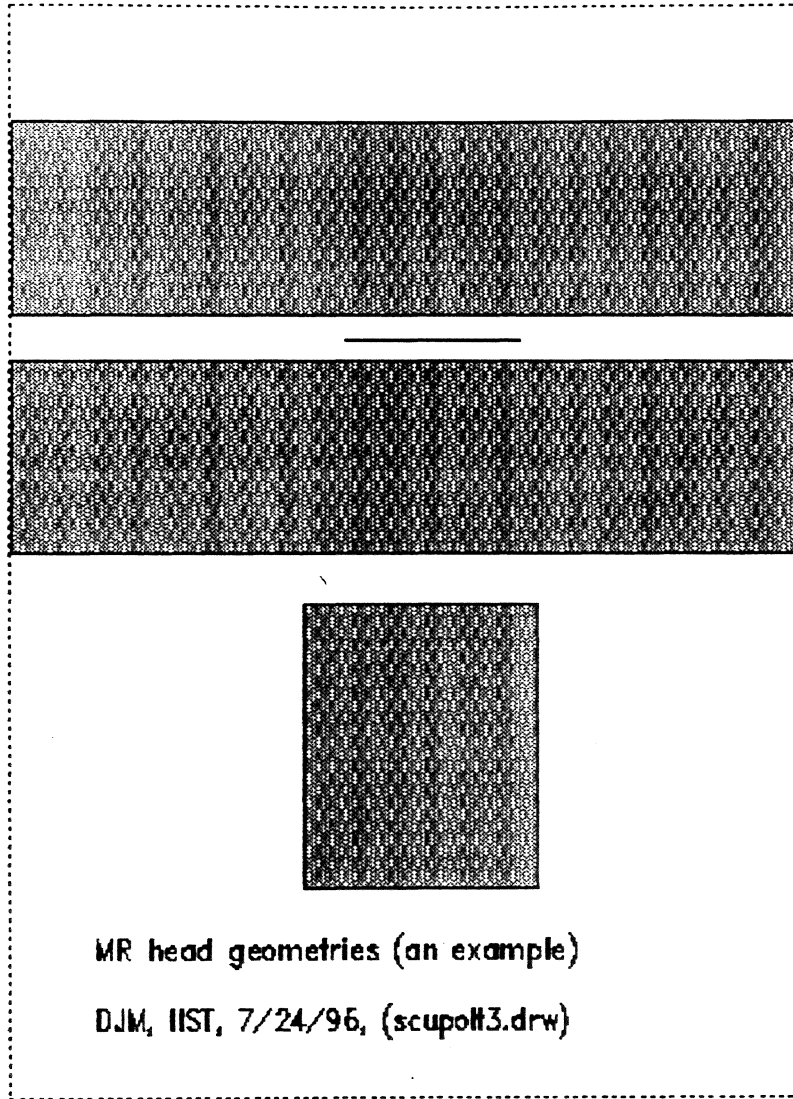
MR head geometries (an example)

DJM, IIST, 7/24/96, (scupoll1.drw)



MR head geometries (an example)

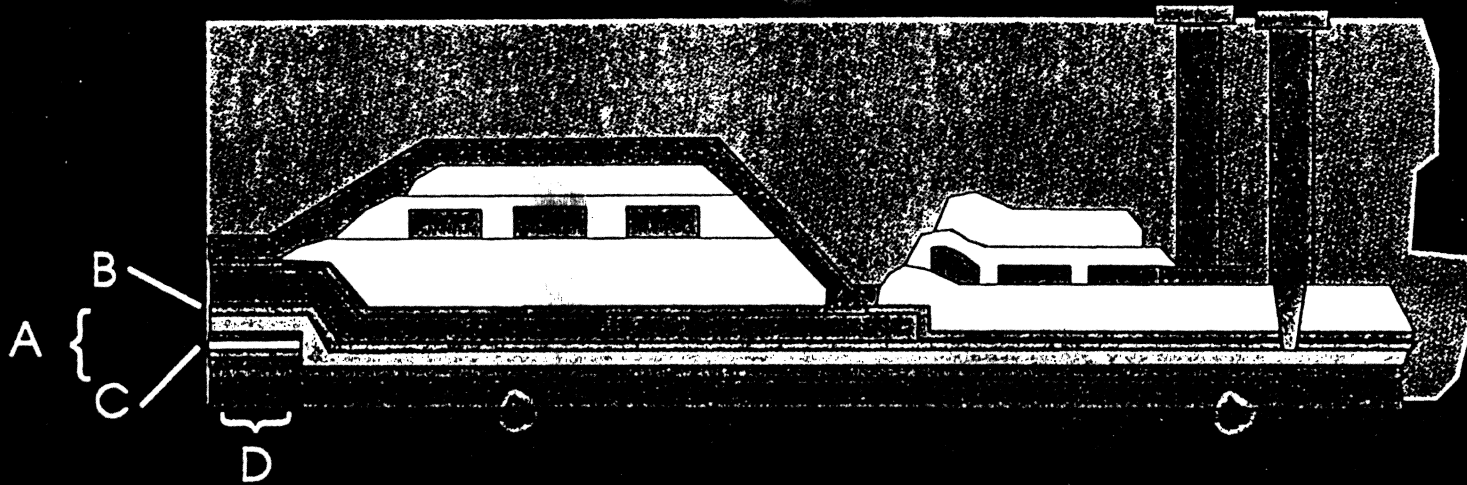
DJM, IIST, 7/24/96, (scupolt2.drw)



MR head geometries (an example)

DJM, IIST, 7/24/96, (scupoll3.drw)

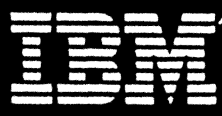
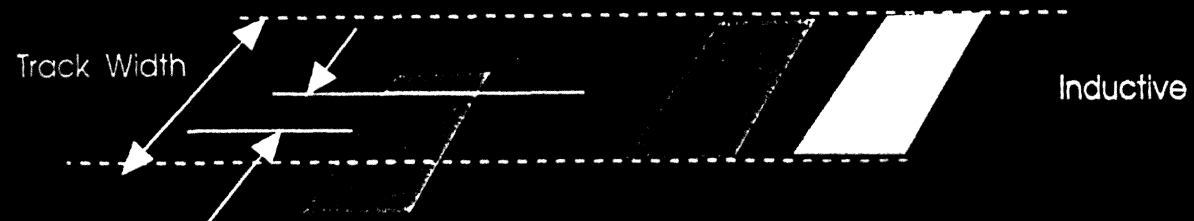
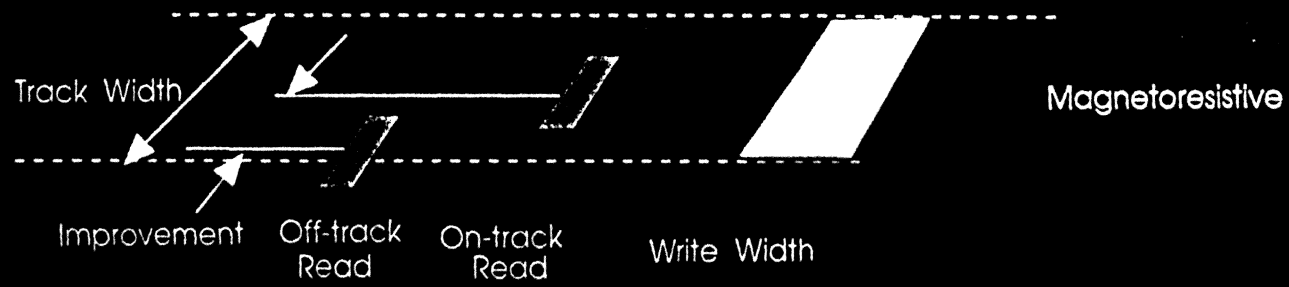
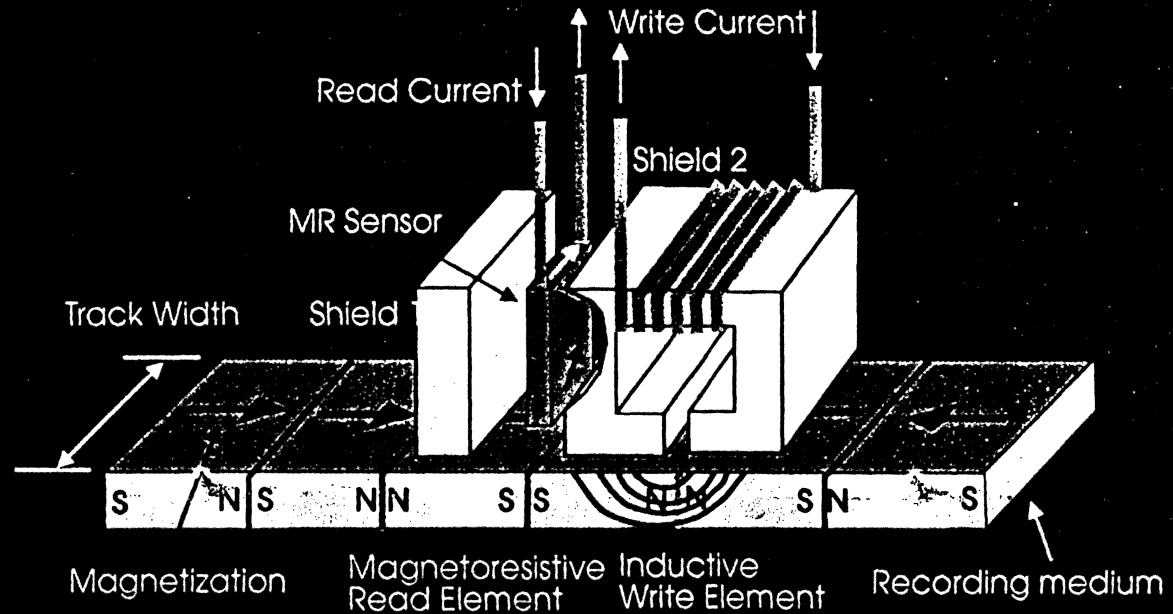
Advanced MR Head Designs



	1 Gbit/in ² Head	3 Gbits/in ² Head	
A	Total Read Gap	0.25 μm	0.20 μm
B	Sensor/Shield Spacing	< 1200 \AA	< 1000 \AA
	Read Trackwidth	2 μm	1.1 μm
C	MR Layer	150 \AA	120 \AA
D	Sensor Height	1.0 μm	0.5 μm
	Flying Height	1.5 $\mu\text{-in}$	1.5 $\mu\text{-in}$

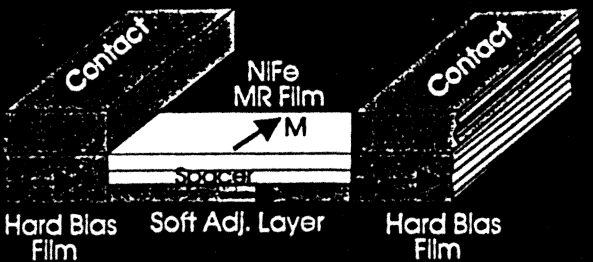
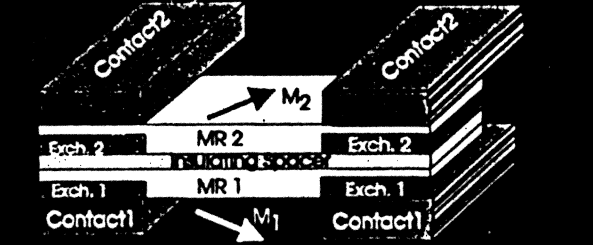
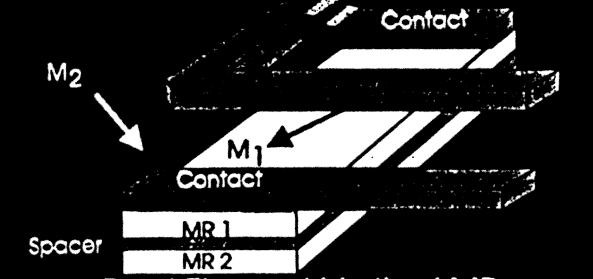
IBM Advanced Technology

Write Wide/Read Narrow Recording Process



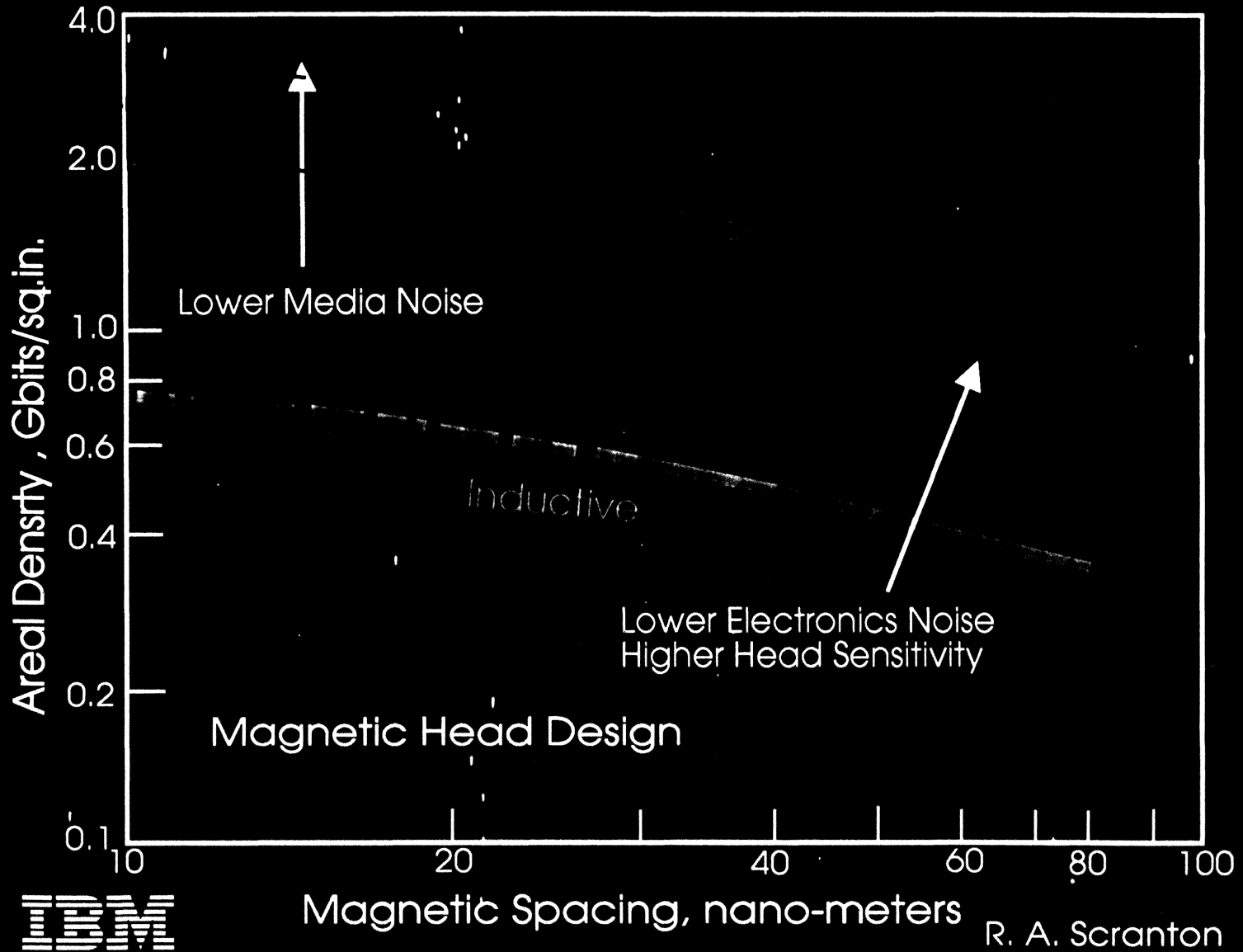
IBM Advanced Technology

Magnetoresistive Head Blasing Alternatives

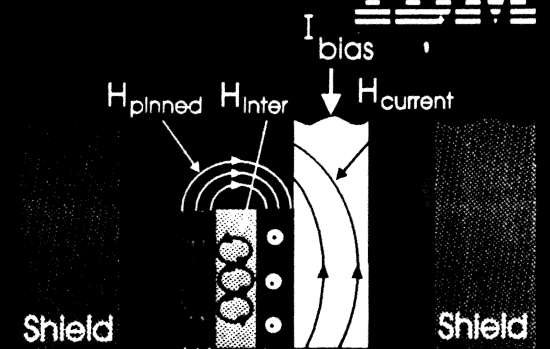
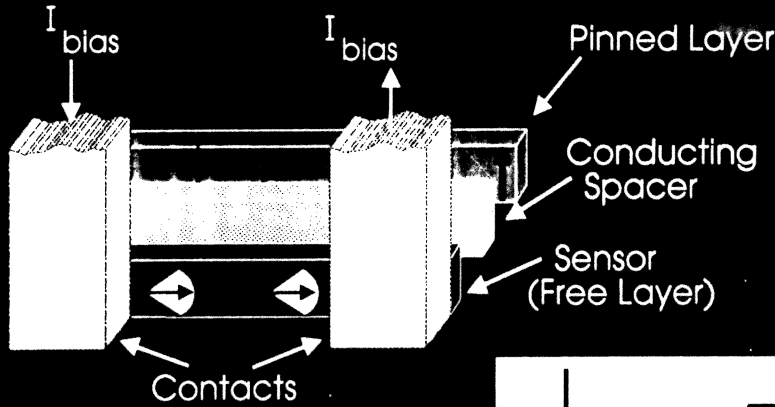
Technology	Advocate	Advantages
 <p>Hard Bias Film Soft Adj. Layer Hard Bias Film</p> <p>Soft Adj. Layer, Hard or Exchange Bias</p>	<p>IBM</p> <p>Quantum Seagate Hitachi Read Rite Fujitsu TDK AMC</p>	<p>Over 100M heads in operation</p> <p>3 Gbit/sq.in. demo</p> <p>Simple, high yield process</p>
 <p>Differential-Dual Stripe/Exchange Bias</p>	<p>Headway</p>	<p>Large output</p> <p>Thermal spike protection</p>
 <p>Dual Element Vertical MR</p>	<p>Sony</p>	<p>Thermal spike protection</p> <p>Constant output with trackwidth</p>



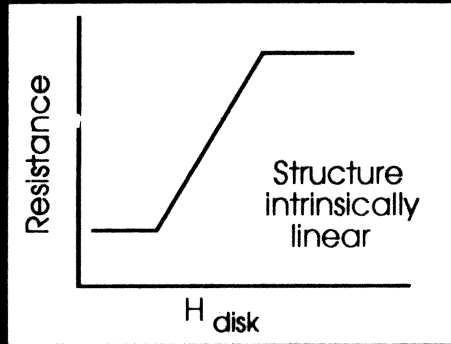
IBM Advanced Technology



Spin Valve Head (Giant MR) Basics

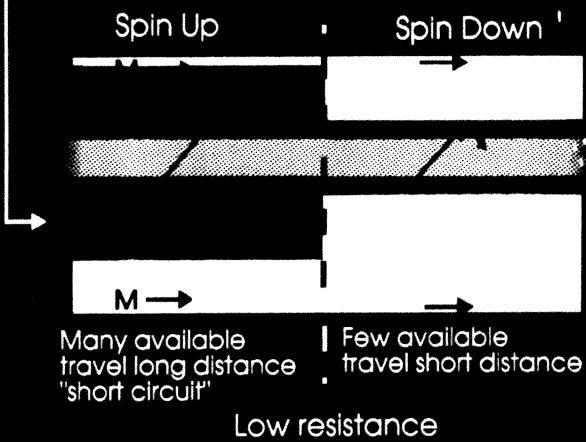


Key: Electrons shared between layers



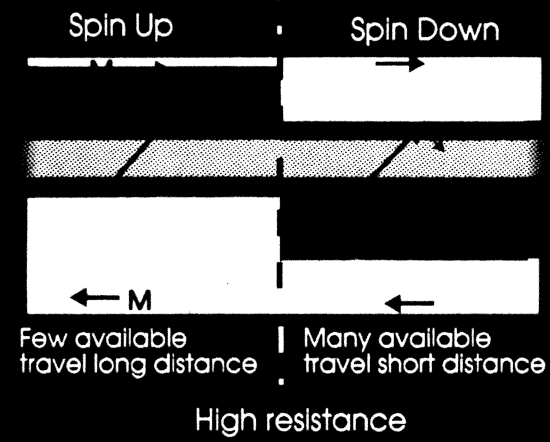
$$H_{\text{pinned}} + H_{\text{inter}} + H_{\text{current}} = 0$$

Electrons available to cross spacer



Low resistance

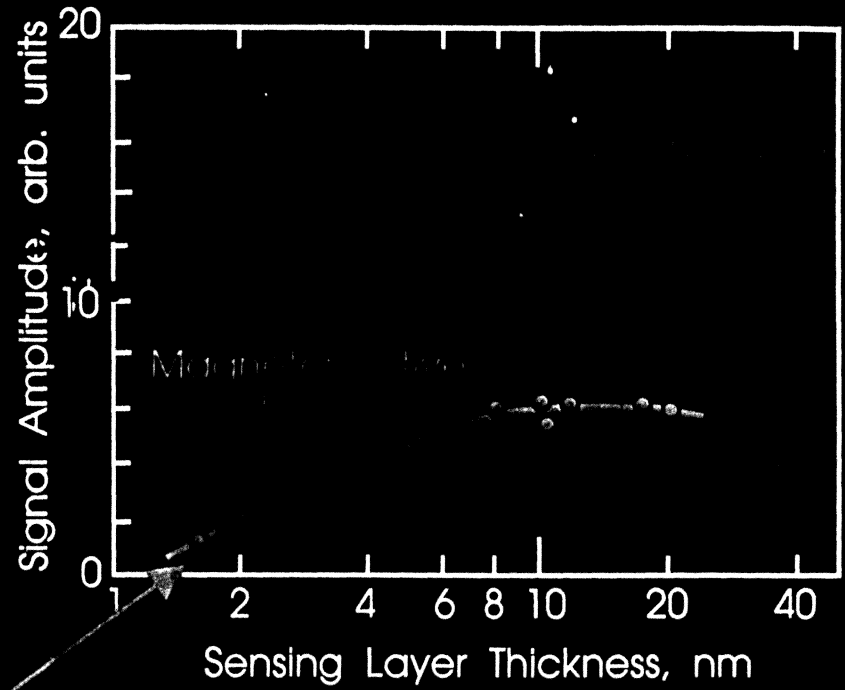
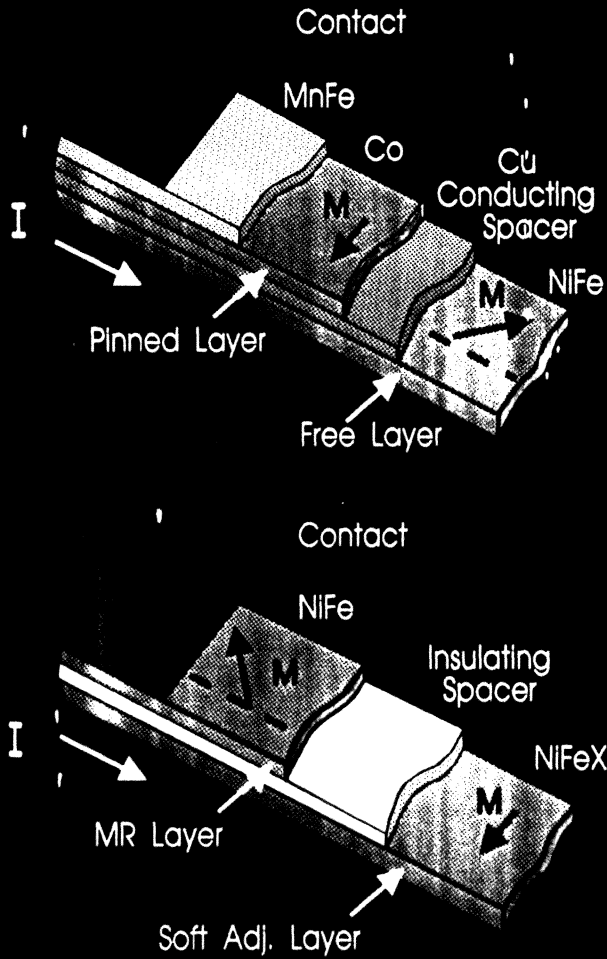
Current direction →



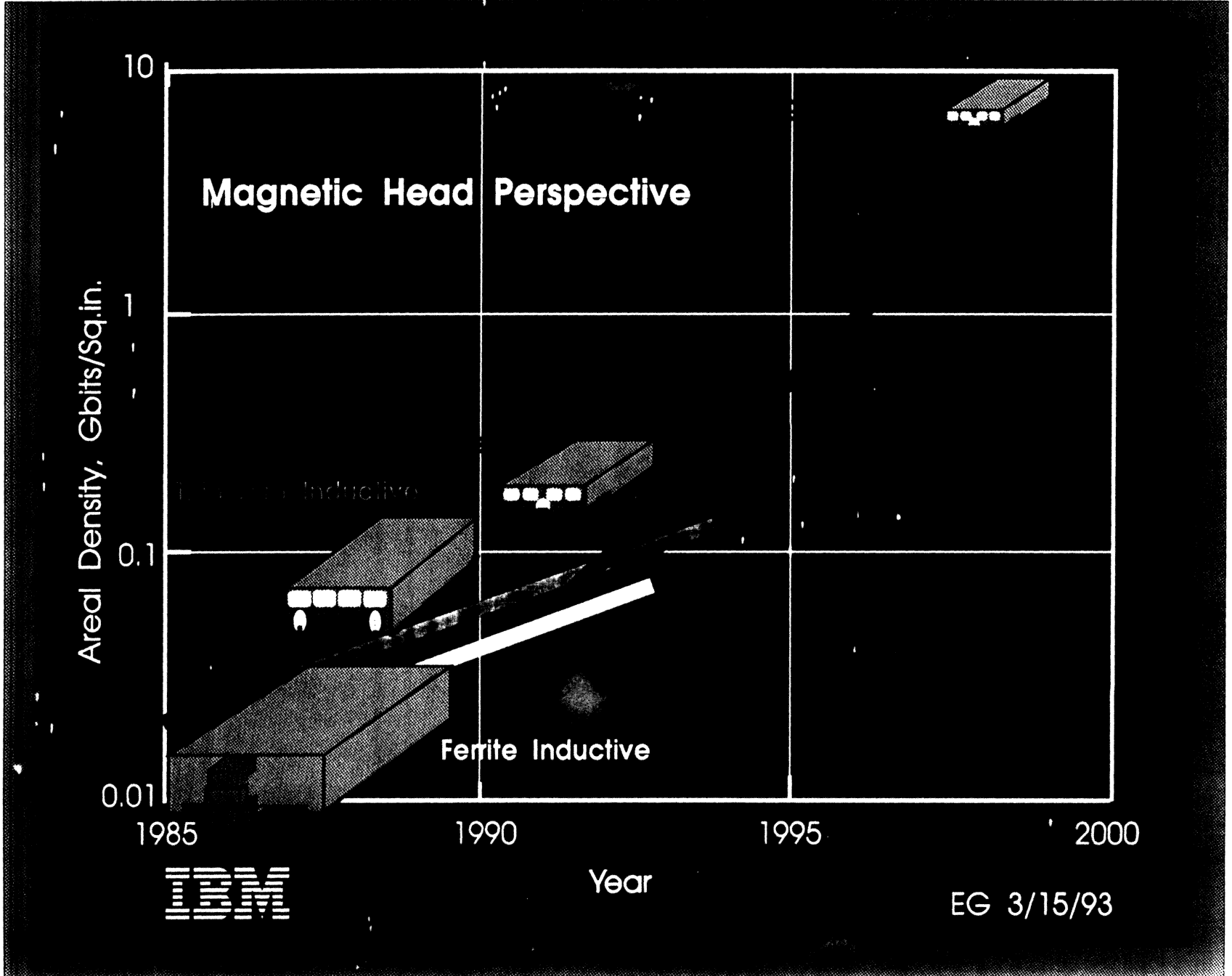
High resistance

Bruce Gurney/Ed Grochowski

MR and GMR/Spin Valve Head Characteristics

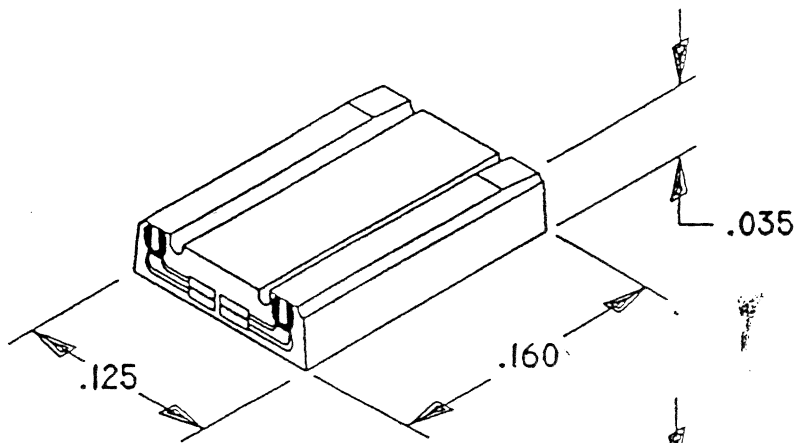


Ed Grochowski/Virgil Speriosu

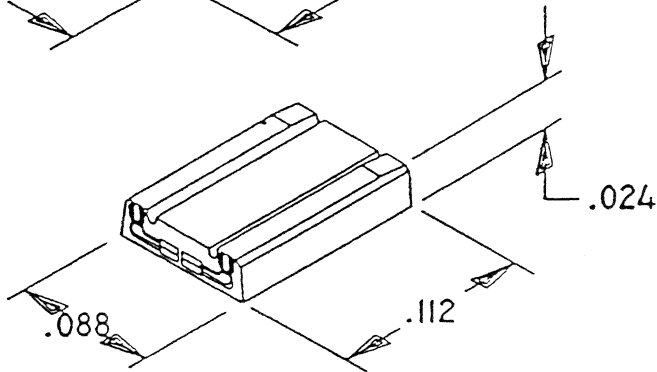


EG 3/15/93

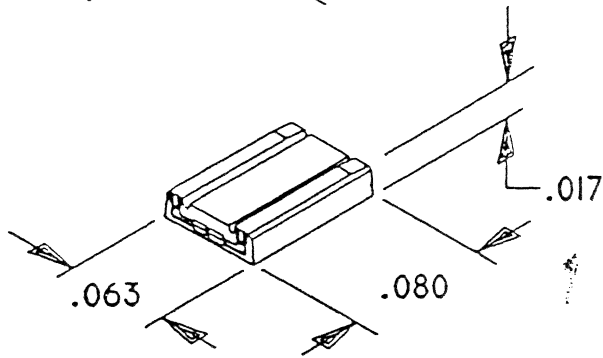
THE INCREDIBLE SHRINKING SLIDER



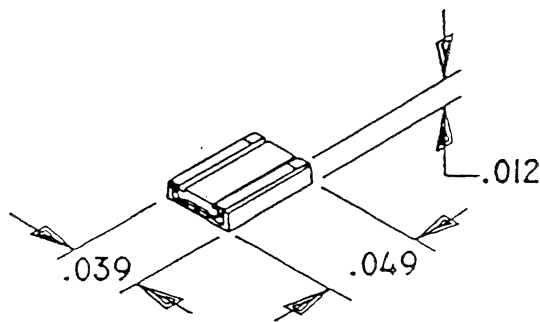
STANDARD
100%



MICRO
70%



NANO
50%



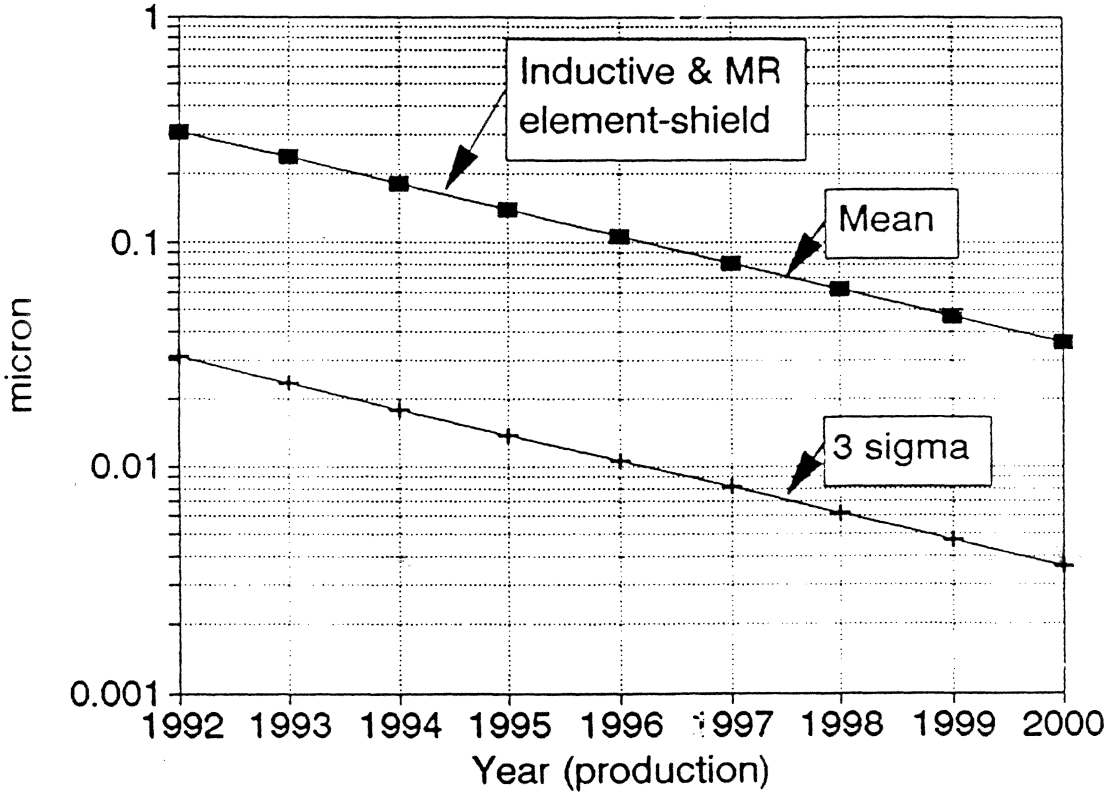
PICO
30%

C. Leung
Read-Rite

④
Emw 11/21/88

Capital Intensive Technology

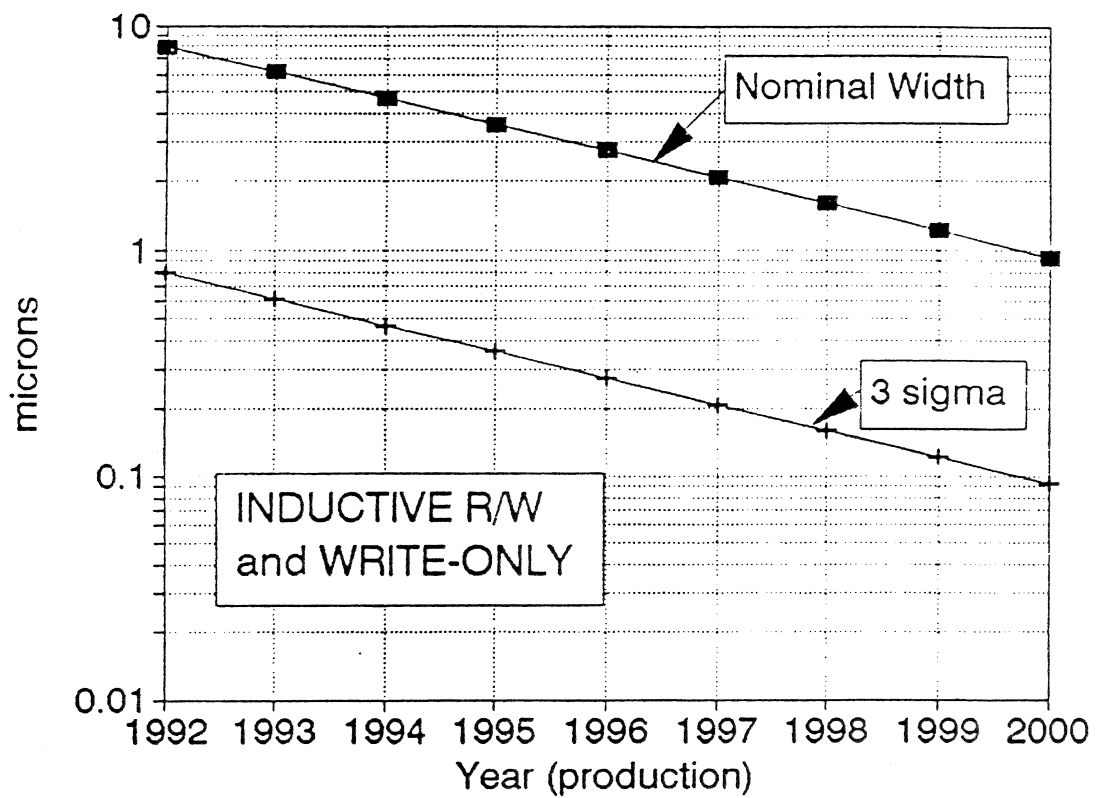
Gap Length Control



IS
EMW
11/21/92

Capital Intensive Technology

Track Width Control



(4)
cmw
11/21/97

Magnetic Recording Disks

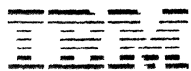
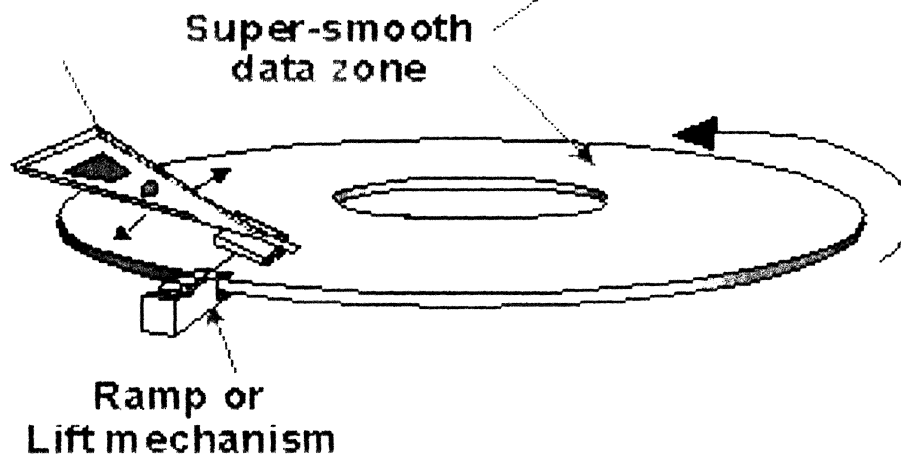
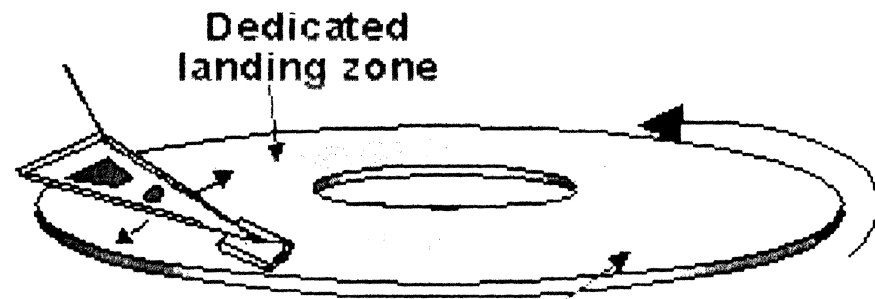
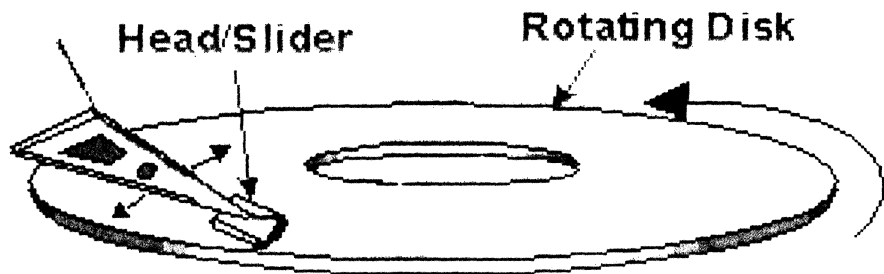
Disk Surface Application



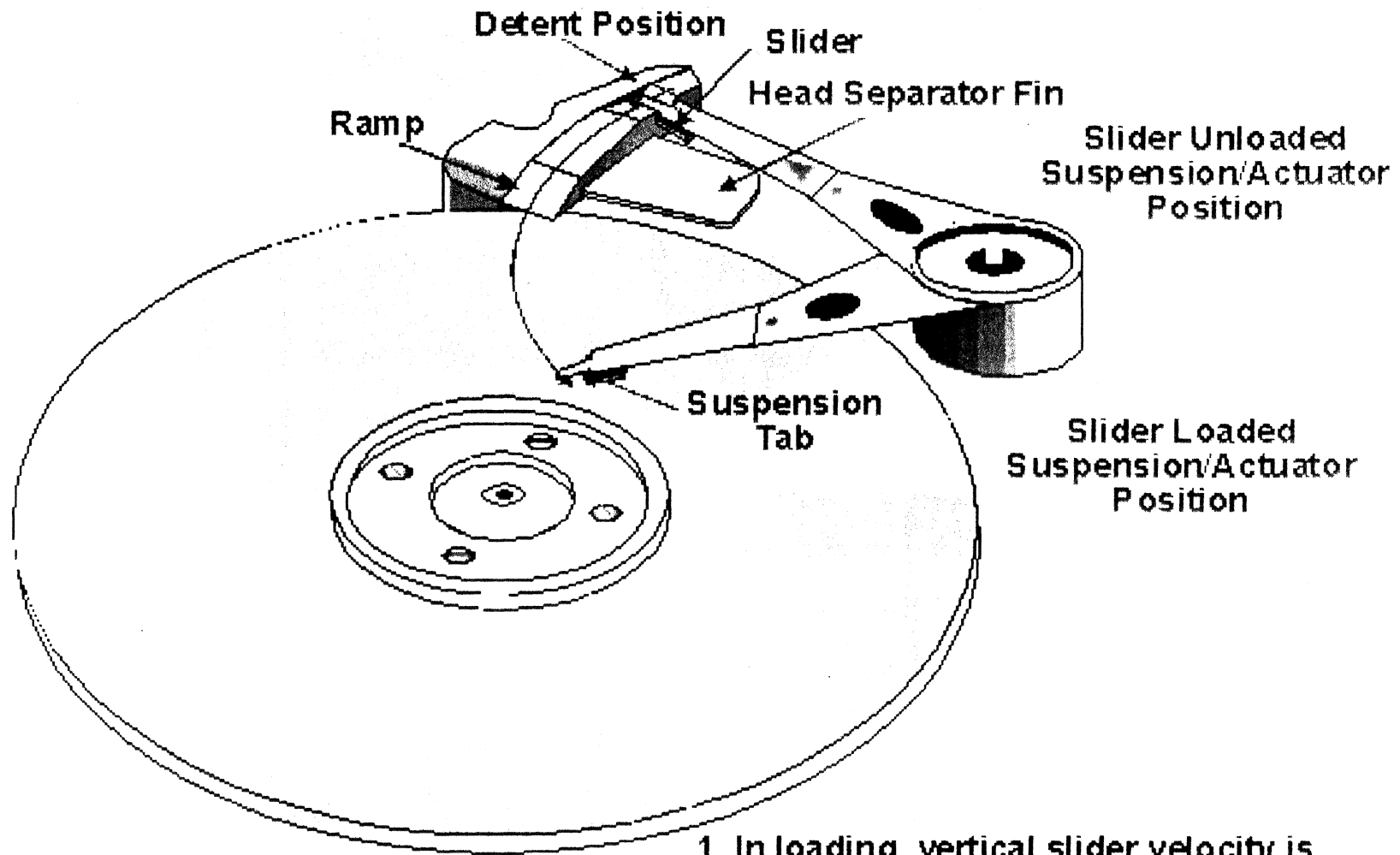
Full-surface Texture
(mechanical or sputter)

Zone Texture
(laser or mechanical)

Load/Unload
(no texture required)



IBM Ramp Load/Unload Dynamics



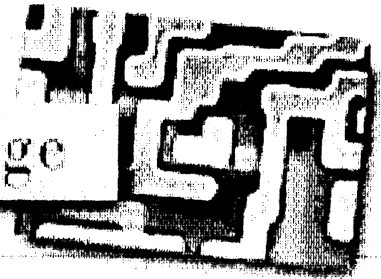
IBM Advanced Technology



1. In loading, vertical slider velocity is servo controlled using back-EMF of actuator motor
2. During power off, back-EMF of spindle motor unloads sliders before disks stop rotating

000000 0000000000 000000 000000
 000000 0000000000 000000 000000
 0000 0000 0000 0000000000
 0000 00000000 000000000000
 0000 0000 0000 0000 0000
 00000000000000000000 000000 000000
 00000000000000000000 000000 000000

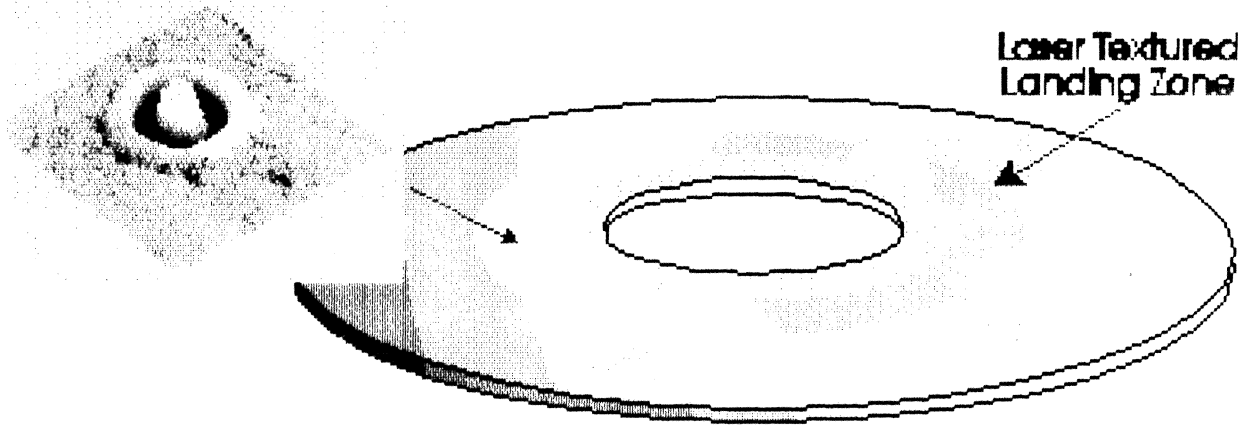
Storage



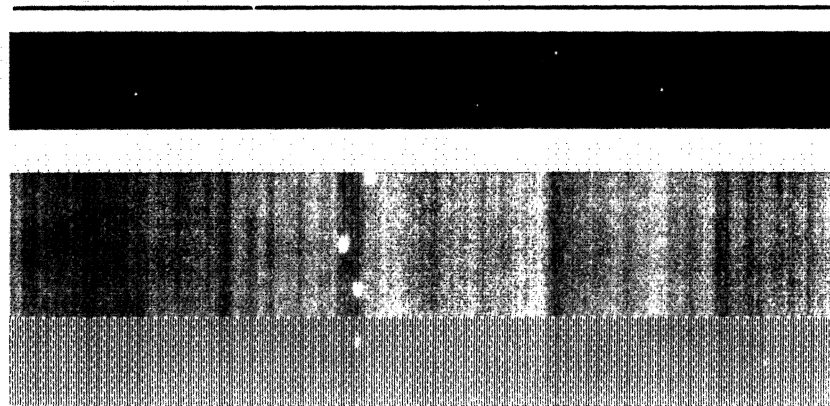
© 1995 IBM Corporation

SECTION 01 ALUMINUM

Disk Technology



Laser Textured
Landing Zone



Lubricant
 Carbon
 CoPtCr
 Cr
 NiP
 AlMg
 Substrate

ity of the disk surface must also be observed, which increase manufacturing costs, Briggs added. So, Iomega began investigating another stabilization technique that would simplify the development of the head/disk interface. This method is now known as "centered-disk stabilization" because the spinning disk is centered between two stationary plates (see Figure 1b). Because of the stable air flow, the media doesn't dip into the access slot. The flexible media is stable up to 3000 rpm.

Iomega's Zip drive uses a special version of Fujitsu ATOMM media. Apparently, the thinner the magnetic coating, the better the output at high frequencies. The media's overwrite characteristics also improve when the coating is very thin. As a rule, the thinner the coating, the rougher the surface finish. Because of this roughness, the head/disk spacing has to be increased, negating the benefits of the thinner coating. Fuji reportedly overcame this problem by using a double-coating process, whereby a relatively thick undercoating of titanium dioxide (TiO_2) sits under a thin layer ($0.4 \mu\text{m}$ for the Zip drive) of metal particle media (see Figure 2).

SEEK, SERVE, FOLLOW

Initially, embedded servo systems weren't widely available. As a result, the floppy was designed with wide tracks (135 tpi) so that, as Briggs noted, an open-loop servo could be used. When the cartridge is inserted into the drive, the media re-centers itself, with an accuracy of about $20 \mu\text{m}$, which is okay for a track pitch of $188 \mu\text{m}$; however, track runout becomes a significant issue as the track width narrows, necessitating a closed-loop track-following servo system.

"To perform track following," says Briggs, "the stepper motor is usually replaced with a voice coil motor (VCM), which is simply a coil of wire centered between strong permanent magnets." The VCM positions the heads on the desired track (seeking) and performs closed-loop track following. There are many schemes for track following on flexible media, most of which rely on magnetically stored servo information rather than on optical patterns. To date, three different types of servo systems have been used in floppy disks: buried servos (Brier); floptical (Iomega, Insite); and sector (Iomega's Zip drive), which are more commonly found in hard disk drives.

Because sector servos are standard in many of today's hard disk drives, integrated circuits are available that perform all the necessary decoding (e.g., Analog Devices' 899 IC), saving Iomega the bother and cost of developing custom ICs. And because Iomega opted to break the chain of backward compatibility when it developed the Zip drive, no additional head-positioning systems are needed, reports Briggs. Finally, by using Winchester-style nano sliders and suspensions, high-speed seeks (29 ms) are possible.

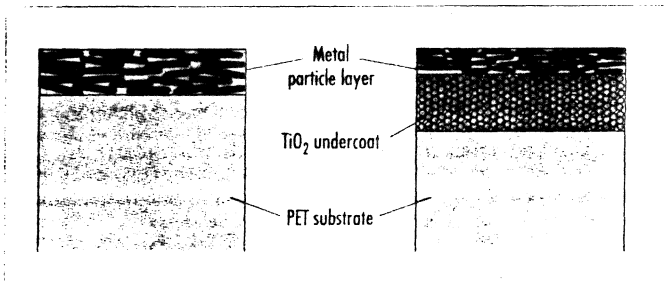
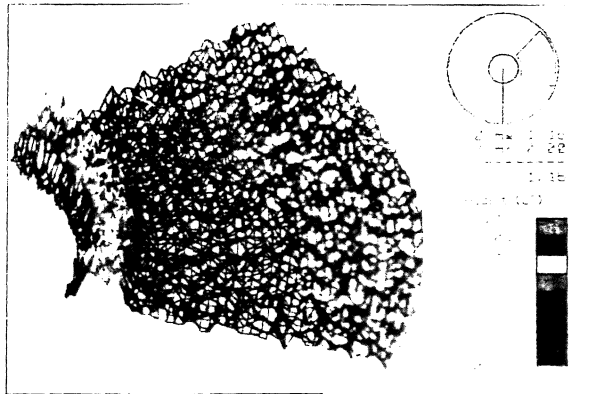


Figure 2. Conventional metal particle (left) versus double-coated, thin film metal particle media (right). Double coating results in a smoother surface.

Disk texture measured by laser

Along with increasing areal densities, hard disks have become correspondingly smoother. Moreover, only an extremely smooth surface can accommodate the low flying heights associated with today's high-performance drives. And with these smooth disks, drive makers have had to learn to deal with a more lethal issue, namely, stiction. Because the disk is so smooth, recording heads can literally get stuck on the disk, and sometimes neither all the king's horses, nor all the king's men can separate the two. A common way of preventing stiction: texturize the surface of the disk, either the entire surface or a small portion of it ("zone texturing"). The textured patterns prevent the heads from sticking to the disk surface. That Technologies (Campbell, CA) has developed an instrument that can measure these textured zones in a production environment. "This is not a laboratory tool," says That's Jim Eckerman. Besides detecting the edge of the textured zone, the laser can measure the height of various textured patterns, including "donut," "somerbrero," and "plateau" patterns, reports Eckerman.



TECHNOLOGY UPDATE

New drives buck trend, revive 5.25-in format

Start-up drive manufacturer Belfort Memory Systems (BMS) of Los Gatos, CA) established a beachhead in the floppy disk market by revisiting the old 5.25-in form factor to produce a low-cost, 100-megabyte drive for desktop computers. The company is currently sampling a 2.5-GB drive that will be officially introduced in August and already has orders for the roughly 100-unit run. The company expects to begin shipping during its first year of operation. The drives will be manufactured in Belfort, France. Initially, the company's marketing effort will focus on Europe.

Tom Finnegan, BMS's VP of business development, says that 2.5-GB capacity is achieved using only two disks with a 1.25-in-gap (MIG) inductive heads. A comparable 3.5-in drive needs four platters and eight heads, making it more expensive. The company also uses MR heads and compatible read/write channel electronics.

ITS Corp. (San Jose, CA), another start-up company, is also using the same strategy, offering an inexpensive 2.5-in drive to compete with 2.5-in drives for notebooks and other portable computers. (See *Data Storage*, March 1996, pp. 17-18.)

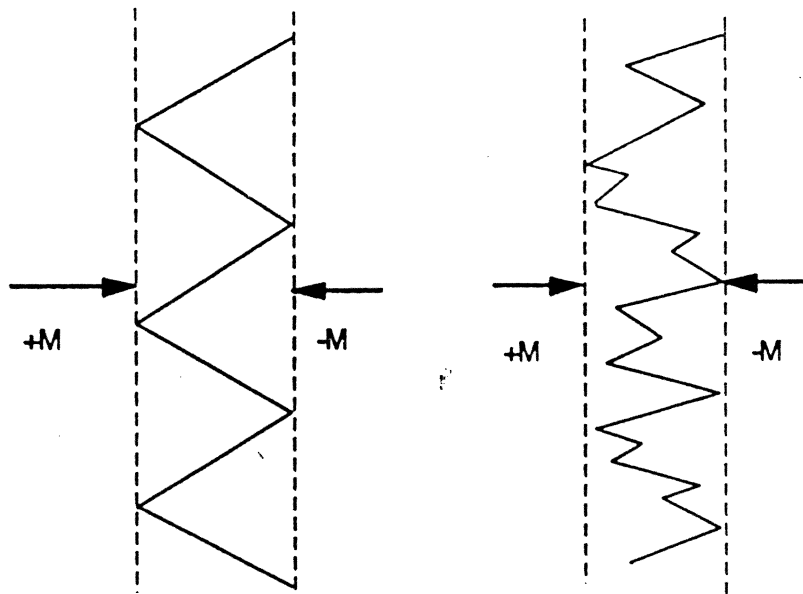


Figure 4. Schematic diagrams of zigzag transitions in thin-film media. The magnetization reverses direction through a transition whose width is the distance between the dotted lines. This width is governed by a parameter formulas. The structure within the dotted lines is governed by the micromagnetic properties. Figure 4a is an idealized picture of a zigzag transition where the sawtooth functionality is periodic. Figure 4b is a more realistic representation showing a more random structure.

become the limiting factor to transition lengths and overshadow simple $M_r \delta / H_c$ arguments, but data to date suggests that the simple macromagnetic approach to transition lengths still applies (Middleton and Miles, 1990). The existence of clusters, is the cause of noise in the transition regions. Magnetization cannot vary smoothly, but rather in discrete units.

4.3.2 Thin-film disk noise vs. recording density

In 1982, it was discovered that thin-film disks showed a noise vs. recorded frequency behavior very different from particulate disks reflecting the cluster model in the transition (Tanaka et al., 1982). Noise in CoNiP plated thin-film disks minimized in the dc saturation condition and increased with recording density. Gamma iron oxide particulate films had an opposite functionality where the noise is greater in the dc state. The now accepted interpretation is that noise in a contiguous plated film is found in the magnetic transitions, while noise in gamma iron oxide particulate media appears uniformly along the recording track.

Later recording experiments extended this work to other alloys and gave deeper insights into the noise vs recording density curves and the implied noise mechanisms (Baugh et al., 1983). Noise power in thin film alloys of CoNi, Co,



Figure 5. Lorentz micrograph of zigzag walls in recorded transitions on a thin-film disk. The sawtooth walls are not regular—the amplitude and pitch of the walls vary (Tong et al., 1984)
© 1984-IEEE.

and CoRe were investigated to densities of 1500 fc/mm as shown in Fig. 8. As Tanaka et al. observed, the noise increased with recording density in a manner exactly opposite to particulate media and sputtered gamma iron oxide. The noise in the thin film media goes up linearly and then increases in slope in a supralinear region prior to reaching a maximum noise level. The noise behavior in the linear region is interpreted as simply the contributions of the extra transitions as the density is increased. The supralinear region indicates that the transitions become intrinsically noisier when they are close together. At very high densities when the transitions overlap, the noise power decreases. An important addition of this work is the suggestion that peak jitter can be predicted by signal to noise analysis, but only by using the maximum noise in the transition density curve.

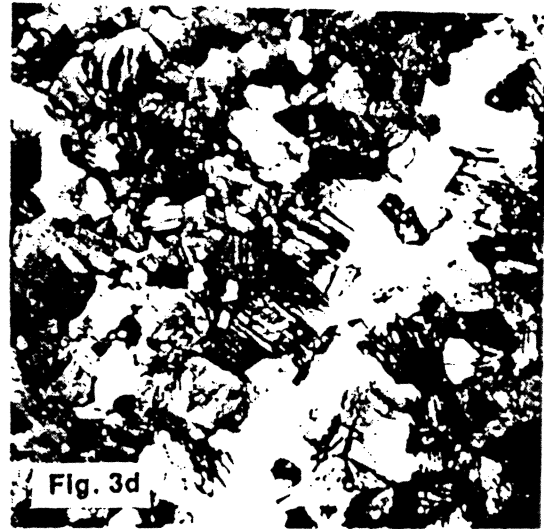
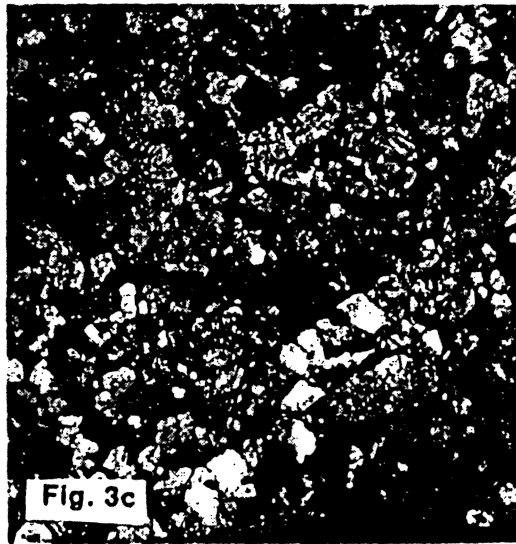
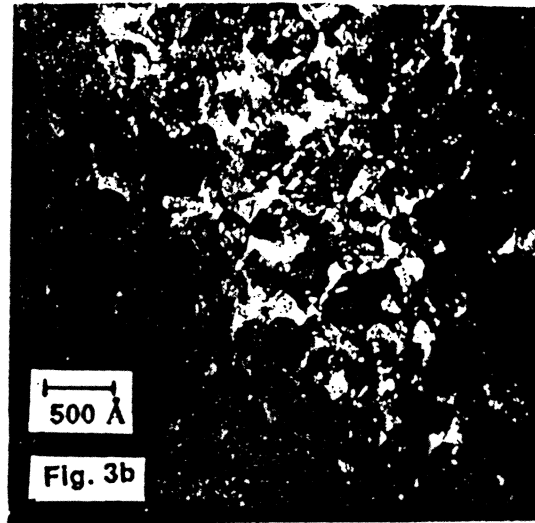
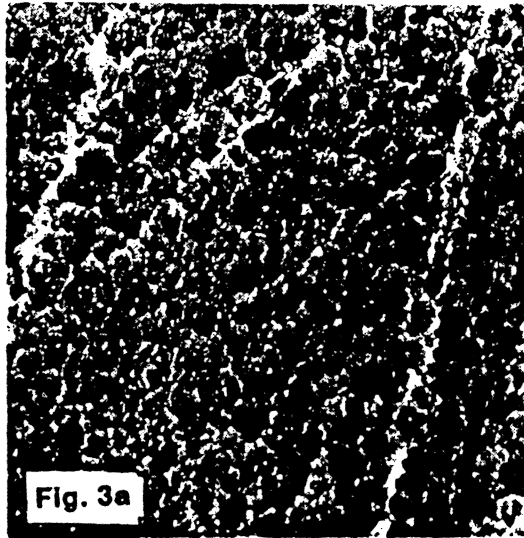


Figure 3. TEM micrographs of four different magnetic films. The fundamental structure is based on grains whose size can range from 100-500 Å. Intergranular spacing varies with different film deposition processes. Figures 3a and 3b show some evidence of grain separation. Figure 17b shows an extreme case of grain segregation through physical voiding.

The realization of a granular structure in thin-film disks has led theoreticians to base their efforts on the model of strongly interacting hcp single crystal grains, each having a uniaxial magnetocrystalline anisotropy. The grains interact

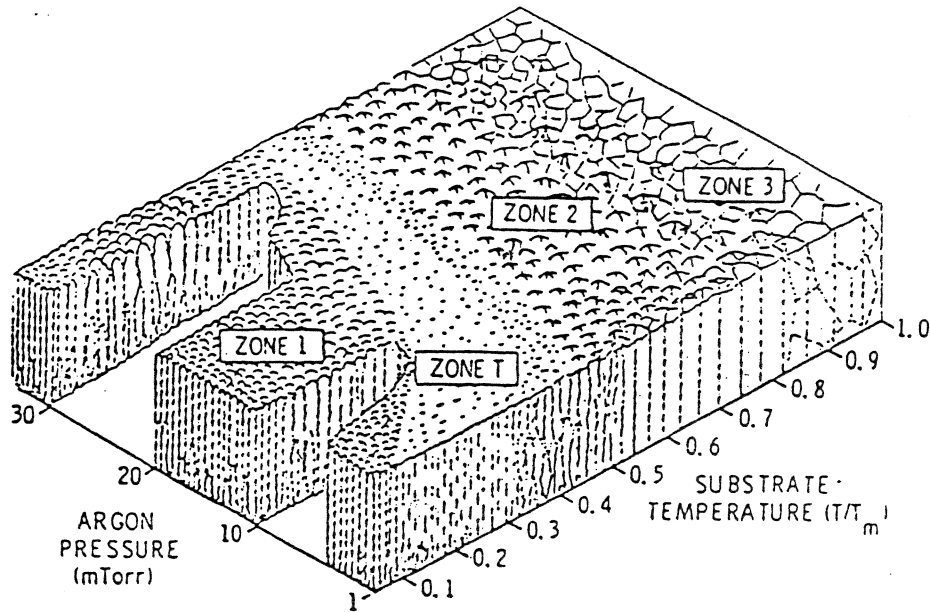


Figure 14. Microstructure zone diagram for metal films deposited by magnetron sputtering. T is the substrate temperature and T_m is the coating material melting point (Thornton, 1986).

5.1.1.1 Pressure and Temperature

Pressure and temperature are two of the important variables used to produce voided grain structures in low noise thin-film media (Yogi et al., 1990; Yogi et al., 1990b). Figure 15 shows the grain structures at low and high temperatures and low and high pressures for CoPtCr/Cr films. The low mobility Zone 1 type disks made at high pressure and room temperature reveal the greater amount of voiding. These disks were quieter and exhibited lower S^* values indicating a reduced amount of exchange coupling. Pressures of 24 mTorr were used to obtain the best results. Similarly, Ar pressures up to 25 mTorr at ambient sputtering temperatures produced the best noise disks in a CoNiCr/Cr system (Ranjan et al., 1990). Sputtered CoNi films on Cr at pressures from 5 to 25 mTorr and temperatures up to 200 °C showed reduced noise (Koga et al., 1989). Low noise results were interpreted in the vein of the low mobility argument, i.e. low kinetic energy conditions lead to films with irregularities on the nm scale.

Many others have observed noise-pressure effects. Chen presented some older work on CoRe revealing marked grain isolation at pressures of 50 and 75 mTorr (Chen and Yamashita, 1988). Noise reduction was observed for a CoCrTa alloy when the sputtering pressure was increased from 0.2 to 10 mTorr (Kawanabe et al., 1990). Prior work by this author, although not providing any noise results, demonstrated that columnar structure appears when sputtering at the higher 10 mTorr pressure. The low mobility of arriving adatoms is invoked

recognized way to represent medium noise in a useful way. If Eq. 9 is used to compute transition jitter, the noise voltage used must be the maximum noise; moreover, it should be referred to the output of the differentiator for peak detection channels (i.e., the noise spectrum at the head terminals should be differentiated).

The realization that noise is concentrated at the transition locations explains the linear portion of the curve in Figure 2. It assumes that the average noise power per transition is a constant, independent of recording density. However, in nearly all types of thin film media it is observed that the noise power increases *faster than linearly* as the density continues to increase, peaking at some higher density. Details of the explanation for this effect will be found in the next section; for now, suffice it to say that a comprehensive understanding of medium noise requires an understanding of this effect.

Consider now a closer look into the character of this transition noise. Figure 3a shows how the observed spectra look on a spectrum analyzer for maximum transition noise and for dc-erased noise³ on a single disk with a thin film head and Figure 3b shows the observed spectra for a low noise and a high noise disk as measured with a ferrite head (the results are the same for a thin film head, with some differences in detailed spectral shapes attributable

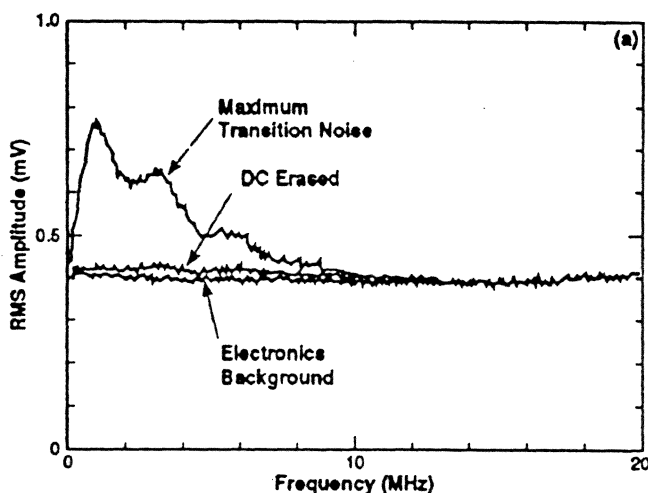


Figure 3a: Measured noise spectra for maximum transition noise and dc-saturated noise on one disk.

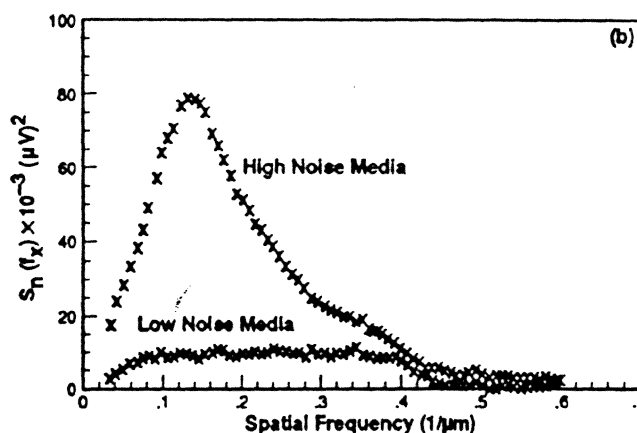


Figure 3b: Measured noise spectra for maximum transition noise from a high noise and a low noise disk.

³ The terms "dc-erased" and "dc-saturated" are used interchangeably to mean a track which has been prepared by applying, for one complete revolution of the disk, a constant, unidirectional head field sufficiently large to saturate the medium and erase any pre-existing transitions.

3.1 Instruments

3.1.1 Spectrum analyzers

For the purpose of studying noise in recording systems the spectrum analyzer is clearly the primary instrument of choice. It measures the frequency content of the noise voltage and thereby provides a tool useful for gaining insight into the causes of the various noise processes, as well as for predicting some of the channel effects of medium noise. Figure 1 shows typical noise voltage spectra measured on one disk at two different recording densities, 3.75 and 15 MHz. The lowest curve shown (c) is the noise spectrum of the head and electronics alone, measured with the disk stopped so there is no contribution from the recording medium.

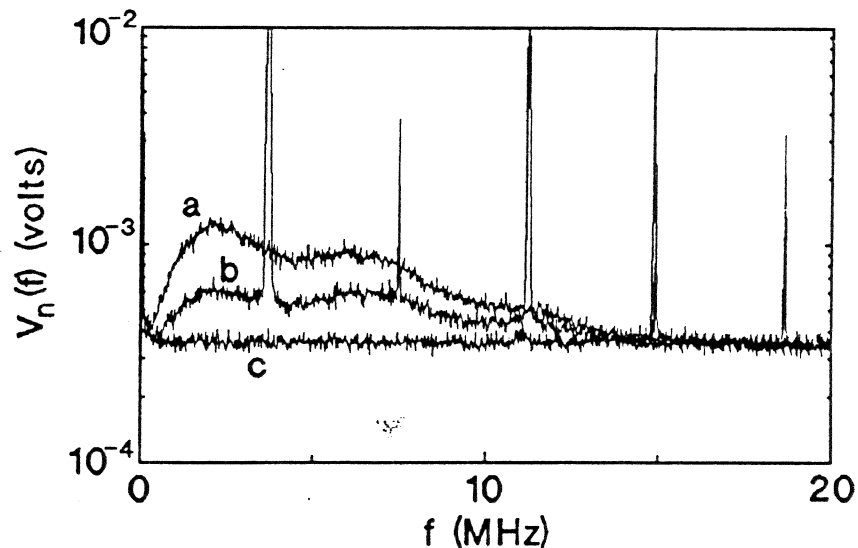


Figure 1: Noise voltage spectra measured on one disk using a thin film head at two different recording frequencies. (a) Recorded at 15 MHz (60 kfc); (b) Recorded at 3.75 MHz (15 kfc); (c) Background noise of head + electronics, measured with disk stopped.

Much of the spectrum analyzer's usefulness is because the reciprocity relation in magnetic recording between the magnetization pattern on the disk and the magnetic field of the sensing head is a correlation integral as seen in Eq. 2 (Bracewell, 1978, pp. 25 and 46).¹ As such it is equally well represented in either the

¹ Most discussions of the reciprocity relation assume that the integral is a convolution integral. Strictly speaking, however, as Bracewell makes clear, an equation of this sort is a cross-correlation integral because of where the minus sign falls in the argument of the magnetization term in the integrand. If the reciprocity equation were a convolution integral its integrand would have the form: $\{h(x)m(vt-x)\}$. However, when calculating $|V(f)|^2$, or power, there is in practice no difference since all quantities in the argument are real functions.

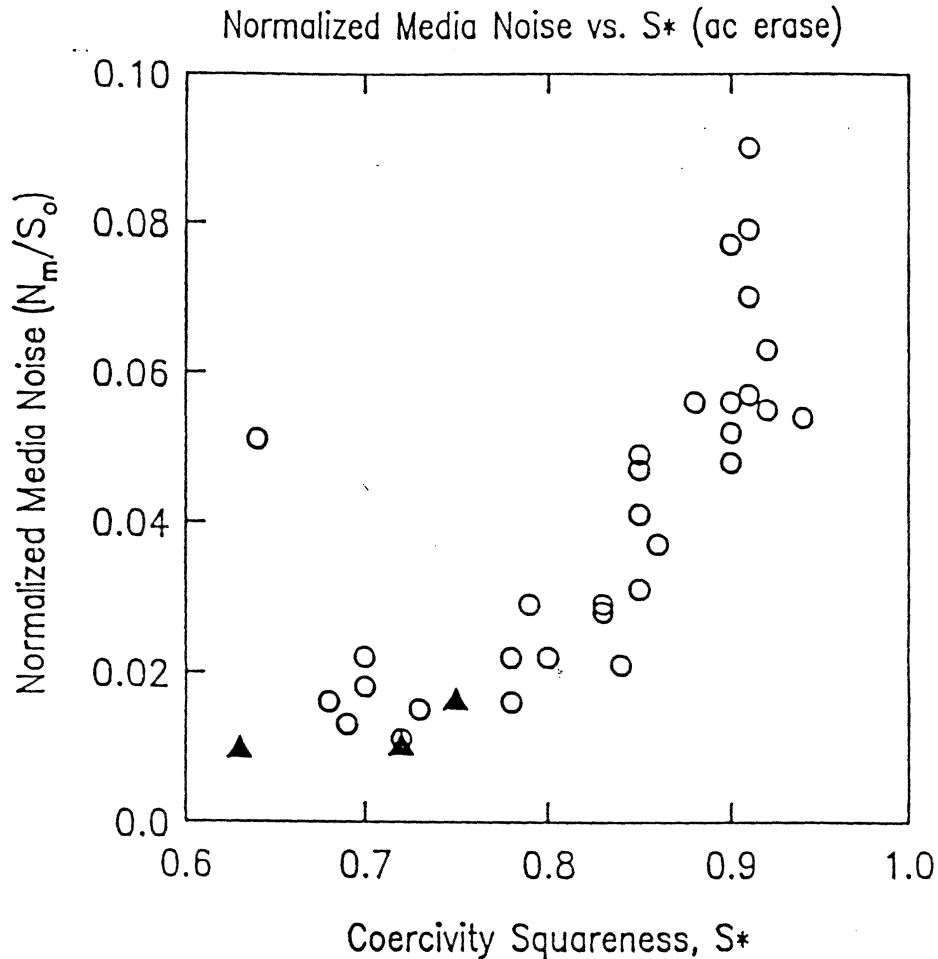


Figure 11. RMS media noise voltage N_m for ac erased media normalized to zero-to-peak isolated pulse amplitude S_0 vs. the coercivity squareness (Sanders et al., 1989).

Speliotis argues that a film can be decoupled having low noise but still have high S^* values from a narrow distribution of anisotropy fields (H_k). This mechanism would explain his results of similar noise values on films with S^* values ranging from 0.70 to 0.93. Khan observed noise to be substantially different between a CoNi and a CoCrTa alloy, even though they both have similar S^* values. The presence of perpendicular anisotropy in the film may be relevant (Sec. 4.3.4.3).

Thin-film media require a mixture of S^* criteria. One wants a reasonably high value of S^* for signal output, writability, and narrow transitions (Yogi et al., 1990b; Speliotis, 1990c; Williams and Comstock, 1971). On the other hand low noise media require uncoupled grains, which is often manifested by a low S^* parameter. The best medium would be one with very high S^* , but uncoupled grains for low noise (Speliotis, 1990c). The S^* parameter would fail to identify such a recording medium. Thus, there has been a search for other measurement



Fig. 3. Transmission electron micro graph of disk with OR = 1. Note that the grains are well packed.

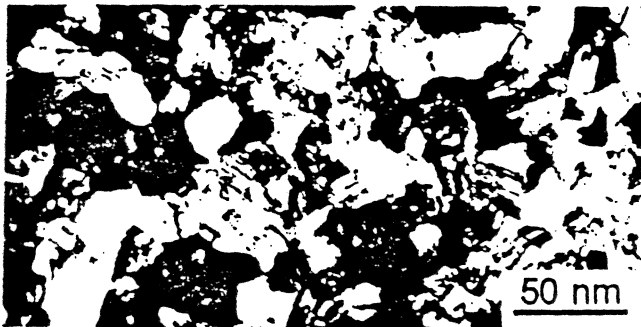


Fig. 4. Transmission electron micro graph of disk with OR = 4.26. Note that the grains are well packed.

Figure 5 shows the overwrite dependence on the write current for disks with various ORs. The overwrite is seen to improve by about 10 dB for disks with $OR > 1$. This result is in contrast with the observation of Simpson et.al., who reported that $OR > 1$ worsened the overwrite performance of the disk [1]. The reason for the better overwrite properties of the disks with $OR > 1$ is not clear at this point. It may be the result of a lower closing field, observed in the hysteresis loops of these films. An alternative explanation, which should be investigated further, is that there may be a less side writing on disks with $OR > 1$.

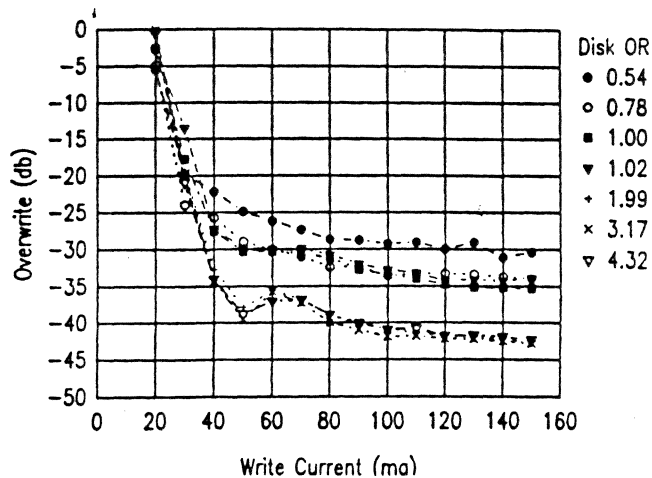


Fig. 5. Overwrite vs write current for disks with various orientation ratio (OR).

Conclusions

The effect of OR on recording characteristics of thin film disks was investigated. An $OR > 1$, for the films with strong intergranular exchange coupling, does not have any effect on So/N of the disk, but it improves the overwrite performance of the disk.

Acknowledgements

The authors would like to thank Thomas Pike for image analysis of the TEM pictures and Jean Horkans for reviewing the manuscript.

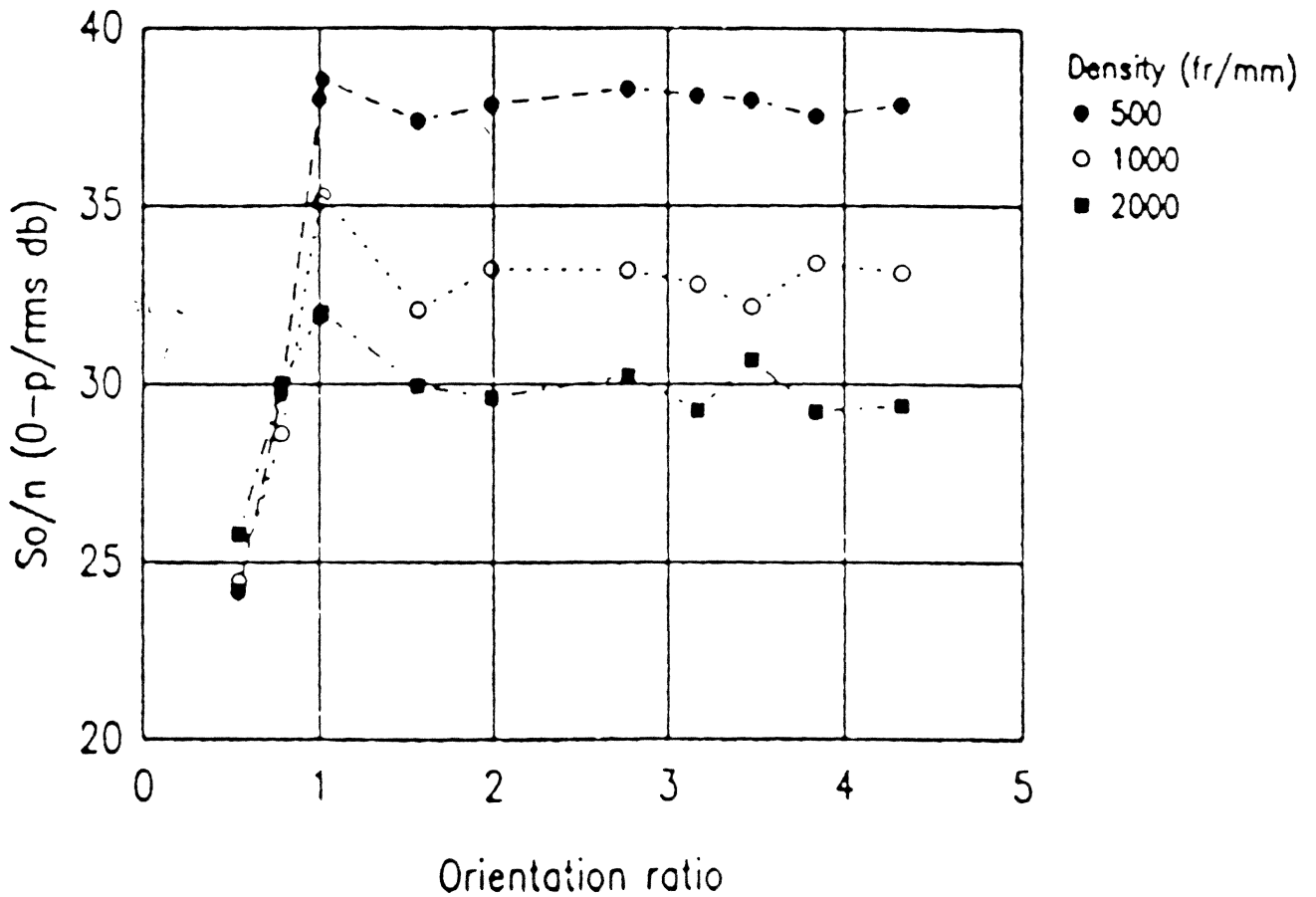
References

- [1] E. M. Simpson, P.B. Narayan, G. T. Swami and J. L. Chao, IEEE Trans. Mag., MAG23, 3405(1987).
- [2] E. Teng and N. Ballard, IEEE Trans. Magn., MAG-22, 579(1986)
- [3] T. Lin, R. Alani and D. Lambeth, J. Magn. and Magn. Mater., 78, 213(1989).
- [4] J. S. Judge and D. E. Speliotis, IEEE Trans. Magn., MAG-23, 3402(1987).
- [5] D.J. Seagle, N.C. Fernelius and M.R. Khan, J. Appl. Phys., 61, 4028(1987).
- [6] R. Nishikawa, T. Hikosaka, K. Igarashi and M. Kanamaru, IEEE Trans. Magn., MAG-25, 3890(1989).
- [7] M. Mirzamaani, K. Johnson, D. Edmonson, P. Ivett and M. Russak, to be published, J. of Appl. Phys., Proc. of 34th mmm conf., 1989.
- [8] J.G. Zhu and N. Bertram, Intermag Conf., Washington DC, 1989.
- [9] T. Coughlin, J. Pressesky, S. Lee, N. Heiman and R. D. Fisher, Proc. of 34th mmm conf., 1989.
- [10] E. Johnson and M.G. Kerr, Intermag Conf. Brighton, UK, 1990.

ercivity
e type
ected
type C
nce of
uld re-

nels at the grain boundaries. Thus, both films had strong, magnetically coupled grains which probably dominated the noise power through an intergranular exchange coupling in such a way that the effect of $OR > 1$ was totally masked. Our observation is somewhat different from theoretical modeling of Zhu and Bertram [8], in that the noise power did not exhibit any appreciable change when OR increased from 1 to 4.26.

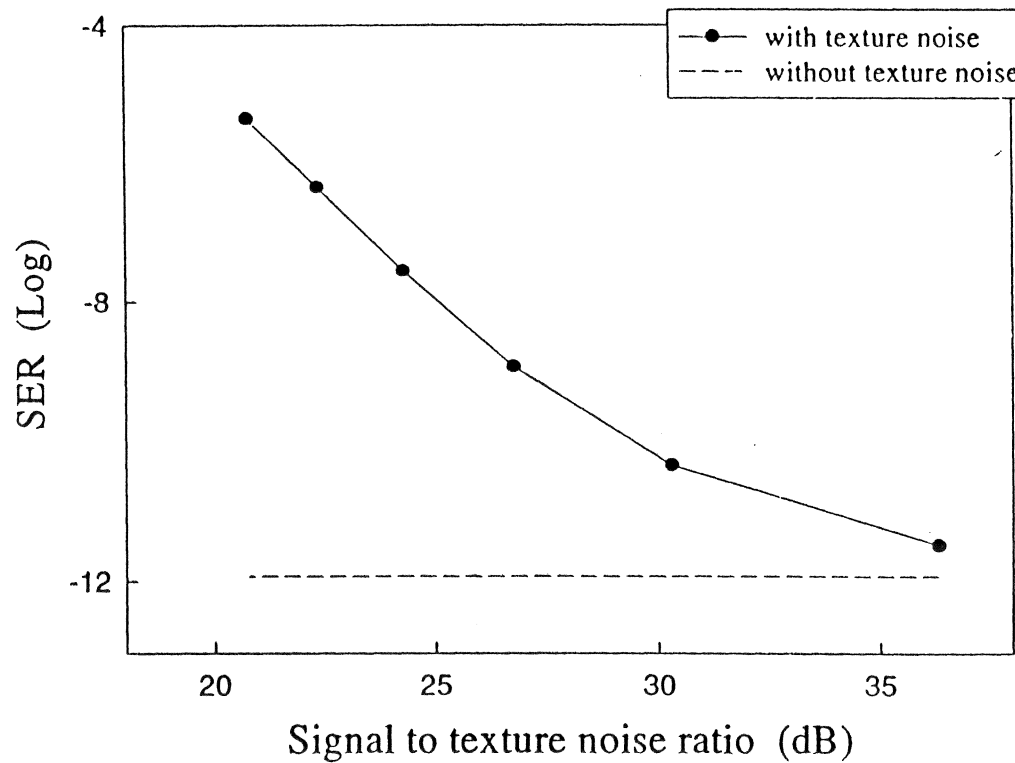
of disk



stating
to 20
nitide
meter
d was
used
in the
ected
e tex-
ess in
ection

Fig. 2. Isolated pulse amplitude over media noise (S_o/N) vs orientation ratio (OR) at different written densities.

Sensitivity to Texture Noise Level



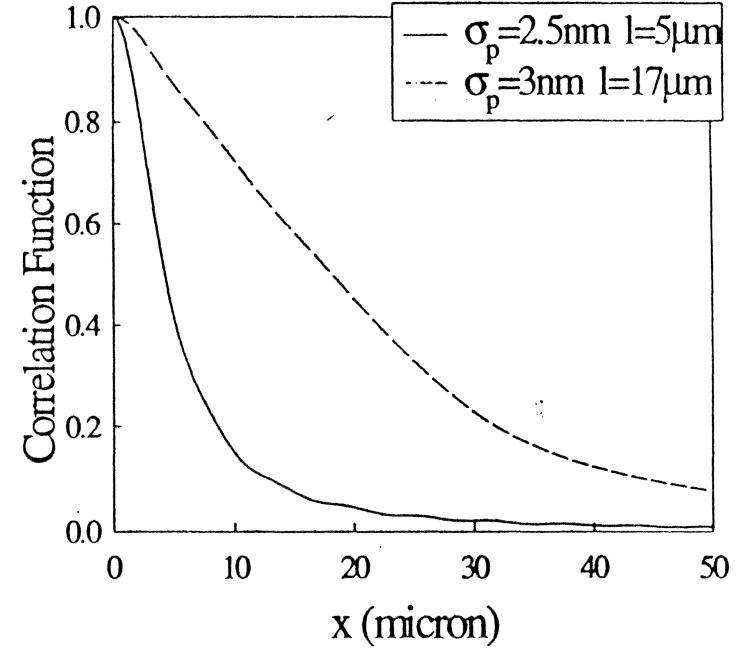
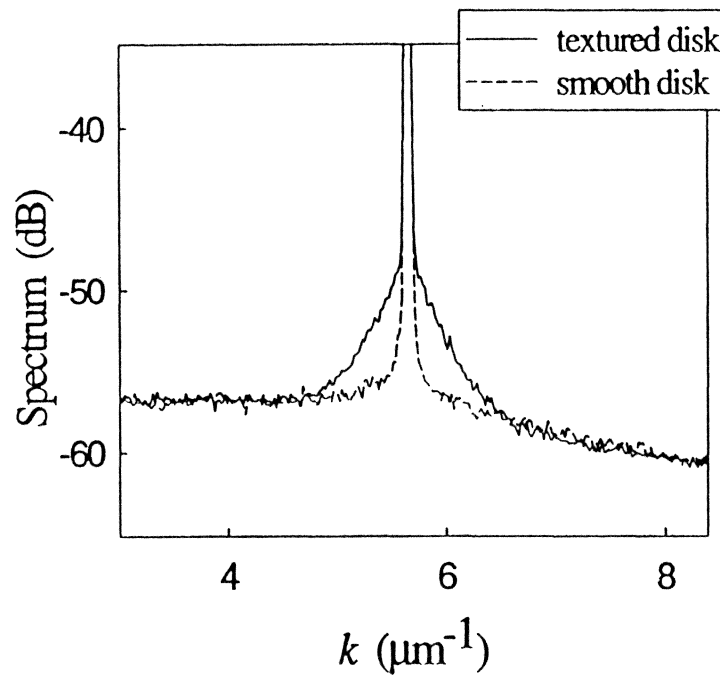
$SNR_e = 30 \text{ dB}$

$SNR_m = 31.75 \text{ dB}$

$Density = 178 \text{ kfc}$

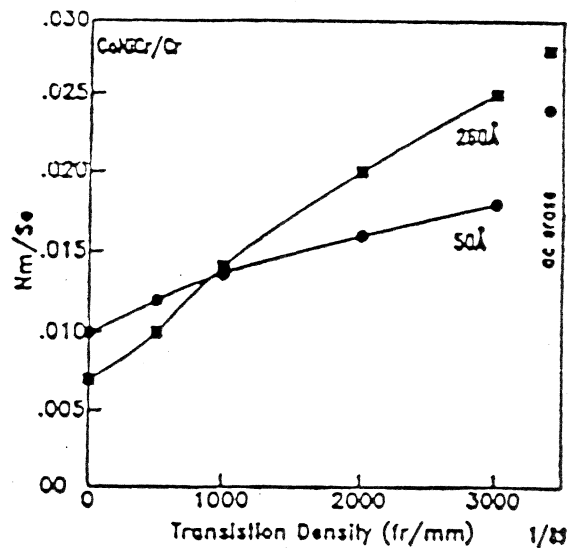
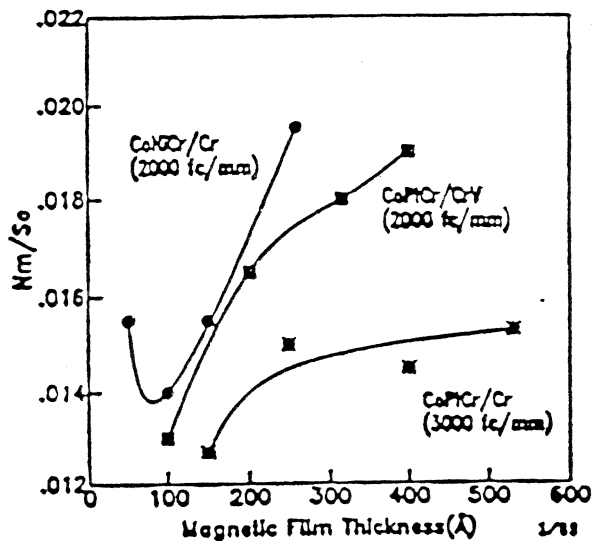
$PW50/B = 2$

Texture Noise Spectrum and Down-Track Correlation

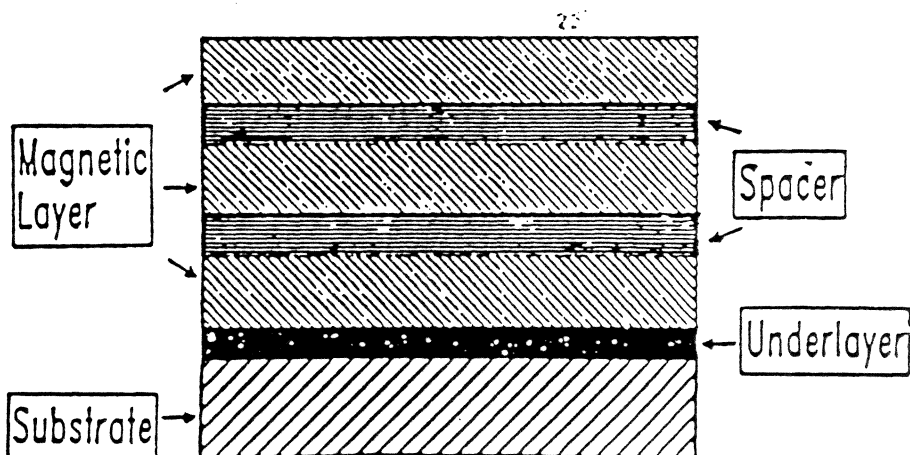


NOISE REDUCTION BY LAMINATION

- Experimentally, it is found that very thin films exhibit enhanced S/N; attributed to favorable grain structure. However, low $M_t t$ reduces signal amplitude.



- A natural extension is to "stack" thin layers to form a laminated structure to regain $M_t t$ and reduce noise:



Media For MR Application

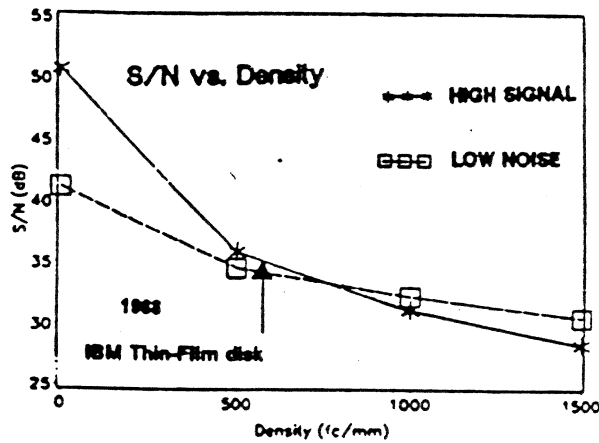
(Supplement)

- MR heads are flux sensitive devices, therefore **more susceptible to noise**.
- Requires lower film thickness (M, t), \therefore more difficult to control properties. On the good side, easier to get higher coercivities.
- MR device is sensitive to electrostatic discharges, \therefore grounding of equipment and operators is important.
- Hard 'asperities' on the media can cause spikes in the output due to rapid thermal changes. This can be corrected with feedback amplifiers.
- Multilayered media:- equipment limited, also should be optimize for the No. of layers.
- Reduced track width and bit length place a constraint on the allowable size of surface imperfection. \therefore reduce debris, handling etc.
- MR media more appropriate on alternative substrates (glass, 'canasite') since they offer lower "**glide height**". However magnetic properties are not as good as Al/NiP due to Cr growth and heating differentials. One solution is to pre-coat the substrates.

Media for MR Heads

For MR heads media noise is of prime importance, owing to *over 10 fold amplification*.

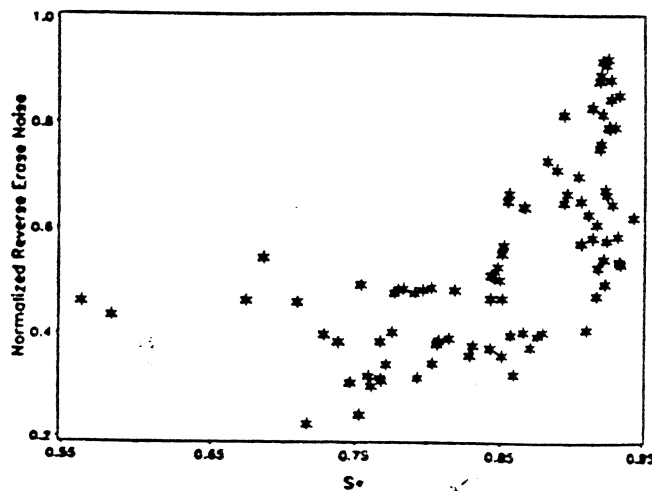
"What used to be appropriate for the 80s" may no longer apply for 90s:-



- Transition noise. This is the dominant noise source for thin film media.

D Coercivity Squareness, S^* .

The role of *macromagnetic properties*, such as ' S^* ', have to be reassessed.



Reverse erase noise vs S^* for a variety of thin-film media. (R. M. White)

Defect Reduction

Increased area density results in narrower tracks and closer bits; critical defect sizes are reduced proportionately.

Potential defect sources include substrate scratches, processing scratches, debris shadows, blisters or delaminations, sputter shadows and handling damage

Critical defect size is declining rapidly at 60% areal density growth rate.

Environment, equipment, process and materials are issues.

Handling and cleanliness are extremely critical

- Cleanrooms**
- Gloves, clothing**
- manual versus automatic handling**

Dan Malone, IIST, 7/24/96, (scudeft1.doc)

SNR and bit cell size

SNR vs tpi (W= track width)

$S \propto W$, $N^2 \propto W$ therefore

$$\text{SNR}_v \propto \sqrt{W} \propto 1/\sqrt{\text{tpi}}$$

?

The bandwidth, B , is the bandwidth through which the measurement is made and is generally wider than the 3 dB bandwidth normally used to characterize actual filters. Johnson noise has a gaussian amplitude distribution. This is illustrated in Figure 1(a). In the frequency domain Johnson noise is white (Figure 1(b)). These properties allow for a convenient measurement and description of Johnson noise.

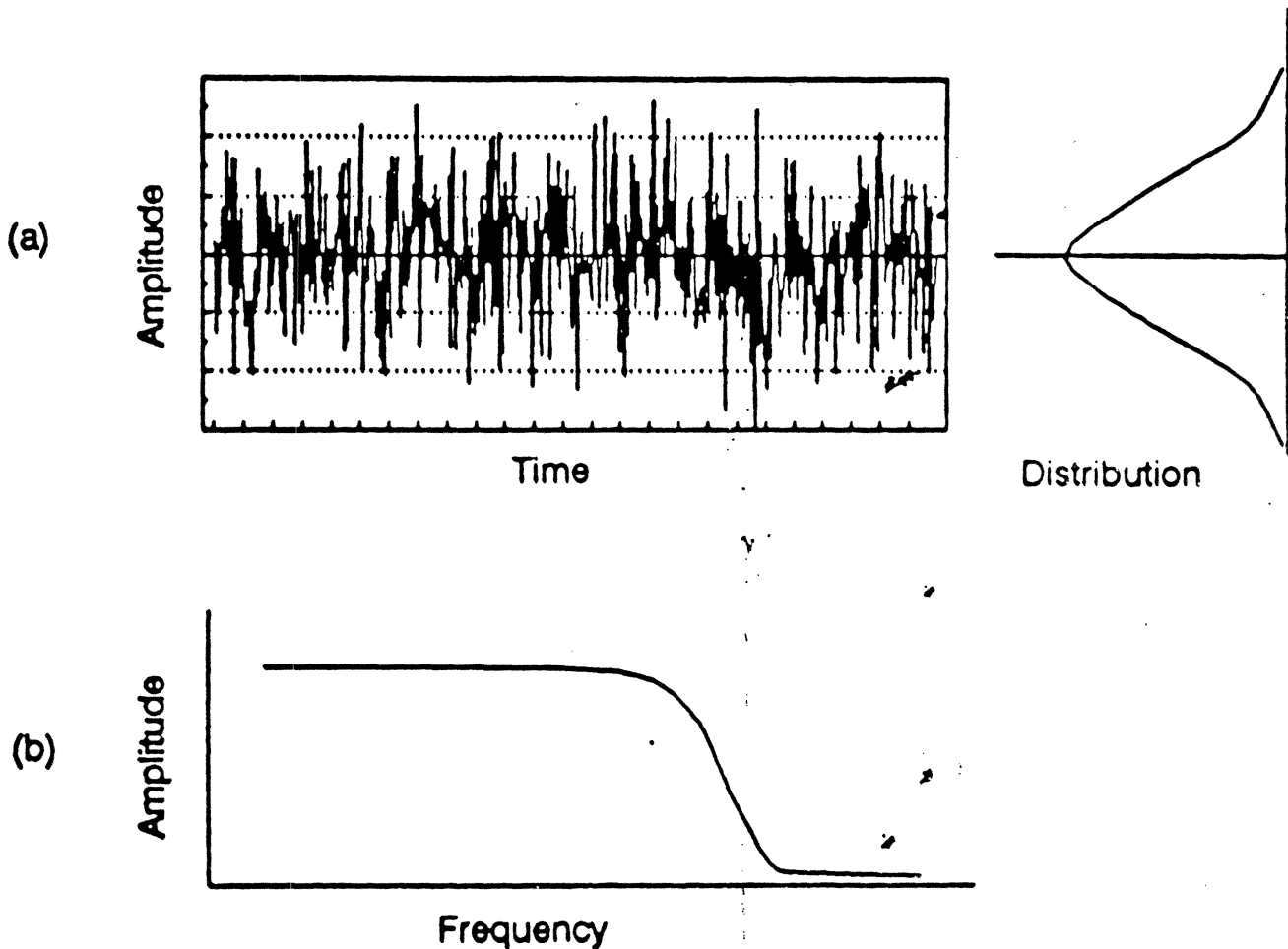


Figure 1. Random (Johnson) Noise: (a) Time domain, (b) Frequency domain.

Noise from thin film media differs in important ways from that of particulate media. One difference has to do with stationarity. Suppose a function, $N(t)$, describes a noise voltage with respect to time. If either the mean or any higher order moment of $N(t)$ is time (or space) dependent, then the noise is non-stationary (Bendat and Piersol, 1980). For media noise the second moment, the variance, given by:

$$\psi^2(t) = \lim_{T \rightarrow \infty} \frac{1}{T} \int_0^T N^2(t) dt \quad (2)$$

Magnetic Recording Noise

The Essential Problems of Magnetic Recording

- 1. Reliably Achieving the Ever-Decreasing Head to Disk Spacing.**
- 2. Improving Error Rate with an Ever-Decreasing Magnetic Signal.**
- 3. Positioning the Head with Ever-Decreasing Speed and Precision.**

Signals, Distortion, Interference and Noise

- **SIGNAL** (desired waveform that we want to read)
e.g. ideal PR4 waveform or peak-detect signal

- **DISTORTION** (average difference between what we get and what we want)
 - **Linear**: intersymbol interference, linear peak-shift
 - **Nonlinear**: Asymmetry, NLTS, Partial erasure

- **Interference** (unwanted signals or other garbage)
 - adjacent track or old information
 - poorly overwritten old data
 - electromagnetic interference (EMI)

- **Noise** (unpredictable random perturbations)
 - thermal (Johnson) noise from head and preamp (AE)
 - domain instability (Barkhausen) in ind. and MR heads
 - media noise (transition-noise and dc-erase noise)

The Principal Noise Sources

- o Media Noise**

- o Electronics Noise**

- o Off-track and adjacent track noise**

- o Electromagnetic interference**

In well engineered systems, none of these is negligible

Electronics Noise

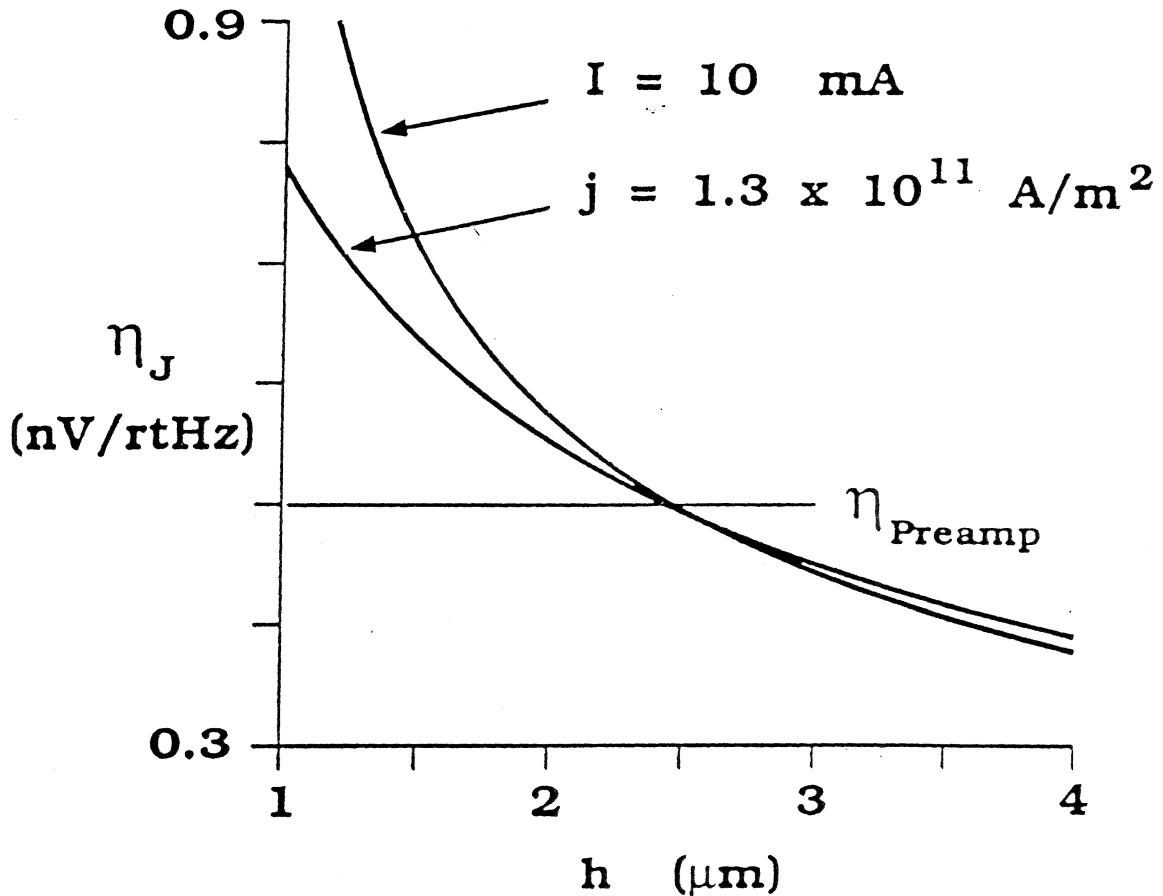
- o Johnson Noise (from the real part of the head impedance as seen at the amplifier input)**
- o Plus the equivalent noise resistance of the read head preamplifier**
- o Tends to be a voltage proportional to (bandwidth)^{0.5}**

Media Noise

- **The only fundamental Noise**
- **Related to the granular nature of ferromagnetism**
- **For independent particles:**
 - media $S/N \sim N$ the number of particles in a bit cell**
- **With particle interactions:**
 - exchange coupling increases noise at the transition, decreases noise in saturated areas**
 - magnetostatic coupling decreases noise**

The fundamental limit on media noise is particle size.

Johnson Noise of MR Heads



Head and Preamp Noise Voltage Spectral Density

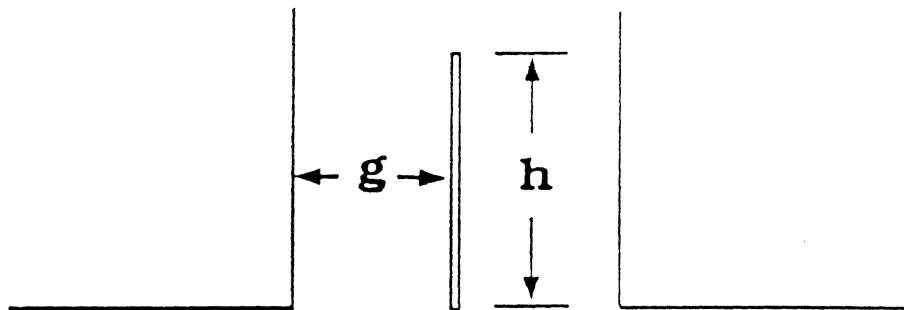
$$\eta = \sqrt{\eta_J^2 + \eta_{\text{Preamp}}^2}$$

Johnson Noise of MR Heads

$$\eta_J = \sqrt{4 k T (R + R_{Leads})}$$

$$R = R_0 (1 + \alpha \Delta T)$$

$$I^2 R = \frac{2Kwh}{g} \Delta T$$



$$k = 1.38 \times 10^{-23} \text{ Joules/K}$$

$$T = 296 \text{ K}$$

$$\rho_0 = 25 \times 10^{-8} \text{ Ohms} \cdot \text{m}$$

$$\alpha = 0.003 \text{ K}^{-1}$$

$$K = 0.75 \text{ Watts/m} \cdot \text{K}$$

$$R_{Leads} = 5 \text{ Ohms}$$

$$t = 300 \text{ \AA}$$

$$g = 0.2 \text{ } \mu\text{m}$$

$$h = 2.5 \text{ } \mu\text{m}$$

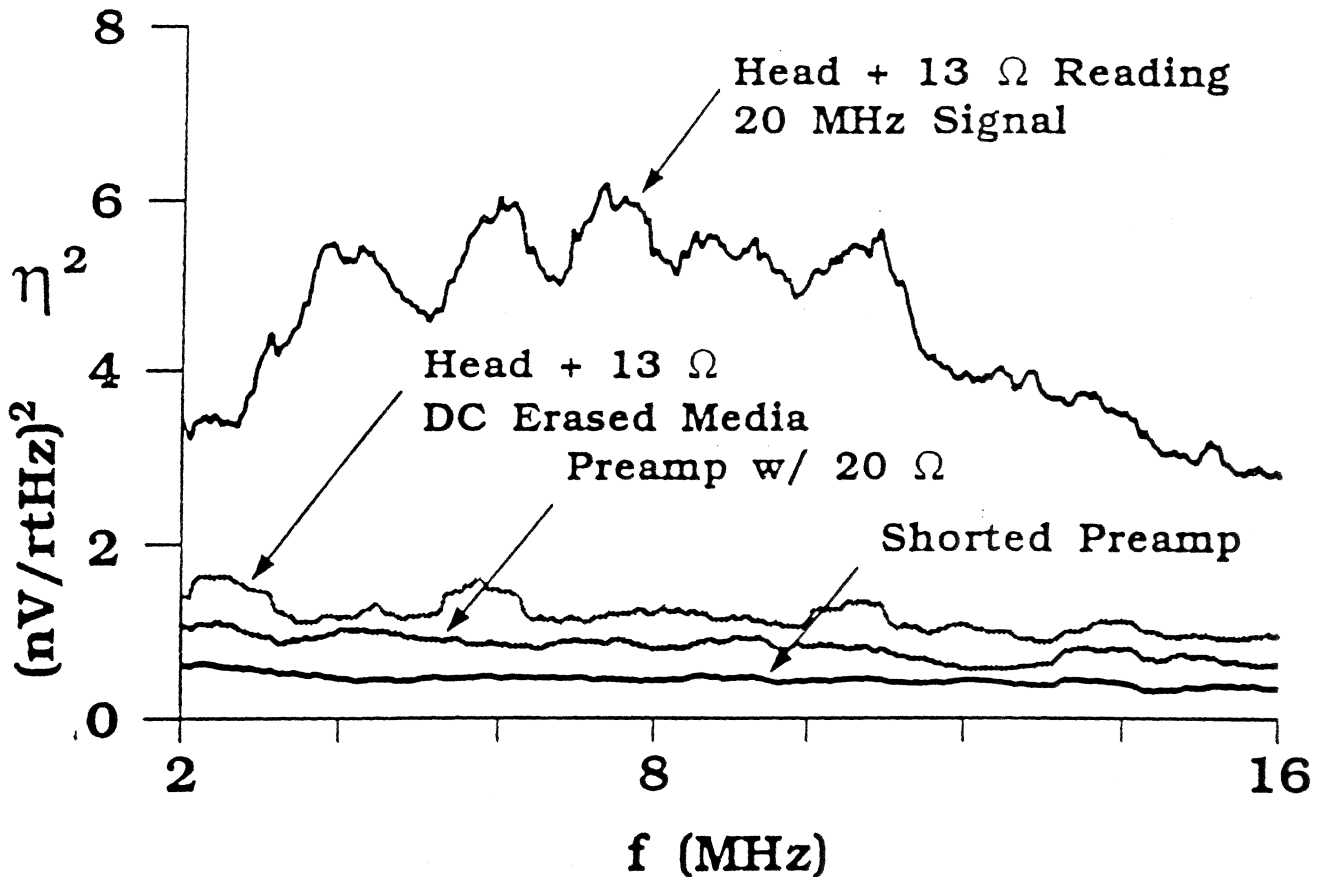
$$w = 4 \text{ } \mu\text{m}$$

At $T=296 \text{ K}$ and with 10 ma

$$R = 19.1 \text{ Ohms} \quad \Delta T = 19 \text{ K}$$

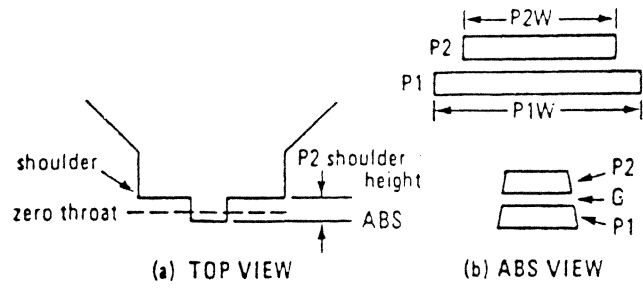
Media Noise with MR Heads

If sensitivity to Signal Flux is improved then sensitivity to Media Noise is also.



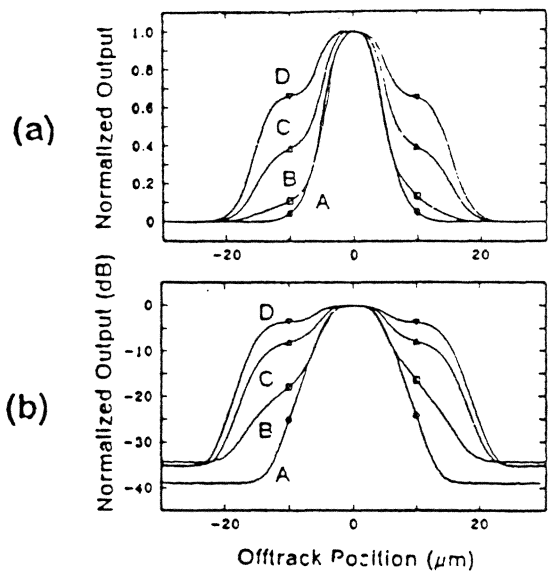
3200 tpi
58 kfc
1.4 memu/cm²
1700 Oe

**Side Writing
Side Reading
Erase Bands**



Before and after pole trimming

(a) Pole-tip shoulder created during pole trimming. (b) Pole-tip geometries before and after trimming viewed from the air bearing surface.



Microtrack profiles of trimmed heads with shoulder heights ranging from 1.8 to 6 μm . (a) Linear scale. (b) Logarithm scale.

FIGURE 7

Su, Ju, Vo, IEEE Trans, SEPT 92
 (PP 2722-2724)

Offtrack Characteristics of Shielded Magneto-resistive Head

Tetsuhiro Suzuki, Yoshihiro Motomura and Katsumichi Tagami
Functional Devices Res. Labs., NEC Corp., Kawasaki 216, Japan

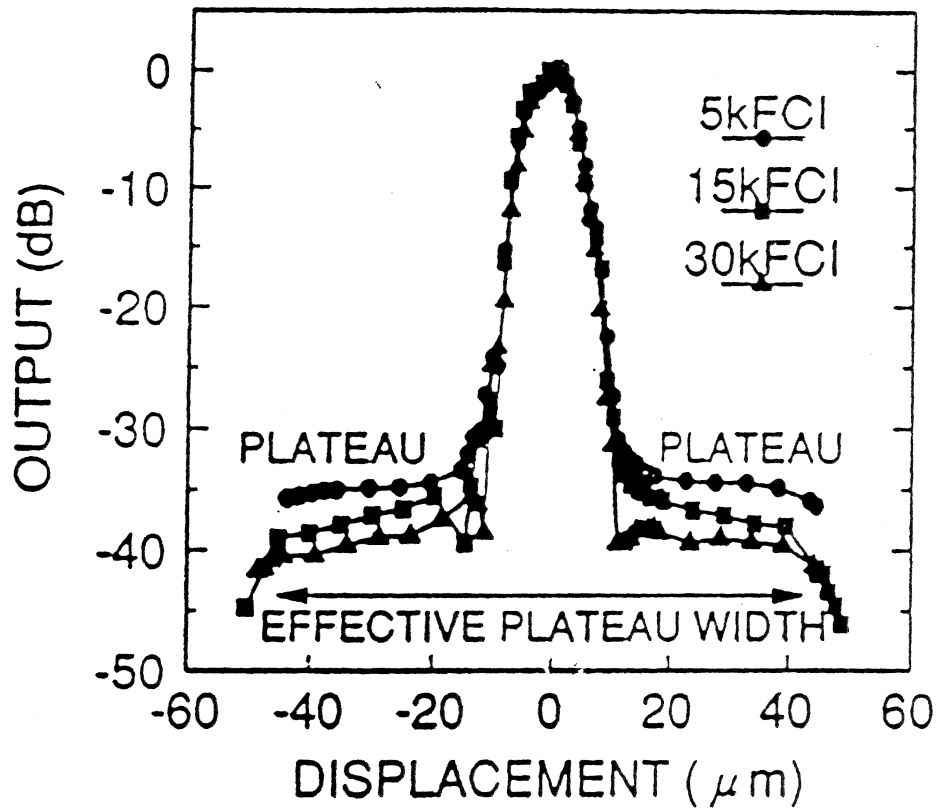


Fig.2 Offtrack characteristics for shielded MR head.

SPATIAL DISTRIBUTION OF OVERWRITE INTERFERENCE ON FILM DISKS

Dean Palmer and James V. Peske
Compact Storage Lab
IBM Corporation, Rochester, MN 55901 USA

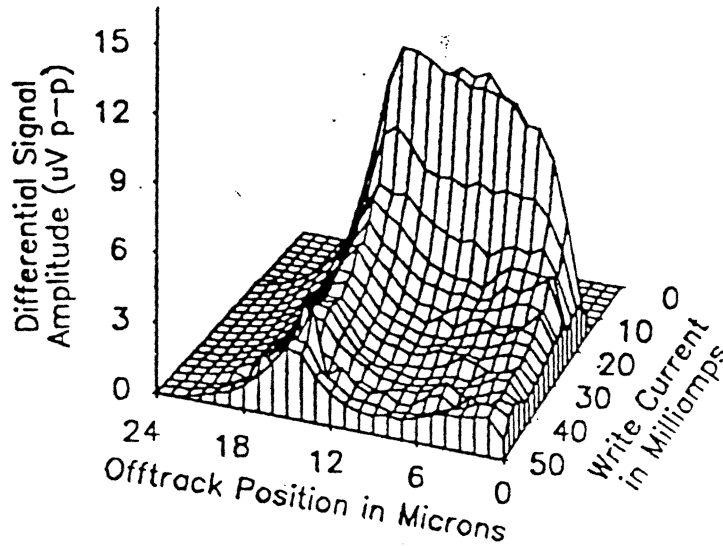


Figure 5: Remaining I:1 Amplitude after Overwrite with 2I: for Ferrite Head as Function of Write Current.

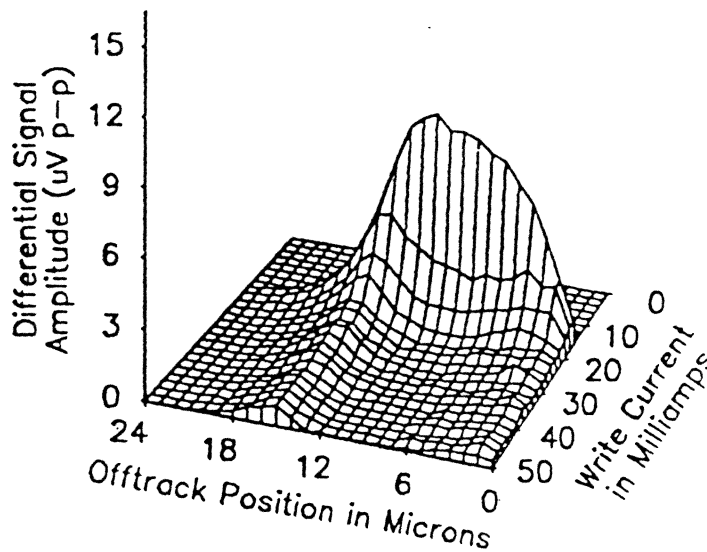


Figure 6: Remaining I:1 Amplitude after Multiple Overwrites with I:2 for Ferrite Head as Function of Write Current.

MAGNETORESISTIVE HEADS

* PHYSICAL STRUCTURE

- Thin layer of NiFe between two large shields
- Separate write element - usually wider
- Resistance changes with angle of magnetization

* BIASING, IMPEDANCE, SENSITIVITY

- needs magnetization biased to correct angle - & stabilized
- needs bias current flowing to sense resistance change
- almost purely resistive impedance, 10 - 100 ohms
- much more sensitive than inductive head
(especially at low velocity - senses fields directly)

* NONLINEAR DISTORTION

- MR transfer function saturated at ends of range
- incorrect bias angle leads to pulse amplitude asymmetry

* SIDEREADING: MR VS. INDUCTIVE

- Inductive heads have extended response at long wavelengths
- MR heads have wavelength-independent response or "skirt"

* DOMAIN-WALL INSTABILITIES

- Inductive heads show "popcorn" noise after writing
- MR heads can end up in quasistable states after writing

THIN-FILM MEDIA

- * PHYSICAL STRUCTURE
 - Thin, very-uniform, high-moment cobalt alloy

- * TRANSITION-SHIFT DISTORTION
 - Transitions displaced from correct positions as they are being written
 - Caused by demag. fields from previous transitions or by poor field risetimes in the head

- * OVERWRITE
 - Associated with shifts in positions of new transitions caused by demag. fields from old data

- * TRANSITION NOISE
 - Noise in thin-film media is localized around transitions
 - Noise is very low in fully magnetized regions

- * EDGE EFFECTS, SIDEWRITING
 - Writing off the side of the head is like writing at a large flying height
 - Poor resolution, large phase-shifts & transition-shifts
 - High noise, poor overwrite

(1986) was the first to report on observations of this type of noise. Using a technique of digitizing and averaging the readback signal and subtracting signals to simulate different widths of readback heads, he found that the recording process induced a narrow band of noisy magnetization along the track edges. (Figure 11) He also found that the width of this band of noise seemed to be independent of track width. As a result, although it constitutes a small fraction of the noise contribution for wide tracks ($> 10 \mu\text{m}$), as track widths are reduced this noise would contribute an increasing portion of the total medium noise and eventually (at, perhaps, $1\text{-}2 \mu\text{m}$ head widths) most medium noise would come from the track edges; further track width reduction would not reduce medium noise any more.

The character of track edge noise is significantly different from transition noise. Work by Muller, et. al. (1990) and Indeck, et. al. (1991b) has shown that track edge noise arises not from magnetization fluctuations caused by a head-on wall, like a transition, but from a different process. Assuming that a recording disk's surface has been prepared by dc-erasing the entire surface in one direction, as is typically done during drive manufacture, along the track edge the magnetization on- and off-track will be either parallel or anti-parallel for alternating bits. Even if the disk has been left in its virgin

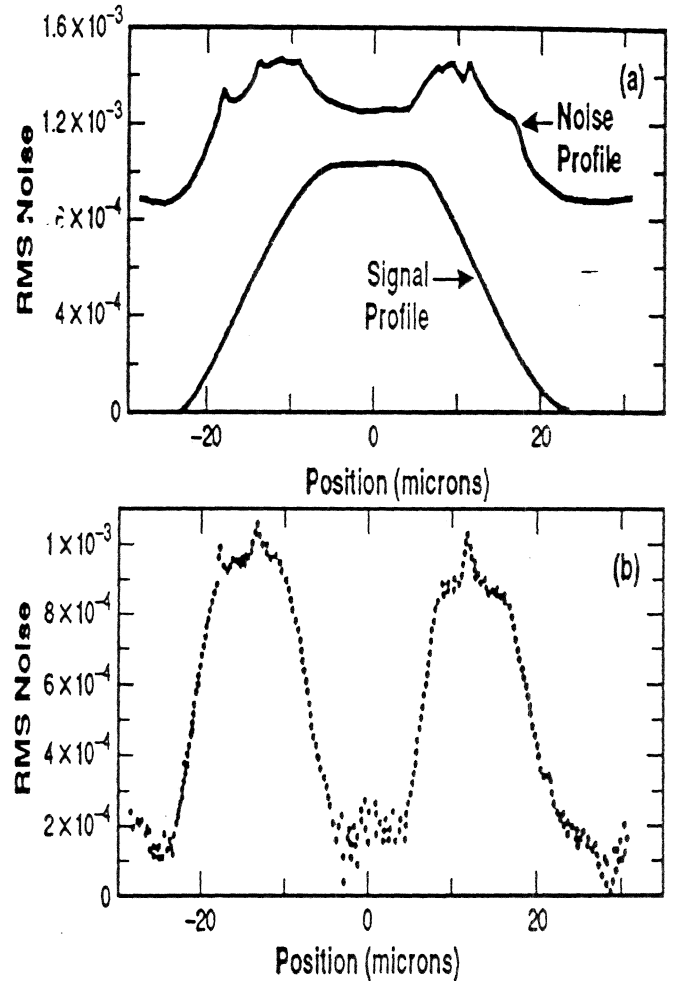


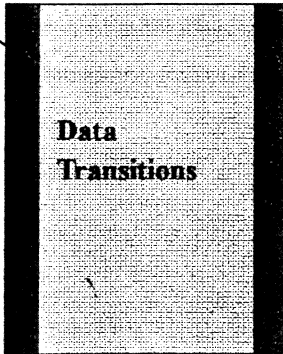
Figure 11: Plot (a) shows the rms noise voltage vs. position as a $12.5 \mu\text{m}$ wide read is scanned across a $28 \mu\text{m}$ wide track. The noise is measured with a spectrum analyzer. For comparison, a plot of signal vs. position is also shown. Plot (b) shows the edge noise component obtained from the total by subtracting the dc-erased and transition noise. (Amplitudes are arbitrary.) (Yarmchuk, 1986)

Erase Bands - who needs them ?

- Erase bands exist at the edges of all written tracks.
- Servo system would prefer no erase band.
- Data handling systems work best with an optimum erase band.
- Erase bands are determined by the magnetic and physical parameters of the heads, disks and recording channel electronics.
 - Magnetic Fly Height
 - Write head geometry's (gap, pole thickness, throat height, shape, edge sharpness)
 - Disk coercivity, orientation, squareness,...
 - Write current and write current risetime.
 - slider skew

Edge Effects

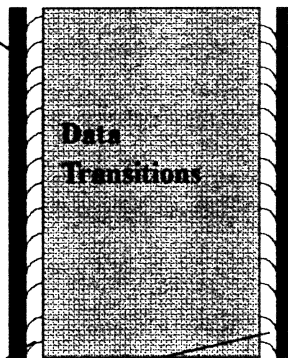
Erase
Bands



Dan Malone
edge2.ppt
4/25/97

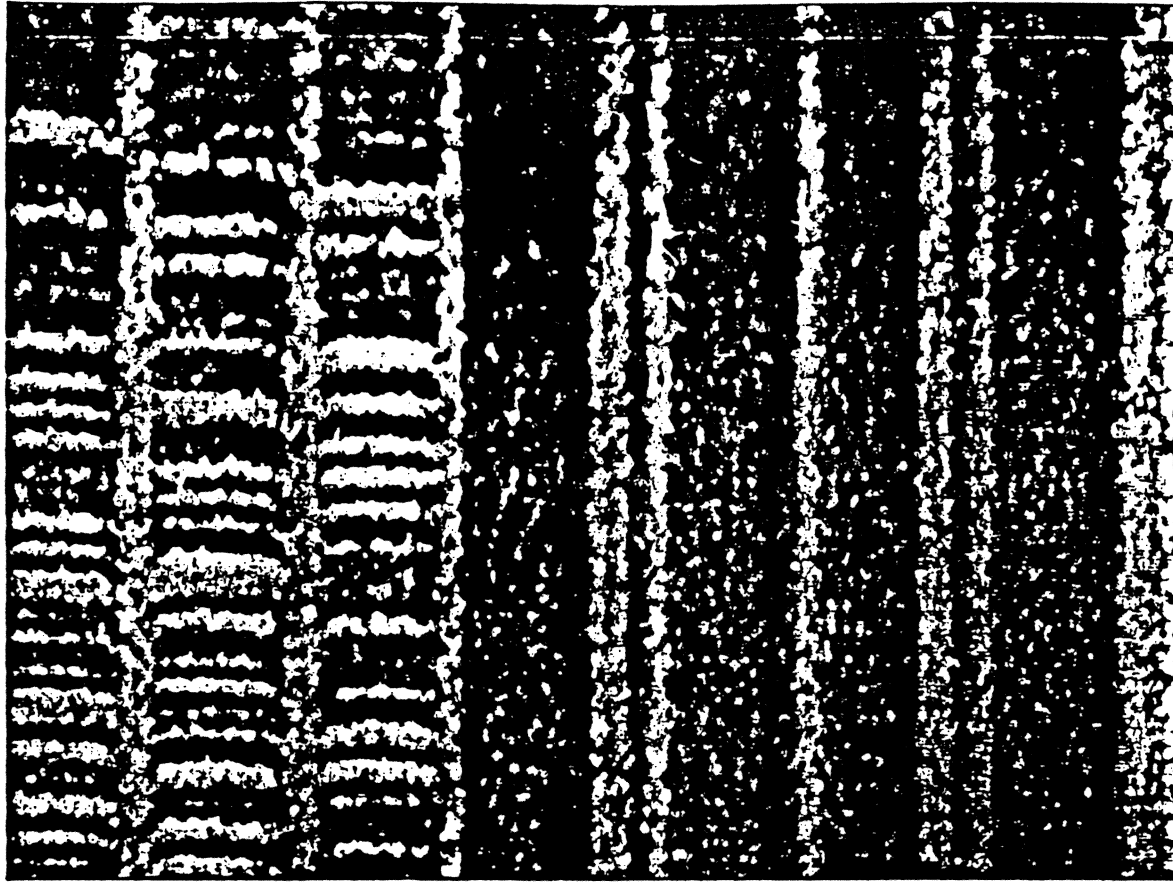
Edge Effects

Erase
Bands

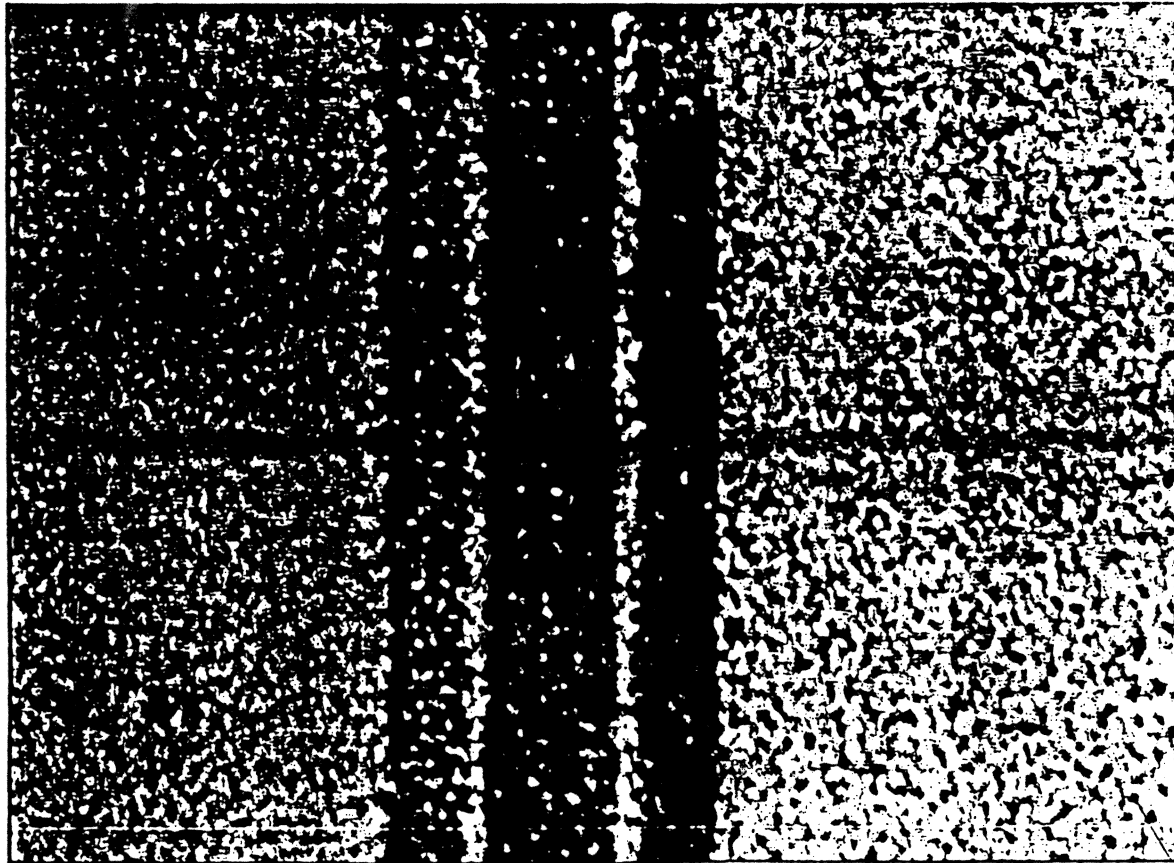


Transition
Hooks

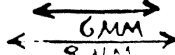
Dan Malone
edge.ppt
4/25/97



HDA808-L-11, DISK # 2B



22120 2F 26120 KTS



Erase Band and Transition Charge - Model and MFM

M. R. Madison, T. C. Arnoldussen, T. Y. Chang, R. W. Wood, and F. D. Scott II

IBM Corp. SSD, San Jose, Ca 95193

Abstract - The three-dimensional magnetic vector field for a magnetic recording head with unequal pole width is used as an input to a two dimensional extension of the Williams Comstock model to calculate transition charge, erase band widths, and to simulate magnetic force microscope images. Modeling results are compared to MFM images.

I. INTRODUCTION

The current trend toward higher areal density in magnetic recording underlines the need for accurate modeling of the "side-erased bands" and the shape of the transition charge at the track edge. The "side-erased bands" function as guard bands between adjacent tracks. The shape of the transition charge affects the pulse shape versus track offset, specifically the linearity of the Position Error Signal (PES) versus track offset.

The Magnetic Force Microscope (MFM) is gaining acceptance as the industry tool for examining the shape of the written transitions. The MFM measures the vertical component of the magnetic field (H_v) or its vertical derivative dH_v/dy from the media charge density. A two-dimensional extension of the Williams-Comstock model [1] is used to calculate the charge density, which leads to the calculation of H_v or dH_v/dy . The charge density calculation and the measured MFM image complement each other to validate our understanding of the write process. We will trace this process to increase our understanding of the erase band and the charge density shapes. We have combined a three-dimensional magnetic vector field from a Finite Element Field (FEF) calculation

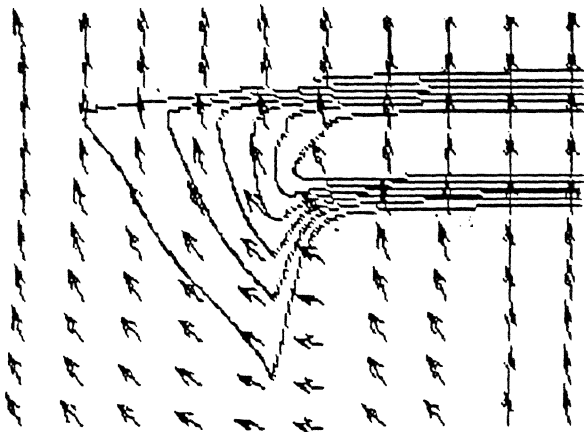


Figure 1 Plot of constant field magnitudes (2-D) contours and in-plane vector field

of the writing head with unequal pole widths, with a two dimension Williams-Comstock model to calculate the transition charge shape, and the erase bands. We have simulated the MFM images and compare these with the measured MFM images. This results in a simple picture of the erase band.

II WRITE MODEL

If we assume we have a sharply written transition with charge $\rho = \delta \nabla \cdot M_1(x')$ a distance "a" below a surface, where δ is the media thickness, M_1 is a sharply written transition, x is along the track direction, z is perpendicular to the track direction, and y is perpendicular to the magnetic film surface. Then the vertical component of the H field is:

$$H_y(x, y, z) = \frac{\delta}{4\pi} \int_{-\infty}^{\infty} \int_{-\infty}^{\infty} dz' \nabla \cdot M_1(x', z') \frac{y-a}{\left[(x-x')^2 + (z-z')^2 + (y-a)^2 \right]^{3/2}} \quad (1)$$

If the charge is a line segment of width W, along the z direction, we can easily do the integration, resulting in:

$$H_y(x, y, z, a) = \frac{\delta}{4\pi} \nabla \cdot M_1 \times \frac{(y-a)}{(x^2+a^2)} \left(\frac{W+z}{\sqrt{x^2+z^2+(y-a)^2}} + \frac{W-z}{\sqrt{x^2+z^2+(y-a)^2}} \right) \quad (2)$$

The charge density times the film thickness is exactly equal to twice the vertical component of the H field, so we use equation 2 to calculate the charge density in the medium.

The Williams-Comstock model assumes the transition contour is written where the trailing head field is equal to the remnant coercivity of the medium. The Williams-Comstock model assumes the competition between the field gradient of the head and the demagnetization effects of the transition results in an arc tangent transition perpendicular to the transition contour. At each point on the transition contour, magnetization is characterized by a local "a" parameter, where the magnetization is:

$$M(x) = 2 \frac{M_r}{\pi} \arctan\left(\frac{x}{a}\right)$$

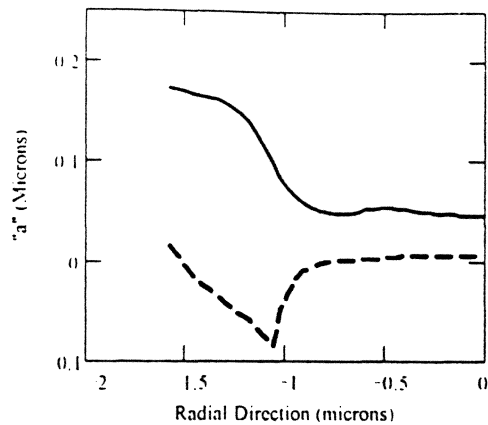


Figure 2 Williams-Comstock "a" (Solid), also shown contour of the transition (Dashed)

The divergence of M is:

$$\frac{dM}{dx} = \frac{2M_y}{\pi} \frac{a}{(a^2 + x^2)}$$

This is the same charge distribution which results from Equation (2) for an infinitely long charge. Therefore, we can think of the Williams-Comstock model as resulting from a sharp charge a distance "a" below the magnetic surface. This is the fundamental concept in Reference [1].

The write model is based on Reference [1], with several computational modifications. We assume we can break the written charges into two components: The first is the charge density written on the coercivity contour during the head field reversal (the transition charge), the second is due to the magnetization rotation left in the media as the head moves away from the transition. Figure 1 shows the field direction and constant field magnitude contours. Notice the field direction is largely perpendicular to the contour right of the "cusp" in the field magnitude contour, and left of the "cusp" the field direction has large components along the constant field contour. At the transition the charges

perpendicular to the field magnitude contour result in what we call the transition charge. After the head reverses direction, writing the charge transition, the head fields are dragged along until the next transition is written. The dragging head fields leave the in-plane magnetization pointing in the direction of the head field between the transitions. A magnetic charge results from the rotation of the magnetization in the direction perpendicular to the head motion. In these calculations a vector head field from a FEF calculation is used instead of the Lindholm field model of Reference [1]. Instead of the convolution integral in Reference [1] Equation (2) is used to calculate the charge densities and the vertical magnetic fields they produce.

First, we present the calculation of the transition charge.

The FEF calculation of the writing head field is used to calculate both the location in the media where the magnitude

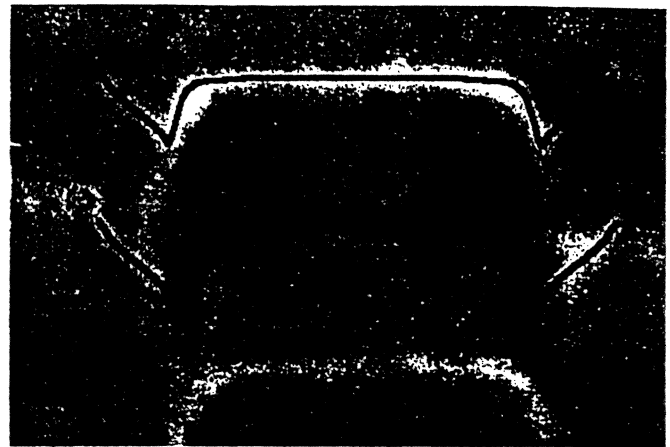


Figure 3 Isolated Transition MFM on DC-erased background Model contour overlaid on transitions.

of the in-plane trailing head field is equal to the remanent coercivity, and the direction of the head field along this contour. In the head model the P1 pole is much wider than the P2 pole. The head model is used to calculate the magnitude and gradient of the head field perpendicular to the coercivity contour. The field gradient is then used to calculate a local Williams-Comstock "a" parameter. The Williams-Comstock "a" parameter is calculated using the actual field gradient, rather than the Lindholm field used in the original paper. The local component of the head field perpendicular to the constant coercivity contour is combined with the local "a" parameter to calculate the transition charge density. Computation of the transition charge density is accelerated by breaking the transition into an equivalent set of line segments placed a local distance "a" below the surface, as in Equation (2). The charge on the line segment is twice the magnetization times the cosine of the head field angle with respect to the perpendicular to the contour. For each line segment this model has two independent components, local "a", and the magnetization divergence.

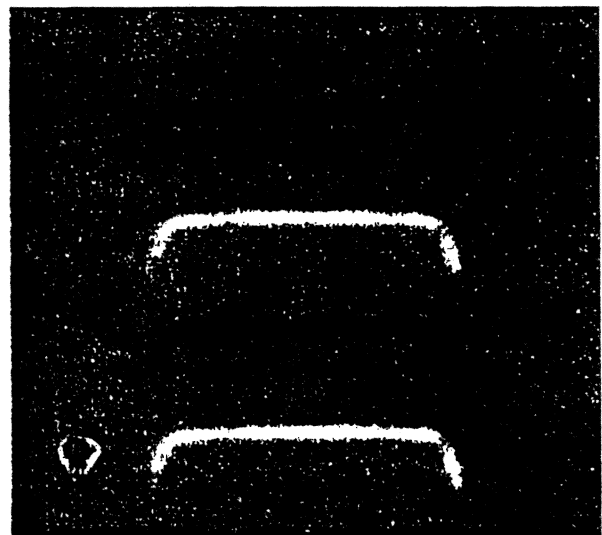


Figure 4 Simulated Isolated Transition MFM

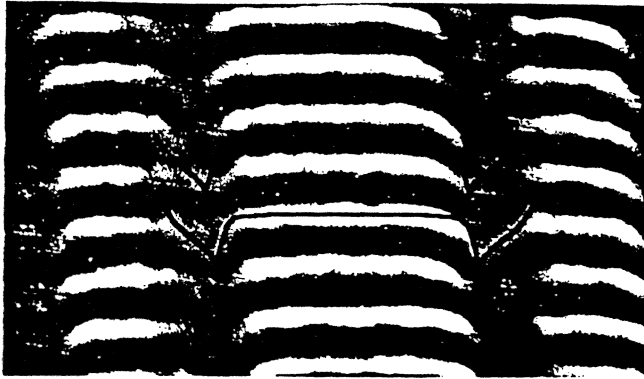
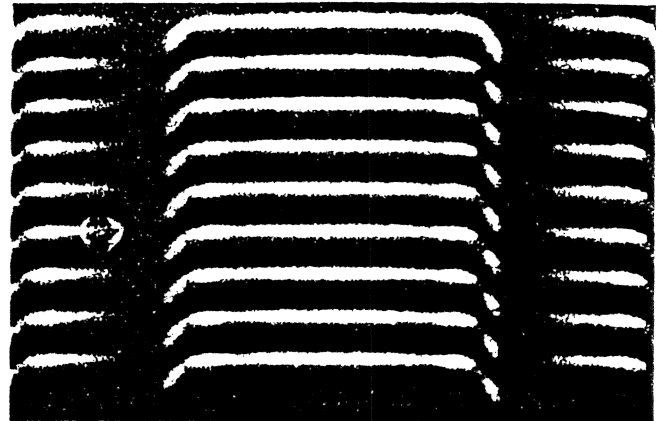


Figure 5 Three Tracks with center track overlaid.

components, local "a", and the magnetization divergence. The components in Equation (2) are rotated for each line segment of charge. In addition to the charge distribution we get the H_y field from the media. dH_y/dy can be easily calculated by differentiating Equation (2) with respect to y and summing over line segments of the constant coercivity contours. The rotation charge is calculated in a similar method to the transition charge. The head field gradient perpendicular to the head motion is used to calculate a Williams-Comstock "a". The rotation charge left in the media is dH_z/dz . For media magnetization M_r , and the head field perpendicular to the direction of motion, H_z , the divergence in Equation (2) is set equal to $M_r \cdot (dH_z/dz) / H_z$. The integral in Equation (1) can then be approximated by a sum of $dx \cdot$ Equation (2) where the line charges are in the direction of motion.

MFM's are set to measure either H_y or dH_y/dy . dH_y/dy is easily calculated by taking the derivative of Equation (2) and then setting y to the tip height above the surface. The charge density of the media is calculated by setting $y = 0$.

Figure 2 shows the local "a" parameter and the constant coercivity contour. Notice to the left of the cusp the "a" increases. This is the result of the low head field gradient perpendicular to the contour. A large "a" results in a diffuse effective charge, and a low charge density, and hence the erase band. The large "a" is a result of the head fields having large components along the coercivity contours. A second contributor to the erase band is the magnetization rotation to the outside of the cusp of the transition region. Figure 3 shows an isolated track MFM measurement with the constant field magnitude contour equal to the medium coercivity. Figure 4 shows the simulation of the MFM by plotting the dH_y/dy fields and assuming the tip is 30 nm above the surface. The image simulation is not convolved with a tip transfer function. Figure 5 shows the MFM scan of the high density triple track pattern and the erase band overlaid with the constant coercivity contour. Notice that the contour is consistent with the observed erase band in the media. The field contour accurately predicts the charge



density contour and the erase band. Figure 6 is the simulation of the triple track measurement. Figure 7 shows the direction of the magnetization, the constant coercivity, and lines delineating the "erase band" and the "transition charge". In this model the erase band results from the same constant field magnitude contour, however, as the simulation shows, since the effective "a" parameter is large and the magnitude of the local gradient of M is small (a result of the field lines not being perpendicular to the transition), the resulting charge in the erase band region is small. In addition, if the head is skewed, the erase band on one side increases while the other side it decreases, consistent with the measurements in Reference [2]. The asymmetry in the charge density resulting from skewing the head is discussed in Reference [3].

REFERENCES

- [1] T.C. Arnoldussen, I.L. Nunnelley, R.P. Ferrier, F. Martin, "Side Writing/reading in magnetic Recording", *J. Appl. Phys.* 69, April 15, 1991 pages 4718-4720.
- [2] Kurt Wiesen, Richard M. Lansky, and Charles Sobey, "Recording Asymmetries at Large Skew Angles" *IEEE Trans. Magn.*, Vol. 29, NO. 6 November 1993, pages 4002-4003.
- [3] Thomas Chang, Mike Salo, Hao Fang, Mike Madison, Jian-Gang Zhu, and Tom Arnoldussen, "Affects of Skew Angle on the Written-in Base Line Shift Signal at High Track Densities", *IEEE Trans. Magn.*, in press.

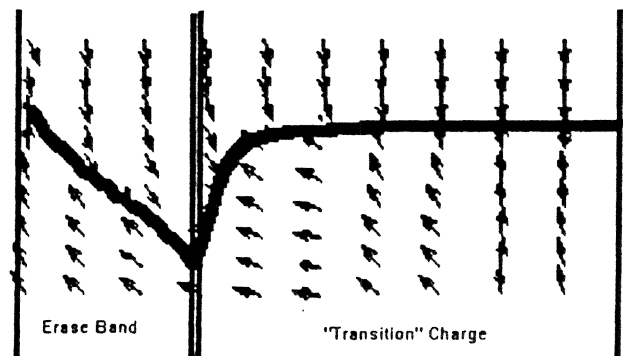
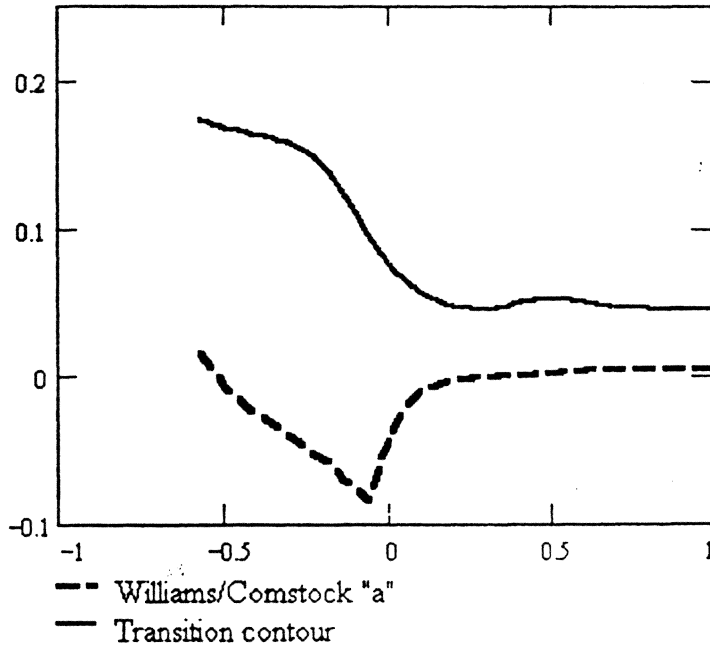
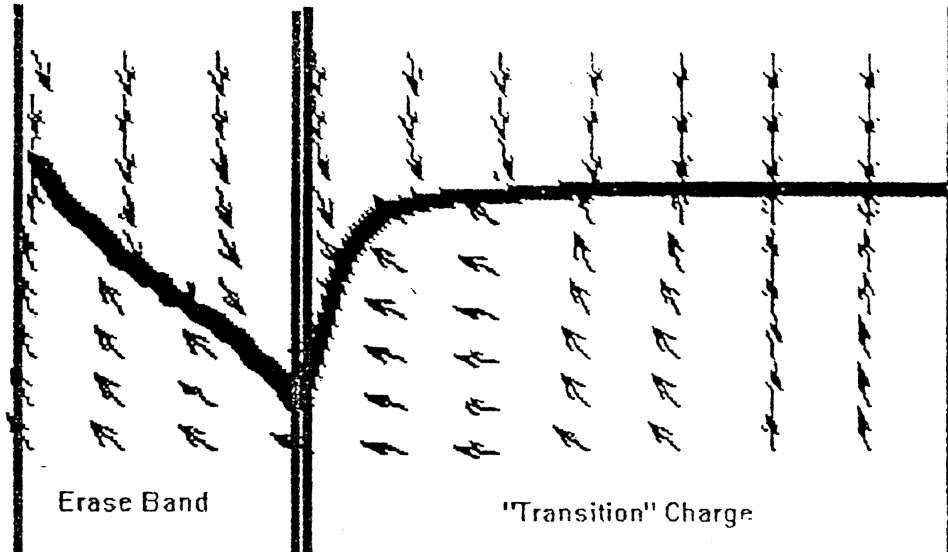
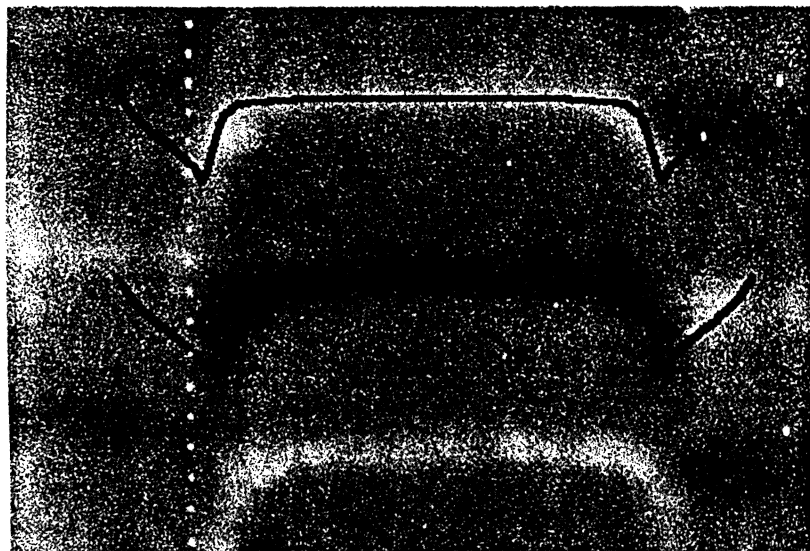


Figure 7 Magnetization vector field at a transition. "Erase band" and "Transition Charge" sections of the constant coercivity contour delineated

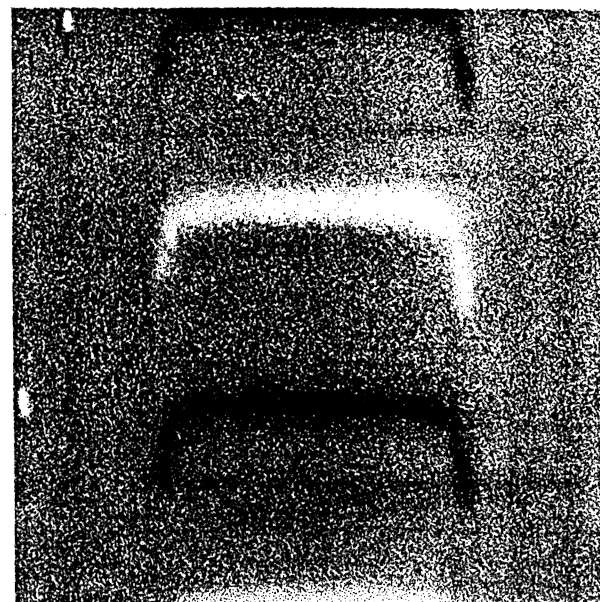
Erase Band



MFM - Experiment and Simulation Low Density

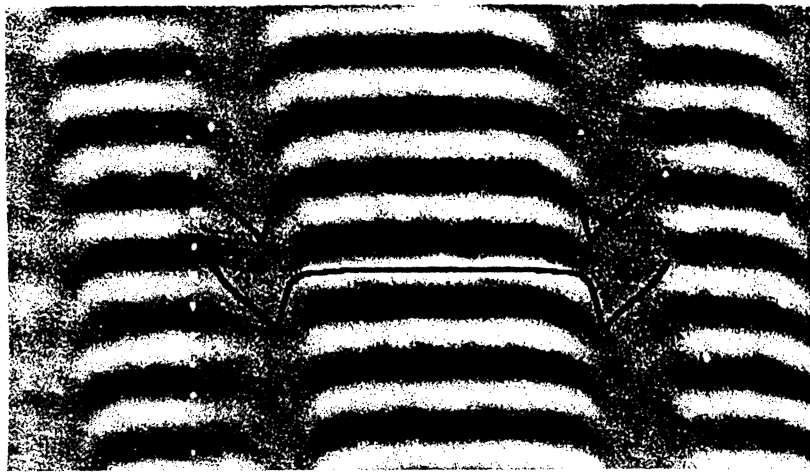


Isolated Transition MFM on DC Erased Background. Model contour overlaid on transitions.

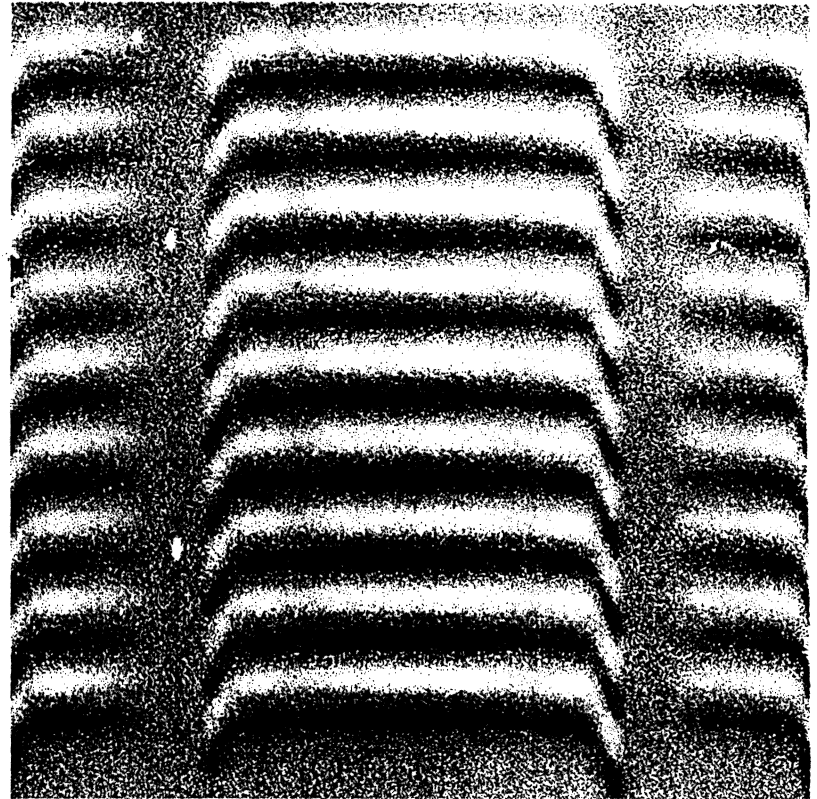


Simulated Isolated Transition MFM.

MFM - Experiment and Simulation Triple Track.

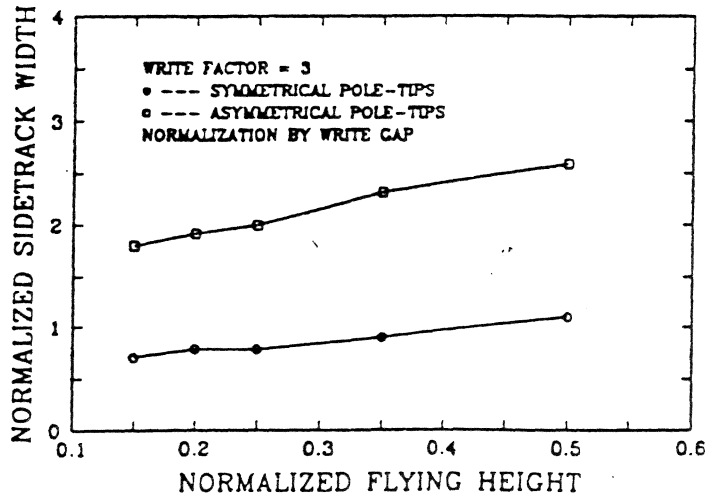


Three Tracks with center track overlaid. Model transition contour overlaid on transitions.



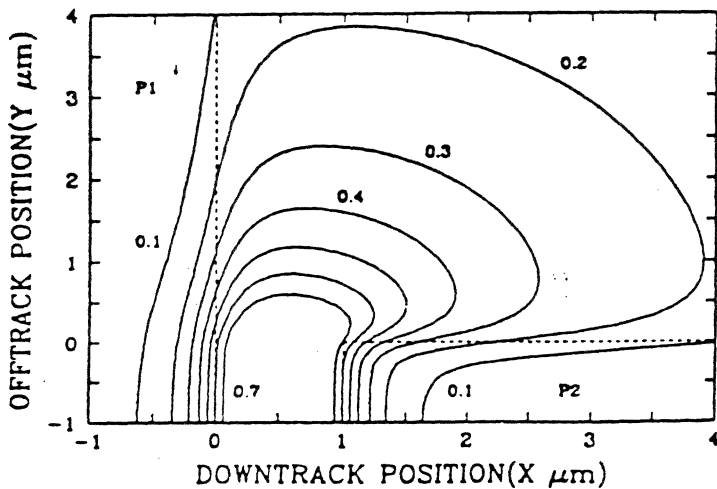
Simulation of MFM high density Triple Track.

II) Reduce head pole asymmetry.

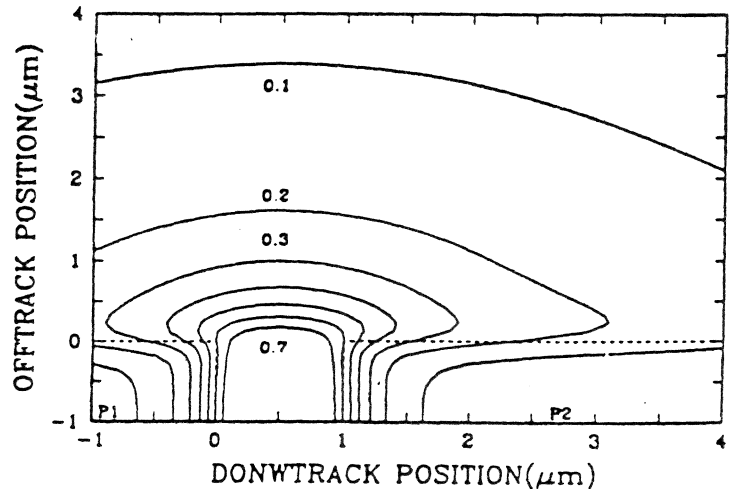


Sidetrack width vs flying height for symmetrical and asymmetrical heads.
(Ching Tsang)

Note that reducing head-disk spacing does not have much effect. However, **reducing pole-tip asymmetry** reduces side-track width considerably.



a) **Non-Ideal case** (unequal P1 and P2)
The contours are highly asymmetrical about the gap center & extend further into side track



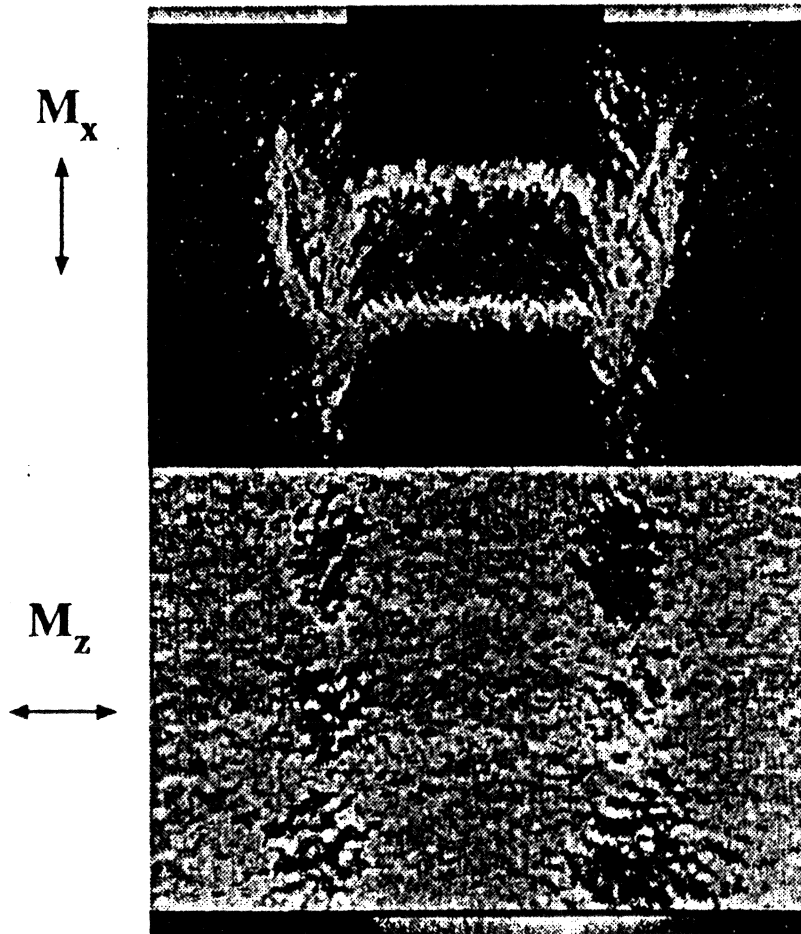
b) **Ideal case** (equal P1 and P2)
Here 0.3 contour, e.g., extends only 0.1 μm , vs 2.4 μm of non-ideal case.

Conclusions:

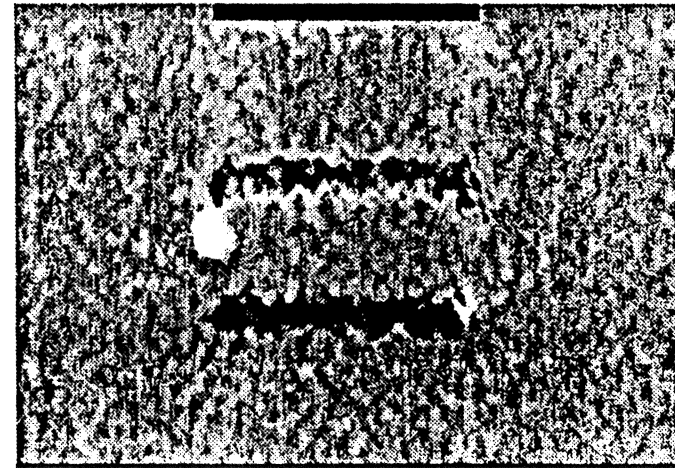
- 1. Erase bands results from the large effective “a” parameter, a result of the field lines not being perpendicular to the transition.**
- 2. MFM’s are effective in evaluating Model.**
- 3. Contours show why head skewing results in asymmetrical erase bands.**

Side Writing in Isotropic Longitudinal Thin Film Media

Magnetization Pattern



Magnetic Pole Density

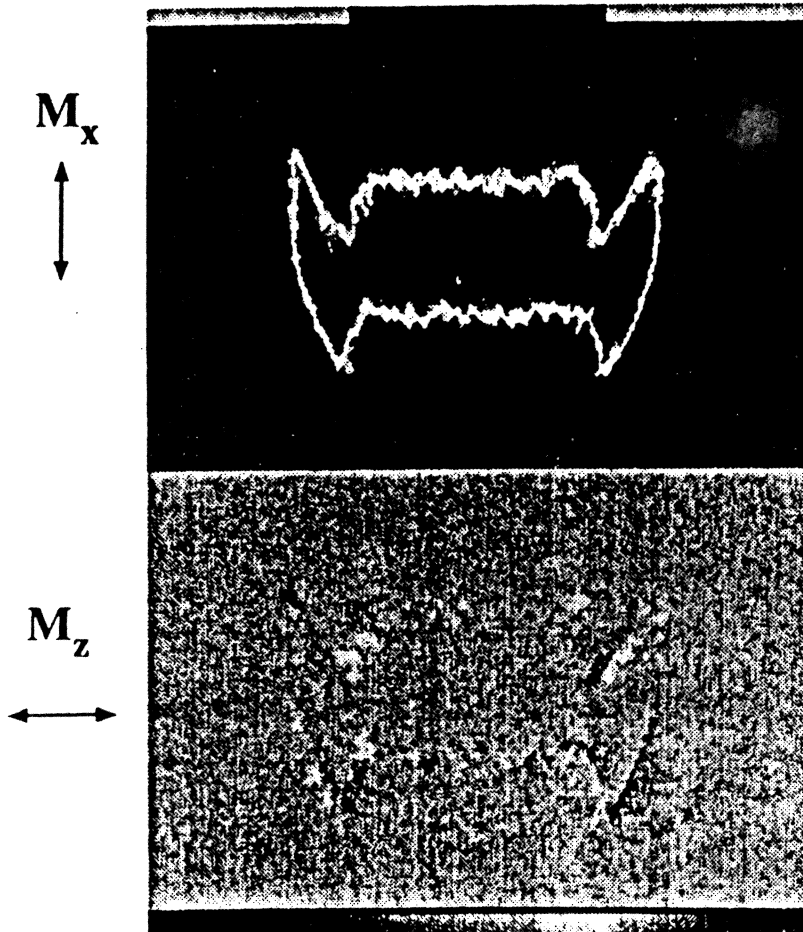


$\nabla \cdot \mathbf{M}$

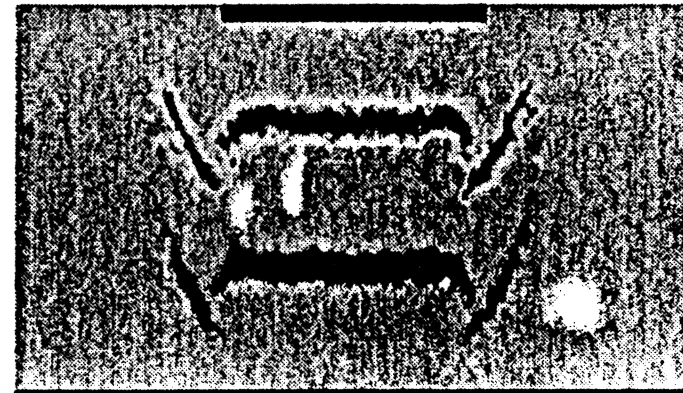
- No edge transitions in side-written band
- Side-written band behaves like an erase band
- Edge erase band suppresses intertrack interference.

Side Writing in Well Oriented Longitudinal Thin Film Media

Magnetization Pattern



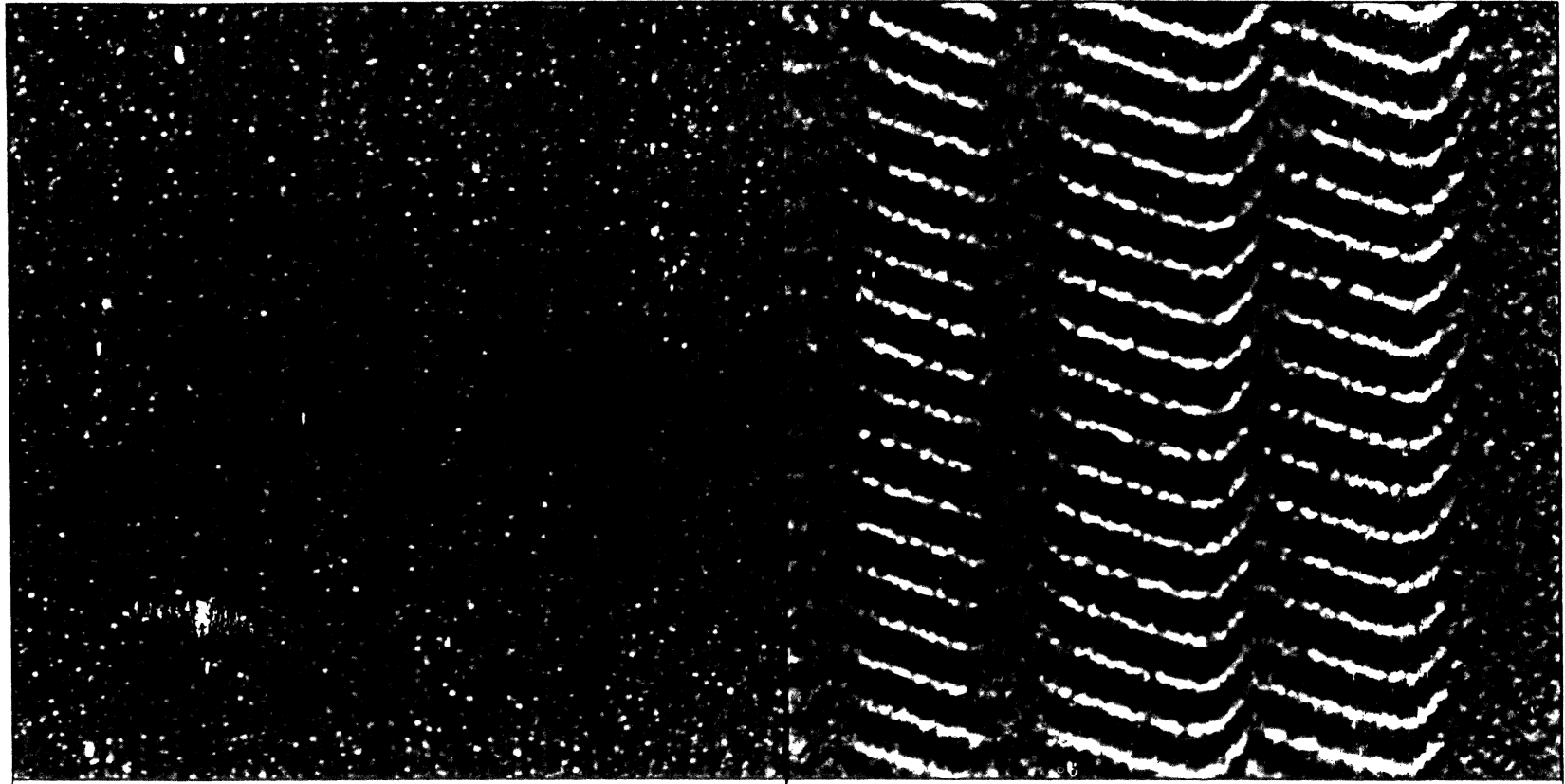
Magnetic Pole Density



$\nabla \cdot \mathbf{M}$

- Edge transitions in side-written band
- Edge transitions introduce phase shift
- Edge transitions enhances intertrack interference.

LSDMAFM Images



0

Data type
Z range

Height
30.0 nm

10.0 μm 0

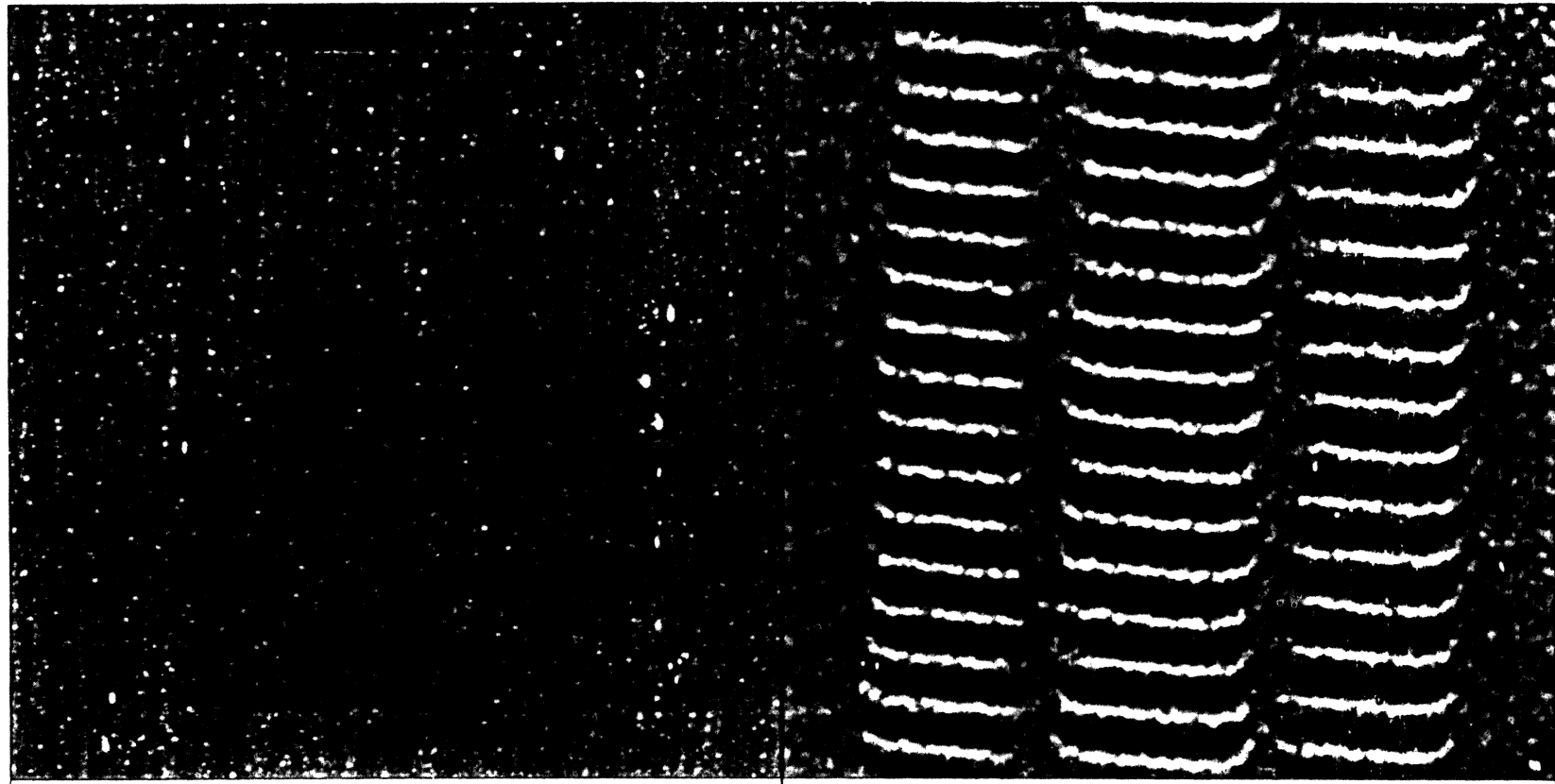
Data type
Z range

Phase
8.00 de

10.0 μm

c12od1tt.002

LSDMAFM Images



0

Data type
Z range

Height
30.0 nm

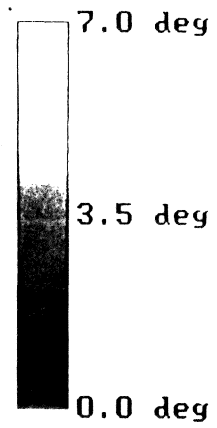
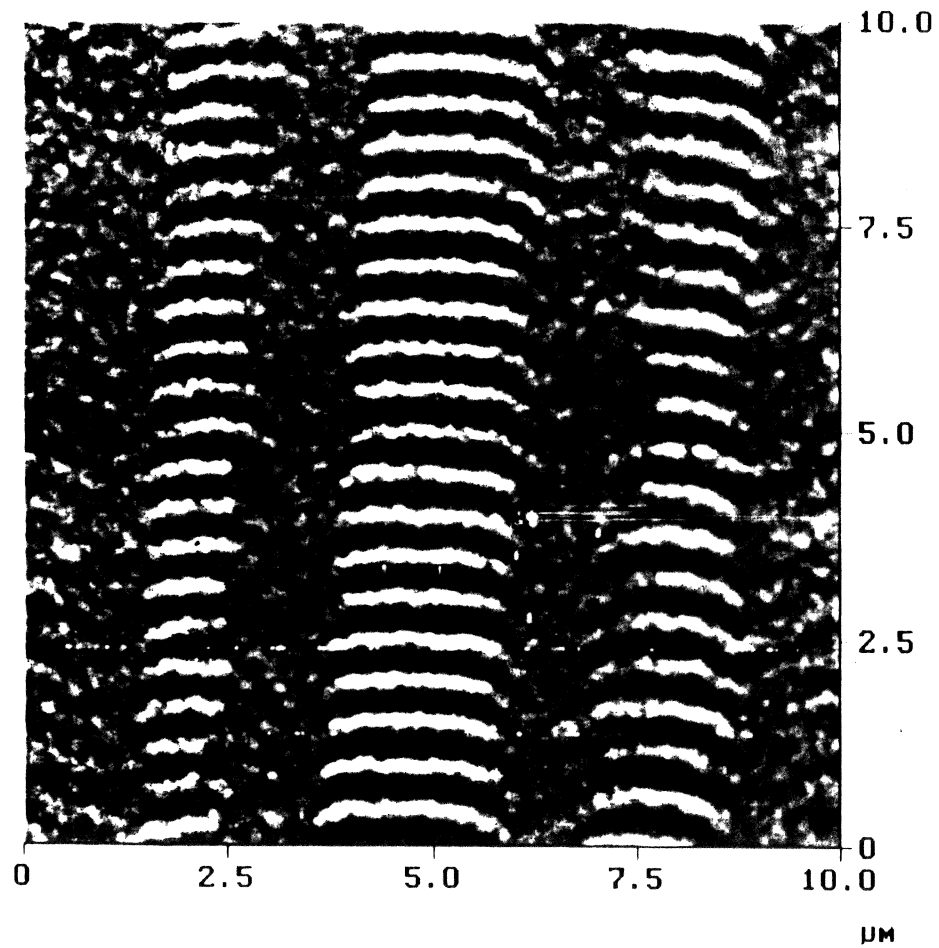
10.0 μm 0

Data type
Z range

Phase
8.00 de

10.0 μm

c12id2tt.002



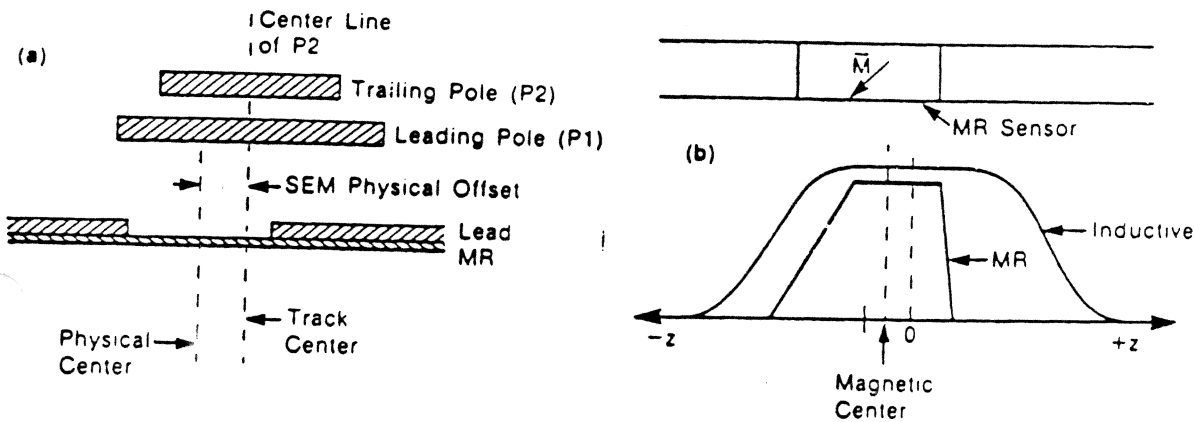
NanoScope		LS_DM_AFM	
Scan size		10.00	μm
Setpoint		1.608	V
Scan rate		1.489	Hz
Number of samples		512	

c1fpidx.003

IV) Off-track Performance

This is characterized by the distance the head can move off track before some specified unacceptable error rate is reached.

- It is affected by read-to-write head alignment.

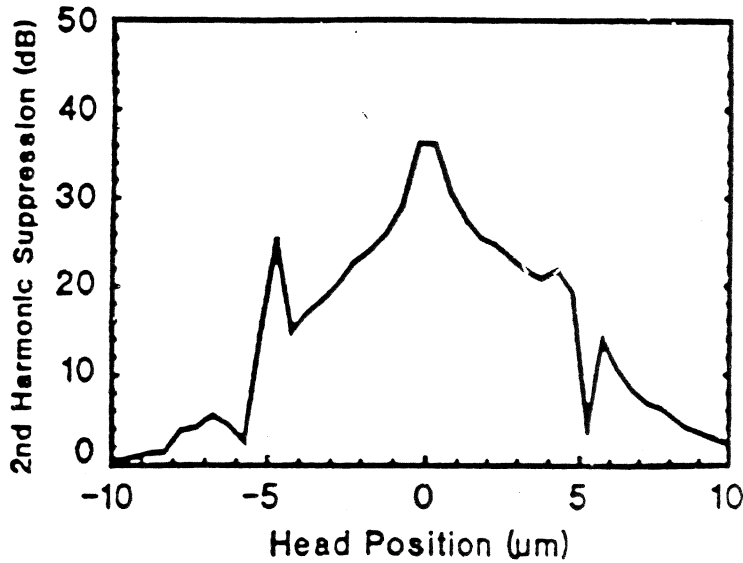


- Note that some well-controlled, **intentional** read/write *offset* which compensates for 'magnetic center' shift *may be necessary*, as is indicated above. However, too much misalignment can be detrimental.
- Excessive **misalignment** can lead to:

a) additional **mechanism for track misregistration (TMR)**.

b) **reduced signal amplitude** (due to anisotropic flux propagation along the directions perpendicular to bias magnetization in MR stripe).

◆ Second harmonic suppression is also strongly a function of head position:

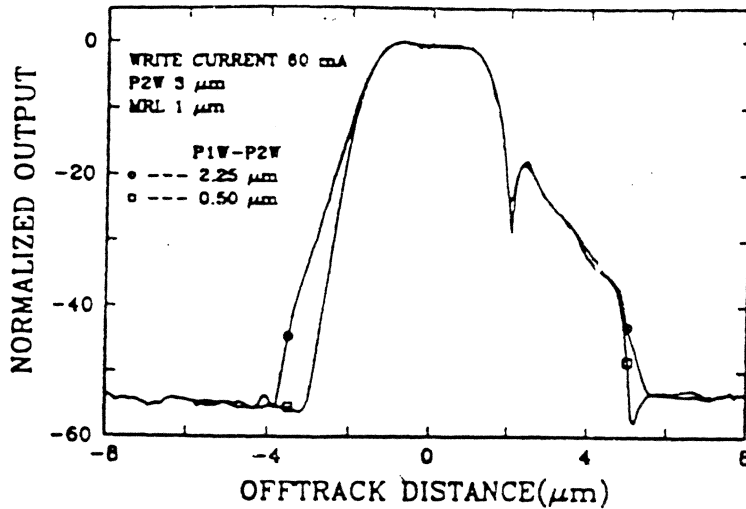


Second harmonic suppression of a 4 μm DSMR read/4.5 μm write head with respect to cross-track position. Linear density=10 kfc/i.

- Keep the flux into the stripe low to avoid saturation.
 - a) Keep **Mrt** low, and
 - b) keep **gap thickness** low. This is limited by sensor-to-shield shorts.

These also improve resolution.

- Keep sensor stripe thickness high, therefore, need more flux to saturate the stripe (this may reduce amplitude and resolution).

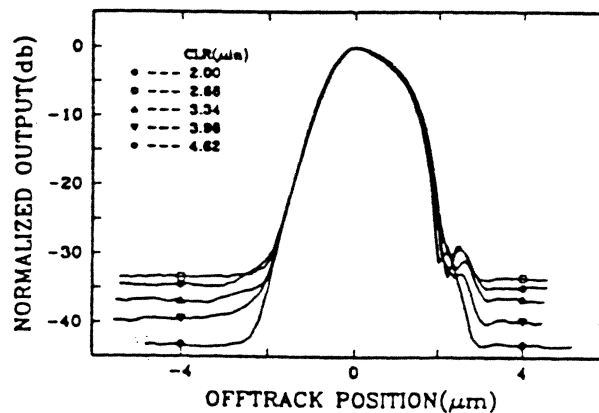


Track profiles of normal vs ion-milled gigabit write heads.

Reducing the upper pole tip to lower pole tip difference to 0.5 μm significantly affects the signal profile (broadening) below -20 dB. (C. Tsang)

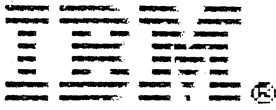
b) Read-head resolution:

- For a shielded MR head the track resolution (ability to resolve closely packed tracks) is limited by the **side reading behavior** of the sensor. (flux from the neighboring tracks is guided from the tail of the sensor to the center).



MR head microtrack profiles for different head-disk clearances.

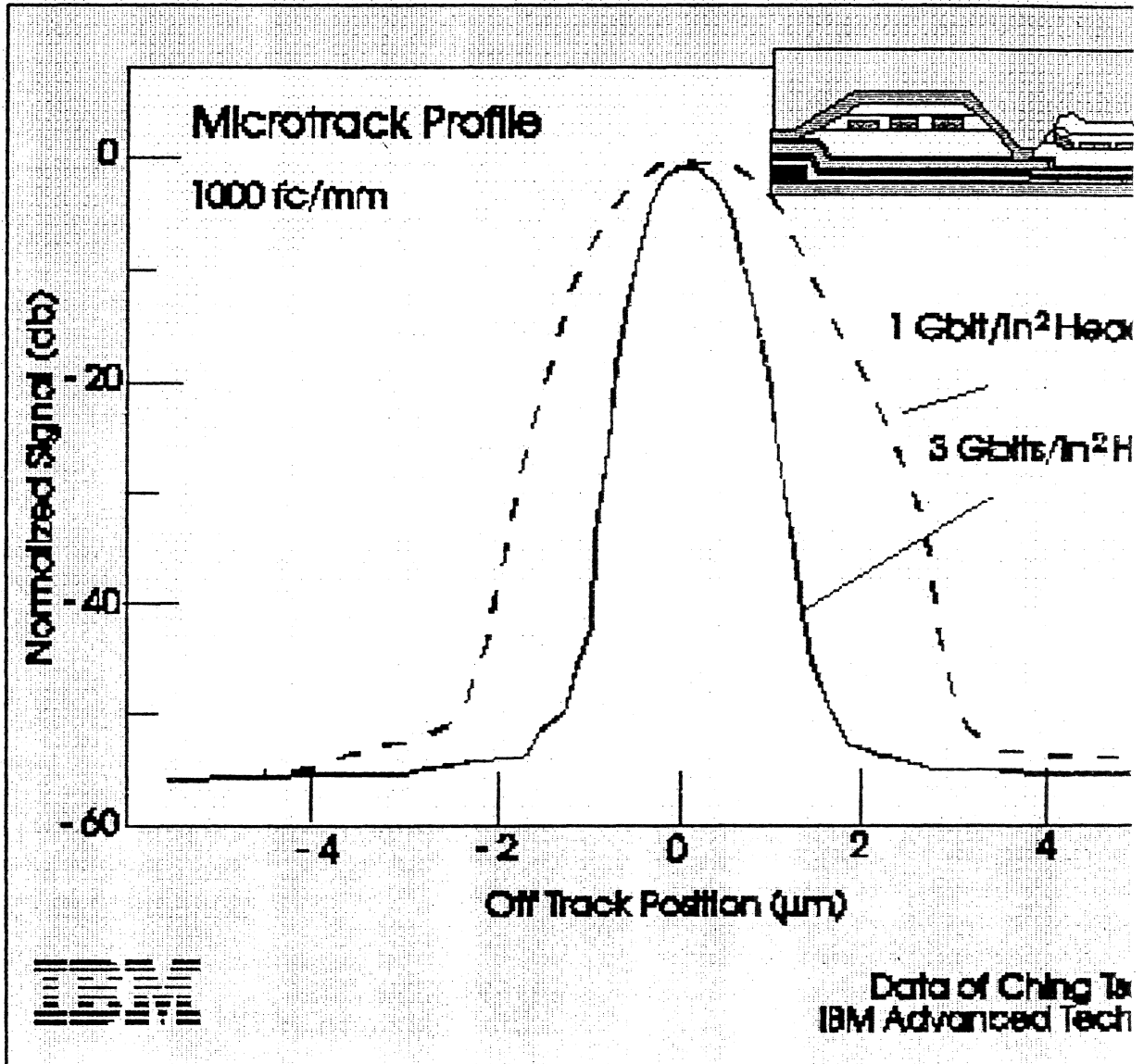
Evidently, the width of track profile is not much affected by flying height. It is better to use *short MR sensors* => may run into domain noise problems. Alternatively reduce permeability of the tail regions (P.E.B).



Storage

© 1995 IBM Corporation

ORCHARD HILL ALABAMA



NEW YORK

(A larger version of this illustration is available.)

The signal amplitudes across a track for the one- and three-gigabit-per square-inch heads indicate how narrow the track profiles are for these advanced MR heads . Three billion bits per square inch will result in a data track profile roughly two microns from the center. IBM leads the world in the manufacturing

Servo: Track Following Seeking

Head Positioning

Two requirements on head positioning:

Track Following

- Sources of track position variation
 - spindle bearing runout
 - disk deflections
 - electronics
 - servo samples
 - erase bands
 - hooks
- Mechanical disturbances
 - windage
 - carriage bearing friction
 - vibration and shock

Track Seeking

- For minimum access time
 - use maximum power
 - max accel / max decel
- bang-bang servo
- design involves choosing switch point.

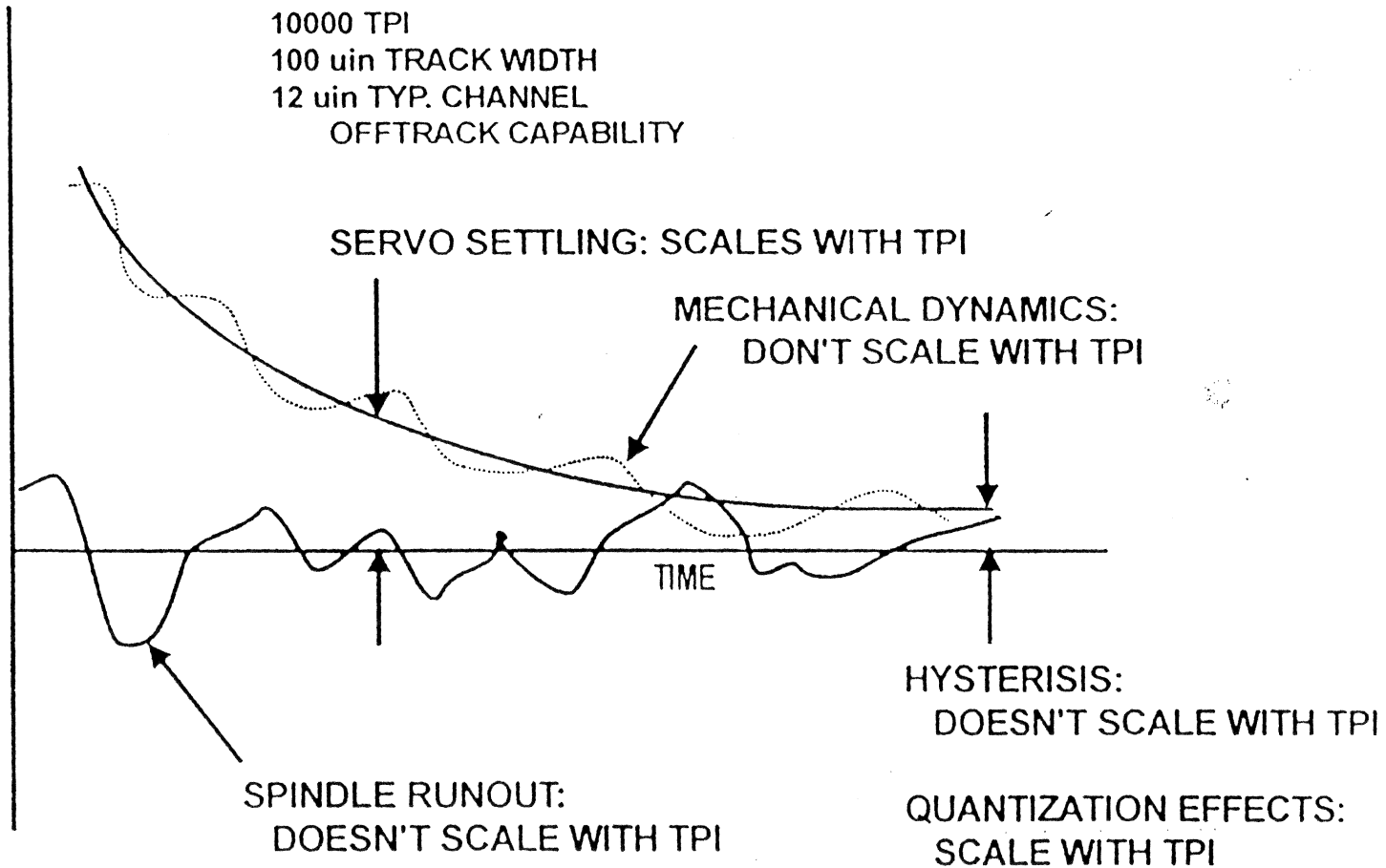
Importance of Servo System

- o Access Time
- o Track Density
- o Positioning accuracy
- o Robustness and Reliability

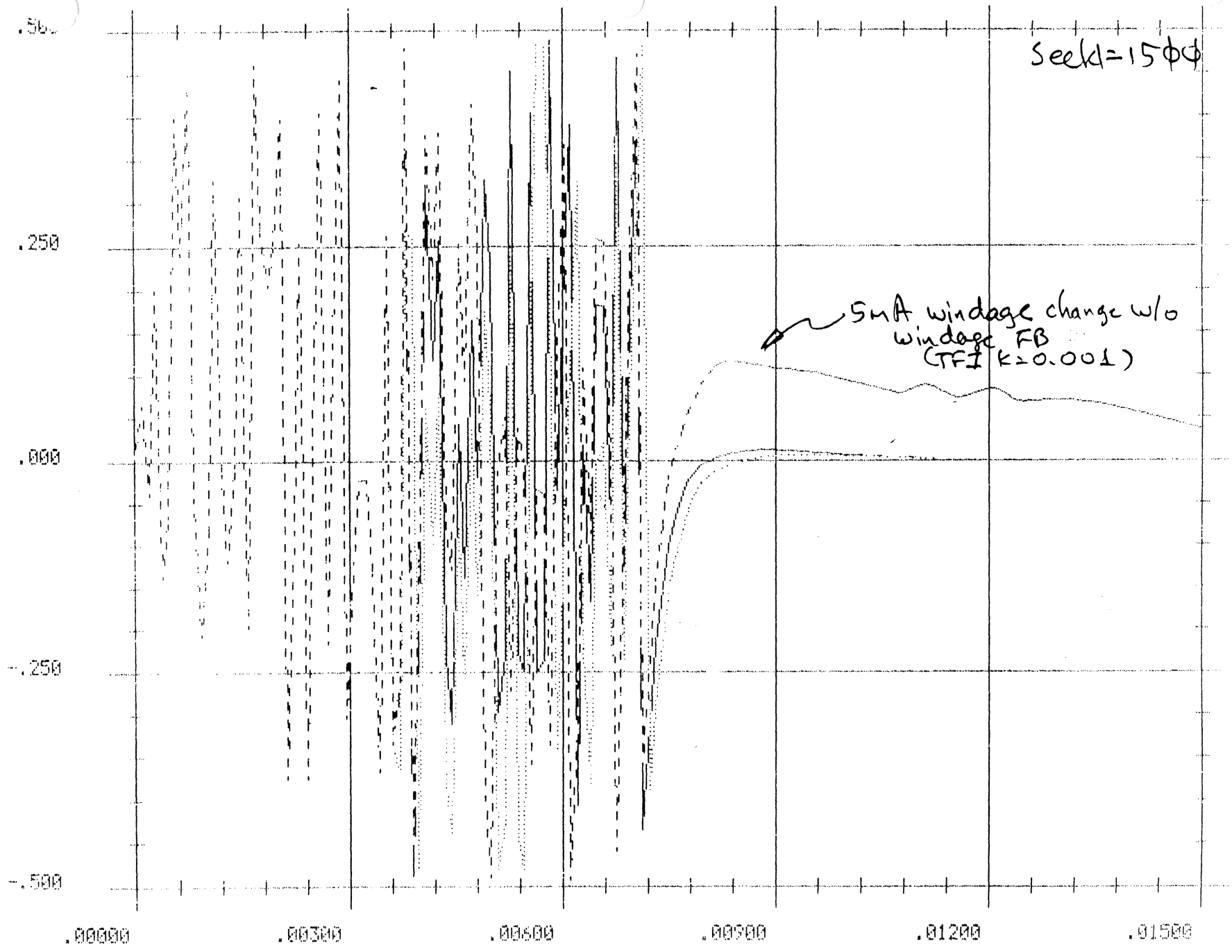
TRACK MISREGISTRATION SOURCES

POSITION

MID 1998
10000 TPI
100 uin TRACK WIDTH
12 uin TYP. CHANNEL
OFFTRACK CAPABILITY



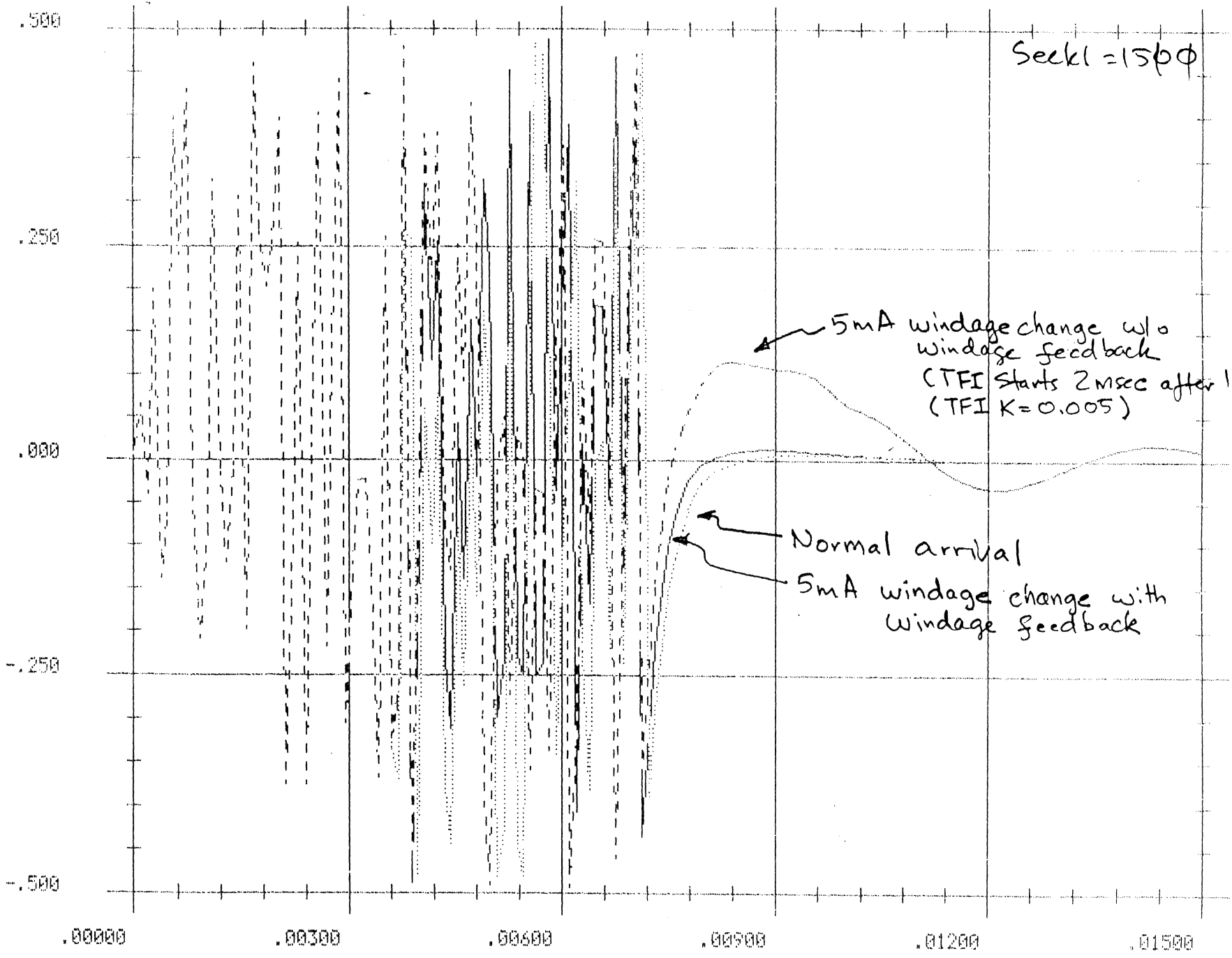
PES RAMP (track)



July 11, 1994

Time (sec)

YES RAMP (tracks)



Seek1 = 1500

5mA windage change w/o windage feedback
(TFI starts 2msec after 1/2 trk)
(TFI K=0.005)

Normal arrival

5mA windage change with windage feedback

July 11, 1994

Time (sec)

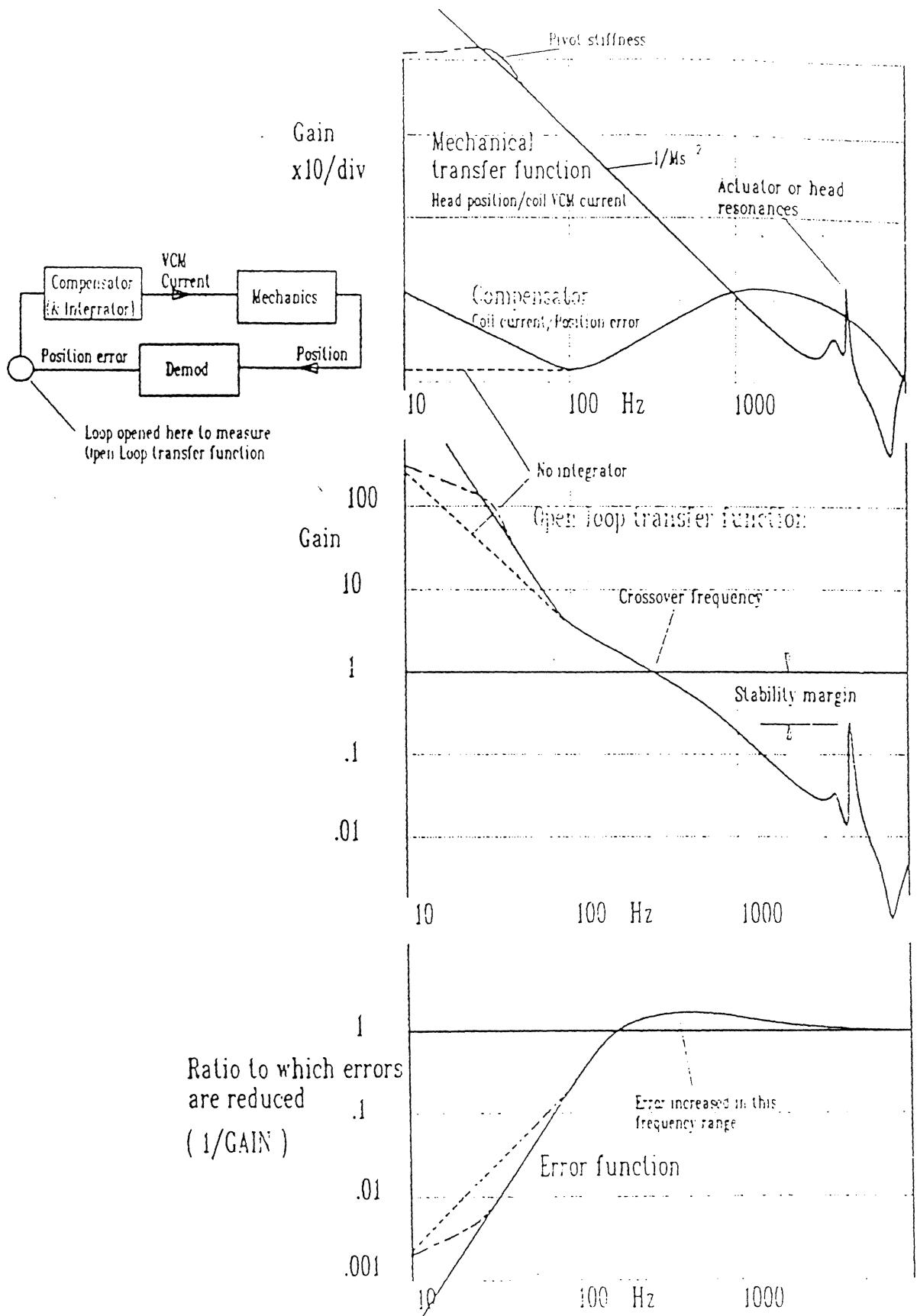


Figure 8. Mechanical and Servo system transfer functions and gain.

Shows mechanical and compensator (electronics) transfer functions. The product of these two is the open loop transfer function, which is drawn to show the potential gain limit due to resonances. The error function (inverse of open loop tfn at low frequencies) is also shown in fig 9

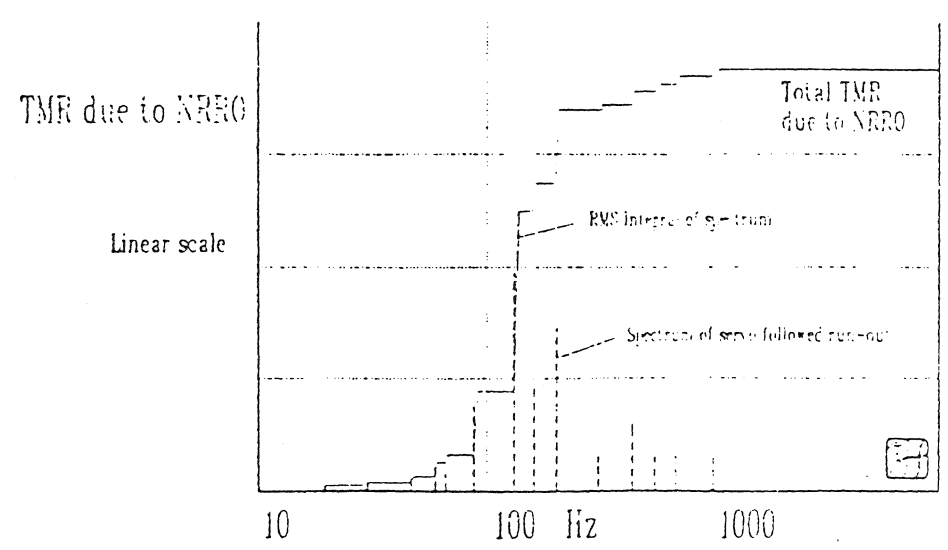
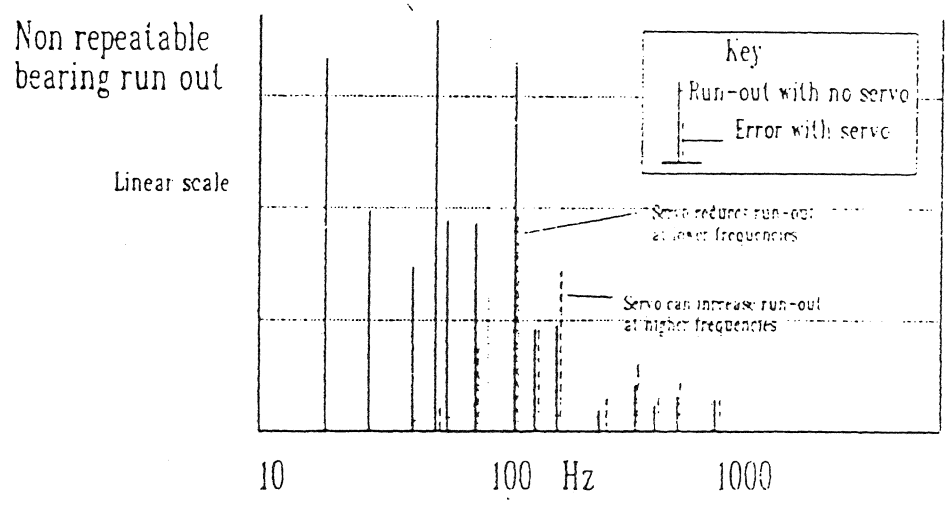
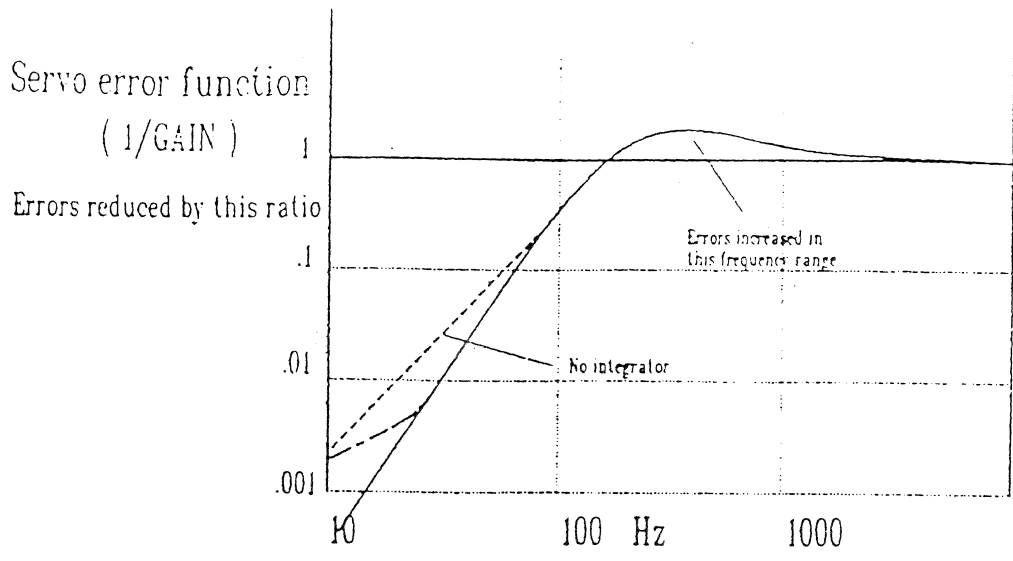


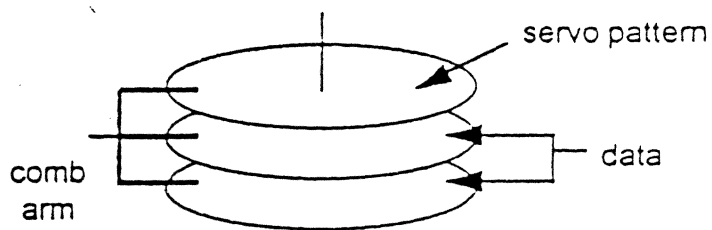
Figure 9. How Gain determines TMR of mechanical disturbances

Bearing non-repeatable run-out is used as an example to show how the servo reduces run-out and also what the limitations are. The same methodology is used to optimise the servo to reduce the other vibrational disturbances of head tracking.

Head Positioning

Open Loop

- Low Cost



Servo

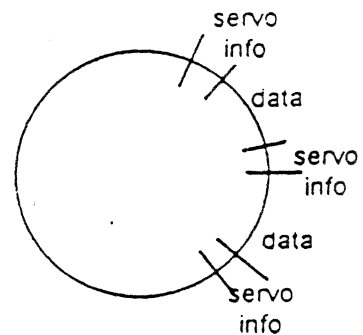
- Dedicated

- Issue - cascaded mechanical & thermal tolerances

- Embedded

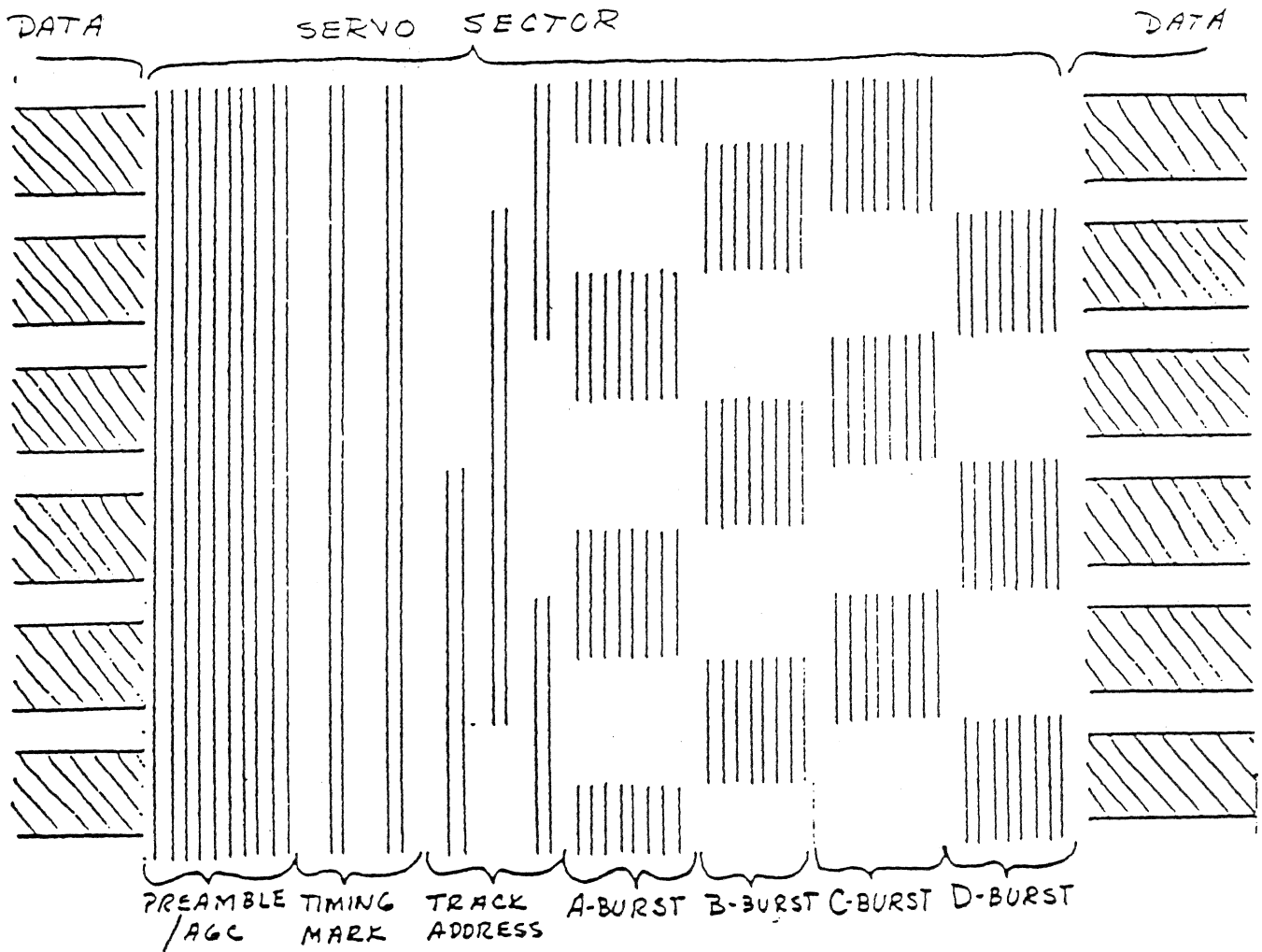
» Sector

- Issues - Open loop when R/W
- real estate
- slew rate
- tolerance to disk defects



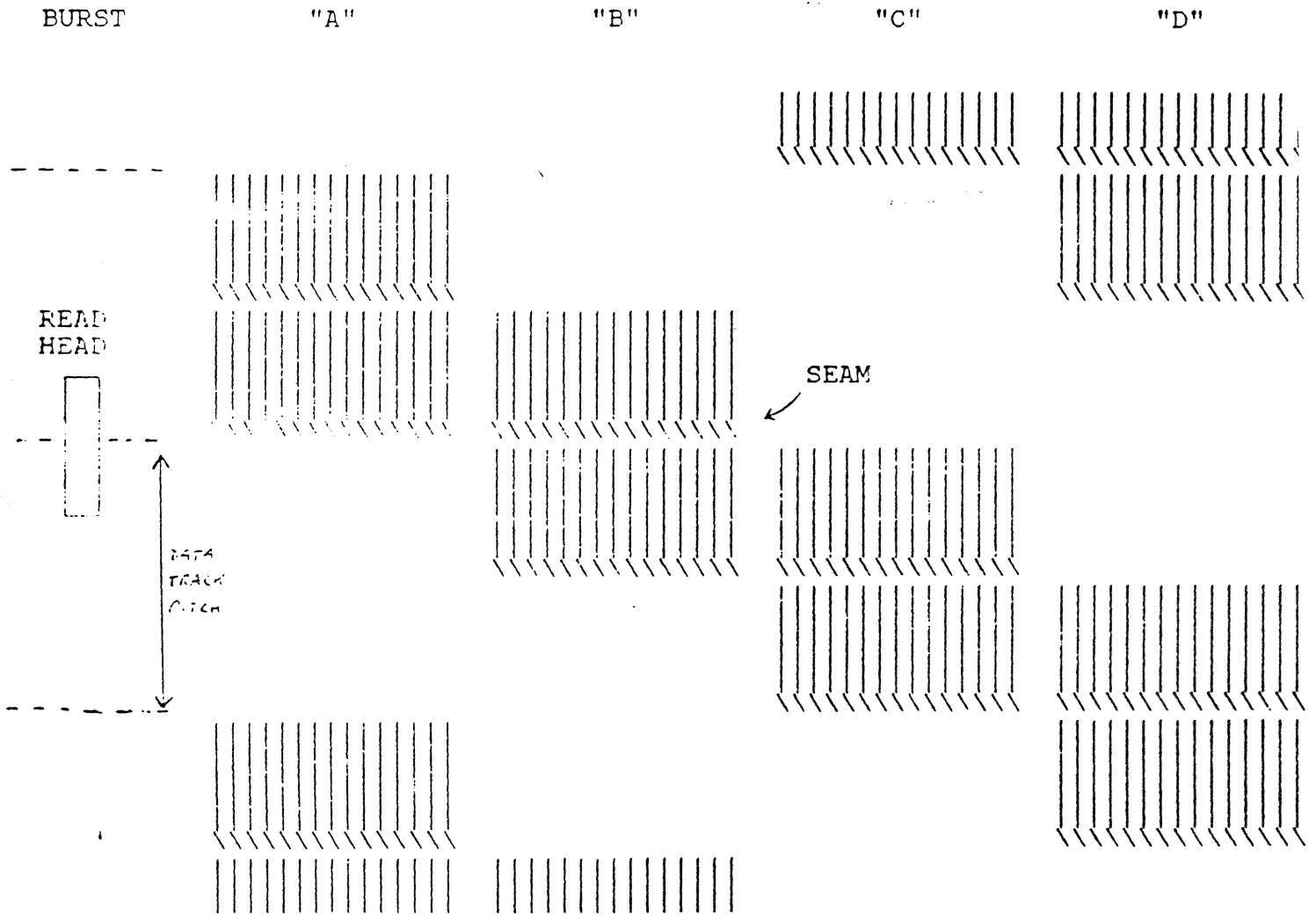
» Continuous

- Issues - Source of PES (Position Error Signal)
- disk fabrication
- sensor
- servo while write



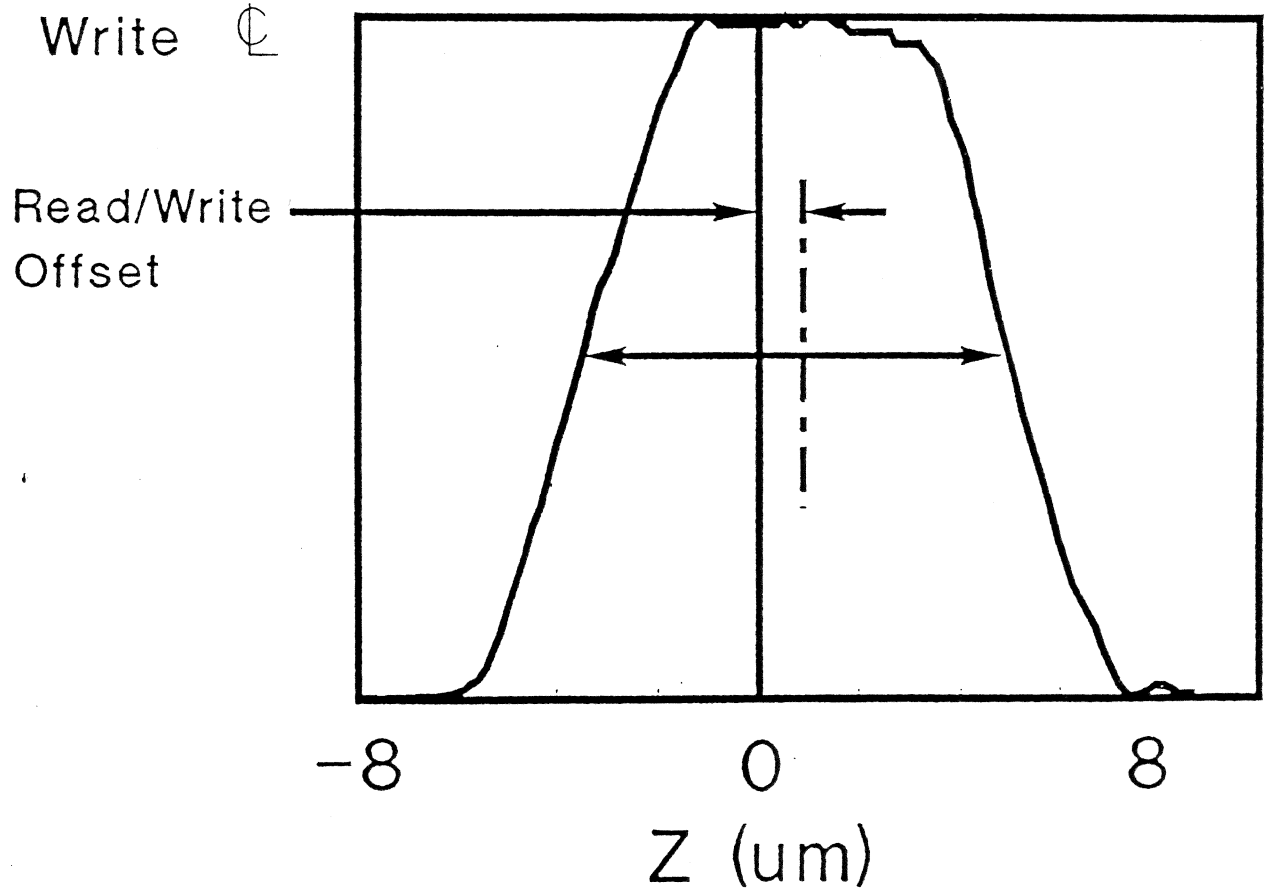
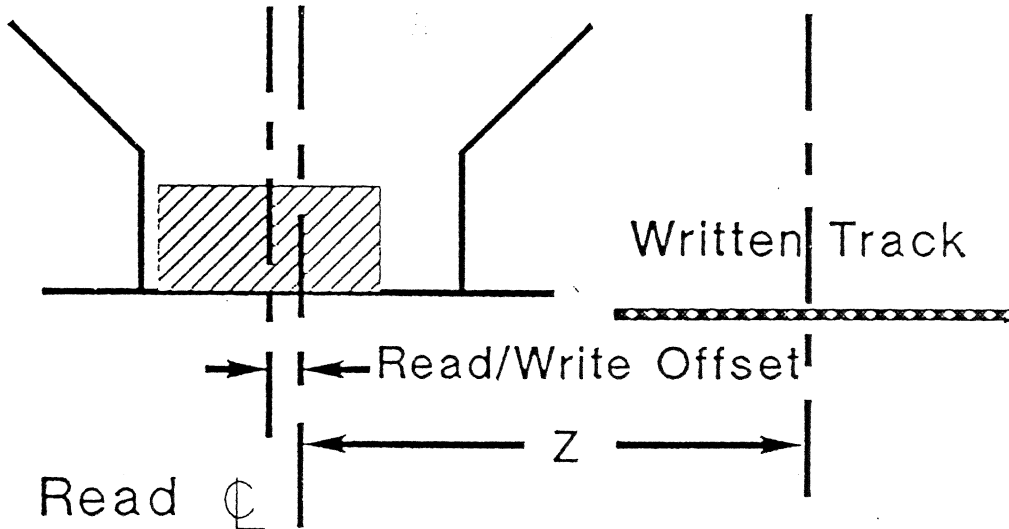
NORMAL AND QUADRATURE SERVO

QUAD-BURST PATTERN

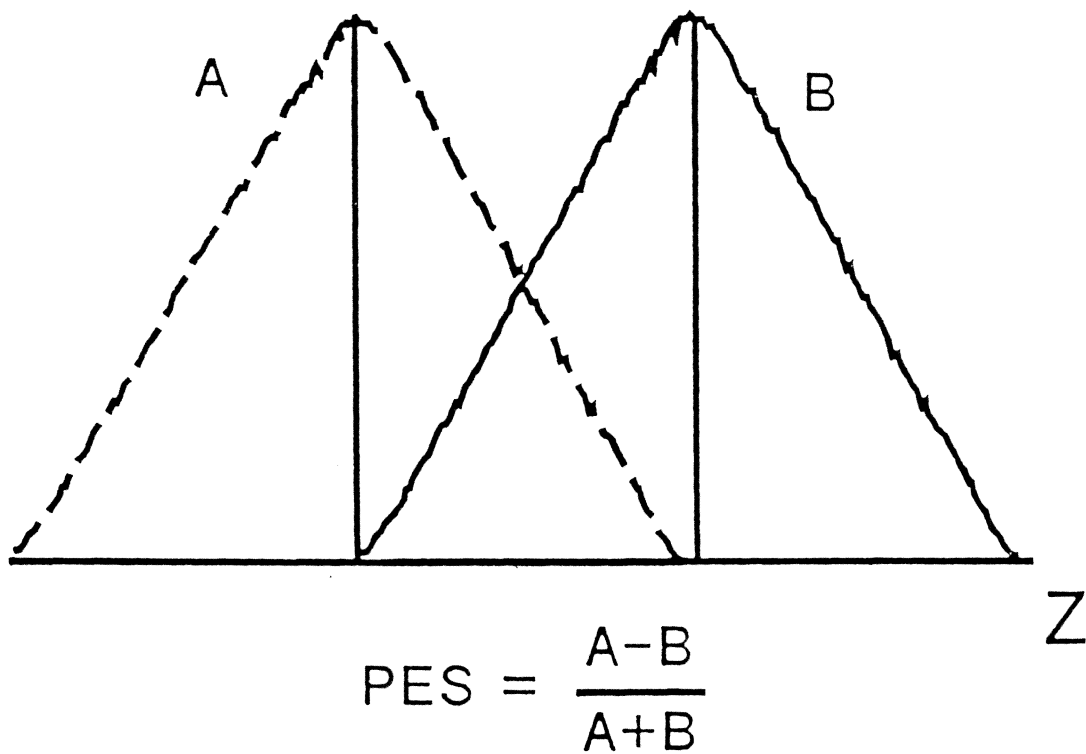
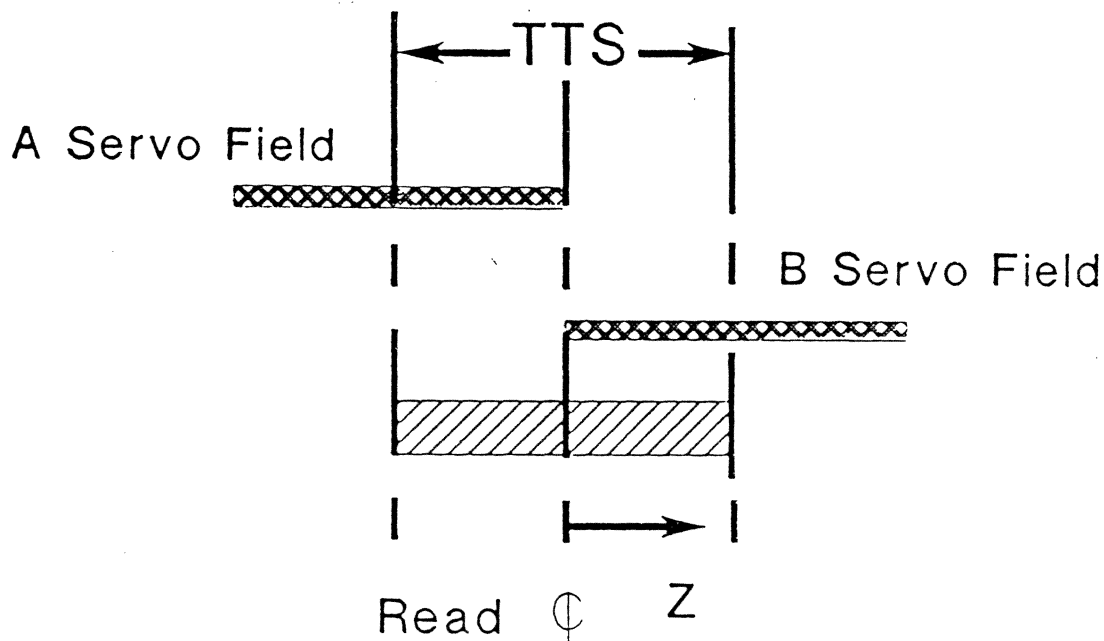


SERVO LOOP SEEKS TO MAINTAIN "A" AND "C" BURST THE SAME SIZE

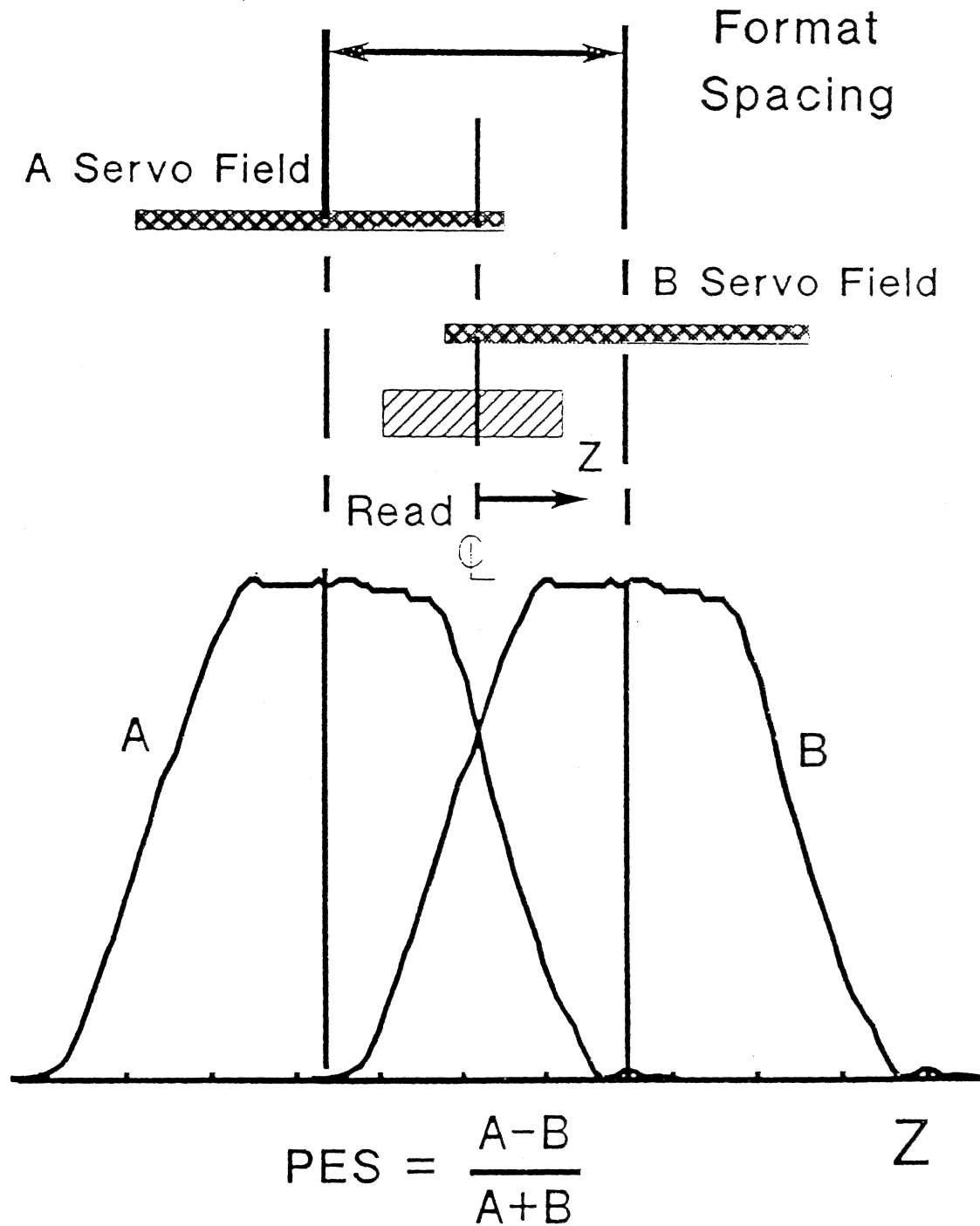
Read/Write Cross Track Capability Track Scan



Read/Write Cross Track Capability Servo

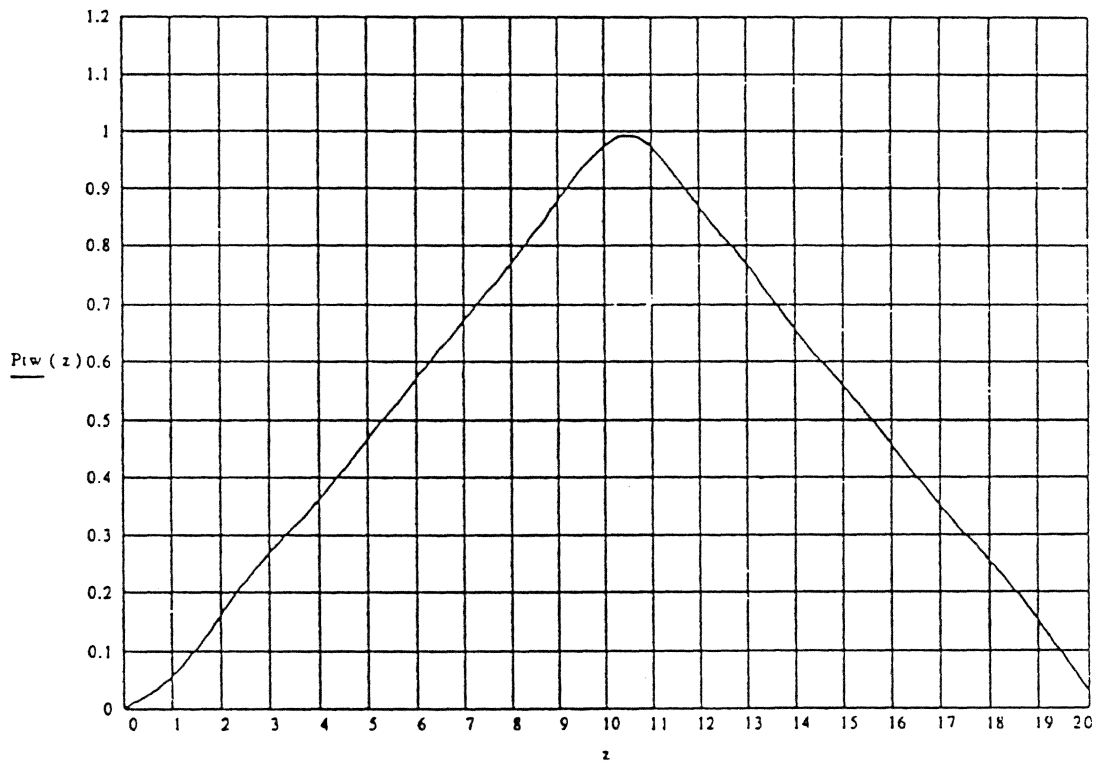


Read/Write Cross Track Capability Servo



Cross Track Scan

Thin Film Inductive Head



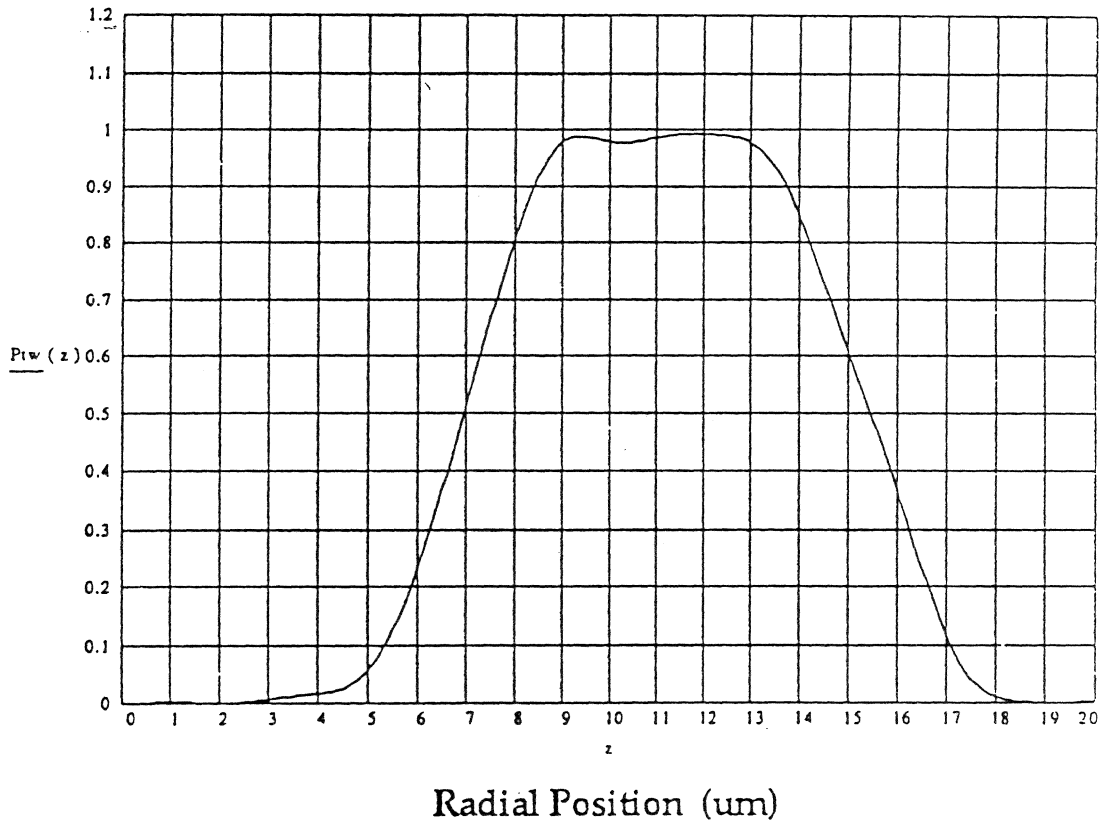
Disk Memory Division
VIST92A.GAL

R. Simmons
11/14/92



Cross Track Scan

Dual Stripe Magnetoresistive Head



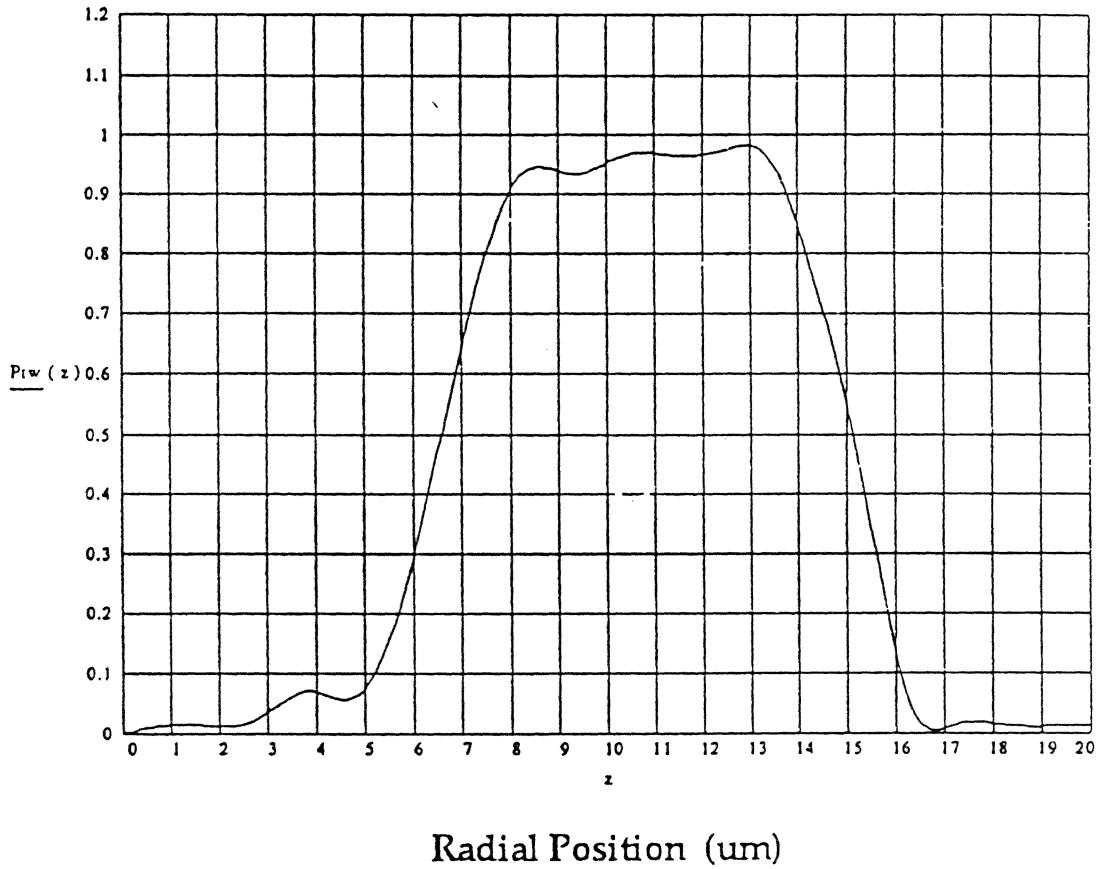
Disk Memory Division
VIST921.GAL

R. Simmons
11/14/92

 HEWLETT
PACKARD

Cross Track Scan

Single Element Magnetoresistive Head



Disk Memory Division
115T921.GAL

R. Simmons
11/14/92



**Track
Misregistration
(TMR)**

TMR - Track Misregistration

- "Static"

- o Thermal expansion
- o Creep
- o Loose Parts
- o Shock Damage
- o Servo Positioning Errors
(can be multiaxial)

- "Dynamic"

- o Seek arrivals and overshoots
- o NRRO, non-repeatable runnout
- o External Vibration
- o Resonances (Mechanical or Electrical)
- o Interference from other drives
- o Electrical noise
- o Magnetic center shift from MR heads

Track Width Considerations - Heads:

This is a read-head and write-head problem.

- **TFI requires a compromise between read and write**
- **MR gives freedom to individually optimize (somewhat)**
- **Tradeoffs still required for optimum solution (resolution vs writeability)**

Nominal values as well as tolerances must be considered.

- **Large tolerances will cause width nominals to be narrower**
- **In some cases, tolerances may prevent a solution for a particular design point**
- **Stripe height and throat heights will affect apparent magnetic widths**

For MR heads, the alignment of read and write elements is critical and affects drive performance.

- **Additional mechanism for track misregistration (TMR)**
- **Increases requirements for microjog**
- **Can affect signal amplitude and cross track asymmetry**

Head Positioning Definitions:

Old Information: Any write operation leaves some old written data on either side of the newly written track. This is due to side writing and mis-positioning at the time of writing. The capability to read off-track in the presence of old information (and other noise sources) is often referred to as OI capability. This can be measured on a precision test stand or at the drive level.

Adjacent Track Interference: Data on the track of interest can be corrupted by the adjacent tracks. This can come in two forms: reading and writing. In the read mode, the adjacent track can sometimes be read even if it is not physically under the head due to side reading effects. In the write mode when the adjacent track is written, there may be an overwrite of the track of interest. This is often referred to as a "squeeze" from the adjacent track towards the track of interest. Both of these effects are affected by the positioning accuracy and TMR parameters.

747 Curve: Named for its shape which resembles a 747 cockpit, the curve results from a test to find the off-track capability when reading over previously written data and with an adjacent track written at a variable distance. (We will show how one gets the curve later)

Write to read track misregistration (TMR_{wr}): This is the mis-positioning of the head over the track of interest as a probability density function (PDF or histogram) It is due to errors in the positioning system of the drive. It is the convolution of the mispositioning of the head and the written track so it is $\sqrt{2}$ wider than the mispositioning of the head alone. While often represented as a gaussian distribution, it usually has long tails.

Write to Write track misregistration (TMR_{ww}): This is the mis-positioning of the adjacent track from the nominal position of the read track. It is also represented as a PDF or histogram. It includes errors in the servo-written track spacing as well as the positioning errors due to the drive. Again this is the convolution of two distributions. While often represented as a gaussian distribution, it usually has long tails.

Optimum Track Density: The optimum track density is the density at which the error rate will be adequate for the product applications. When there is an optimum, it is a compromise between off-track and adjacent track considerations. (more to come on this topic)

Complications Summary

- o Data Banding**
- o Read/Write Offset**
- o Rotary Actuators**
- o Sector Servo**

Track Density Impacts

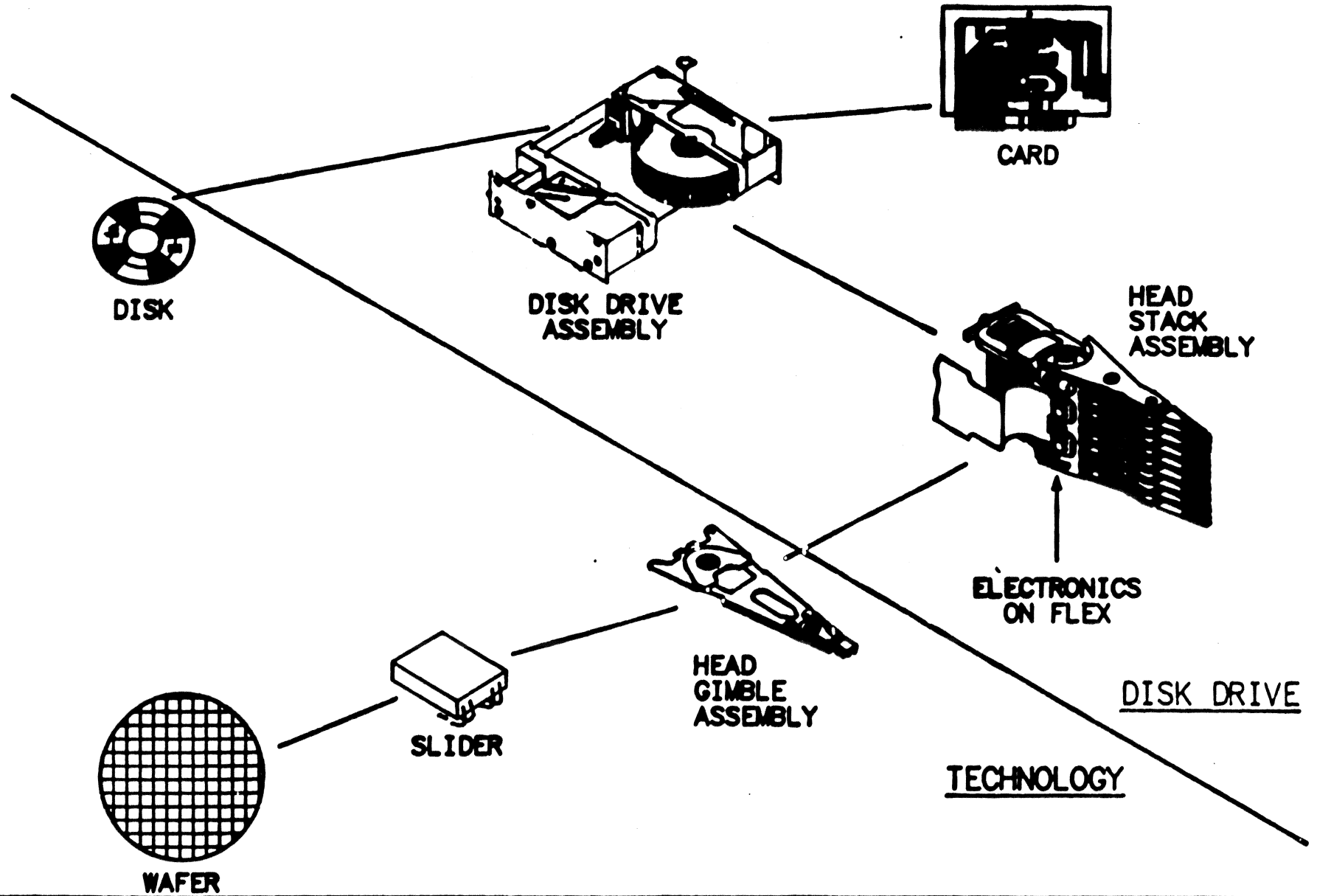
Track Misregistration

- Settling
- Dynamics
- Runout
- Hysteresis
- Quantization

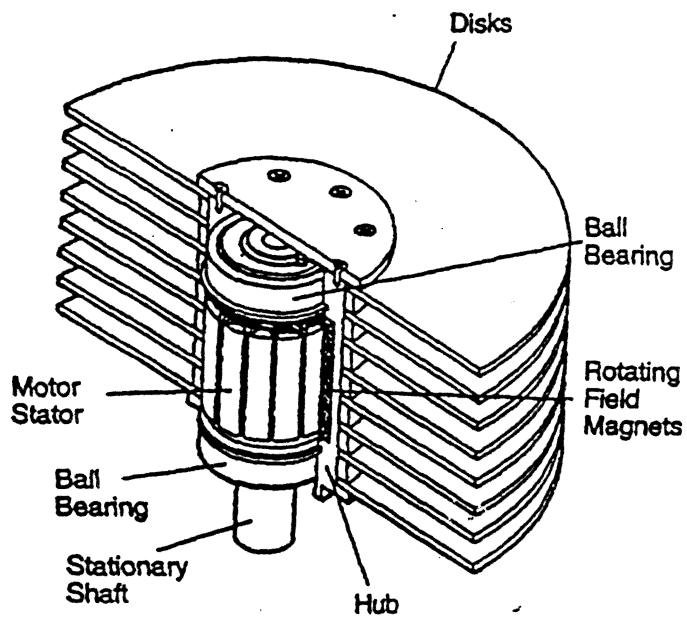
MR Unique Items:

- Read/Write offset
- Cross Track Linearity
- Track center stability
- Net: Good design required

EXPLOSION OF DISK DRIVE



Spindle Assembly, Maxtor XT-1000 (6)



NRRO - NonRepeatable Runout

- Caused primarily by spindle motor bearings
- Is often affected by the quality/sophistication of the servo.
- Sampled servos cannot remove the higher frequency components.
- Can be affected by mounting method
- One of the major components of TMR

Dan Malone, IIST, 6/28/97, (scunrro1.doc)

Seeking considerations:

- Designers try to minimize the seek times to maximize performance.

- Seek arrivals are not always “pretty”

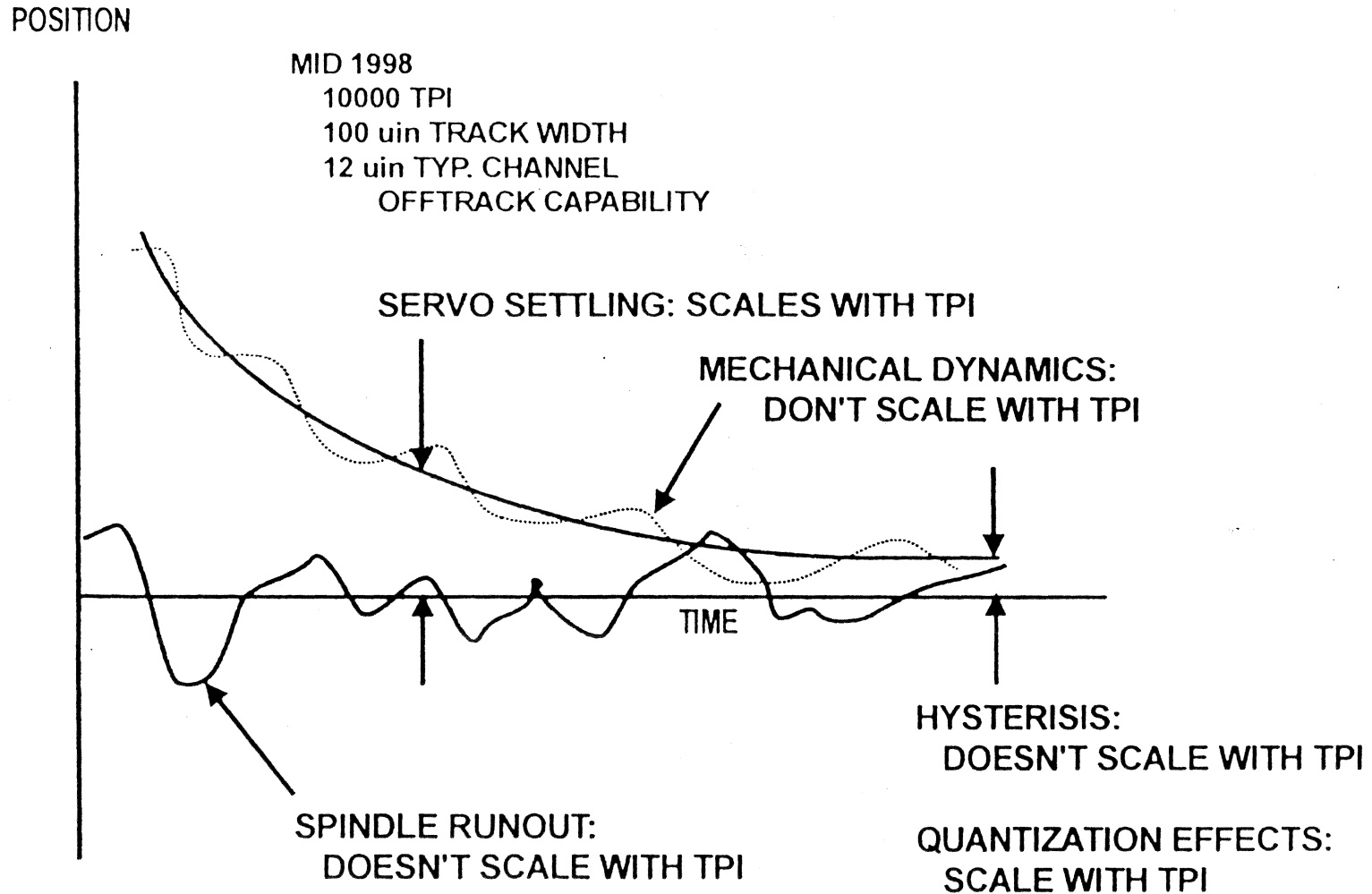
- When is it okay to read?

- When is it okay to write ?

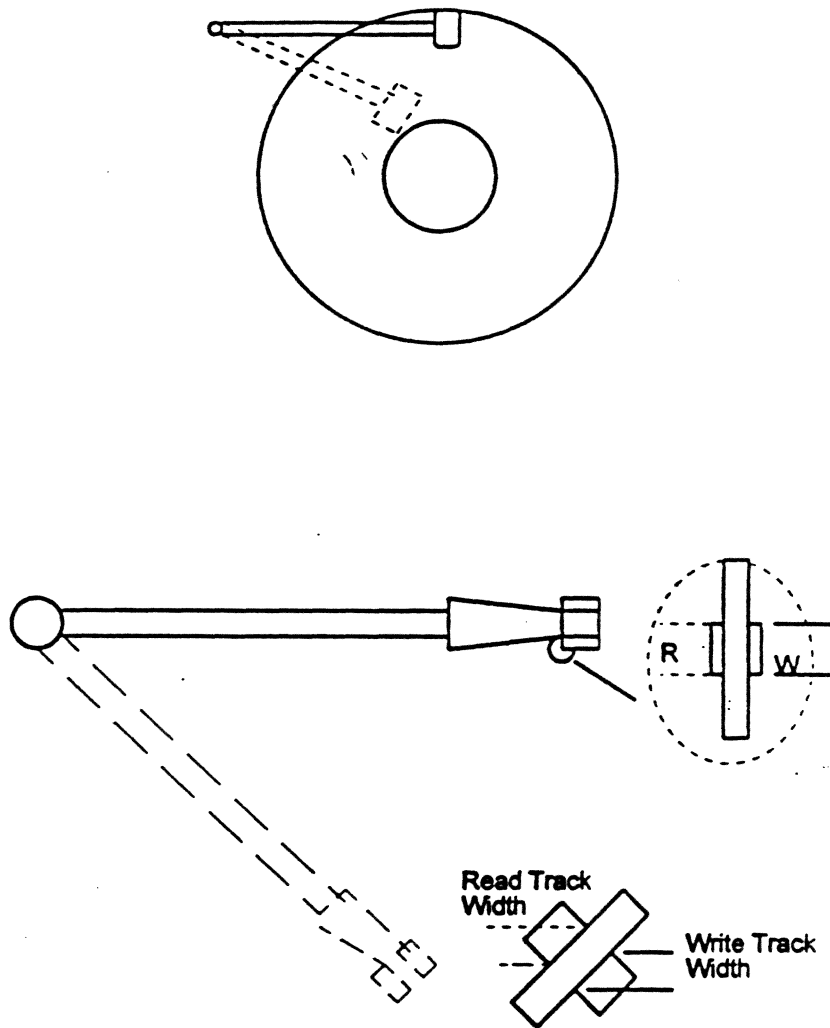
- Data Integrity is of utmost importance.

Dan Malone, IIST, 6/28/97, (scusrvo1.doc)

TRACK MISREGISTRATION SOURCES



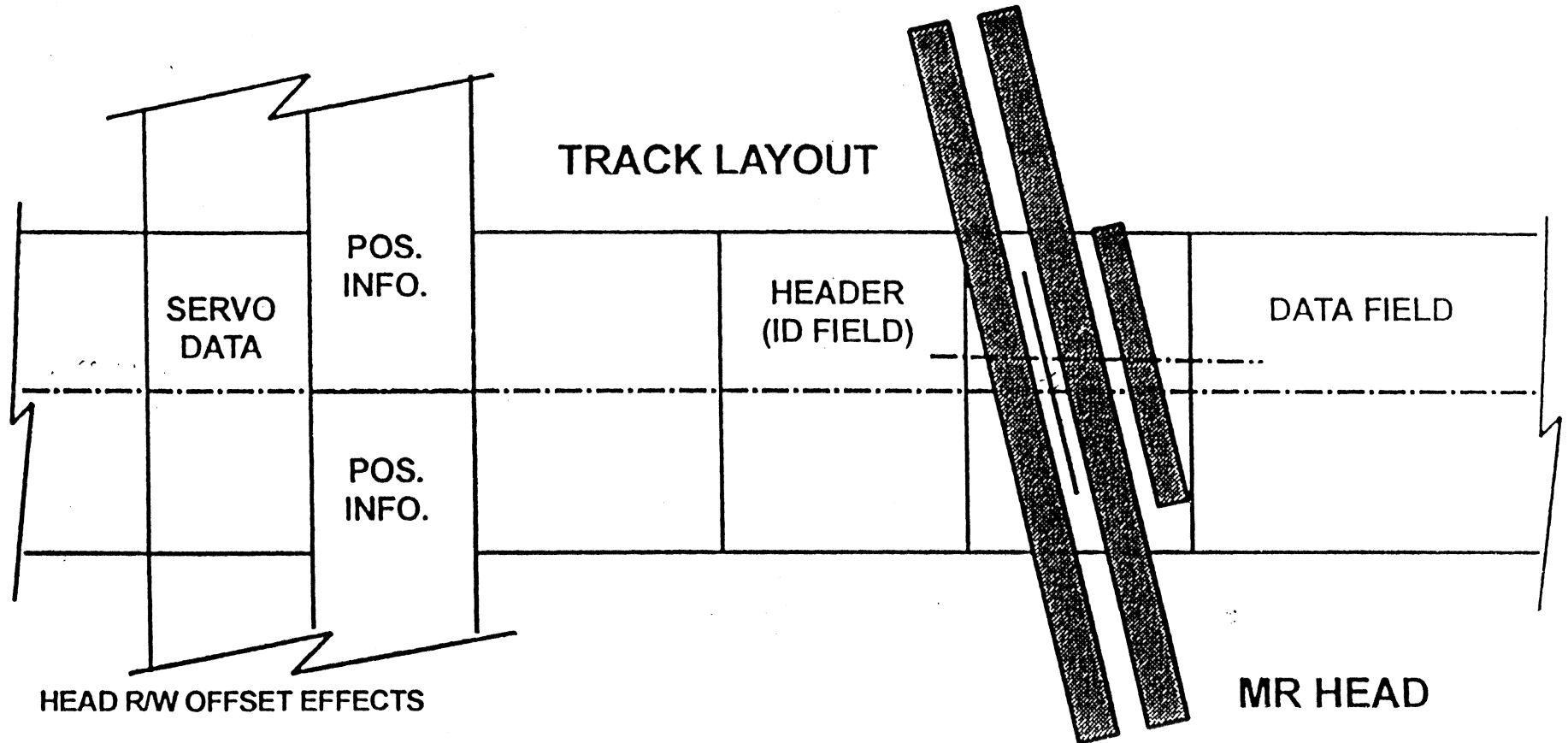
Skew And Crosstrack Asymmetry



Solution?

- *'Micro-jogging'* can help reduce asymmetry resulting from skew.

MR HEAD TMR EFFECTS



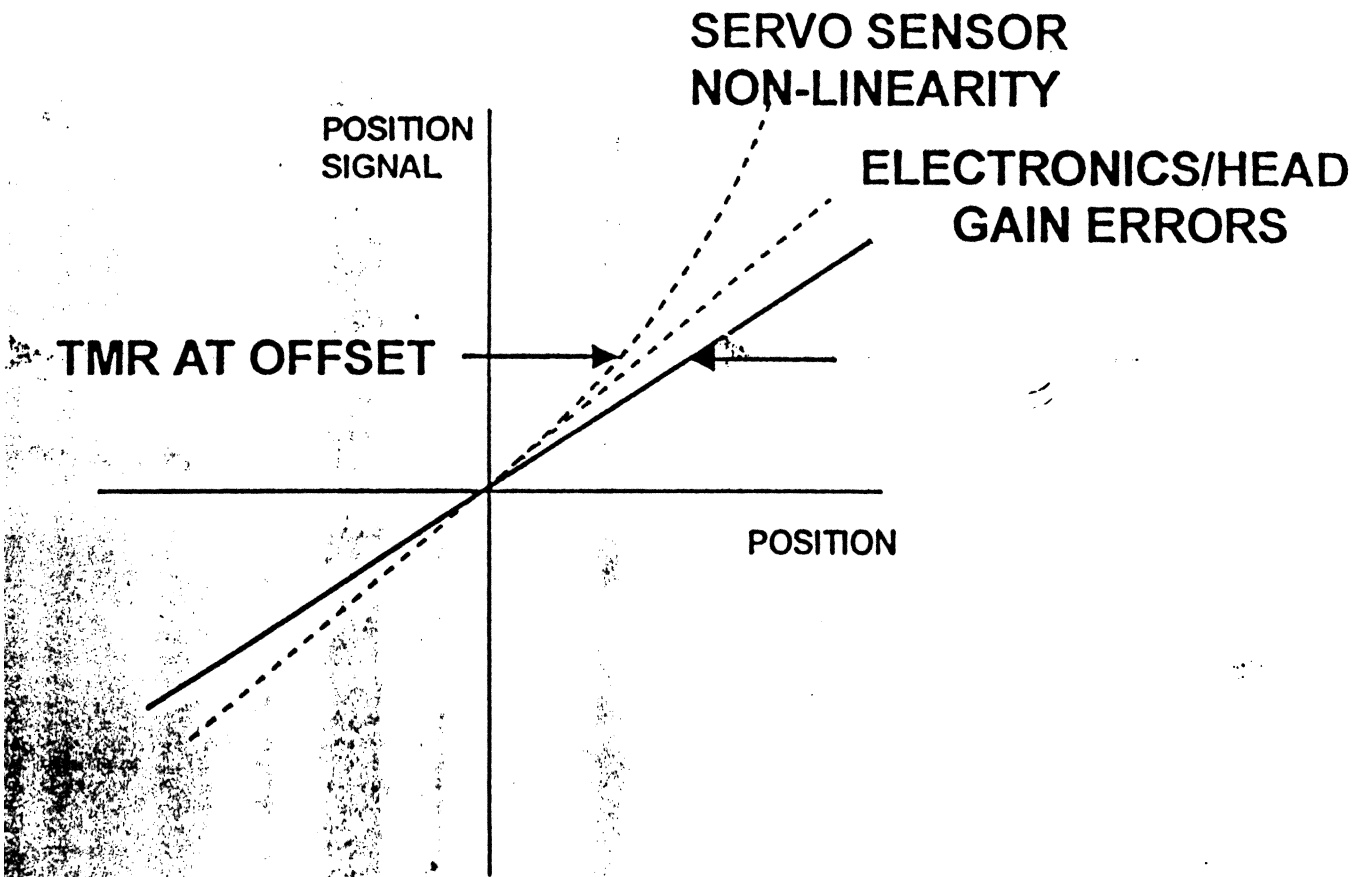
HEAD R/W OFFSET EFFECTS

READ ELEMENT OFFSET:
CALIBRATION IN DRIVE TEST

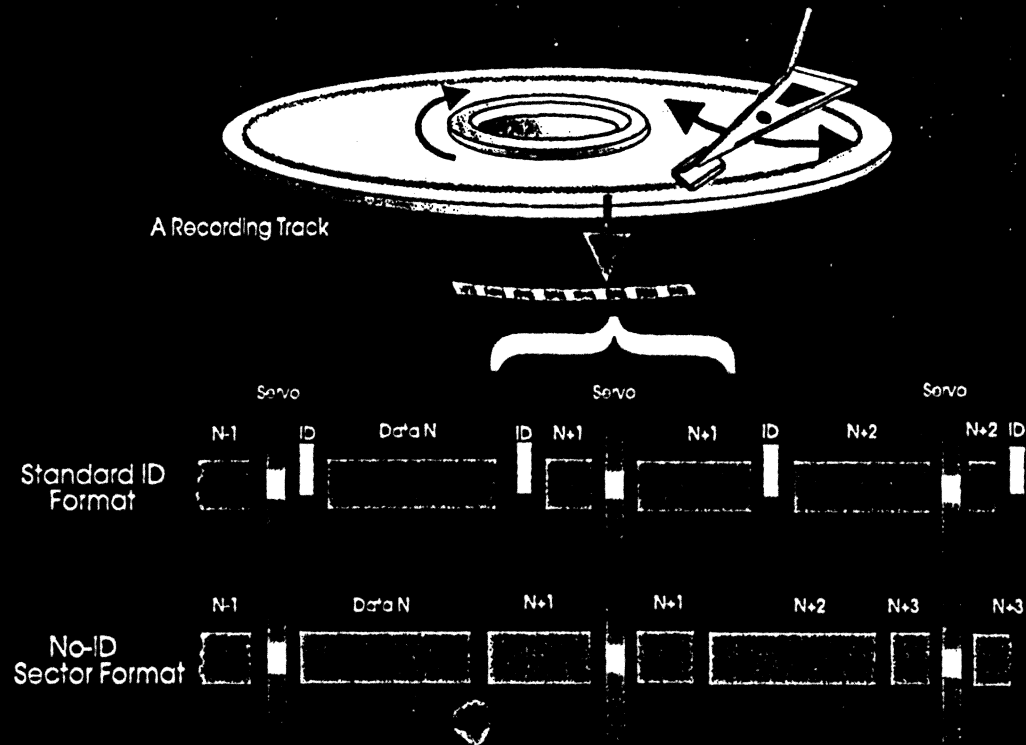
ACTUATOR SKEW:
DETERMINISTIC DURING DESIGN

READ ID/WRITE DATA OPERATION
R/W OFFSET SCALES W/ TIP OR
NO HEADERS

MR TMR EFFECTS



IBM No-ID™ Sector Format

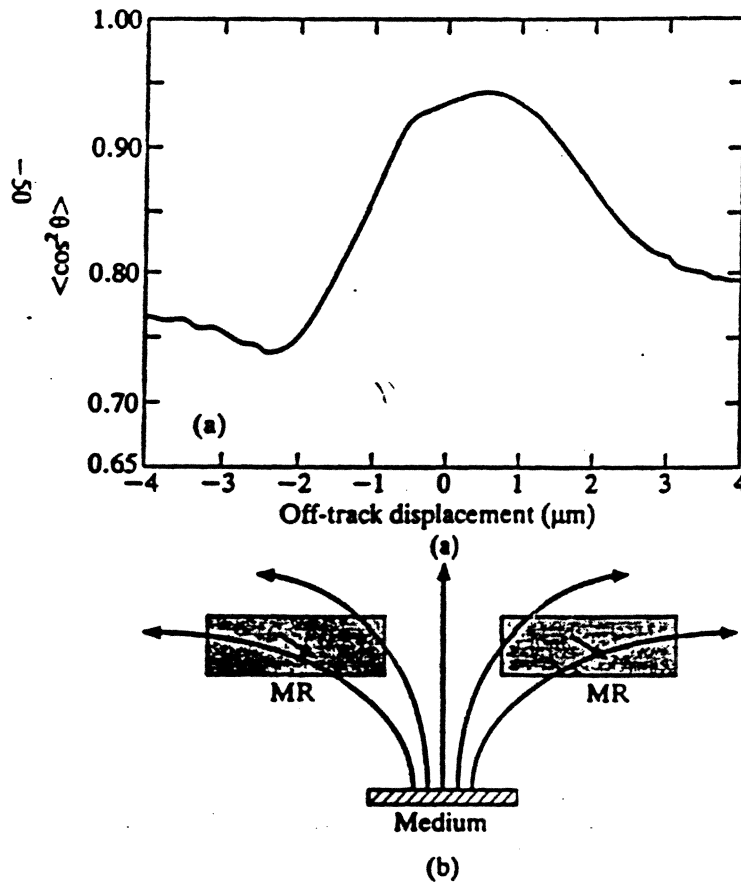


Advantages:

- More Disk Space For Data Storage (ID Fields to Electronics, Write to Read Recovery Eliminated)
- Improved Formatting Efficiency
- Potential To Reduce ECC Bytes (Eliminates ID Field Disk Errors)
- Potential To Increase TPI (Based on MR Head R/W Offset)



IBM Advanced Technology

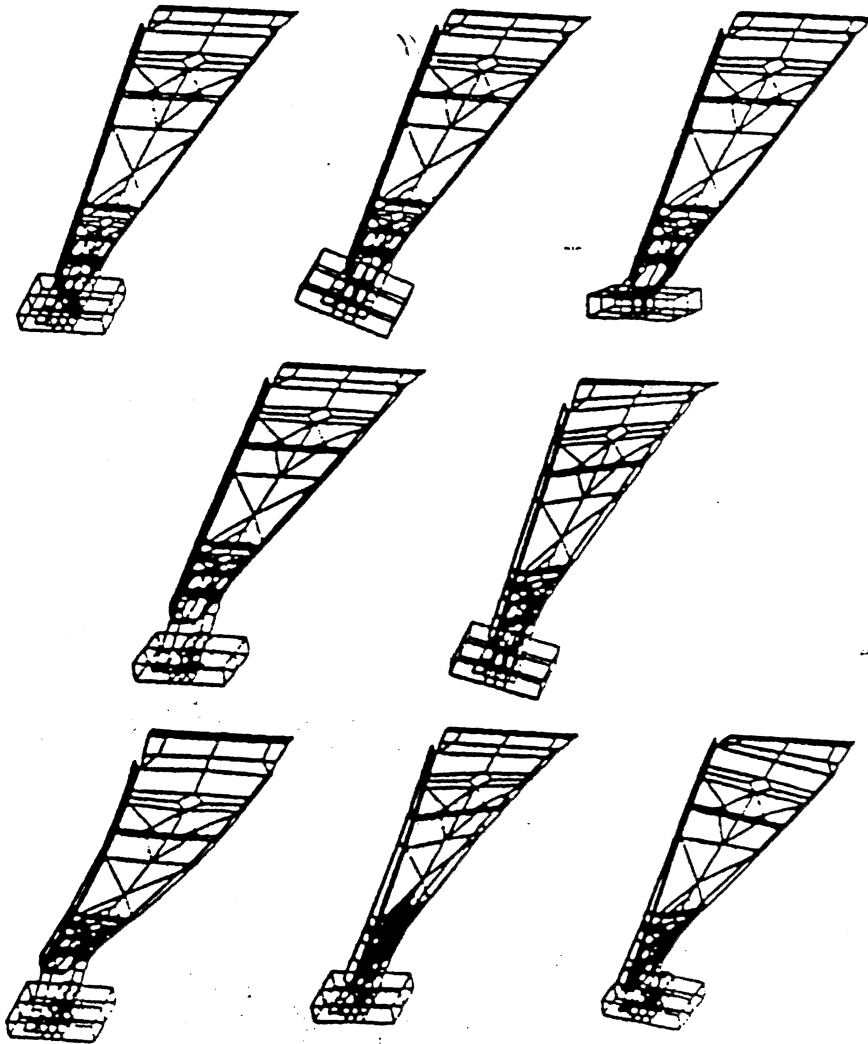


- For the element on the right ($\Delta z > 0$) the signal field is generally orthogonal to the MR bias magnetization. \therefore torque on the magnetization is large.
- As the element is moved off-track towards $\Delta z < 0$, at a specific location the field is approximately parallel to MR magnetization minimizing the response.
- On track ($\Delta z = 0$) the response is not the largest due to non-uniform bias magnetization.

Typical Suspension Resonance Modes

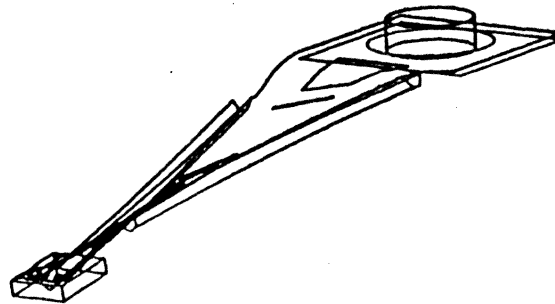
Numerous Modes

Off-Track Most Troublesome



First Torsion Mode

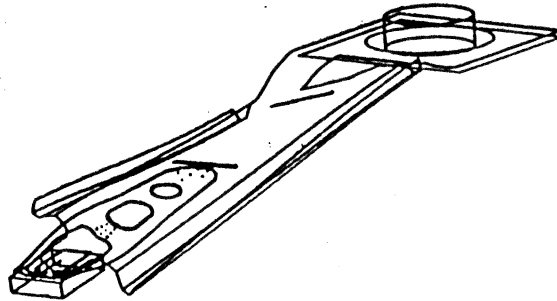
- This mode has a significant influence on off-track errors.
- Radius length, load beam width, rail design, and material thickness have a significant influence on this mode.



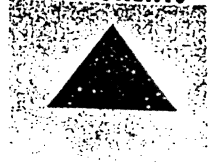
T-1950 (14U Rail): First Torsion Frequency = 2040 Hz

Second Torsion Mode

- Like first torsion, this mode also contributes to off-track errors.
- Radius length, load beam width, rail design, and material thickness have a significant influence on this mode.



T-1950 (14U Rail): Second Torsion Frequency = 5633 Hz



Cover Feature

Smart shock sensors preserve data integrity in hard drives

Lloyd Levy, Micropolis Corp.

The high capacity of today's hard drives has been achieved through steady advances in head technology and digital servo positioning systems. The former has yielded higher bit densities; the latter, higher track densities. Drive makers have arrived at the point where each new advance represents some kind of technical feat.

For example, as the track pitch falls below 200 μm , maintaining the data heads within acceptable limits of track center under shock conditions is a significant technical challenge. A shock of fairly short duration (under 5 ms) can knock the head off track, affecting data integrity—the seriousness of the shock depends on whether the off-track motion occurs during a read or write operation.

Shock or vibration during a read operation may cause a soft error, that is, the head may read data on an adjacent track. When this occurs, error correction

information contained in the data indicates an invalid read, causing the data to be reread. The data can be fully recovered through repeated reads, and data throughput is only briefly affected.

On the other hand, if the head is knocked off track while data is being written, the data that's overwritten is permanently lost.

This type of error (i.e., a hard error) is not recoverable (see Figure 1).

An ideal position servo would stay on track center at all times. However, practical systems aren't sufficiently stiff to stay on track center when the shock or vibration lasts for only a few milliseconds.

An alternative is a system that detects a potential off-track excursion and then prevents data from being written before the head moves off track. Standard digital servo systems have sample intervals in the 40- to 150- μs range, thus they are unable to respond to brief off-track excursions quickly enough.

FAST-ACTING SENSORS



KEEP DATA FROM BEING

OVERWRITTEN UNDER

SHOCK CONDITIONS

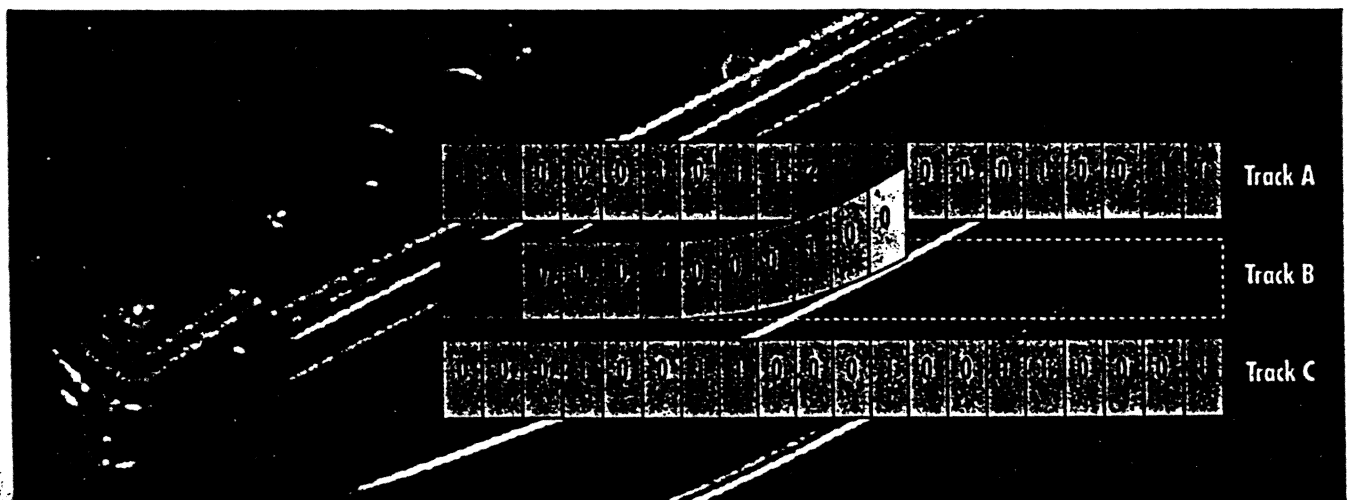


Figure 1. How data becomes corrupted. Data is written on Track A. While the head is writing on Track B, the drive is "bumped," knocking the head onto Track A. However, data continues to be written until an off-track condition is detected. Consequently, some of the original data on Track A is overwritten and permanently lost. Unrecoverable data loss is referred to as a hard error. Shock during reads (Track C) causes soft errors.

he current 60-MHz version has 3-W power and was fabricated with 0.5- μ m CMOS technology. Models of 66 and 75 MHz will also be available.

The multimedia authoring chip set (CLM440) consists of hardware plus software. It meets the full MPEG-1 requirements and the specification for MPEG-2.

The 4720 set for storage encoding (e.g., for video file compression) uses chips and uses variable-bit-rate (VBR) encoding to meet requirements by 20 percent. It supports both NTSC and digital video formats. The most expensive chip set targets broadcast encoding and is based on seven processor chips plus software.

The full MPEG-2 standard and features low data rates—an essential feature in broadcast applications where bandwidth is expensive and limited.

C-Cube's early entry into the MPEG encoder business has given the company an impressive roster of customers, including major TV and satellite-communication heavyweights (such as Compression Labs, COMSAT Labs, and Scientific

Cube had a head start in the fledgling MPEG-2 market for multimedia PCs and DVD recording. According to Mele, executive VP for sales and marketing at C-Cube, "The reduced chip count and lower power requirements of the C-3 provide new opportunities for delivering MPEG-2 on the PC platform."

The lower prices and improved performance of the new chip sets should allow C-Cube to maintain its market momentum. All three chip sets are sampling now, with full production scheduled to begin sometime this quarter. —M.E.

Tiny sensor measures g-forces in mobile drives

Mobile drives are exposed to a lot of rough handling. When the tiny sensor in the mobile drive detects an external shock, it sends a voltage signal to the CPU, which processes the signal and stops the drive from writing, thereby minimizing errors in data recording. The new g-force sensor from Toshiba America (Irving, CA) draws one half the power (2 ma in the active mode, 0.1 μ a in the power-saving mode) and is about one third the size of an earlier design offered by the company.

It is also more sensitive. The sensor input terminal has a high impedance of 50 meg-ohm and can be correlated with a pressure-to-voltage sensor, accurately detecting small shock signals. In addition, the sensitivity of the sensor can be adjusted externally through such devices as a capacitor and resistor. A built-in low-pass frequency circuit with a cutoff frequency of 7 KHz prevents harmless vibrations from interfering with disk-drive operation. The g-force sensor, which operates from a single 5-V power supply, sells for \$1.12 in production quantities.

QUALITY AND SERVICE MAKE THE DIFFERENCE

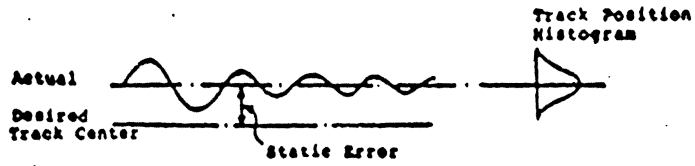
**PR Hoffman has been Committed
to Quality and Service Since 1938.**

- Double Sided Planetary Lapping /Polishing Machines to 48"
- Customized Carriers for Virtually all Machines
- Complete Line of Expendable Plates and Gears
- Waxless Mount Polishing Templates

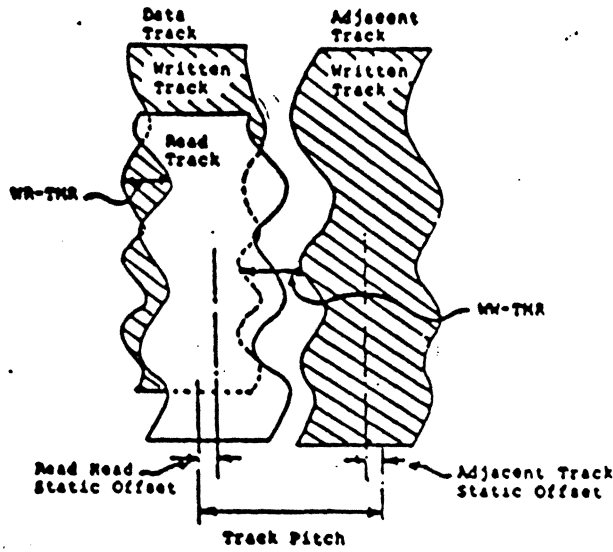
TEL: 717-243-9900

**FAX: 800-776-3830
717-243-4542**

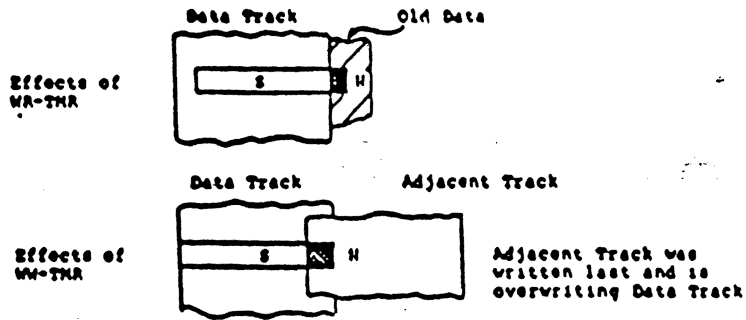
Error Rate Modeling History



Track Position Error during a single seek.

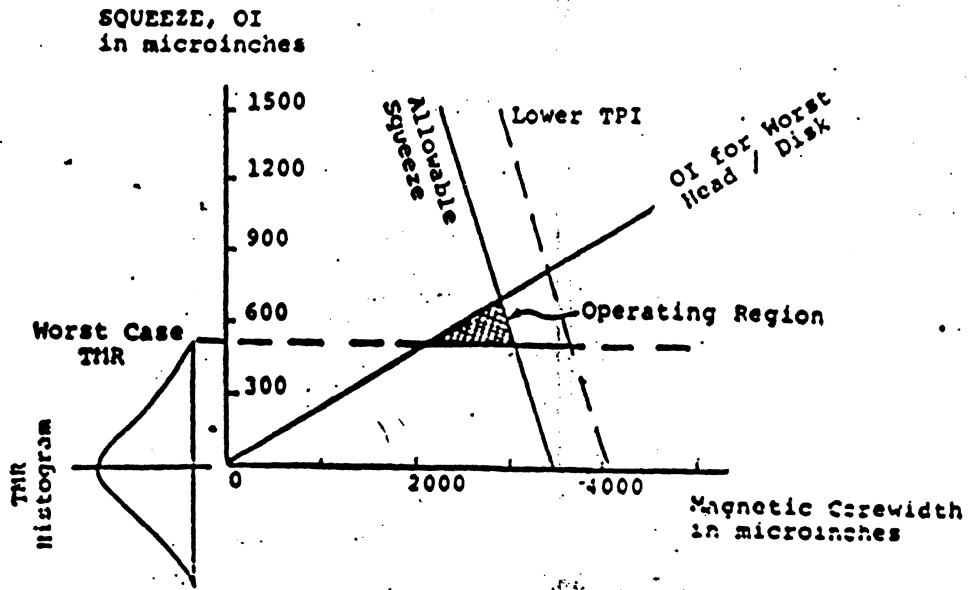


Example of Combined WR and MW TMR



S/N Ratio degradation from TMR

FIGURE 4



LAMBDA CURVE
FIGURE 12

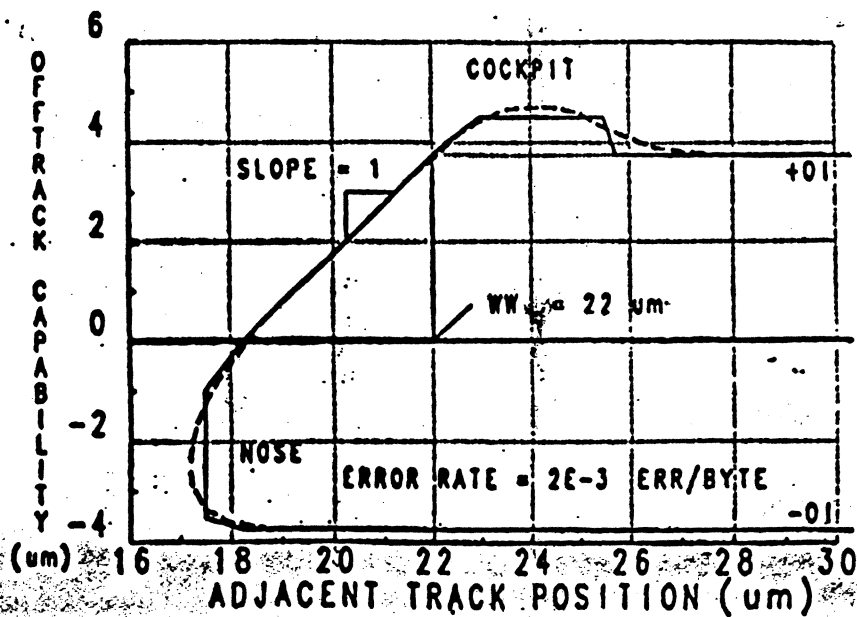
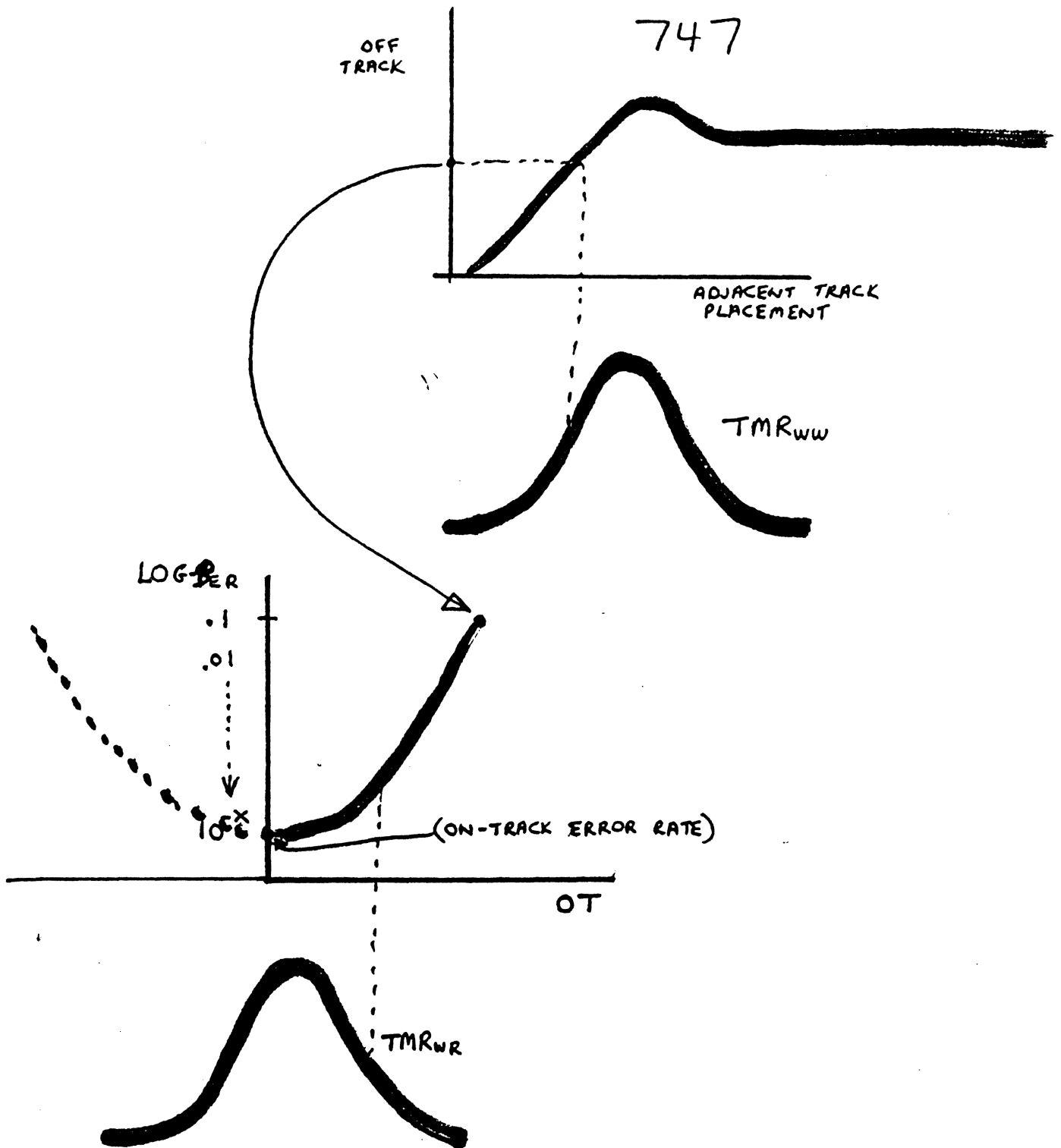


FIGURE 13

SOFT ERROR RATE MODELING



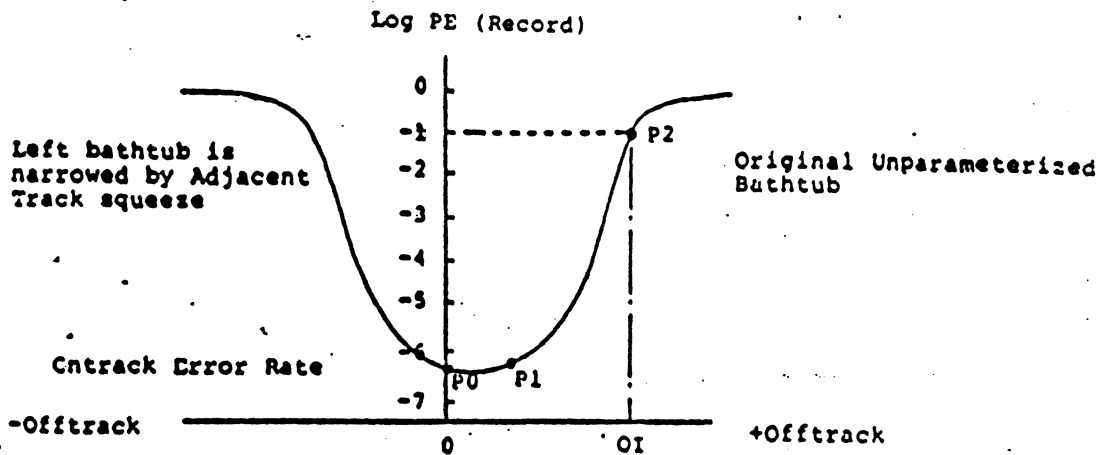


FIGURE 10A -Offtrack

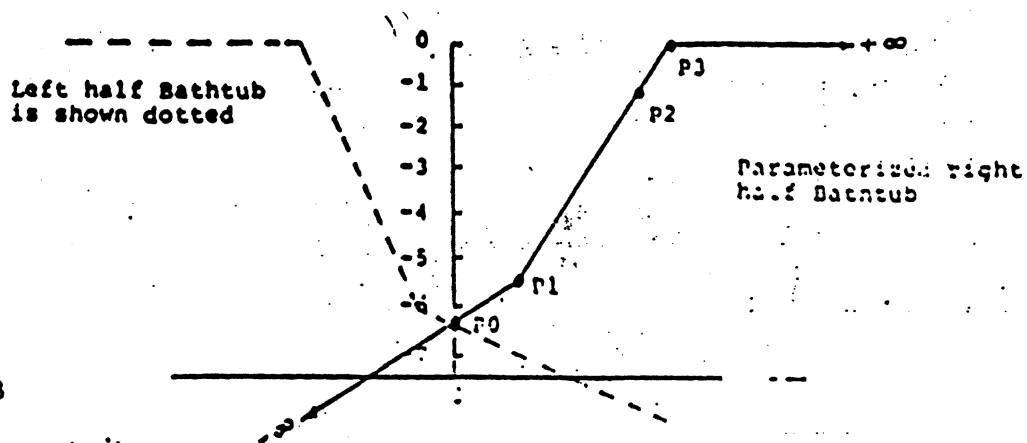


FIGURE 10B

case4 nom hd/disk

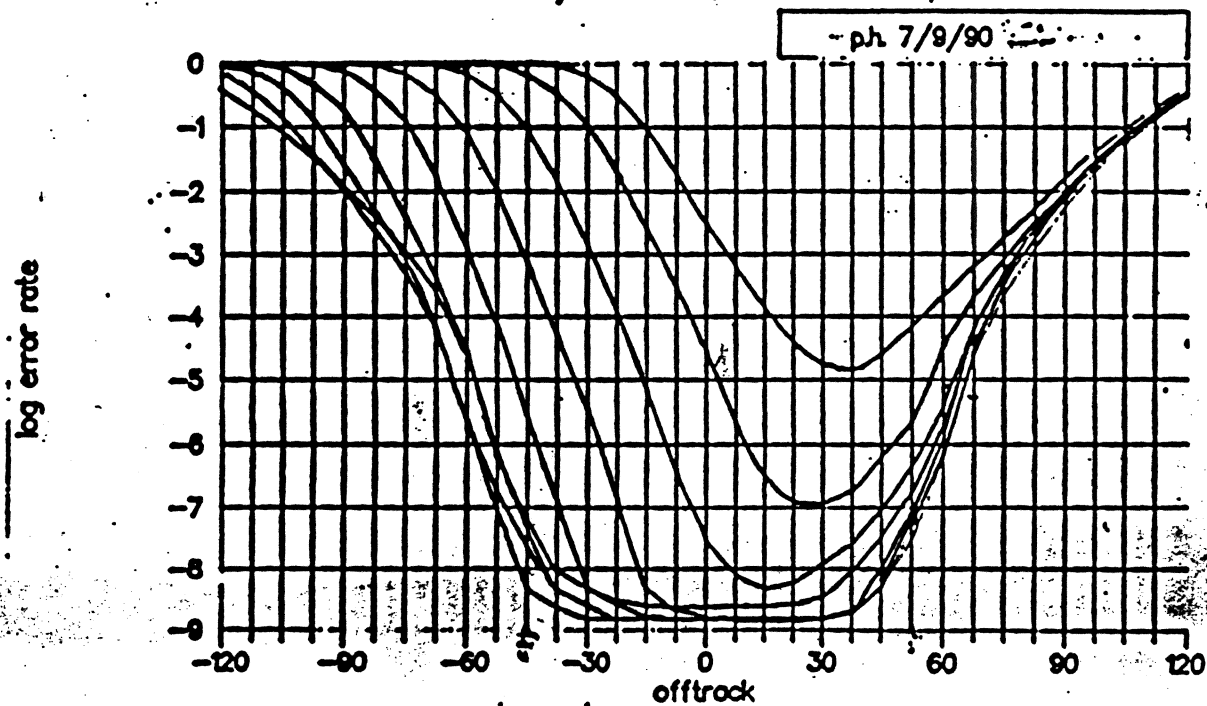
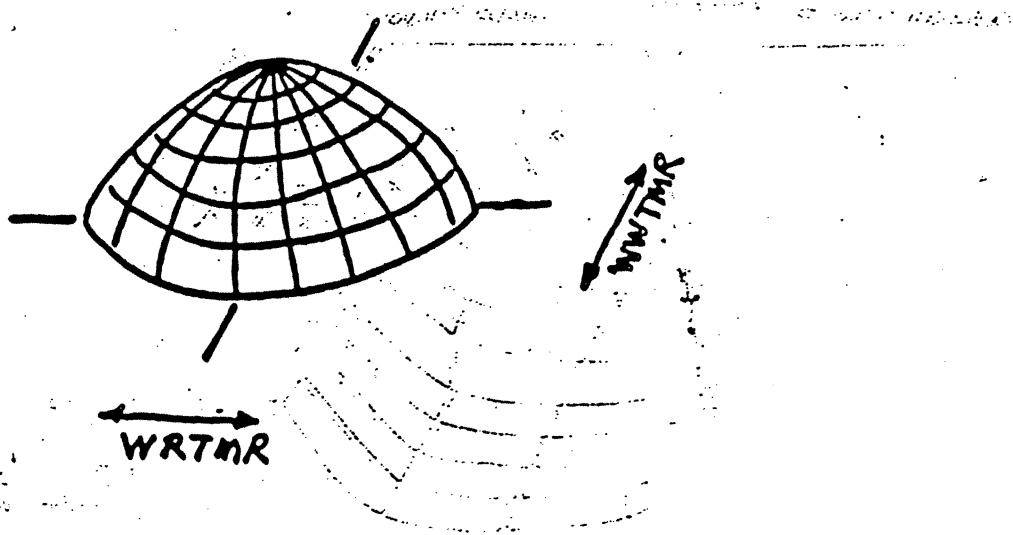
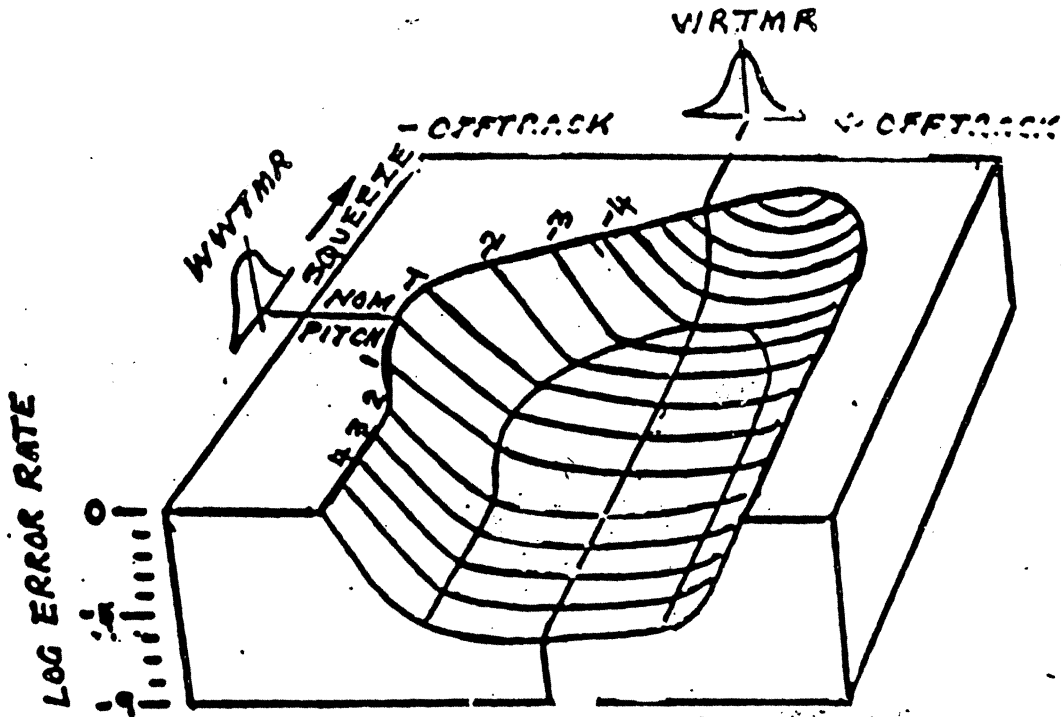


FIGURE 11



DEMONSTRATION OF 500 MEGABITS PER SQUARE INCH WITH DIGITAL MAGNETIC RECORDING

Roy A. Jensen, Joost Mortelmans and Robin Hauswitzer
 IBM Corporation, Magnetic Recording Institute, San Jose, CA 95193, U.S.A.

Abstract - This paper describes the testing and modeling methods undertaken to demonstrate and verify an areal density of 500 million bits/in.² with a combined inductive, thin film write head and a magneto-resistive read head on an advanced, state of the art thin film disk. The linear density was 100,000 bits/in. (3937 bits/mm), the track density was 5,000 tracks/in. (196.9 tracks/mm) and the flying height was 2.5 μ m. (64 nm).

INTRODUCTION

The IBM Magnetic Recording Institute set an objective to demonstrate an areal density of 500 million bits/in.² (3937 bits/mm²), in an environment where the most aggressive products were just approaching 100 million bits/in.². The criteria for success were set as: a flying height of 64 nm (2.5 μ m), with a 3 σ write-to-read track misregistration (TMRw/r), including read-write misalignment, of no less than 760 nm (30 μ m) and a total raw soft error rate (SER) of 10⁻⁴ (errors/byte). The flying height and TMRw/r criteria were selected as obtainable mid-nineties product objectives. This paper describes the characterizations of the head, disk and channel, the linear and track density measurements, and the test and modeling methodologies used to verify the soft error rate and TMRw/r for the measurements made.

COMPONENT CHARACTERIZATIONS

The narrow track recording head was a combination of a thin-film inductive write element and a magnetoresistive read element. The read head was similar to the type described in paper[1]. The head gap was .4 μ m and the element width was 3.6 μ m. The recording was done on a CoPtCr thin-film disk, similar to the type described in paper[2], but with a coercivity of 1335 Oe and remanence-thickness product of .8x10⁻³ emu/cm². Many of the geometric and magnetic target values for the head and disk were set by use of modeling techniques described below. The following were used to gain our objectives: a peak detection channel with a data rate of 4.5 megabytes per seconds (MB/s), a second derivative equalization boost of 10 dB at 17.5 MHz, a five-pole low-pass filter with a 3 dB attenuation at 22 MHz and a (1,7) run length limited encoding scheme. The magnetic head-disk separation was approximately 102 nm (4 μ m) with a flying height of 64 nm. The difference was split between head recession and disk overcoat. The head output at low density was 643 μ V_{p-p} with a 3 dB roll-off point at 2400 flux changes per mm (fc/mm). Figure 1 shows both unequalized and equalized isolated pulses. Figure 2 shows the micro-track profile of the read head. The low frequency track profile of the written track was very uniform, had fairly steep sides and the width was 4.3 μ m. The total signal to noise ratio was 28 dB, defined as base to peak isolated pulse divided by rms noise. The disk noise was measured with high density data present.

SELECTION OF LINEAR AND TRACK DENSITIES

To determine the linear and track densities and the required TMRw/r for the desired soft error rate, a combination of off-track tests and modeling was used. Many of the

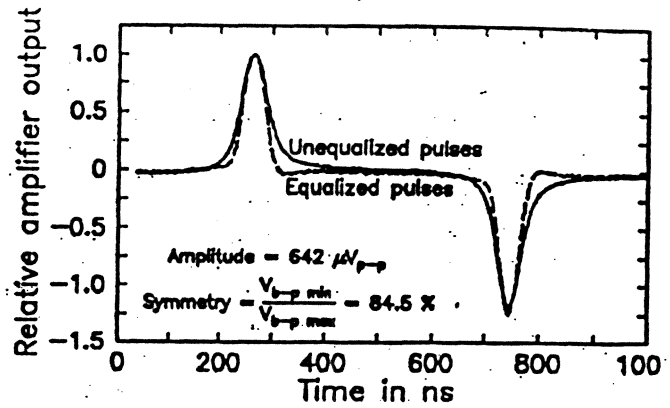


Figure 1. Normalized, equalized and unequalized isolated pulses.

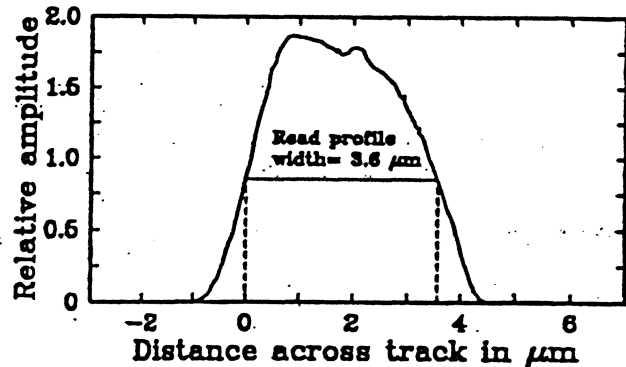


Figure 2. Read head micro-track profile using a .5 μ m written track width.

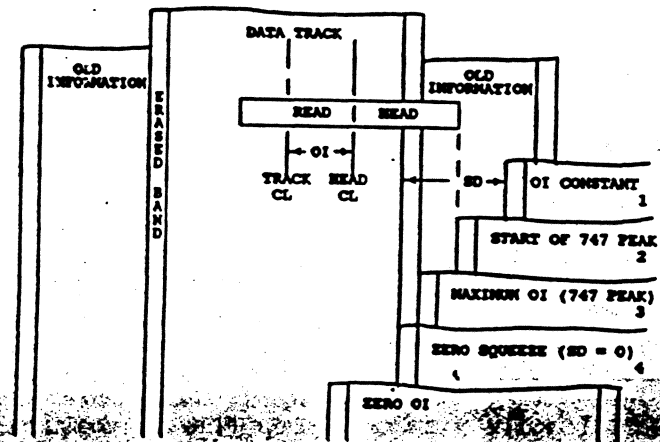


Figure 3. Old information and 747 curve test schematics. SD is the squeeze distance, OI the old information distance. Numbers on the left refer to points in Figure 4.

test procedures described were developed in IBM the mid seventies. These tests measure performance, expressed as error rates, under all off-track combinations of the head during reading and writing. The Track Density Error Rate Model, developed by Joost Mortelmans, simulates these tests by using as input some 20 geometric and magnetic component parameters, and calculates the SER from the signal to Gaussian noise ratio (SNR) [3] and the amount of signal type noise from adjacent tracks. This enables the model to compute the total SER as a function of assumed TMRw/; and the write-to-write track misregistration (TMRw/w).

The first step was to determine the approximate track density capability of the test head by generating a 747 curve (so named for its resemblance to the front of a 747 airplane). This test consists of finding the off-track capability when a track of random data is centered at the boundary of two previously written tracks and an adjacent track is written at a variable distance. Figure 3 shows the basic background pattern with the approaching adjacent track in the lower half. It also shows the presence of erased bands at the edge of each recorded tracks. For a given track pitch, the head is moved off-track in small increments until all written sectors have failed three times in 30 read operations. The mean of the resulting histogram of failed sectors versus off-track distance is called OI and this corresponds to a byte error rate of about 8×10^{-5} . Figure 4 shows OI versus adjacent track pitch for the 500 MB/in.² components. Referring again to Figure 3, when the adjacent track is far removed from the center track, it will have no impact on OI which will remain constant. However, as the old information band, between the data and the squeezing tracks becomes smaller, the off-track capability will increase and reach a maximum when the two erased bands about. Further squeezing will result in a decrease of OI and to a position where the two erased bands overlap; this is point A in Figure 4, where OI is the same as the initial point where the adjacent track is far removed from the center track. For yet smaller track pitches, the adjacent track erases or overwrites the center track, which causes OI to decrease precipitously. The track density at which the 747 curve peaks is close to the optimum for that head. Figure 4 shows this peak in the vicinity of 5 μm (200 $\mu\text{in.}$) or 5000 t/in.

The second step was to determine the linear density to use for tests involving large quantities of data. This was accomplished by running the old information test as a function of linear density. This test also measures off-track capability and consists only of the initial step of the 747 procedure; no adjacent track is recorded. Figure 5 indicates OI as a function of linear density. Three trials were run at three different equalizer and detector clip level settings. Since the 747 curve showed that our track density would be close to 5000 t/in and since our goal was 500 Mb/in.², we selected 100 kbp/in with the settings of trial #3 for the testing of large quantities of data.

SER AND TMR TEST AND MODELING RESULTS

The solid line bathtub curve, shown in Figure 6, was obtained by measuring the error rate as a function of off-track position of the read head, while collecting in excess of 10^9 bytes of data from 20 tracks in an overnight test run. The track configuration is that of the OI test geometry, which is equivalent to a separation between center and adjacent tracks of one erased band width. In this case SD of Figure 3 is 0 which corresponds to 5344 t/in. We initially tested the tracks at a 65% defect clipping level to identify the sectors to be skipped, however, no skips were required. The track density for the desired SER was determined as a function of TMRw/r and TMRw/w. The latter was assumed

to be 33% larger than the former. The track density analysis consists of two steps, one for the write-to-read and one for the write-to-write TMR.

In the first step, a bathtub curve is calculated (smooth curve in Figure 6) for the same track geometry as described in the test procedure to obtain the data bathtub. Minor adjust-

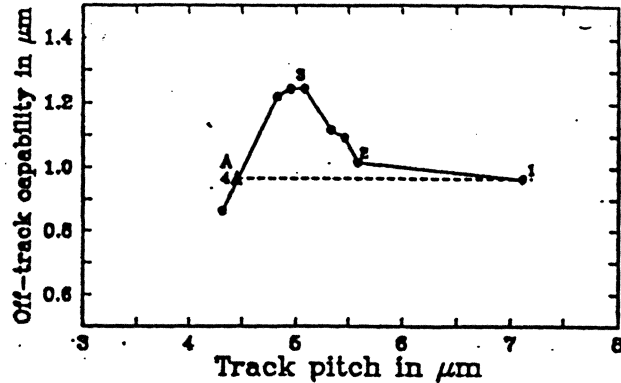


Figure 4. 747 curve for 500 Mb/in². Point A occurs when the erased bands of the adjacent and center tracks overlap. Numbers refer to Figure 3.

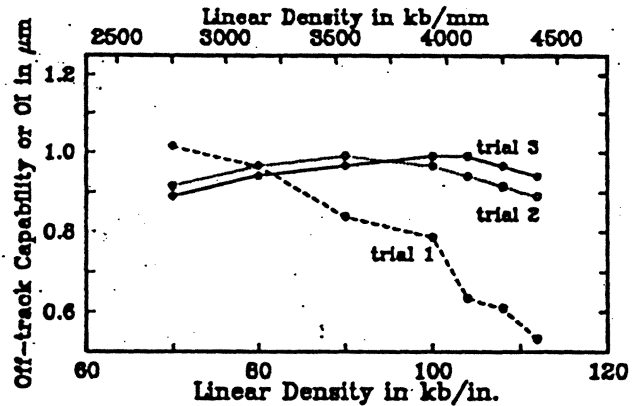


Figure 5. OI or off-track capability versus linear density for three settings of the equalizer and the detector clip level, using the OI test.

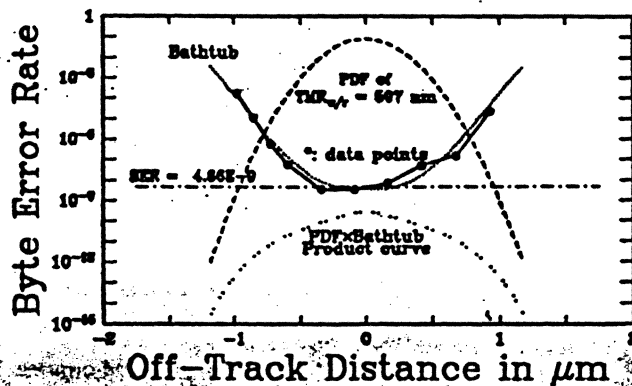


Figure 6. Measured and calculated bathtub, when no adjacent track is recorded. Also shown are, PDF of TMRw/r, the product curve and its integral value (horizontal line) which yields the expected error rate and point B in Figures 7 and 8.

ments, within the uncertainty of the parameters, were made for a better match to the data. An expected error rate value was obtained by integrating the product of the bathtub and the (Gaussian) probability density function (PDF) of the assumed TMRw/r. The width of the PDF relates to the 3σ value of the TMRw/r which is equal to 597 nm (23.5 μm). This error rate is point B in Figures 7 and 8. Similarly, for each other value of TMRw/r, the bathtubs will correspondingly yield expected error rates which are plotted in the lower part of Figure 7 as the dotted curve. The solid curve results from using the data bathtub of Figure 6.

In the second step, both TMRs are kept constant and a series of bathtubs are calculated as a function of adjacent track distance. The expected error rates of the bathtubs and the fixed TMRw/r yield the squeeze curve shown in Figure 8. Also shown are the PDF of the TMRw/w, the product curve and its integral, the overall error rate. This PDF of the TMRw/w is centered at a squeeze distance of $SD = 0$, which corresponds to the OI test geometry and to 5344 t/in. (210.4 t/mm). This track density is very high and also results in a high error rate as shown in Figure 8. The left hump of the product curve corresponds to the over-writing of the center track by the adjacent track (TMRw/w), while the right hump, which is suppressed here because of the close proximity of the adjacent track, corresponds to the amount of old information between the two erased bands. At the optimum track density of the components, the two humps would have equal heights, indicating a balance between too high and too low a track density. This calculation was repeated for a range of TMRw/w values to obtain the upper curve, in Figure 7. The SER value at 10^{-4} is point C, also shown on Figures 8 and 9. The total process of Figure 7 is repeated at different nominal track densities to generate Figure 9 which is a plot of the track density versus TMRw/r for a total soft error rate of 10^{-4} (byte). TMRw/r for 5000 t/in. (210.4 t/in.) is 30.8 μm (772 nm), which met the TMR objective of not less than 30 μm (760 nm).

CONCLUSION

We have demonstrated longitudinal magnetic recording and playback at 100 kb/in. (3937 b/mm) and 5000 t/in. (196.9 t/mm) equivalent to an areal density of 500 Mb/in.². The components were characterized in great detail including write, read, erased band and read profile skirt widths. A combination of off-track measurements and the Track Density Error Rate Model showed that the target density was obtained for a soft error rate of 10^{-4} and a TMRw/r of 30.8 μm (772 nm). Although this was accomplished in a laboratory environment, the capability of magnetic components to record and read back at these high linear and track densities was clearly demonstrated. Incorporation of these densities into a product with the associated flying height and TMRs still represents significant engineering challenges.

REFERENCES

- [1] C. Tsang et al., "Gigabit Density Recording using Dual-element MR/inductive heads on thin film disks", CA-10 this conference (1990)
- [2] T. Yogi et al., "Role of Atomic Mobility in the Transition Noise of Longitudinal Media", BP-01 this conference, (1990)
- [3] P. H. Siegel, "Applications of a Peak Detection Channel Model" IEEE Trans. on Magnetics, vol.18, pp.1250-1252, Nov. 1982.

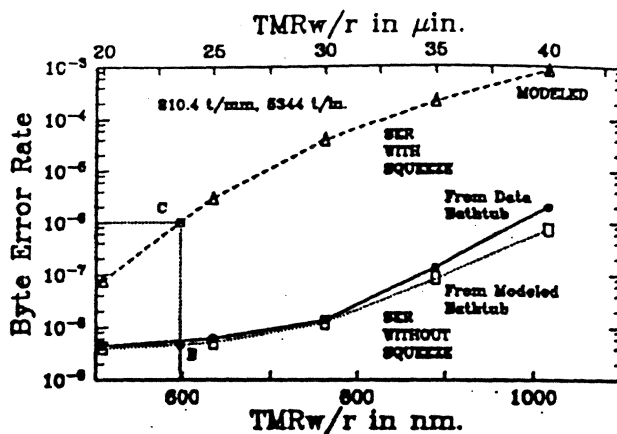


Figure 7. Overall SER with squeeze (top) and SER from data and calculated bathtub without squeeze.

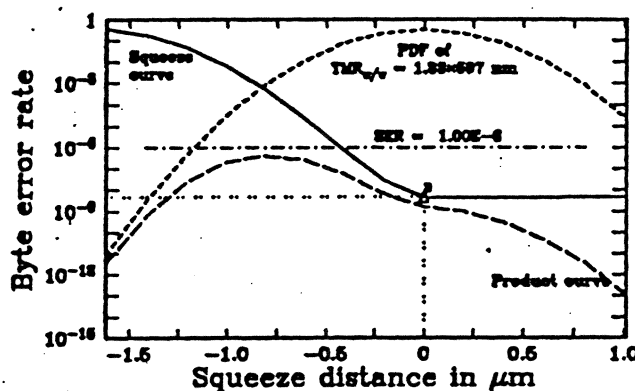


Figure 8. Calculated squeeze, PDF of TMRw/w, the product curve and its integral value which yields the overall expected error rate.

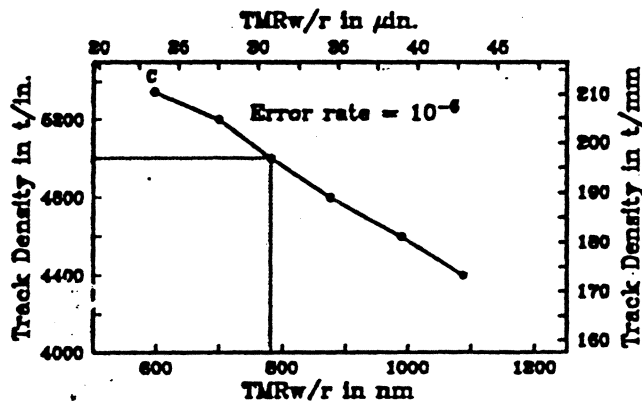


Figure 9. Track density versus TMRw/r at a SER of 10^{-4}

EVOLUTION OF THE SOFT ERROR RATE MODEL AND SOFT ERROR

BY

P. Hardy and D. J. Malone
 Channel Technology,
 IBM, San Jose, CA. 95193

ABSTRACT:

Soft error rate models have been used, within IBM, since the early sixties to determine the capacity capabilities of diskfiles. Most models consider the data handling capabilities and the mechanical misregistration to determine the TPI for a given system error rate. Recent models have been used to estimate factory yields, field performance distributions, and also the effects of manufacturing tolerances. This paper describes the most recent hybrid models which are used for estimating Soft error rates on high TPI designs.

INTRODUCTION

The task of Channel Technology is to integrate the head, disk, and channel design to obtain the best overall soft error rate (SER) from a new product. The SER model is used in this context to explore the effects of different parameter settings on the soft error rate.

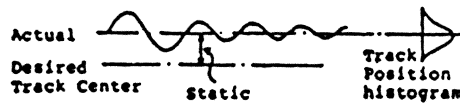
SER models simulate the building and operation of a large number of disk files and estimate the average SER when the files are operated in a typical customer environment. SER models are used during initial product development to evaluate alternative designs and later on with data from production parts to fine tune the manufacturing process for better quality and higher yields. The key ingredients in a SER model are the track mis-registration (THR) distribution and offtrack performance curves (OTP). These are convolved together to obtain the SER.

The SER models used within IBM San Jose today have evolved over the past 25 years. Early models used Monte Carlo methods to convolve the THR and OTP for determining the SER. Later on the THR and OTP double overlap integral was solved analytically which saved much time compared with the Monte Carlo method. Today's models have been extended to consider many head and disk combinations and manufacturing tolerances. In these hybrid models we select from the head, disk, and THR tolerances using Monte Carlo methods, but perform the SER overlap integral analytically. The accuracy of these experiments showed that the SER could be predicted within a factor of 3 of the measured SER. Since recent models use only real measured data from fully functioning machines, they are capable of predicting the SER within a factor of 2 or better.

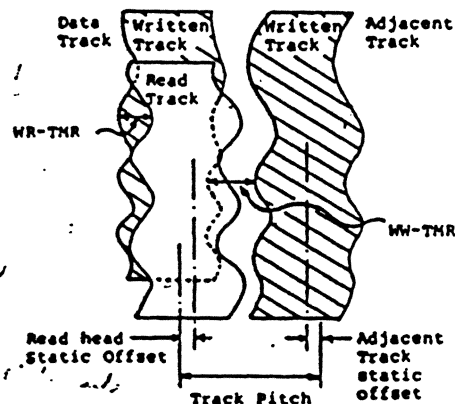
TRACK MISREGISTRATION (THR)

The track position histogram indicates how accurately a head can seek to, and track follow a specific track. The histogram is obtained by making numerous random length seeks to a chosen track and measuring the track following error at many points around the track (Fig. 1a). The various factors contributing to track position error such as non repeatable runout or thermal offsets can be classified as either static or dynamic relative to the time taken to read a record. The effects of static offsets can be removed by shifting the head position before reading. This does not work for dynamic factors which are therefore more of a problem for the data channel to withstand.

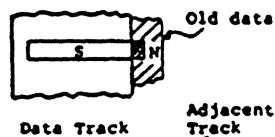
What matters is the difference in head position between writing and reading the record. (fig. 1b) This is called track misregistration or THR. The THR distribution quantifies the amount of radial misalignment we can expect while reading a record. Because of the effects of THR the inter-track gap becomes cluttered with increased old data. When the head is on track the signal to noise ratio is maximum. As the head is misaligned radially the signal decreases, while simultaneously the noise from old data increases. (fig. 1c) This causes a rapid drop in the signal to noise ratio and increases the SER. Old data noise cannot be filtered out since it has characteristics which are similar to the desired data signal. THR causes radial misalignment both while writing and reading. THR while writing can cause the data on the adjacent track to be overwritten, which may result in hard errors in extreme cases. (fig. 1d) The THR between two written tracks is known as WRTHR. THR between writing and reading is known as WRTHR.



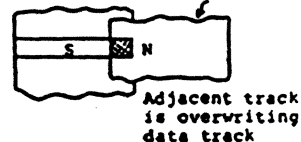
(a) Track position error during a single seek



(b) Example of combined WR and WW THR



(c) WRTHR effects



(d) WWTHR effects

Fig. 1. Showing effects of Track Misregistration.

A Soft Error Rate Model for Predicting Off-Track Performance

Mathew P. Veal, *Member, IEEE* and Thomas D. Howell, *Senior Member, IEEE*

Abstract—Specifying the head and determining the track density are critical, interdependent decisions made early in the development of a hard disk drive. We have created a soft error rate model to be used as a tool to aid in making these decisions. We have also developed methods to estimate the side reading and writing parameters of a head using well known spindant tests. In addition to these four reading and writing parameters, the model requires an estimate of the track misregistration (TMR) and a sixth input parameter, the effective on-track signal-to-noise ratio (SNR_{eff}) of the channel. The utility of the model is demonstrated in a test case based on a system with a thin film head/medium and a peak detection channel. The model is used to predict error rate both as a function of track density for a given head and as a function of head width for a given track density. The validity of the model is demonstrated by the close agreement of simulated 747 curves generated by the model with experimental 747 curves measured as a spindant.

I. INTRODUCTION

SOFT error rate modeling is a method for estimating the average raw error rate of disk drive systems [1], [2]. In this technique, the read channel raw error rate is measured as a function of track spacing and head-to-track registration. This function is referred to as the error rate response surface (ERRS) [3], or alternately as the error rate profile [4]. The ERRS is integrated with the probability distribution of the track misregistration to yield the average system error rate. Soft error rate models are used in selecting the track density for a specific system [4], [5] as well as for verification of system error performance under operating conditions. One drawback of this method is the time and equipment required to collect data for the ERRS measurement. The measurement requires a precision spindant, the head/medium, a fully operational read channel, and a data collection system. Such a measurement is often impractical because track pitch must be decided early in the development cycle.

We propose an approach to soft error rate modeling in which the ERRS is generated by a computer model rather than by direct measurement. Our model specifies the side reading and writing properties of the head/medium with

four parameters. These parameters can be easily estimated from simple spindant measurements. The on-track performance is specified by a single parameter, the effective signal-to-noise ratio (SNR_{eff}) of the channel. As a result of our approach, the model can be used to study any design parameter whose variation can be measured or characterized as a function of the model parameters. In particular, we show how the model can be used to predict system error rate as a function of track pitch and/or head width. The head width study depends on simple assumptions about the variation of side reading and side writing widths. These assumptions allow the extrapolation of off-track performance estimates over moderate ranges of head widths. We demonstrate the utility and validity of the model with a test case involving a system with a thin film inductive head. Our approach might also be used to predict performance of systems with magnetoresistive (MR) heads. The model would have to be modified slightly to account for the asymmetric side reading characteristic of the MR head. Finally, the model can be used to compare and evaluate different head geometries [6].

Section II contains a description and derivation of the soft error rate model, including the method used to generate the ERRS and the assumptions that were placed on the signals and interferences. Section III describes four simple tests to estimate the model's read and write parameters from spindant measurements. These parameters were used in the test case that is described in Section IV. Our conclusions are summarized in Section V.

II. DERIVATION OF THE MODEL

A block diagram of the model is shown in Figure 1. Four parameters (w_r , w_e , w_{r1} and w_{r2}) describe the side reading and writing properties of the head. Side writing is defined by the width of the track (w_t) and the width of the erased band (w_e). Side reading is characterized by the read width (w_r) and the side reading width (w_{r1}). A fifth parameter, SNR_{eff} , characterizes the on-track error performance of the channel. These five parameters plus the track density and the three standard deviation value of track misregistration ($TMR_{3\sigma}$) are sufficient to estimate the probability of error of the system. In addition, the model can simulate a "747" curve, so named because its shape resembles the profile of the nose of the Boeing 747 airplane [7].

The effect of interfering signals from adjacent tracks

Manuscript received December 22, 1992; revised July 27, 1994. This material is based in part on work supported by the National Science Foundation under grant no. ECD-8907068.

M. P. Veal is with Quantum Corporation, 333 South Street, SHR 1-3/E29, Shrewsbury, MA 01545.

T. D. Howell is with Quantum Corp., 500 McCarthy Blvd, Milpitas, CA 95035.

Log Number 9405615.

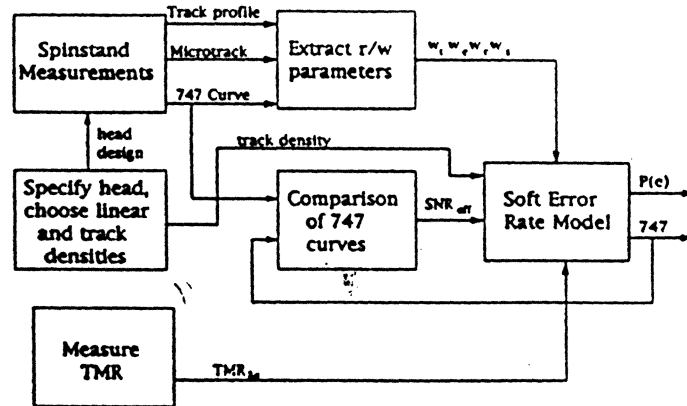


Fig. 5. Soft error rate model with spinstand measurements.

mation of the four read and write widths. These tests are described in the following section. The fifth parameter, SNR_{eff} , is estimated by matching a measured 747 curve to a set of 747 curves generated by the model. The designer also must measure or model track misregistration ($TMR_{3\sigma}$). An alternative use of the soft error rate model is to use a three dimensional head/medium model to estimate the four read and write widths. In this case, a detailed on-track channel model is required to estimate SNR_{eff} . Use of the on-track channel model allows performance studies that trade off linear density with track density.

III. SPINSTAND MEASUREMENTS

We use three spinstand tests to estimate the four read/write width parameters required by the soft error rate model. The three tests are a track profile, a microtrack profile, and a 747 curve. The measure taken from the track profile is $w_r + w_w$. The measures taken from the microtrack profile are w_r and $w_r - w_w$. The 747 curve is used to measure $w_r + w_w$. The model parameters are recovered from the appropriate linear combinations of these measurements.

The fifth model parameter, SNR_{eff} , can be estimated by comparing a 747 curve generated on the spinstand to 747 curves generated by the model. These procedures are derived below, and a short discussion of track misregistration measurement is included.

A. Track Profile Test

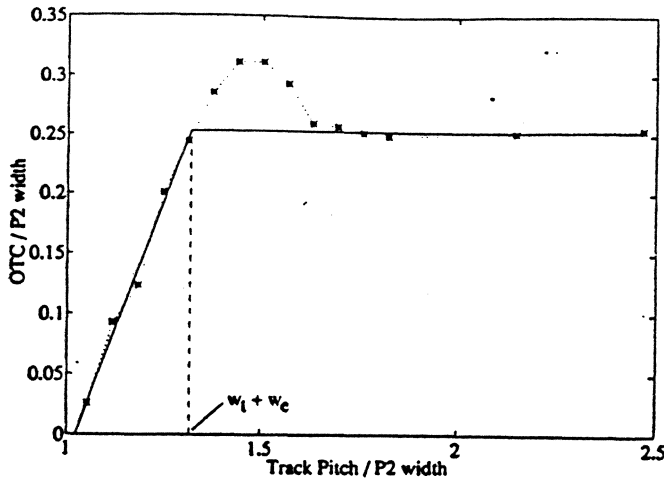
radial head position on the y-axis. The points that fall outside the profile of the two sets of tracks as shown in Fig. 2 intercept with these intercepts

B. Microtrack Test

The second test is a microtrack test. A microtrack test involves moving the head across the track and performing a series of measurements that is much thinner than the track width. One of the advantages of this test is that it allows the measurement of the thin track width (the area between the track edges) in the limit of zero. The track width with $M(y)$, will be zero in the limit.

An example of a track profile is shown in Fig. 3. The track profile typically has a trapezoidal shape. The track density supports the track width. It is a trapezoid function that measures that area under the curve and the "plateau" of the trapezoid. Since the microtrack head function, the corresponding head function, these parameters, these respectively.

The procedure for the microtrack test is similar to the track profile test. The track profile is fitted to the linear portion of the track. A line is fitted to the maximum amplitude of the average value of the track. The half height of the

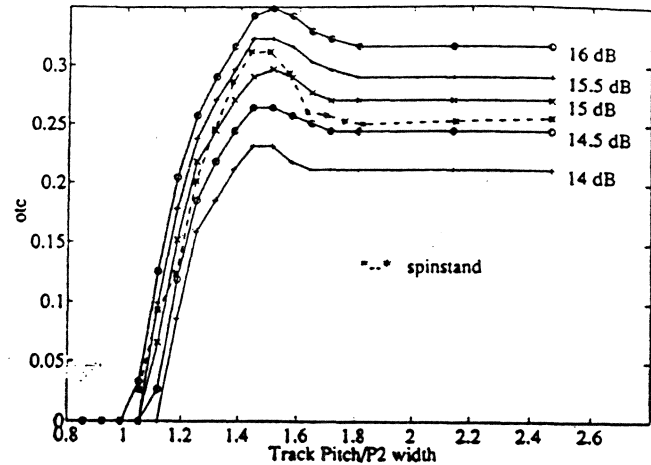
Fig. 8. 747 curve estimation of $w_l + w_e$.

w_e }. An example of the matching procedure is shown in Fig. 9, where SNR_{eff} values of 14, 14.5, 15, 15.5 and 16 dB were used to generate five 747 curves. The value of SNR_{eff} is chosen by selecting the model-generated 747 curve that most closely matches the spindisk curve. This method is appropriate because the 747 curve is a contour line for the error rate response surface (ERRS). The ERRS viewed in three dimensions is a plot of error rate, or $P(e)$, as a function of ϵ_{wv} and ϵ_{wr} . The 747 curve is a plot of the value of ϵ_{wr} corresponding to a specified $P(e)$ as a function of ϵ_{wv} . Thus, the 747 curve is traced by a plane of constant $P(e)$ that slices the ERRS.

E. Estimation of Track Misregistration

The measurement of track misregistration (TMR) is typically handled by classifying the causes of TMR and conducting a separate test to measure each cause. Such sources of TMR include spindle non-repeatable runout (NRRO), servo prediction error and thermal track shift. The total system TMR, specified at its 3σ value, is computed by adding the individual variances due to the different sources. If all the sources are independent, then the total TMR is just equal to the square root of the sum of the squares of the individual 3σ values. Otherwise, the total TMR value can be computed by Monte Carlo methods.

A complete discussion of TMR measurement is beyond the scope of this paper, but it is of interest to note that some sources of TMR are under the control of the designer. For instance, allowance in the TMR budget is usually made for seek settling. In order to achieve faster access times, a disk system will try to read before the head is completely settled. Thus, there is a tradeoff between disk access time and TMR tolerance of the system. The soft error rate model described here has the ability to predict error performance as a function of TMR. This curve can be used to determine the tolerance of the system to increased levels of TMR, and to set the margin for settling time.

Fig. 9. Selection of SNR_{eff} by matching an experimental 747 curve to family of model-generated curves.

F. Alternate Measurement Methods

The track profile and microtrack profile tests described above were chosen because they are easy to conduct and require no special equipment beyond a spindisk. In particular, the estimate of the erased band width w_e can be improved. The procedure outlined above requires a measurement from each of the track profile, microtrack profile, and 747 tests to estimate w_e , and the uncertainty in each of these measurements adds to the uncertainty in the w_e estimate. Other, more accurate techniques may be used to measure the parameters if time and equipment are available. Hoyt and Sussner describe a single head technique for measuring erased width [15]. Their technique can be modified to measure $w_l + w_e$ as a function of frequency using a spectrum analyzer. Van Herk and Bijl describe two techniques, one which directly measures track width w_l and one which measures $w_l + w_e$ [16]. These techniques are more complicated, requiring several heads of different widths, but they promise better accuracy. Finally, the erased band might be measured directly using ferrofluid and an optical microscope or using magnetic microscopy techniques [17].

IV. TEST CASE

We have conducted a single test case to verify the accuracy of the model and illustrate its uses. We followed the parameter estimation tests described in Section III to estimate parameters for the model. The head and medium on which the measurements were made, as well as the operating conditions (linear density, write current, etc.), were taken from a system representative of the state of the art in late 1991. Both the head and medium were high performance thin film components. The primary error mode of the channel was assumed to be bit shift.

The parameter estimation tests were made at different data frequencies and disk radii because the read/write properties vary with both frequency and track position. We conducted tests at both the inside diameter (ID) and outside diameter (OD) of the disk, and at the maximum

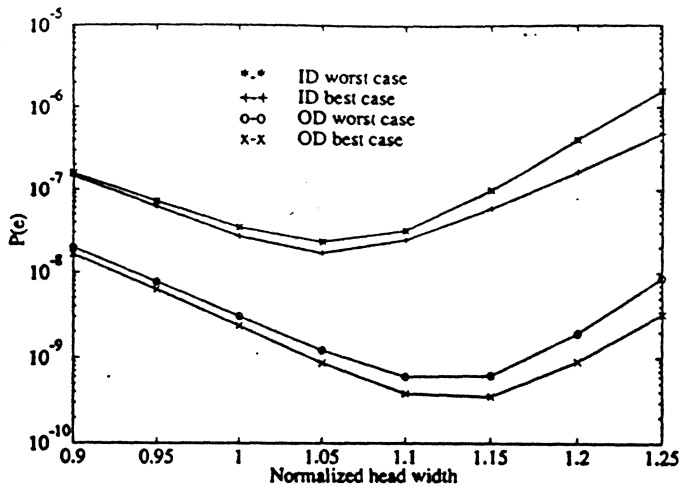


Fig. 13. $P(e)$ versus head width for a fixed track pitch.

The other points in the plot are generated by the model using parameters extrapolated according to the assumptions describe above. Remember that the true error rate at a given track radius is bounded by the worst case and best case curves. Again, note the higher error rate at the ID. As is shown by this plot, the head is slightly more narrow than the width that is optimal for the chosen track pitch.

The performance curves in Fig. 13 have a well-defined minimum point due to two competing effects. The on-track performance improves with increasing head width as the track width (and therefore the signal power) increases. The off-track performance is relatively constant for small head widths. After the head width passes a critical width, corresponding to the knee in the error rate versus track pitch curve, the off-track performance degrades with increasing head width as the guard band shrinks. This second effect dominates at large head widths, and the curves follow a roughly linear (on this log scale plot) slope. The $P(e)$ increases an order of magnitude for an increase of about 8.5% increase in head width at this slope. At small head widths, the $P(e)$ increases about an order of magnitude for a 12% decrease in head width.

A second use of the type of plot shown in Fig. 13 is to study the effect of component variation once the product is in production. The effect of variation in the head width can be easily viewed by inspecting the plot at, say, +5% and -10% of head width, if those are the specifications given to the head manufacturer. Another way to view this plot is to draw a line at the system specification for error rate, say $P(e) = 10^{-7}$, to determine which head widths meet the specification.

The final performance study is a plot of error rate versus track misregistration (TMR). This plot shows the sensitivity of the model's error rate prediction to variation in TMR. In addition, this plot could be used to determine budgeting of TMR sources. As discussed in Section III, certain sources of TMR are under control of the designer. In such cases, the designer wishes to know how much margin the system has in its off-track performance curve. The four cases of track radii and frequency are plotted in

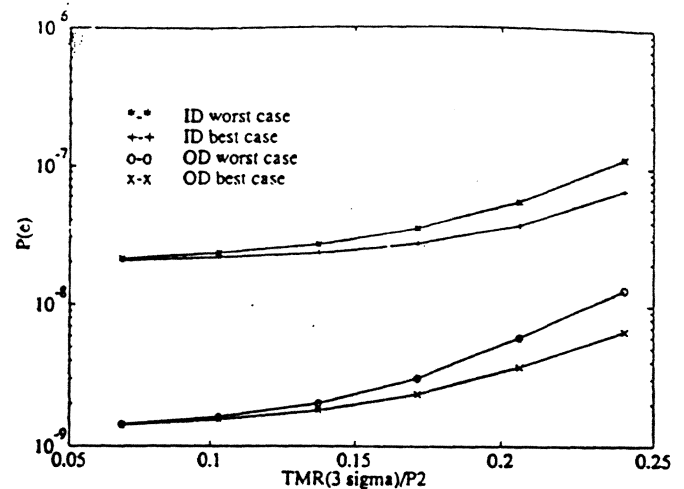


Fig. 14. $P(e)$ versus TMR 3σ for fixed head width and track pitch.

Fig. 14. The best and worst case conditions are defined as in the previous plots. Again, the error rate is significantly higher at the ID than at the OD. The nominal TMR 3σ value used in the studies of Fig. 12 and 13 was 0.172 in units of $P2$ width. As shown in Fig. 14, the performance curves are somewhat sensitive to the TMR assumption, although the sensitivity of error rate to TMR is less than the sensitivity to head width. The TMR margin for seek settling can be determined from a plot such as shown in Fig. 14. The normal sources of TMR are added together. The worst case performance curve (of the four shown) at this level of TMR should be less than the system specification for error rate, say 10^{-7} . The TMR value on the worst case curve which yields a 10^{-7} error rate is determined. The TMR margin is the difference between these two values.

V. CONCLUSIONS

We have developed a soft error rate model to predict off-track performance for disk drives. Our model uses the accepted method of system error rate estimation, in which the track misregistration distribution is integrated with the error rate response surface (ERRS). The ERRS is estimated with a computer model based on a few parameters that describe the side writing and side reading properties of the head/medium. We used a number of simplifying assumptions in generating this model. In particular, we assumed that the effect of all sources of on-track errors can be represented with an error function whose performance is characterized by a single parameter. The effect of our assumptions is twofold: the computational demands are reduced, and the model is focused on those system parameters that affect off-track performance, particularly track pitch, head width, and track misregistration.

The utility of this model was demonstrated in a test case, in which error rate was predicted as a function of track pitch, head width and track misregistration. The test case was based on parameters estimated from spindstand

RPS - Recording Process Simulator

Roscamp Engineering Inc.

Designed to aid disk drive component suppliers and disk drive designers in understanding performance and yields.

First version of RPS was in 1986 for understanding magnetic head behavior. Current version completely models the data portion of a disk drive. Future versions will model servo with 3D solvers.

Model is currently used by 24 industry leaders in magnetic disk drive design and manufacture as well as head and disk suppliers in both the US and Japan.

Signal to Noise Calculations

Signal to Noise for DASD

$$\text{SNR} \cong \frac{\text{Signal from Track of Interest}}{\text{RMS of Noise Sources}}$$

N_d = Disk Noise

N_{hr} = real part of the head noise

N_{ampl} = amplifier noise

N_{oi} = Sig-oi = Noise from old information

N_{adj} = Sig-adj = Noise from adjacent track

$$\text{SNR} \cong \frac{\text{Signal from Track of Interest}}{(N_d^2 + N_{hr}^2 + N_{ampl}^2 + N_{oi}^2 + N_{adj}^2)^{0.5}}$$

SNR AND BER

Gaussian distribution

where e_n = noise voltage and σ = standard deviation. $p(e_n)$ is probability density function.

$$p(e_n) = \frac{e^{-\left(\frac{e_n^2}{2\sigma^2}\right)}}{\sqrt{2\pi}\sigma}$$

$$BER = P(|e_n| \geq K) = \text{erfc}\left(\frac{K}{\sqrt{2}\sigma}\right)$$

K is a detection threshold and $P(e_n)$ is the cumulative probability that the noise voltage exceeds the threshold (an error results whenever a pulse is transmitted and not detected or no pulse is transmitted but a pulse is detected).

If we define:

$$SNR = \frac{E_{0-pk}}{\sigma}, \text{ then } K = \frac{E_{0-pk}}{2}$$

and

$$BER = \text{erfc}\left(\frac{SNR}{2\sqrt{2}}\right) = 2Q\left(\frac{SNR}{2}\right)$$

where

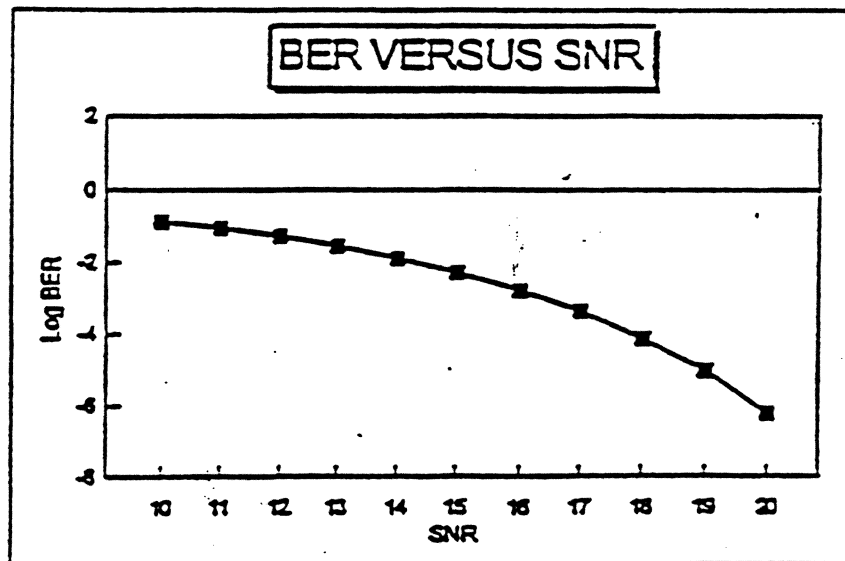
$$Q(x) = \frac{1}{\sqrt{2\pi}} \int_x^{\infty} e^{-\frac{z^2}{2}} dz$$

For reasonable values of SNR we can approximate the BER as follows:

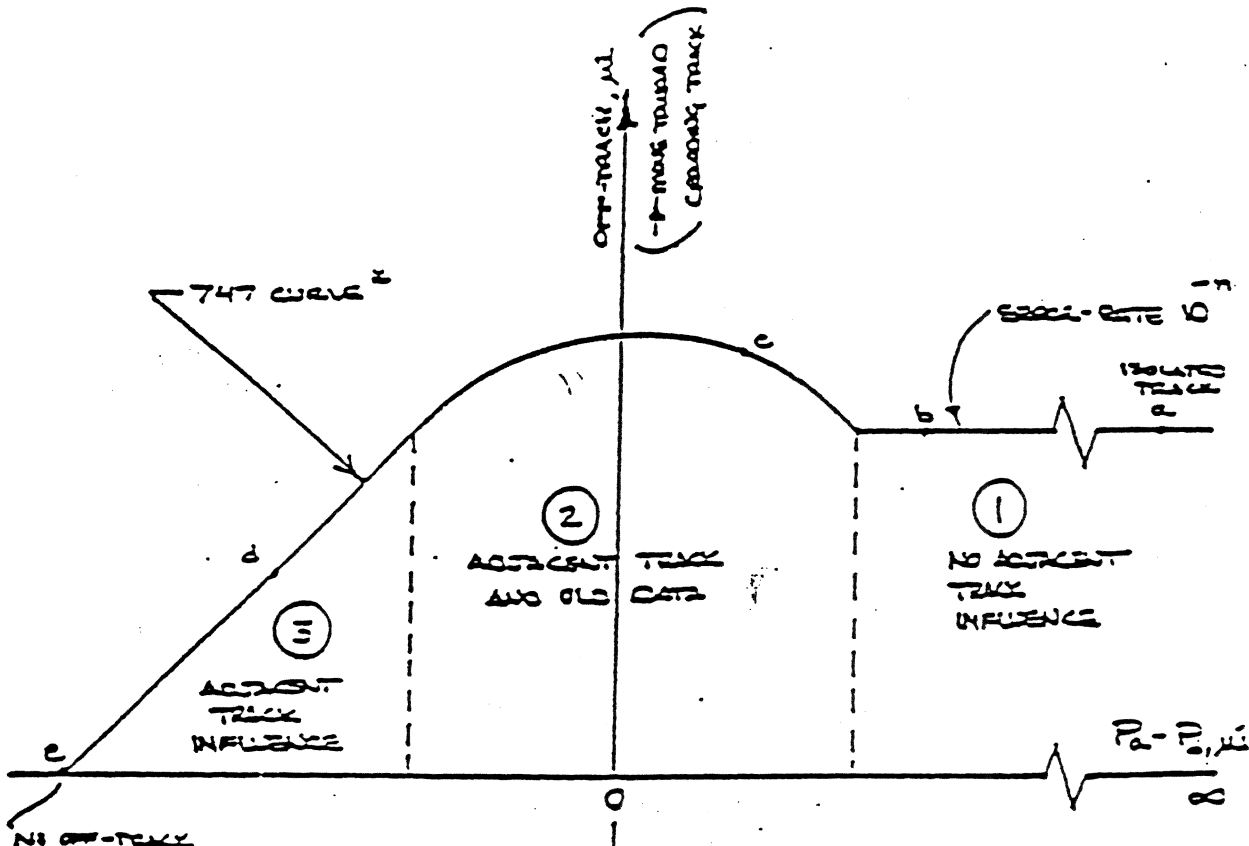
$$BER \approx \frac{e^{-z^2}}{\sqrt{\pi}z}$$

where

$$z = \left(\frac{SNR}{2\sqrt{2}} \right)$$

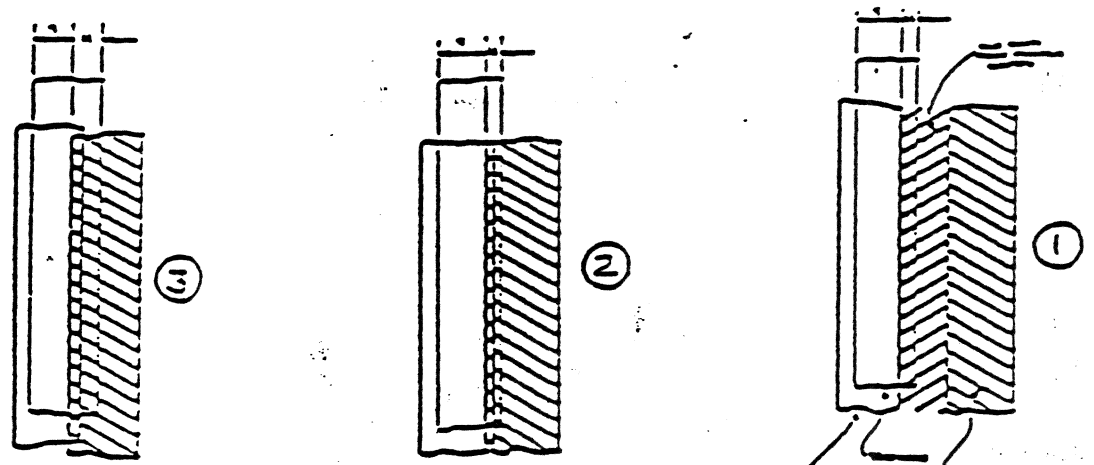


747 OTC CURVE



ACTIVATION TRACK ERROR GREATER THAN μ

ACTIVATION TRACK ERROR GREATER THAN μ



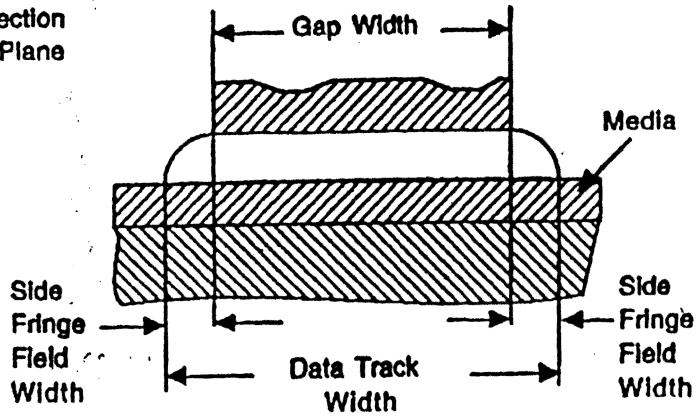
IIST

A. Hoagland 390

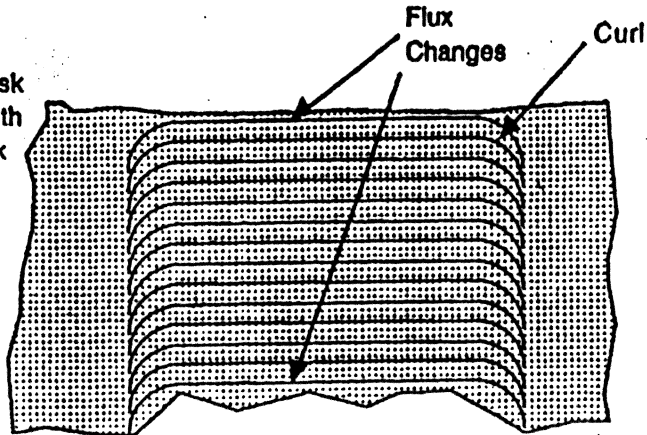
120

Gap Width and Data Track Width

Cross Section through Plane of Gap

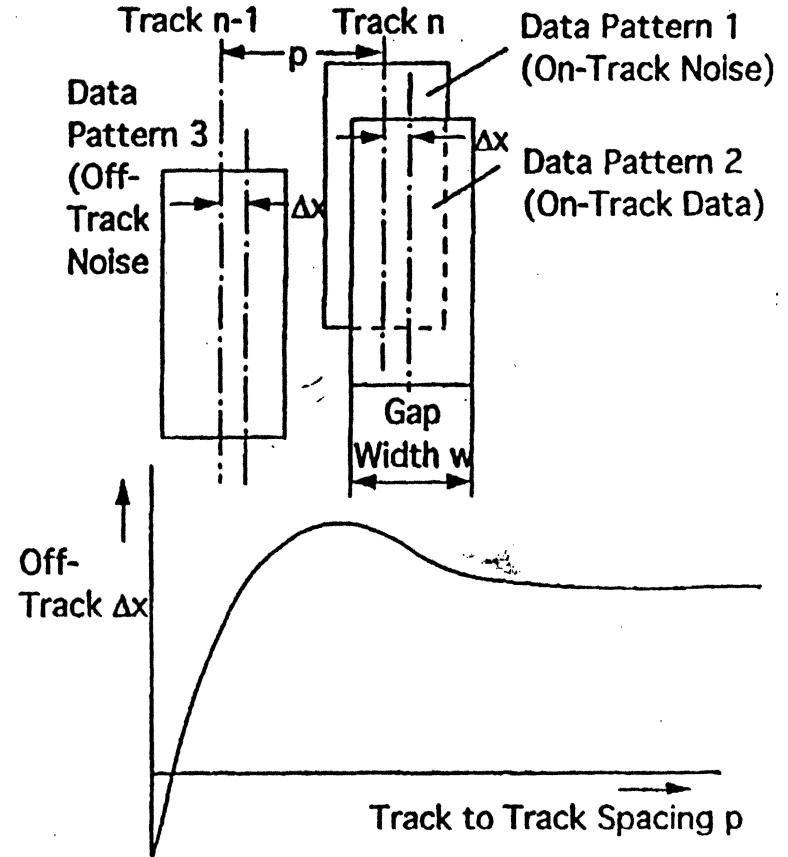


View of Disk Surface with Data Track



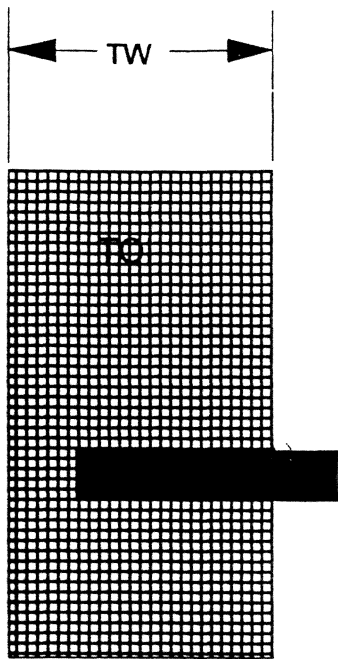
Rigid Disk Drives
Hans H. Gatzert

Optimal Track to Track Spacing



Rigid Disk Drives
Hans H. Gatzert

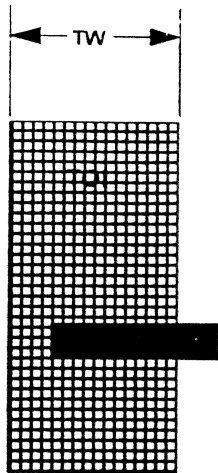
Track Layout Examples & Error Rate Calculations



Track Layout

(scuoffa4.drw)

Dan Malone, May 1995



Track Layout

(scuoffa4.drw)

Dan Malone, May 1995

Head sensitivity can be defined as a certain number of volts (microvolts) per unit track width.

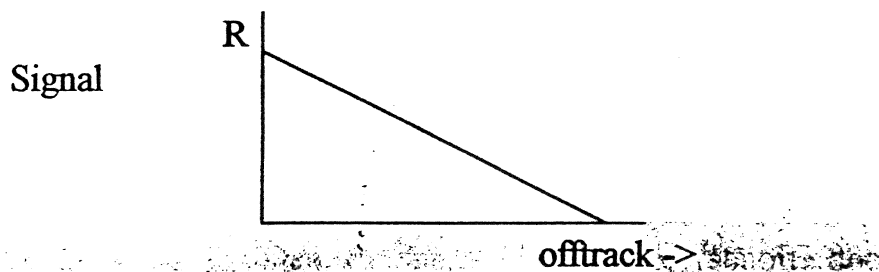
e.g. 80 uvolts/micron

Comes from the amplitude equation:

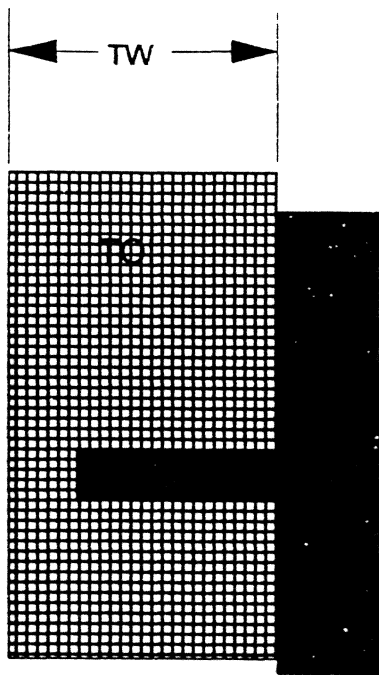
$$V_{out} = N \epsilon M_r V_L \mu_0 K W \cdot (\text{losses})$$

$$HS = \text{Head Sensitivity} = \frac{V_{out}}{W}, \quad Tw = \text{Written track width}$$

$$D = Tw \cdot Hs, \quad OFF = (\text{offtrack-distance}) \cdot Hs, \quad OT = \text{offtrack distance}$$



(scuoff4.doc)



Track Layout

(scuoffa3.drw)

Dan Malone, May 1995

$$\text{Signal} = R = D - \text{OFF}$$

$$\text{Noise} = N_{\text{TOT}} = \sqrt{N_s * N_s + N_{\text{off1}} * N_{\text{off1}}} \quad (\text{uncorrelated})$$

$$\text{Signal to Noise Ratio} = \frac{R}{N_{\text{TOT}}}$$

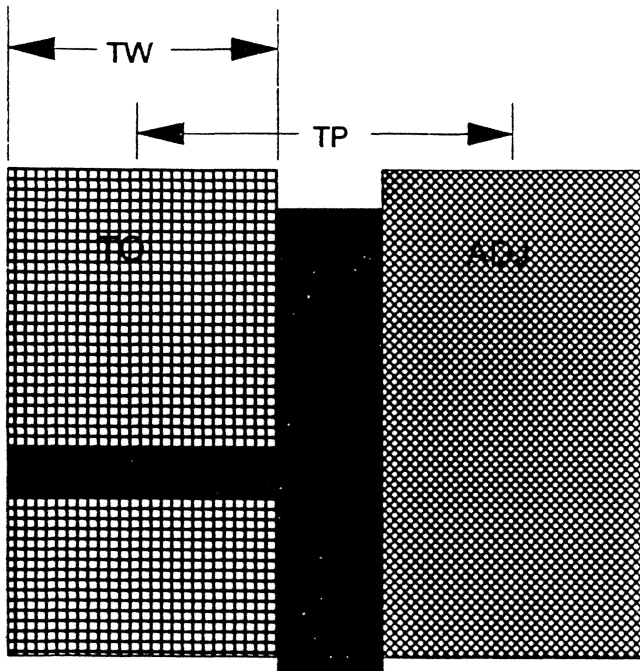
$$Z = \frac{\text{SNR}}{2\sqrt{2}}, \quad \text{erfc}(z) \cong \frac{e^{-z^2}}{\sqrt{\pi} Z}$$

OFF	R	Ns	Noff	Ntot	SNR
0	D	Ns	0	Ns	D/Ns
off1	D-off1	Ns	off1	$\sqrt{N_s * N_s + \text{off1} * \text{off1}}$	
off2	D-off2	Ns	off2

So,

General expression for the simplified case:

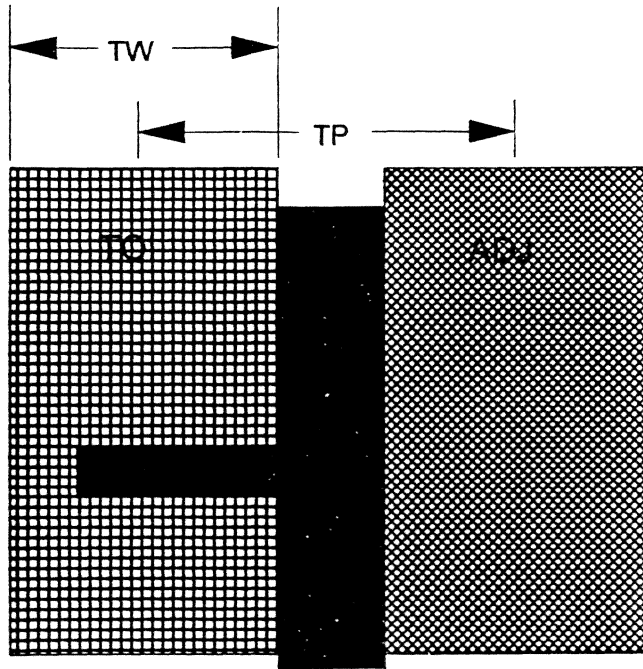
$$\text{SNR} = \frac{D - \text{Off}}{(N_s^2 + \text{off}^2)^{0.5}}$$



Track Layout

(scuoffa1.drw)

Dan Malone, May 1995



Track Layout

(scuoffa2.drw)

Dan Malone, May 1995

A	B	C	D	E	F	G	H	I	J	K	L
---	---	---	---	---	---	---	---	---	---	---	---

```

1 Signal to Noise Ratio          -12 Signal and Noises ver
2                               -60 Dan Malone, ELEN 463,
3 EB          0      microinches  0      0Error Rate vs Offtrac
4 Noise       10      uvolts      80     50Signal to Noise Ratio
5 TPI         4000    TPI
6 TP-uin      250    track pitch
7 TW-uin      200    80% RULE      406.4
8 TW-mic      5.00   in microns     406.4
9 Hs          80     uv/micron
10 Hs         2.032   uv/uinch
11 DetLos     10     db

```

12	uin	offtrack(uin)	Signal	dist	dist	uv	uv	uv	SNRR(db)	Z
13	OT	TW-OT	R(uv)	OT-EB	OI(uin)	Ns(uv)	Nold	Ntot	SNR	
14	2	0	200	406.4	0	0	10	0	10	40.6 32.2 14.37
15		2	198	402.3	2	2	10	4.06	10.8	37.3 31.4 13.18
16		4	196	398.3	4	4	10	8.13	12.9	30.9 29.8 10.93
17		6	194	394.2	6	6	10	12.2	15.8	25.0 28.0 8.839
18		8	192	390.1	8	8	10	16.3	19.1	20.4 26.2 7.227
19		10	190	386.1	10	10	10	20.3	22.6	17.0 24.6 6.027
20		12	188	382.0	12	12	10	24.4	26.4	14.5 23.2 5.125

```

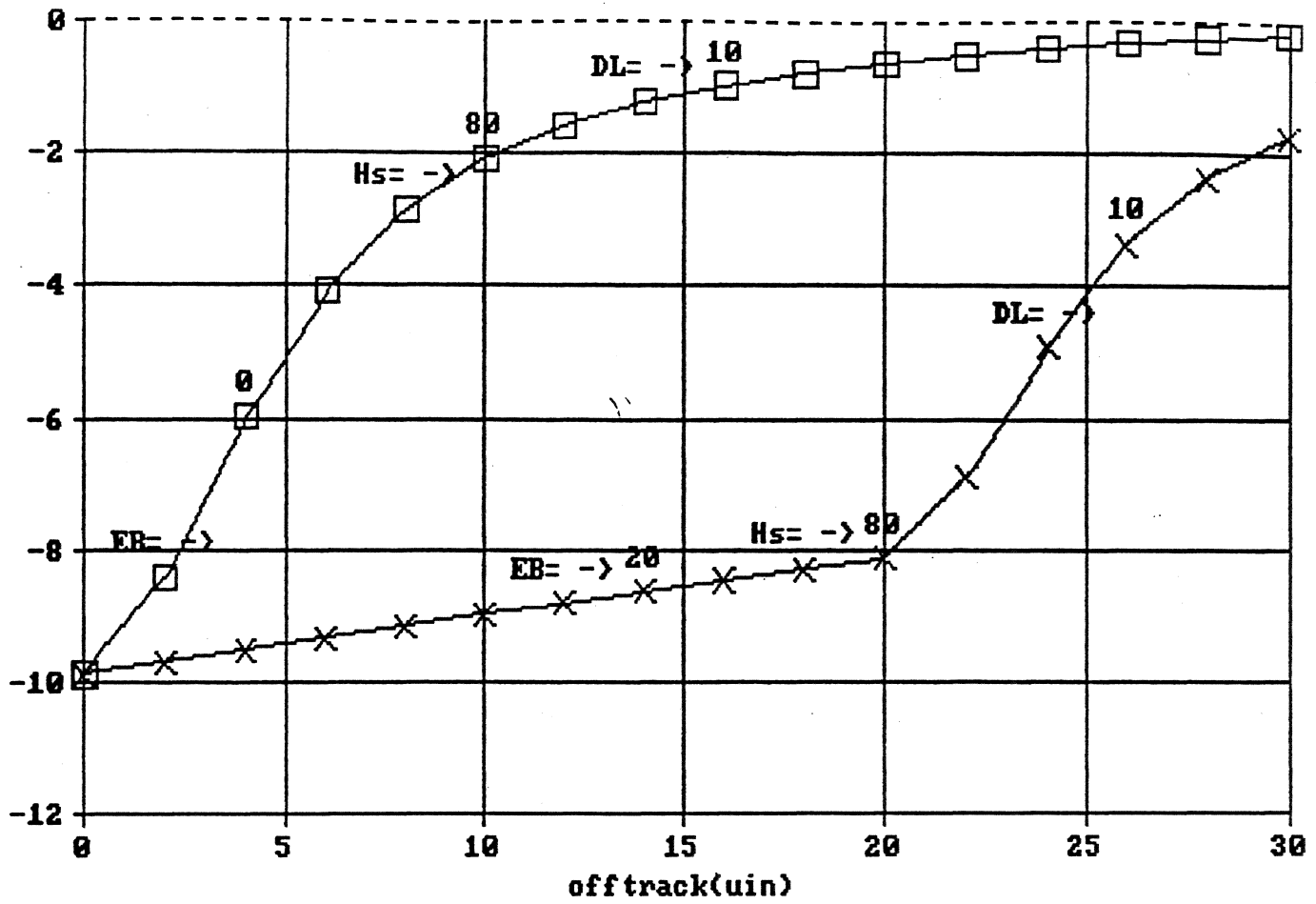
21 TL      Text="offtrack(uin)
Width: 9 Memory: 156 Last Col/Row:T74

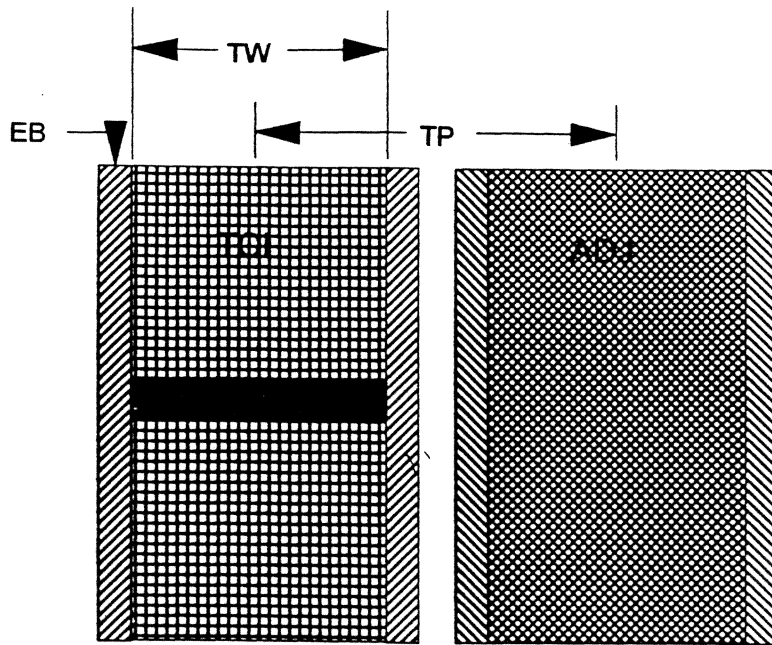
```

READY F1:Help F3:Names Ctrl-Break:Cancel

NUM

Error Rate vs Offtrack distance
 SNR(db)-DetLoss(db)

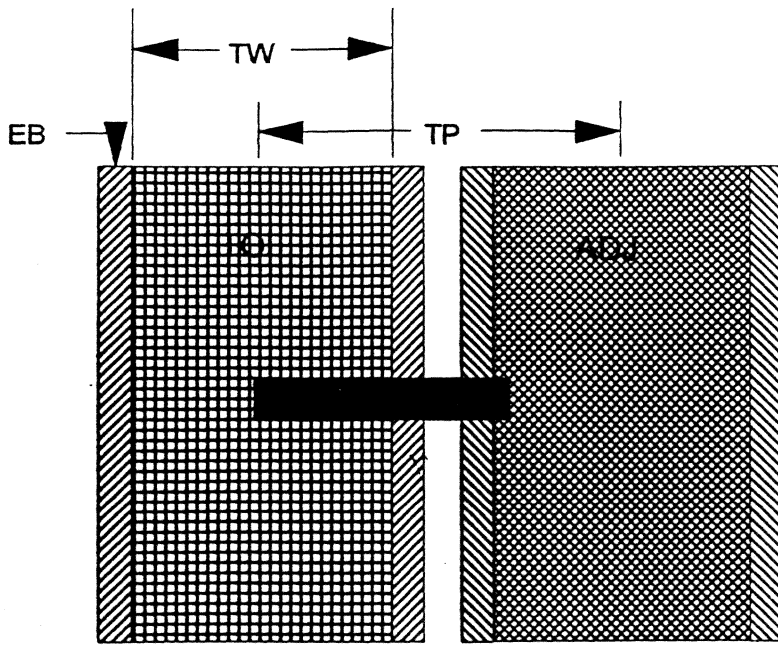




Track Layout
and Read head position

(scuoffe.drw)

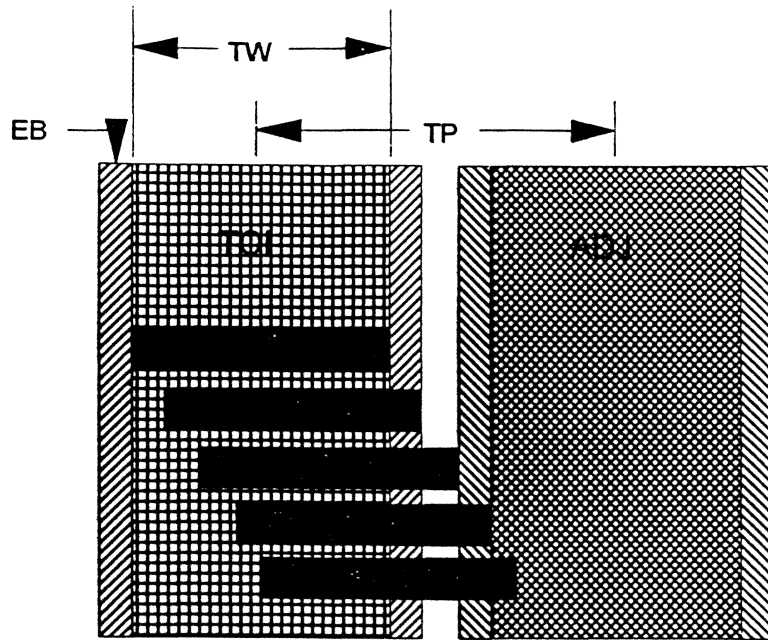
Dan Malone, May 1995



Offtrack Reading

(scuoff.drw)

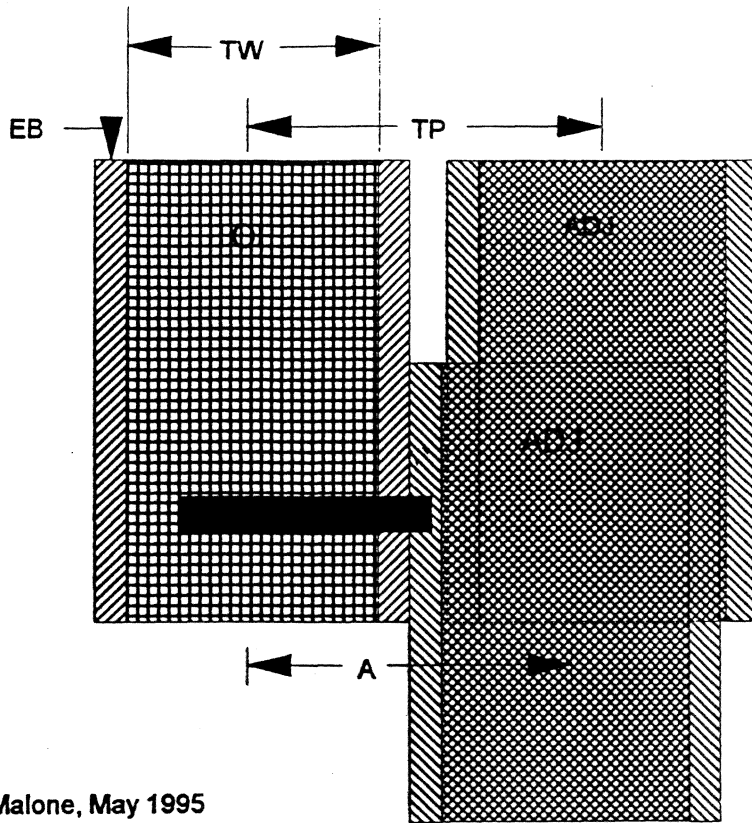
Dan Malone, May 1995



Offtrack Cases

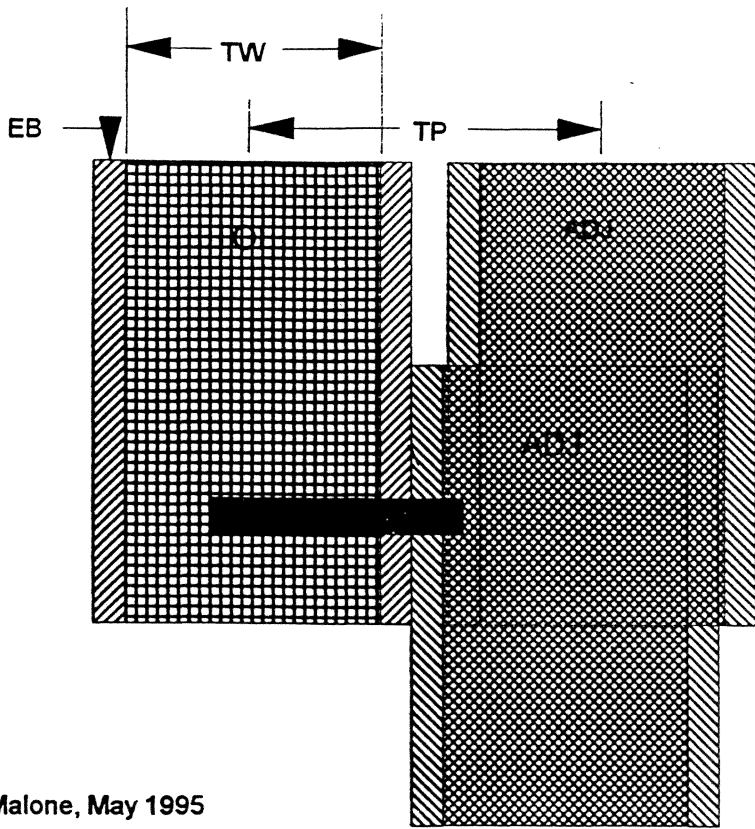
(scuoffg.drw)

Dan Malone, May 1995



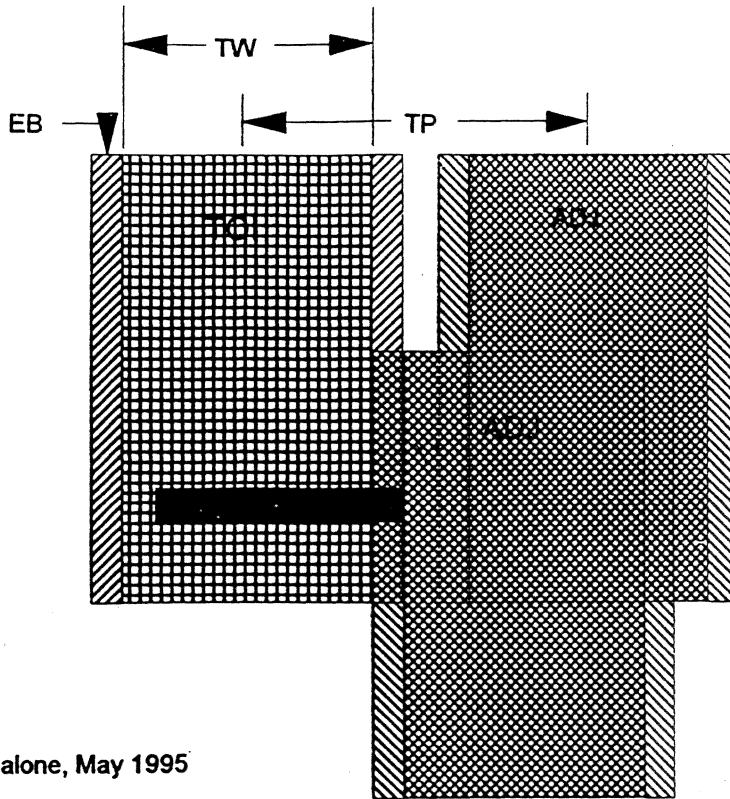
Adjacent
Track
Squeeze
(scuoffh.drw)

Dan Malone, May 1995



Adjacent
Track
Squeeze
(scuoffi.drw)

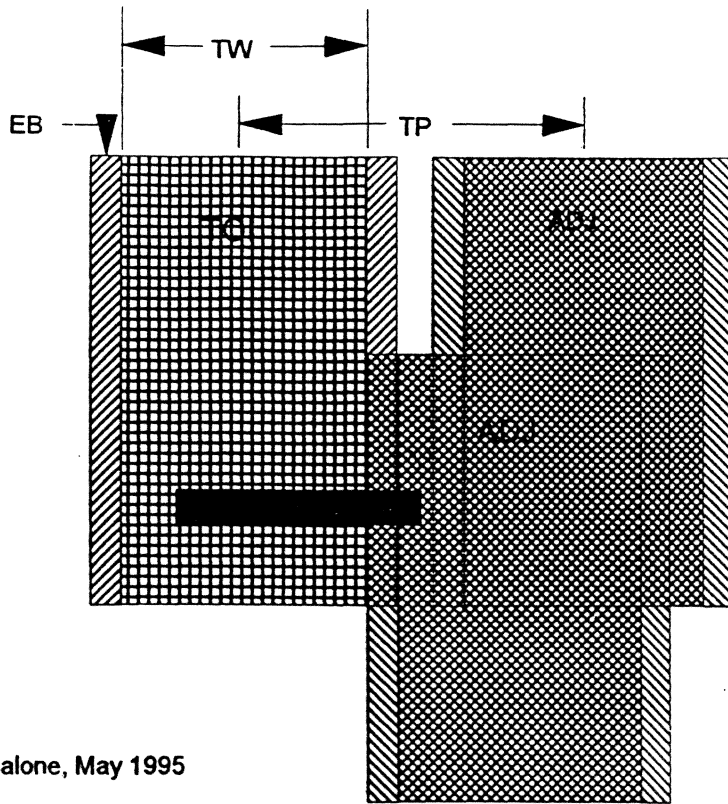
Dan Malone, May 1995



More Squeeze
EB Overlap

Dan Malone, May 1995

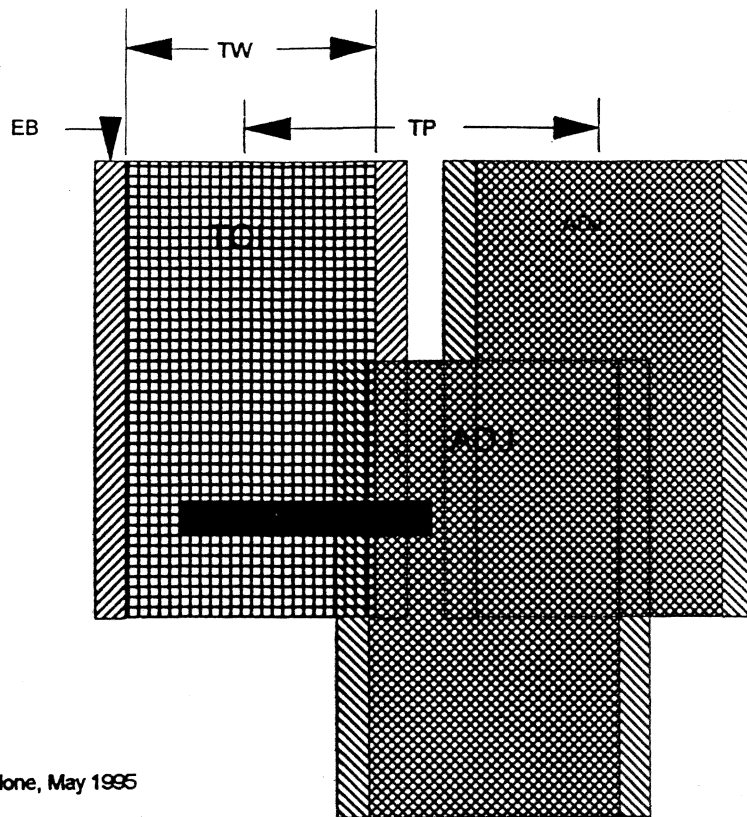
(scuoffj.drw)



More Squeeze
EB Overlap

Dan Malone, May 1995

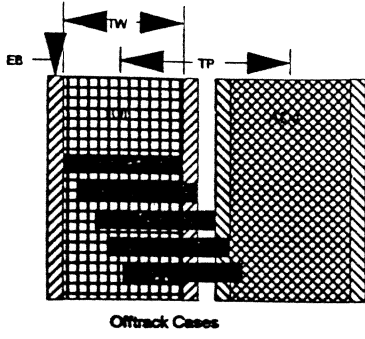
(scuoffk.drw)



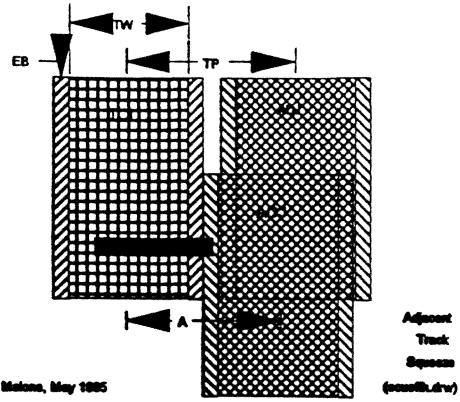
More Squeeze
EB Overlap

Dan Malone, May 1995

(scuoffl.drw)



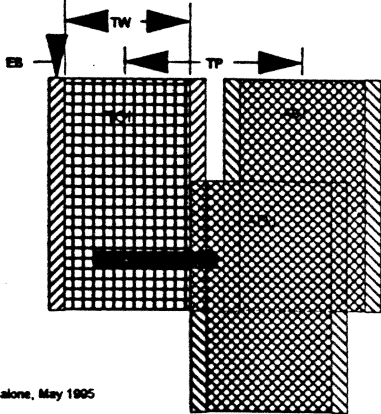
Offtrack Cases



Adjacent
Track
Squeezes
(scsoffl.drv)

Den Malone, May 1995

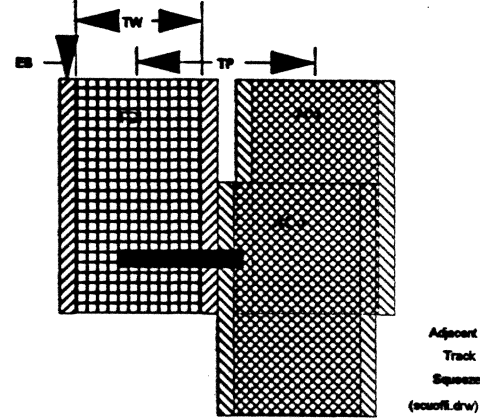
(scsoffl.drv)



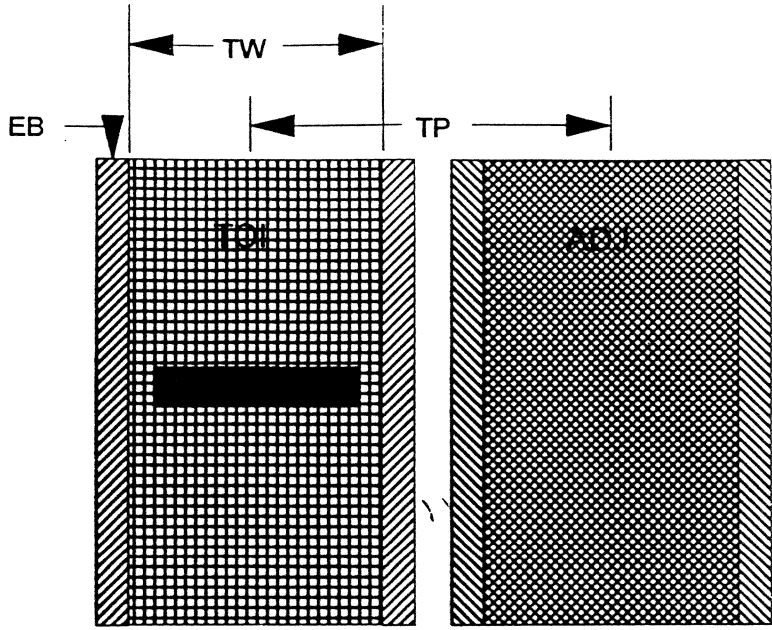
More Squeeze
EB Overlap

Den Malone, May 1995

(scsoffl.drv)



Adjacent
Track
Squeezes
(scsoffl.drv)

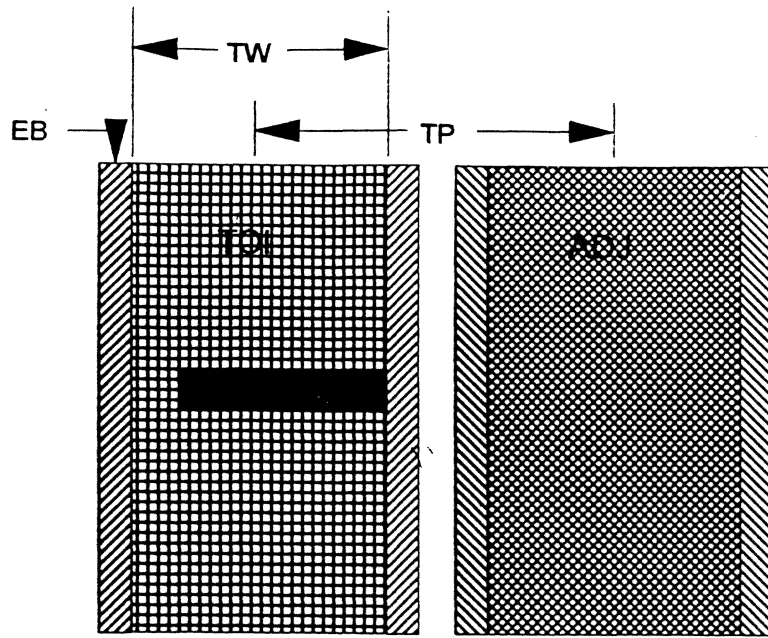


Offtrack Reading

Write wide / Read Narrow

(scuoffm.drw)

Dan Malone, July 1996

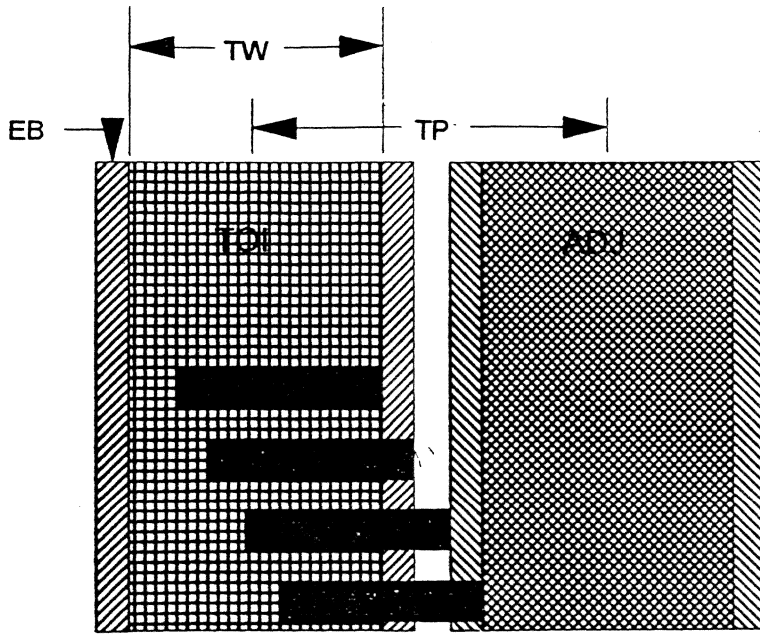


Offtrack Reading

Write wide / Read Narrow

(scuoffn.drw)

Dan Malone, July 1996



Offtrack Reading

Write wide / Read Narrow

(scuoffo.drw)

Dan Malone, July 1996

Data Recovery Procedures

Goals of Error Correction and Error Tolerance

- Achieve an acceptable re-read rate
- Achieve an acceptable unrecoverable error rate
- Achieve higher recording densities through coding

Goals of Error Detection

- Achieve acceptable rate for undetected errors

The Goal of Error Retry

- Recover otherwise unrecoverable data by repeating the operation without any changes or by repeating the operation after changing parameters of the recording channel or positioning system

Errors in Disk Drive Systems

Errors in Storage systems result from:

- **Defects**

- **Noise**

 - Media noise**

 - Electrical Noise**

 - Barkhausen Noise**

- **Offtrack noise**

- **Adjacent track interference**

The number of bits or bytes associated with an error event can be extended by:

- **Error propagation due to the detection method (DFE, or other sequence detector)**
- **Loss of synchronization due to a defect**
- **Recovery from a thermal asperity (TA)**

ECC and DRP

Goals of Error Corrections and Data Recovery

- **Achieve an acceptable reread rate**
- **Achieve an acceptable unrecoverable error rate**
- **Achieve an acceptable miscorrect rate**

Goals of Error Detection

- **Achieve an acceptable rate for undetected Errors**

Goals of Data Recovery Procedures

- **Recover otherwise unrecoverable data by Repeating the operation without any changes or by repeating the operations after changing parameters of the recording channel or positioning system or ECC**

Higher TPI - System Considerations

"It's a vicious circle"

- Designs are dictated by read, write and erase widths, side reading and writing, skew due to the rotary actuator, and TMR

- Decreased track width of the read/write element gives:
 - o lower amplitudes

 - o for the same linear density, this requires a lower magnetic flying height to maintain SNR

 - o lower fly height means smoother media

 - o narrow tracks drives the defects higher
----> still smoother media

 - o narrow tracks drive better servo positioning

 - o need more ECC to cope with higher error rates, disk defects and thermal asperities

 - o tolerances of the head geometry's, disk parameters, fly heights, etc. make the job even tougher.

\$ \$ \$ \$ \$ \$ \$ \$ \$ \$

Dan Malone, IIST, 5/22/98, (scutpi1.doc)